Das Cyclodepsipeptid FR900359: Ein Insektizid mit neuem Wirkmechanismus aus *Cand.* Burkholderia crenata und *Chromobacterium vaccinii*

Dissertation

zur

Erlangung des Doktorgrades (Dr. rer. nat.)

der

Mathematisch-Naturwissenschaftlichen Fakultät

der

Rheinischen Friedrich-Wilhelms-Universität Bonn

vorgelegt von

Wiebke Hanke

aus Ratingen

Bonn 2023

Angefertigt mit Genehmigung der Mathematisch-Naturwissenschaftlichen Fakultät der Rheinischen Friedrich-Wilhelms-Universität Bonn

Erste Gutachterin: Prof. Dr. Gabriele M. König

Zweiter Gutachter: Prof. Dr. Werner Knöss

Tag der Promotion: 19. Dezember 2023

Erscheinungsjahr: 2024

Das Projekt wurde durch als Promotionsstipendium durch die Deutsche Bundesstiftung Umwelt (DBU) gefördert.

Teile dieser Arbeit wurden als begutachtete (Peer Review) Forschungsartikel, Zusammenfassungen und Poster veröffentlicht. Textpassagen und Abbildungen dieser Arbeiten wurden teilweise als Vorlagen übernommen und teilweise direkt für diese Arbeit zitiert.

Publikationen (Peer-Reviewed):

Teile der Publikation wurden in **chapter 3.1** mit der Erlaubnis von den folgenden Autoren wiederverwendet: "Wiebke Hanke, Julian Patt, Judith Alenfelder, Jan H. Voss, Mitja M. Zdouc, Stefan Kehraus, Jung Bong Kim, Goran V. Grujičić, Vigneshwaran Namasivayam, Raphael Reher, Christa E. Müller, Evi Kostenis, Max Crüsemann and Gabriele M. König. Feature-Based Molecular Networking for the Targeted Identification of G_q Inhibiting FR900359 Derivatives. Journal of Natural Products **2021**, 84 (7), pp. 1941–1953. Copyright 2021 American Chemical Society.
DOI: https://doi.org/10.1021/acs.jnatprod.1c00194
ACS Articles on Request author-directed link:
https://pubs.acs.org/articlesonrequest/AOR-UIEDBFJIXYI6M4UFSI8M
Reference number: 1

Teile des folgenden Papers wurden für die Erstellung von **chapter 3.3** und **3.4** verwendet: Wiebke Hanke, Judith Alenfelder, Jun Liu, Philipp Gutbrod, Stefan Kehraus, Max Crüsemann, Peter Dörmann, Evi Kostenis, Monika Scholz, and Gabriele M. König. The Bacterial G_q Signal Transduction Inhibitor FR900359 Impairs Soil-associated Nematodes. Journal of Chemical Ecology **2023**, Open Access under a Creative Commons Attribution 4.0 International License.
DOI: https://doi.org/10.1007/s10886-023-01442-1
Reference number: 2

Wissenschaftliche Zusammenfassungen und Poster:

Internationaler VAAM-Workshop zu “Biology of Microorganisms Producing Natural Products”. Jena, Deutschland. 15.-17. September 2019. The cyclic depsipeptide FR900359: An insecticide with a novel mode of action from *Cand.* Burkholderia crenata. *Wiebke Hanke, Christian Seiffert, Stefan Kehraus, Gabriele M. König, and Max Crüsemann.*

John Innes/Rudjer Bošković "summer schools in applied molecular microbiology" focused on "Microbial Specialised Metabolites: Discovery, Biosynthesis, and Evolution". Online. 1.-29. September 2020. Role of FR900359 as $G\alpha_q$ inhibitor and insecticide in the soil environment of its natural producer. *Wiebke Hanke, Philipp Gutbrod, Christian Seiffert, Stefan Kehraus, Max Crüsemann, and Gabriele M. König.*

VAAM-Workshop zu "Biology of Bacteria Producing Natural Products". Online. 22.-23. September 2021. Influence of the $G\alpha_q$ inhibitor FR900359 on the plant-pathogenic nematode *Heterodera schachtii*. *Wiebke Hanke, Philipp Gutbrod, Judith Alenfelder, Evi Kostenis, Jun Liu, Monika Scholz, Stefan Kehraus, Max Crüsemann, and Gabriele M. König.*

International VAAM workshop on "Biology of Microorganisms Producing Natural Products". Dortmund, Germany. 7.-9. September 2022. Effects of the G_q inhibitor FR900359 on soil nematodes. *Wiebke Hanke, Judith Alenfelder, Philipp Gutbrod, Jun Liu, Stefan Kehraus, Peter Dörmann, Max Crüsemann, Monika Scholz, Evi Kostenis, and Gabriele M. König.*

Für meine Großeltern.

Table of Content

Abbreviations

Ac	Acetyl
A domain	Adenylation domain
AHL	*N*-acyl homoserine lactone
Ala	Alanine
ANOVA	Analysis of variance
AUC	Area under the curve
b°	b-Ions without water
β-HyLeu	β-Hydroxyleucine
β-PLC	β-Isoform of the phospholipase C
BLAST	Basic Local Alignment Search Tool
BGC	Biosynthetic gene cluster
Cand. Burkholderia crenata	*Candidatus* Burkholderia crenata
Cch	Carbachol
cDNA	Complementary deoxyribonucleic acid
C. elegans	*Caenorhabditis elegans*
C domain	Condensation domain
CFU	Colony-forming units
CRISPR/Cas9	Clustered regularly interspaced short palindromic repeats/Caspase 9
C. vaccinii MWU205	*Chromobacterium vaccinii* MWU205
Da	Dalton
DAG	Diacylglycerol
Dgk-1	Diacylglycerol kinase
dH_2O	Distilled water
Dha	Dehydroalanine
DMR	Dynamic mass redistribution
DMSO	Dimethyl sulfoxide
DSMZ	German collection of microorganisms and cell cultures
E. coli	*Escherichia coli* OP50
EDTA	Ethylenediaminetetraacetic acid
Egl	Egg-laying defective
EIC	Extracted ion chromatogram
FBMN	Feature-based molecular networking

FR	FR900359
GDP	Guanosine diphosphate
GNPS	Global natural product social molecular networking
GPCR	G protein-coupled receptor
GTP	Guanosine triphosphate
HEK293 cells	Human embryonic kidney 293 cells
H. schachtii	*Heterodera schachtii*
HPLC	High-performance liquid chromatography
HTRF	Homogeneous time resolved fluorescence
HyPla	Hydroxylated phenyllactic acid
iBA	Isobutyric acid
IP_1	myo-Inositol 1 phosphate
IP_3	D-myo-Inositol 1,4,5-triphosphate
iVA	Isovaleric acid
J2	Juvenile stage 2
KO	Knock-out
LB	Lysogeny broth
Leu	Leucine
M3 receptor	Muscarinic acetylcholine receptor type 3
MBT	Modified two sample binomial test
Me	Methyl
Me_2	Dimethyl
MLP	MbtH-like protein
MOPS	3-(*N*-morpholino) propanesulfonic acid
MS	Mass spectrometry
MS^2	Tandem mass spectrometry or MS/MS
m/z	Mass-to-charge
NE	NaOH extract
NGM	Nematode growth medium
NMR	Nuclear magnetic resonance
NP	Natural product
NRPS	Nonribosomal peptide synthetase
NSE	New soil extract
OA	Octopamine

Abbreviations

PA	Propionic acid
PEI	Polyethylenimine
PDB	Protein data bank
pEC_{50}/pIC_{50}	Negative logarithm of the half maximal effective/inhibitory concentration
PGPB	Plant-growth promoting bacteria
PIP_2	Phosphatidylinositol bisphosphate
pK_i	Negative logarithm of the inhibitor constant
PKS	Polyketide synthase
Pla	Phenyllactic acid
PNP	Peptidic natural product
P. pacificus	*Pristionchus pacificus*
Prop	Propionyl
QS	Quorum-sensing
RIC-8A	Resistance to inhibitors of cholinesterase 8A
RT	Retention time
SEM	Standard error of the mean
SESOM	Soil-extracted solubilized organic matter
SESOM+	SESOM with chitin added to the medium
SM	Sekundärmetabolite
T domain	Thiolation domain
TE domain	Thioesterase domain
Thr	Threonine
VA	Valeric acid
WE	Water extract
WT	Wildtype
YM	YM-254890

Zusammenfassung

Sekundärmetabolite (SM) oder auch Naturstoffe sind für ihr breites Spektrum an Bioaktivitäten bekannt und daher eine wichtige Quelle für neue Arzneimittelkandidaten. Neben ihrer Relevanz für die Therapie von Erkrankungen sind SM und ihre Produzenten ebenso von Bedeutung für ein gesundes Pflanzenwachstum und fungieren in der Landwirtschaft als natürlich vorhandene oder auch ausgebrachte Pflanzenschutzmittel.

Das freilebende Bodenbakterium *Chromobacterium vaccinii* MWU205 ist dafür bekannt, dass es verschiedene SM produziert, darunter das zyklische Depsipeptid FR900359 (FR). FR ist ein hoch aktiver und selektiver $G\alpha_q$-Protein-Inhibitor, der erstmalig aus den Blättern der Pflanze *Ardisia crenata* gewonnen wurde. Er wird in der pharmakologischen Forschung zur Untersuchung der intrazellulären Signalübertragung von G-Protein-gekoppelten Rezeptoren verwendet. Im Rahmen dieser Studie wurde die Analyse der FR/G_q Interaktion durch Kernspinresonanzspektroskopie innerhalb der Forschergruppe FOR2372 unterstützt, in dem vollständig $^{13}C/^{15}N$-markiertes FR durch Isotopenfütterungs-Experimente hergestellt wurde. Es zeigte sich, dass die Fütterung mit Propionsäure die FR-Produktion von *C. vaccinii* MWU205 steigert und die Isolierung von vollständig $^{13}C/^{15}N$-markiertem FR im großen Maßstab ermöglicht.

FR ist auch von ökologischer Bedeutung, da es G_q-Proteine von Säugetieren und Insekten hemmt, was für diese schwerwiegende physiologischen Folgen hat. Aufgrund ihrer hochgradig konservierten Struktur ist die G_q-Proteinfamilie ein hervorragendes ökologisches Zielmolekül für FR-produzierende Organismen und FR ist somit geeignet um sich gegen ein breites Spektrum von Schadorganismen zu verteidigen.

Ein wichtiges Ziel dieser Studie war es, das Metabolom von *C. vaccinii* MWU205 nach bioaktiven SM zu durchsuchen, mit besonderem Augenmerk auf neue FR-Derivate. Um ökologische Aspekte zu beleuchten, fokussierte sich diese Arbeit des Weiteren auf die FR-Produktion unter bodenähnlichen Bedingungen, und nachfolgend auf die Aktivität von FR gegenüber Bodenorganismen, z. B. bodenassoziierte Nematoden.

Um die Plastizität des Metaboloms von *C. vaccinii* MWU205 zu charakterisieren, wurden dessen Extrakte und die Depsipeptid-haltige Fraktion der Blätter von *A. crenata* mittels Massenspektrometrie untersucht und in einem merkmalsbasierten molekularen Netzwerk verglichen. Die molekulare Familie von FR wurde im Netzwerk identifiziert und im Detail untersucht. Dieser Analyse folgend wurde ein neues FR-Derivat, FR-6, isoliert

und seine exakte Struktur aufgeklärt. In pharmakologischen Assays unterdrückte FR-6 die G_q-Signalübertragung.

Experimente, in denen *C. vaccinii* MWU205in Bodenextrakten kultiviert wurde zeigten, dass FR unter bodenähnlichen Bedingungen hergestellt und vom Produzenten an die Umgebung abgegeben wird. Dies ist auf den Boden übertragbar, so dass FR über seine Bioaktivität das umgebende Habitat beeinflusst.

In silico-, *in vitro*- und *in vivo*-Untersuchungen lieferten Erkenntnisse zu ökologisch relevanten Wirkungen von FR auf bodenassoziierte Nematoden. $G\alpha_q$-Proteinsequenzen bodenassoziierter Nematoden wurden *in silico* auf ihre FR-Bindestelle hin untersucht, und eine Bindung der untersuchen Zielstrukturen wurde vorausgesagt. In der Tat konnte anschließend die Hemmung von heterolog exprimierten $G\alpha_q$-Proteinen der Nematoden *Caenorhabditis elegans* und *Heterodera schachtii* durch FR bewiesen werden. *In vivo*-Experimente zeigten, dass FR die Fortbewegung beider Nematoden reduziert, die Eiablage von *C. elegans* hemmt und das Schlüpfen von *H. schachtii* aus seinen Zysten verringert. Diese Ergebnisse deuten darauf hin, dass FR die Ausbreitung und Vermehrung von Nematoden im Boden reduzieren könnte.

Diese Doktorarbeit stützt die Hypothese, dass *C. vaccinii* MWU205und das von ihm produzierte FR zu einem ökologischen Gleichgewicht im Boden beitragen könnten, und hierrüber das erfolgreiche Wachstum von Pflanzen fördern. Insgesamt weist auch diese Studie darauf hin, dass die mikrobielle Vielfalt im Erdreich von weitreichender Bedeutung ist.

Abstract

Natural products (NPs) also named secondary metabolites are known for their broad range of bioactivities, which makes them an important source for novel drug candidates. Besides their application for human health, NPs and their producers are important to sustain plant health by functioning as natural existing or also applied crop protectants in agriculture.

The free-living soil bacterium *Chromobacterium vaccinii* MWU205 is known to produce various NPs including violacein and the depsipeptides valhidepsins A-F and FR900359 (FR). FR is a potent and selective $G\alpha_q$ protein inhibitor that is used extensively to investigate the intracellular signaling of G protein-coupled receptors. In the scope of this study, isotope feeding experiments were conducted to generate completely $^{13}C/^{15}N$-labeled FR for detailed investigations of the FR/G_q interaction with nuclear magnetic resonance spectroscopy within the research group FOR2372. Feeding of propionic acid was found to shift the depsipeptide production of *C. vaccinii* MWU205 from FR-2 (FR derivative with *N*-acetyl-β-hydroxyleucine instead of *N*-propionyl-β-hydroxyleucine as side chain) to FR. This way, the big scale isolation of completely $^{13}C/^{15}N$-labeled FR was enabled.

FR is also of ecological importance, as it binds to G_q proteins of mammals and insects, leading to severe physiological consequences. Due to its highly conserved structure, the G_q protein family is an excellent ecological target for FR producing organisms and suitable as a defense towards a wide range of harmful organisms.

The overall aim of this study was to search for bioactive secondary metabolites, with special emphasize on new FR derivatives, in the genome and the metabolome of *C. vaccinii* MWU205. To shed light on the ecological relevance of FR, its production was investigated under soil-like conditions. Subsequently, its bioactivity on soil organisms, e.g., nematodes, was assayed.

A first bioinformatic analysis of the genome of *C. vaccinii* MWU205 revealed ten biosynthetic gene cluster (BGC), including the BGC of FR, violacein, 2,4-diacetylphloroglucinol, and the siderophores viobactin and chromobactin. To characterize the plasticity of the metabolome of *C. vaccinii* MWU205 it was cultivated in different laboratory media and the resulting extracts combined with the depsipeptide-containing fraction of *A. crenata* leaves were investigated and compared using feature-

based molecular networking. The molecular families of violacein, valhidepsins, and FR were identified in the network and further investigated for new derivatives. As a result, thirty to date unknown FR derivatives, one third of which being unique to *C. vaccinii* MWU205, and eight unknown valhidepsins were identified. Guided by mass spectrometry, a novel FR derivative, FR-6 (**Fig. 1**), was isolated, and its exact structure unambiguously established. In pharmacological assays FR-6 suppressed G_q signaling with micromolar potency, which was confirmed in radioligand binding assays. In conclusion, molecular networking is a powerful tool that guided the way to a novel G_q inhibiting FR derivative, which underlines the potency of FR as G_q inhibitor[1].

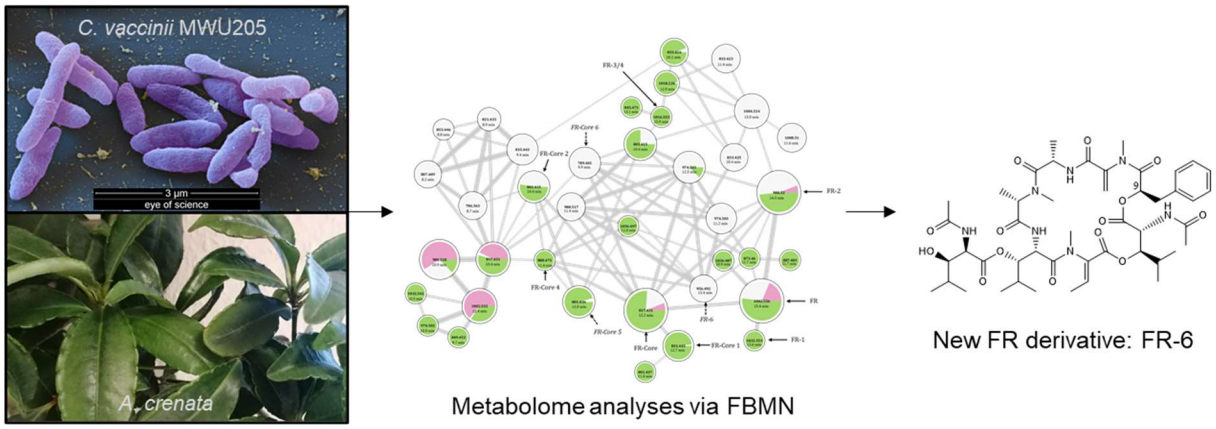

Fig. 1: Analysis of the molecular family of FR900359 (FR) detected in the metabolome of *Chromobacterium vaccinii* MWU205 and the depsipeptide-containing fraction of *Ardisia crenata* leaves lead to the isolation of the new FR derivative FR-6[1]. FBMN=Feature-based molecular network. Scanning electron microscope recording of *C. vaccinii* MWU205 was performed by "eye of science".

After the successful isolation of FR-5 by feeding butyric acid to *C. vaccinii* MWU205, further precursor experiments with branched or longer acids revealed a small incorporation determined by mass spectrometry, however, the incorporation was not sufficient for the isolation of the respective compounds. Finally, feeding of *meta*- and *ortho*-fluorinated phenylalanine led to the increased production of a novel FR derivative, while the *para*-fluorinated phenylalanine was not accepted. The isolation of the *meta*-fluorinated FR was started and is still in progress. These findings underline the strength of feeding experiments as tools to improve FR production and investigate the specificity of biosynthetic enzymes.

Following the investigation of the metabolome in laboratory media, experiments with soil-extracted solubilized organic matter were conducted to shed light on the ecological significance of FR production. These experiments revealed that FR is produced under soil-like conditions and a subsequent examination of its distribution confirmed that

FR is excreted by *C. vaccinii* MWU205 (**Fig. 2**). Thus, FR is most likely present in *C. vaccinii*-inhabited soil and supposedly impacts the surrounding habitat[2].

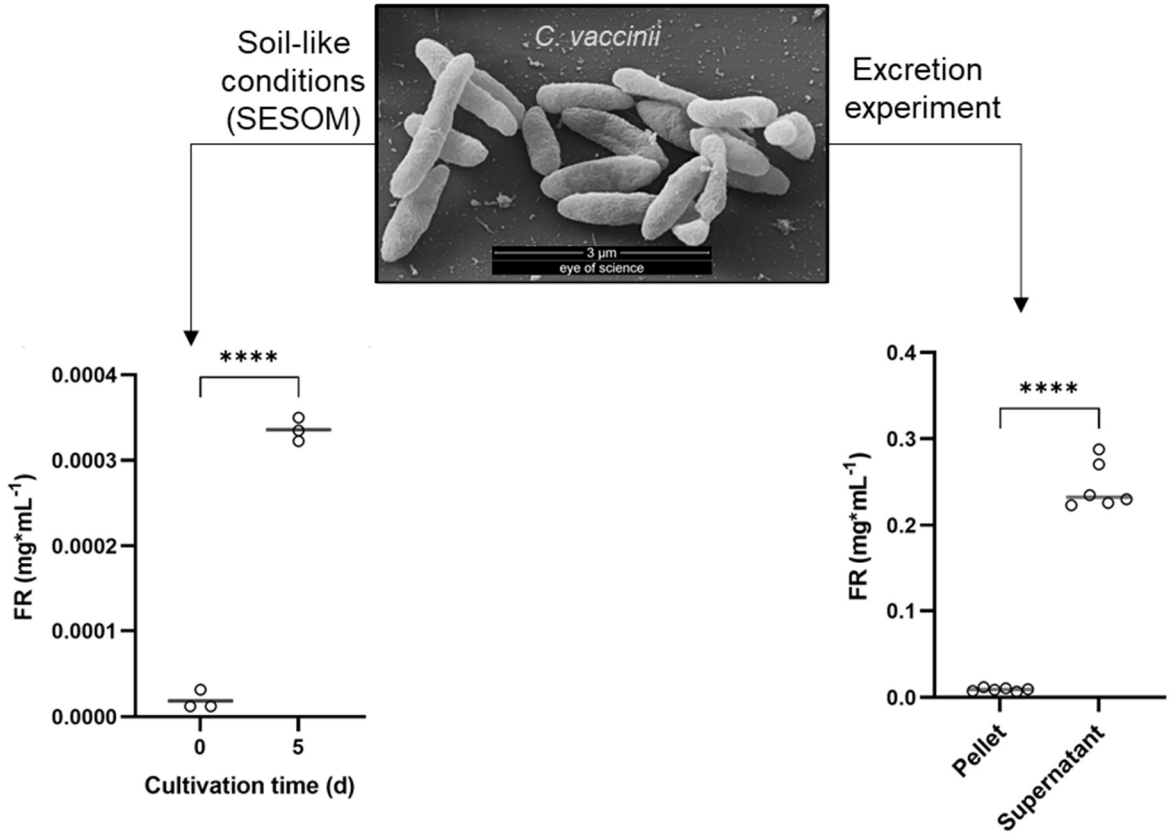

Fig. 2: FR900359 (FR) production under soil-like conditions by *Chromobacterium vaccinii* MWU205 and excretion of FR into the surrounding LB medium by *C. vaccinii* MWU205[2]. Scanning electron microscope recording of *C. vaccinii* MWU205 was performed by "eye of science".

Most importantly, *in silico*, *in vitro*, and *in vivo* investigations of this study revealed insights into the ecological relevant effects of FR on soil-associated nematodes (**Fig. 3**). A bioinformatic search and analysis of nematode $G\alpha_q$ protein sequences predicted the binding of FR to the investigated target proteins. In fact, subsequent *in vitro* experiments confirmed that FR inhibited IP_1 accumulation of heterologously expressed $G\alpha_q$ proteins of the nematodes *Caenorhabditis elegans* and *Heterodera schachtii* in the micromolar range. *In vivo* experiments with *C. elegans* and the plant parasitic cyst nematode *H. schachtii* demonstrated that FR reduces locomotion of *C. elegans* and *H. schachtii*. Furthermore, FR inhibited egg-laying of *C. elegans* and hatching of juvenile stage 2 of *H. schachtii* from its cysts. In conclusion, the results suggest that FR might reduce nematode dispersion and proliferation[2].

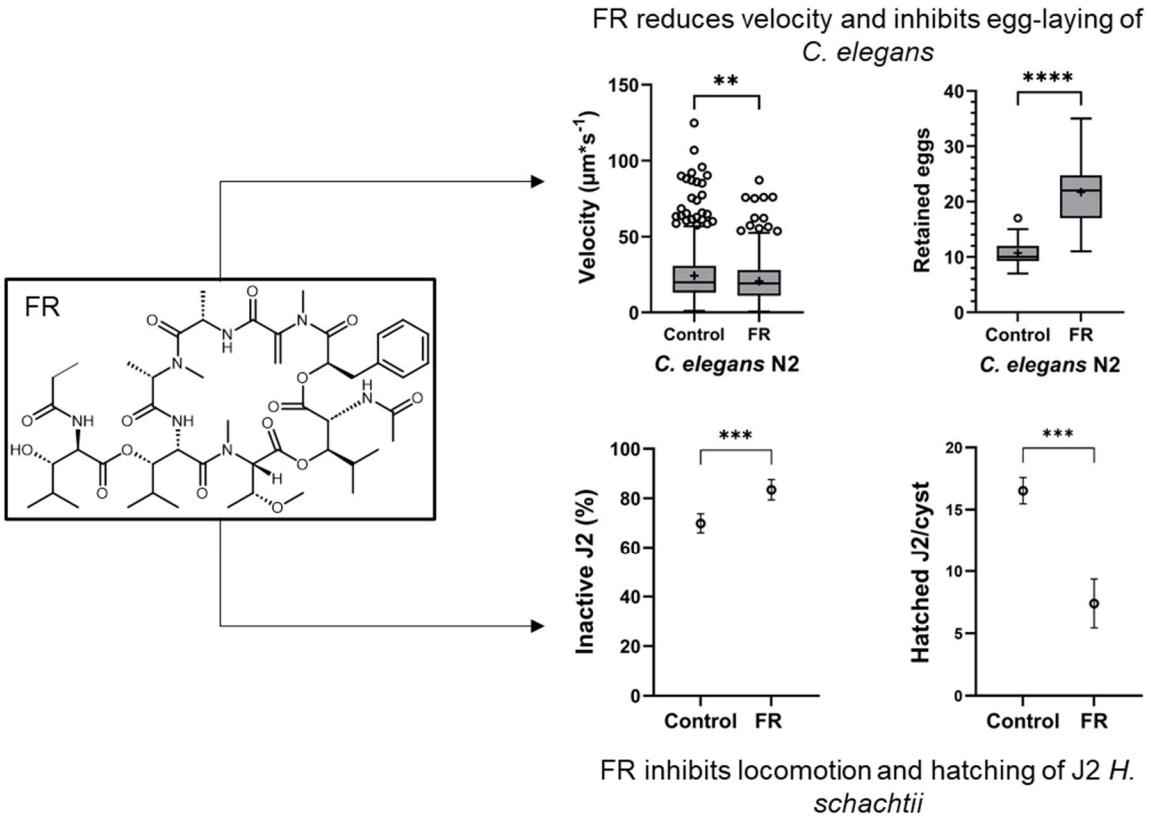

Fig. 3: Effects of FR900359 (FR) on the free-living soil nematode *Caenorhabditis elegans* and the plant parasitic cyst nematode *Heterodera schachtii*[2]. Scanning electron microscope recording of *C. vaccinii* MWU205 was performed by "eye of science".

These experiments support the hypothesis that *C. vaccinii* MWU205 and the excreted FR in soil might contribute to an ecological equilibrium, maintaining and establishing the successful growth of plants[2]. Overall, this study also indicates that microbial diversity in soil is of far-reaching importance.

1. Introduction

1.1. Soil Microbiome

This thesis deals with the detailed chemical and ecological investigation of *Chromobacterium vaccinii* MWU205 and its natural product (NP) FR900359 (FR), to reveal their role in the context of the soil microbiome, especially regarding the protection of plants from nematodes.

The soil is habitat for numerous organisms, e.g. bacteria, fungi, arthropods, and nematodes[3–5]. Microorganisms form the soil microbiome, which is described as "black box in need of unboxing"[6] as it is defined by complex and dynamic interactions of multiple species[7]. The soil microbiome is responsible for water purification, nutrient uptake and cycling, plant growth promotion, disease and pathogen suppression, carbon sequestration, and many more[6,8]. Therefore, global challenges like climate change[9], food demand[10,11], and antibiotic-resistant bacteria[8] are directly and indirectly connected to the soil microbiome, revealing the importance of research in this field.

As soil is not one single environment but rather multiple environments, numerous microbial communities exist next to each other, which makes research challenging[3]. A common tool to investigate the soil microbiome is the metagenome, which examines the taxonomic composition of the soil microbiome, using extraction of all deoxyribonucleic acids (DNAs) of one soil sample and subsequent high-throughput sequencing[12]. As the metagenome approach lacks the connection of taxa found in soil to their function, further approaches[13], like metatranscriptomics, metaproteomics, metabolomics, and finally the metaphenome are used to close this gap[14–16]. Apart from "omics" methods, the investigation and cultivation of a single microbial member and its interaction with other members of the microbiome is necessary to reveal the ecological role in its soil environment[3,17].

The plant microbiome unites the microbes living above-ground (phyllosphere), underground (rhizosphere), and in the plant (endosphere)[10]. As plant health and growth is influenced by its microbiome, scientists aim to engineer plant microbiota to support plant growth and inhibit plant pathogens[10,11,18]. Methods used to engineer include soil conditioning through organic soil amendments, the use of root exudates, the design of artificial microbial consortia, engineering the seed microbiome, 'microbe-friendly' plants, microbiome breeding, and microbiome transplantation[7,19,20].

The beneficial effects of the microbiota on the plant health can be observed in nature, e.g., disease-suppressive soils[21] and plant growth-promoting bacteria (PGPB)[22,23]. PGPB are free-living bacteria and rhizobacteria, which promote plant growth by direct and indirect mechanisms. Biofertilization by nitrogen fixation, phosphate solubilization, biostimulation by metabolites like auxins, cytokines, and 1-aminocyclopropane-1-carboxylate deaminases, and biocontrol by protecting the plant against pathogens for example with chitinases and antibiotics, are the three main effects of PGPB[24,25]. The use of single or multiple beneficial microbial species as bioinoculants is a sustainable method to fight pathogens in agriculture[18], making them an important replacement option for chemical pesticides[22,25,26]. The most prominent example for a biological control agent used in agriculture is *Bacillus thuringiensis*, a gram-positive bacterium that produces an endotoxin with insecticidal effect[27,28]. However, unlike *B. thurengiensis* most bioinoculants aim to invade the plant-associated microbiome and colonize the roots, e.g., *Rhizobium*, and *Azospirillum*[22]. Bioinoculants are not only used as biocontrol agents, but also as sustainable and eco-friendly biofertilizers to increase crop production[26]. One successful example is the inoculation of soybean (*Glycine max*) with *Bradyrhizobium*, which increased yield through nitrogen fixation[29]. The development of new bioinoculants to invade the plants soil microbiota is difficult due to the complexity of the invasion, unknown interactions between the microorganisms, and undiscovered activities of microorganisms[18,22]. Therefore, investigations to reveal the role of certain soil members and their interaction with other organisms are crucial for solving the complex puzzle that is the soil microbiome.

Opposing the beneficial effects of microbiome members, plant pathogens, i.e., fungi, bacteria, viruses, protozoa, and nematodes, present a huge threat for plant health[30]. Relevant pathogens for this study are nematodes, a widespread phylum with huge diversity[31–34] that is ubiquitously distributed in soil[35,36]. The functional role of nematodes in soil has been examined intensively due to their impact on the soil food web and soil health[34,37–40]. Nematodes are divided according to their food source, i.e., bacterivore, fungivore, omnivore, herbivore, and predator[36,41]. Herbivorous nematodes, i.e., plant parasitic nematodes, are plant pathogens causing 12.3 % of crop losses, equal to 157 billion US Dollar per year[42]. Over 4100 species are known, e.g., sedentary endoparasites that are divided into cyst nematodes (*Heterodera* spp.) and root-knot nematodes (*Meloidogyne* spp.), stem and bulb nematodes (*Ditylenchus* spp.), foliar nematodes

(*Aphelenchoides* spp.), seed gall nematodes (*Anguina* spp.), migratory endoparasites (*Pratylenchus* spp., *Radopholus* spp.), ectoparasites (*Xiphinema* spp.), and semi-endoparasites (*Rotylenchulus reniformi*)[43,44]. The other four trophic groups are beneficial nematodes[45], e.g., predators like entomopathogenic nematodes[46] are lethal for insect pests and used as biocontrol agents in agriculture[47,48].

Chemical nematicides, divided into fumigants and non-fumigants, have been developed since 1881 and are often the simplest tool to control nematodes due to their efficient protection[49]. However, their effects on non-target organisms present risks for the environment that are accompanied by the development of resistances and exposure of the consumer with these xenobiotic substances[50,51]. Other methods are agronomic methods, e.g., biofumigants, crop rotation, and soil amendments, physical methods, plant extracts, PGPB, and biopesticides[51–53]. The trend for biocontrol agents points towards sustainable nematicides, which are safe for humans and the environment[54,55]. To sustain plant health, it is crucial to understand the equilibrium of beneficial and pathogenic effects present in soil. This can be achieved through investigations of interactions of soil organisms and their excreted metabolites, like the herein investigated effect of metabolites from *C. vaccinii*.

1.2. Secondary metabolites produced by the genus *Chromobacterium*

Chromobacterium vaccinii MWU205, is a gram-negative bacterium isolated from wild cranberry bogs and a representative of the genus *Chromobacterium*. The genus *Chromobacterium* belongs to the family Neisseriaceae and consists of fourteen species, i.e., *C. violaceum*[56], *C. subtsugae*[57], *C. aquaticum*[58], *C. haemolyticum*[59], *C. piscinae*[60], *C. vaccinii*[61], *C. amazonense*[62], *C. alkanivorans*[63], *C. rhizoryzae*[64], *C. sphagni*[65], *C. phragmitis*[66], *C. paludis*[67], *C. alticapitis*, and *C. sinusclupearum*[68]. Most species were isolated from soil or water samples and human pathogenicity has only been reported for *C. haemolyticum* and *C. violaceum*[59]. *C. violaceum* is the best known, most investigated representative of the genus, and producer of the purple pigment violacein (**Figure 1**)[69–71]. Many, but not all species of the genus *Chromobacterium* are able to form the violet pigment, however, the production of violacein is not unique for the genus, as other genus like *Janthinobacterium* are known to produce it[72].

Violacein is a well-studied molecule, as its structure, biosynthesis, and bioactivities have been the focus of multiple studies[73–78]. The biosynthetic gene cluster consists of five genes, *vioA-E*, encoding the five enzymes VioA-E which are responsible for the violacein biosynthesis[74,79,80]. Its biosynthesis is regulated via quorum sensing (QS)[81], a mechanism of bacterial communities to cooperate and coordinate their adaptive response to the dynamic environment[72,82,83]. Due to the production of violacein as colorful indicator of QS, *C. violaceum* is an excellent tool to study substances interfering with this communication, so called QS-quencher[72]. Violacein harbors multiple bioactivities[75], i.e., cytotoxicity[84], antitumoral[85–90], antiviral[84,91,92], antibacterial activities against gram-positive bacteria[91,93–95], antifungal[77], antiprotozoal[96,97], and antiparasitary[98–100].

NPs, also known as secondary metabolites, like violacein harbor a broad range of bioactivities, which makes them an important source for new drug candidates[101]. Members of the genus *Chromobacterium*, e.g., *C. violaceum* ATCC 12472, are known to produce other secondary metabolites like the two siderophores viobactin and chromobactin, the structures of which are still elusive[102], and romidepsin (FK228, previously named FR901228) a bicyclic depsipeptide[103]. Romidepsin shows anti-plasmodial activity[104–106] and its reduced form functions as an ATP-competitive PI3K inhibitor and selective inhibitor of class I histone deacetylases[107,108].

Insecticidal activities have been observed for various of the above mentioned *Chromobacterium* spp., demonstrating the ecological importance of this genus as potential biopesticides. *C. subtsugae* PRAA4-1^T has shown activity against various insects, which is probably caused by a heat-stable toxin, and is used as an insecticide under the name Grandevo® sold by Marrone BioInnovations[57,109]. *C. piscinae* produces an insecticidal protein, GNIP1Aa[110], showing toxicity against western corn rootworm, *Diabrotica virgifera virgifera*. *C. sphagni*, *C. phragmitis*, and *C. vaccinii* cultures are toxic for several insects[65,111–113]. The *C.* sp. strain C61 has been isolated from the rhizosphere of eggplants[114,115] and is used as biocontrol against fungal plant pathogens[116–118]. An extracellular chitinase and a cyclic lipopeptide, chromobactomycin, are contributing to the antifungal effect[119–121]. Another strain called *C.* species Panama has been isolated from *Aedes aegypti*[122]and reported to have activity against vector mosquito larvae[123,124], which is mediated by romidepsin[104–106], and corn rootworm strains (*Diabrotica* spp.)[125].

The species *C. vaccinii* was first discovered ten years ago[61], and consists, together with the novel isolates from Brazil[126], of ten strains, which have been isolated on different

continents from various environments, i.e., bog soil of cranberries[61], biofilms in quaking bogs[127], and aquatic environments[126]. Nine of these ten strains have been sequenced, i.e., strain 21-1 discovered in a bog in Maryland (USA, Accession number Genbank: GCA_001855275.1), strains MWU328 and MWU205 located in cranberry bog soil in Massachusetts (USA, Accession numbers Genbank: GCA_000971355.1, GCF_000971335.1)[61], strains GIMC1602:ChrSima_v and GIMC1601:ChrSima_w isolated from biofilms in the quaking bog near Moscow (Russia, Accession numbers Genbank: GCA_020882175.1, GCA_020882155.1)[127], strain XC0014 found in soil in the Zhejiang Province (China, Accession number GenBank: GCA_002952135.1), the reclassified strain NCTC9370 (Accession number GenBank: GCA_900446815.1), and CR1 and CR5 discovered in aquatic environment in Goiás (Brazil, Accession numbers GenBank: GCA_021083355.1, GCA_021083405.1)[126].

C. vaccinii MWU205 has been reported to produce violacein[61] and nonribosomal peptides, i.e., the lipopeptides valhidepsin A-F[128] and cyclic depsipeptides known as chromodepsins, e.g., FR900359 (FR)[129,130]. Valhidepsin A and B might act as biosurfactant as they reduce the surface tension of water[128], while FR is a $G\alpha_q$ inhibitor[131] with various bioactivities (**Figure 1**).

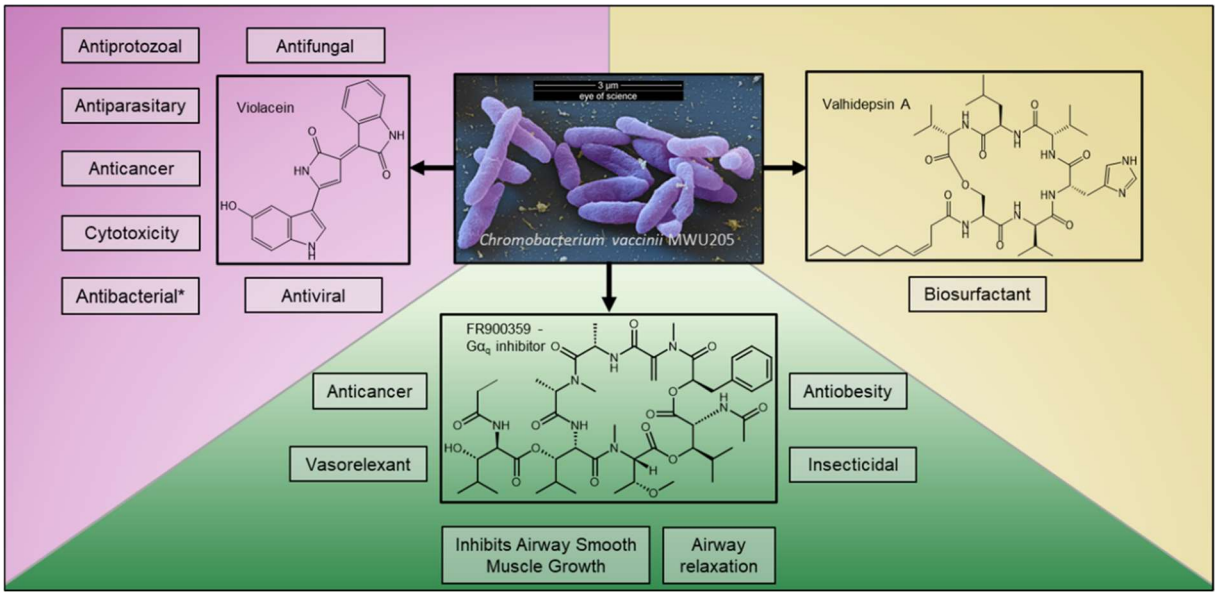

Figure 1: Natural products produced by *Chromobacterium vaccinii* MWU205 and their reported bioactivities. *Antibacterial against gram-positive bacteria.

1.3. The cyclic depsipeptide FR900359

FR (**Figure 1** and **Figure 2**) is a cyclic nonribosomal depsipeptide and has first been described in 1988 as a NP[132]. The following eight building blocks form FR, i.e., *N*-acetyl-L-

hydroxyleucine (*N*-Ac-β-HyLeu/L'), *N*-propionyl-L-hydroxyleucine (*N*-Prop-β-HyLeu/L'''), L-hydroxyleucine (β-HyLeu/L''), *N*,*O*-dimethyl-L-threonine (*N*,*O*-Me_2-Thr/T'), L-alanine (Ala/A), *N*-methyl-L-alanine (*N*-Me-Ala/A'), *N*-methyl-dehydroalanine (*N*-Me-Dha/A''), and D-phenyllactic acid (Pla/F'). *N*-Prop-β-HyLeu constitutes the side chain connected to the hydroxy group of the β-HyLeu, while all other building blocks form the cyclic moiety including two ester bonds between Pla and *N*-Ac-β-HyLeu and *N*-Ac-β-HyLeu and *N*,*O*-Me_2-Thr[132].

Nonribosomal peptides like FR are synthesized by nonribosomal peptide synthetases (NRPS), which are divided into five types. The herein described NRPS is a type I NRPS, which consists of several connected enzymes with modular organization forming megasynthetases[133]. One module specifically recognizes, recruits, and incorporates one precursor leading to the elongation of the peptide chain. Each module may harbor different domains changing the precursor, e.g., methylation, but the smallest and essential NRPS incorporates the building block using an adenylation (A) domain, a thiolation (T) domain, and a condensation (C) domain. The A domain recruits and activates the targeted precursor molecule, e.g., (modified) proteinogenic amino acids, non-proteinogenic amino acids, fatty acids and carboxylic acids[134–140]. If the latter is incorporated, esters are formed instead of a peptide bond and the resulting molecule is called depsipeptide[141]. After activation, the precursor is bound to the T domain via a thioester and is condensed into a dipeptide via the C domain, which unites the precursors bound to the T domains of the first and the second module and transfers the resulting peptide onto the T domain of the second module, where it is further elongated. In the last module, a thioesterase (TE) domain cleaves off the molecule bound to the enzyme[134–140]. As proven for the FR biosynthesis, thioesterases may transfer their product onto another molecule and, as shown for the TE domain of the tyrocidine synthetase, they may cyclize linear peptide chains[142].

The FR biosynthesis gene cluster consists of eight genes (*frsA*-*frsG*) encoding two NRPS, the mono-modular NRPS FrsA and the seven-modular NRPS FrsD-FrsG. The small NRPS is responsible for the formation of the side chain, while the bigger NRPS forms the cyclic moiety onto which the side chain is transferred via the TE domain of FrsA (**Figure 2**)[130,143]. Additionally, *frsB* encodes for an MbtH-like protein (MLP), which is a group of proteins known to beneficially effect solubility and stability of A domains[144–147]. The precursor phenylpyruvic acid is transformed during the FR biosynthesis by FrsC and FrsE

module 3 into D-Pla[148,149]. In recent studies, FrsH was revealed to hydroxylate the L-leucines[150].

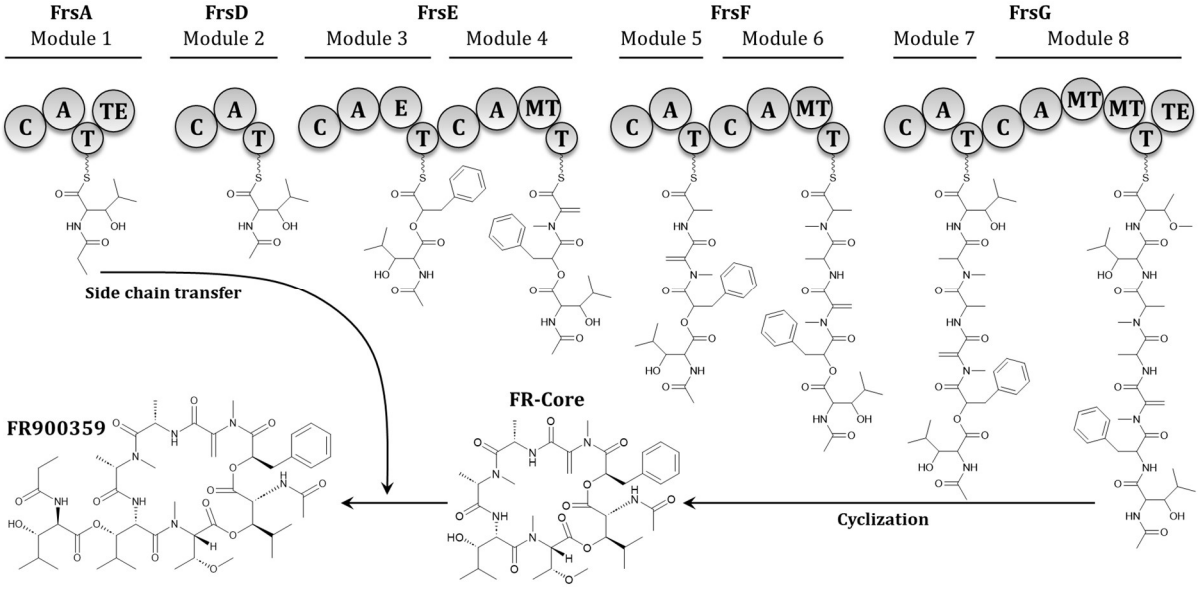

Figure 2: FR biosynthesis. Figure adapted from Crüsemann et al, 2018[143].

FR belongs to the group called chromodepsins, which include all derivatives of FR and of YM-254890 (YM) (natural occurring chromodepsins are shown in (**Figure 3**)[151]). YM was discovered in 2003 and differs at two positions from FR, (i) *N*-Ac-β-HyLeu for the side chain instead of *N*-Prop-β-HyLeu, and (ii) *N*-Ac-Thr instead of *N*-Ac-β-HyLeu[152,153]. The biosynthetic gene cluster was revealed to have the same structure as the *frs* gene cluster (Genbank: LC380916.1).

Chromodepsins are of interest for drug development, as they are specific and potent inhibitors of $G\alpha_q$. G proteins consist of three subunits, α, β, and γ, and are bound in their inactive state to the inside of the cell membrane to a G protein-coupled receptor (GPCR). The Gα subunit harbors a GTPase activity and binds a guanosine diphosphate (GDP) in its dormant form. Once a ligand binds to the GPCR, the G protein translates the external signal into an internal signal by activating further effectors or transmitters. In detail, the GDP bound by Gα is exchanged for a guanosine triphosphate (GTP), which leads to the dissociation of the G protein into Gβγ and Gα, affecting further effectors separately[154,155].

Gα subunits are divided into four major families in humans, $G\alpha_s$, $G\alpha_i$, $G\alpha_q$, and $G\alpha_{12/13}$. $G\alpha_s$ activates, while $G\alpha_i$ inhibits adenylate cyclase and $G\alpha_{12/13}$ stimulates Rho GTPases[156]. $G\alpha_q$ triggers the β-isoform of the phospholipase C (β-PLC) to cleave phosphatidylinositol bisphosphate (PIP_2) into inositol triphosphate (IP_3) and diacylglycerol (DAG) leading to calcium mobilization[157].

Chromodepsins interact with $G\alpha_q$ proteins and thereby inhibit $G\alpha_q$-mediated nucleotide exchange with high selectivity at micromolar potency[131]. YM and FR differ in their residence time, but not in their binding affinity or inhibitory potency towards $G\alpha_q$[158,159]. Hence, they are both extremely useful tools to study G_q-mediated signaling of GPCRs[154,160].

As GPCRs are responsible for many major physiological processes due to their multifaceted functionality[161], approx. 35 % of our pharmaceutical drugs target them[162]. Up until now, approx. 800 GPCRs but only four Gα families are known[163], a phenomenon that may be used to treat multifactorial diseases by inhibiting G proteins, where the selective targeting of one GPCR may prove not effective[154]. Therefore, chromodepsins, like FR and YM, may be highly relevant for a possible medical use in the treatment of airway disorders[164,165], reduction of adipositas[166], maintenance of colony formation of murine embryonic stem cells[167], and suppression of uveal melanoma[168–170].

Chromodepsins were isolated from various ecosystems, i.e., FR from the plant *Ardisia crenata* and the free-living soil bacterium *C. vaccinii* MWU205, YM from the culture broth of *Chromobacterium* sp. QS3666 isolated from soil samples collected in Okutama, Tokyo, Japan, and sameuramide (same structure as FR-3) isolated in Japan from a didemnid ascidian (**Figure 3**). This shows that chromodepsins are widely spread in nature.

First investigations regarding the ecological role of FR for the plant *A. crenata* have revealed that the endosymbiotic bacterium *Candidatus* Burkholderia crenata lives in the leaf nodules and produces FR. Previous experiments towards insects and mammals confirm FR to probably serve in nature as a defense for the bacterial producer and, as in the case of endosymbiotic bacteria, its host plants. In experiments using Sf9 insect cell membranes and G_q proteins of the *Bombyx mori* and *Bemisia tabaci* FR displays strong affinity towards the membranes and proteins. The effect of FR on nymphs of the beetle *Riptortus pedestris* has been evaluated by measuring their survival rate after exposure to different FR concentrations over nine days. For the two highest FR concentrations, 40 µM and 200 µM, the survival rate begun to decrease drastically after four days, with all insects being dead after seven days[143]. FR activity was also tested in mice[164] and rats[171] to examine its effects on mammals. While the intratracheal application of FR in mice lead to airway relaxation, which may be of medical importance[164], the systemic oral application

in mice and rats resulted in decreased blood pressure and transient bradycardia, which surely is of ecological importance if FR is consumed by mammals in nature [164,171,172].

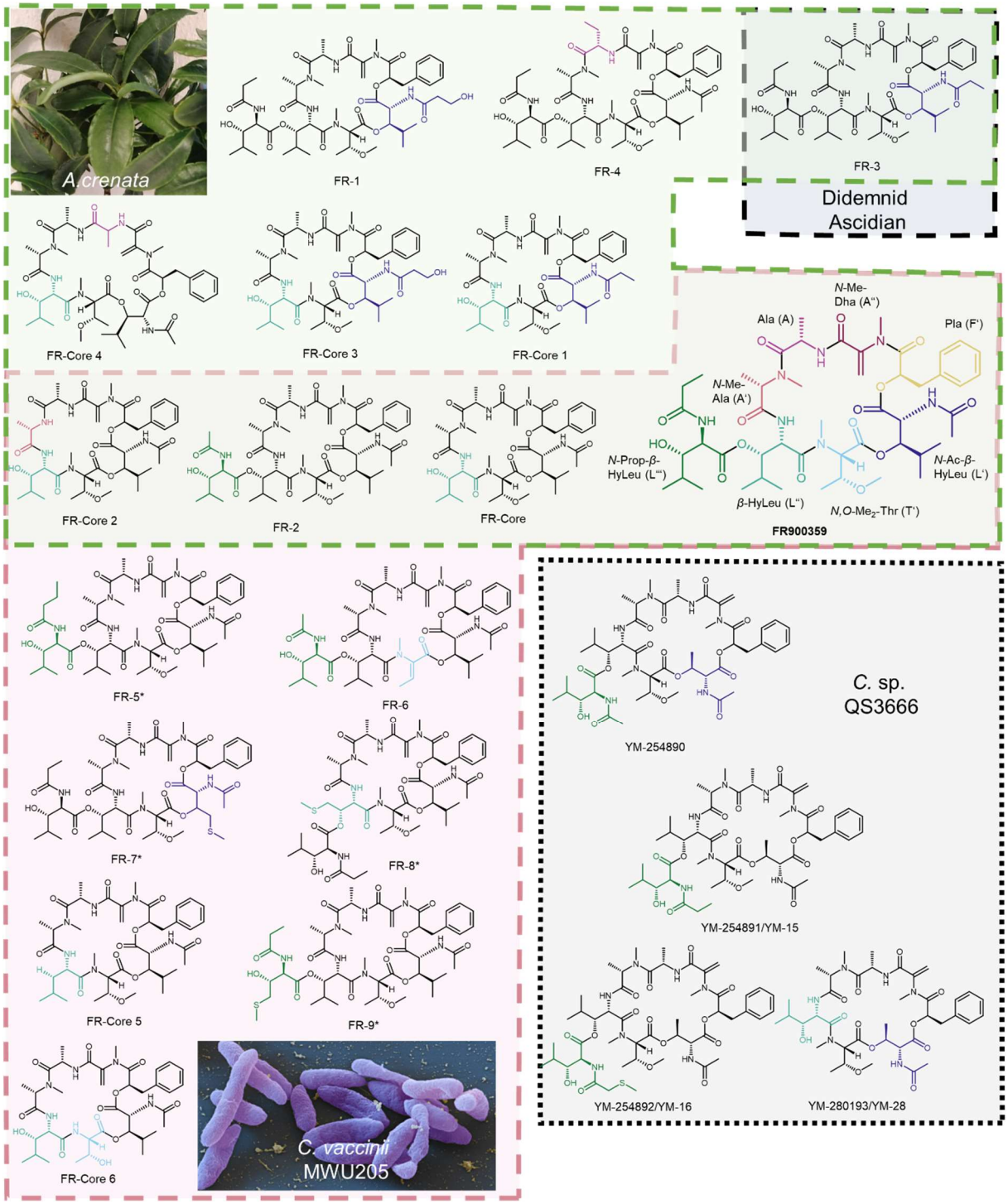

Figure 3: All naturally occurring FR (dashed line)[1,129,143,173] and YM derivatives (round dots)[152,174] arranged in groups according to their origin (green: *Ardisia crenata*, red: *Chromobacterium vaccinii* MWU205, black and dashed line: Didemnid ascidian, black and round dots: *C.* sp. QS3666). All building blocks of FR are labeled and colored. For all other derivatives the building block that is different compared to FR is colored. Compounds marked with an asterisk (*) are derivatives isolated after feeding experiments. Scanning electron microscope recording of *C. vaccinii* MWU205 was performed by "eye of science".

2. Aim of the study

The investigation of the ecological role of the soil microbiome is still in its infancy, however, most important to secure or re-establish a healthy nature and agriculture. The here investigated *Chromobacterium vaccinii* MWU205 has originally been isolated from the soil surrounding *Vaccinium macrocarpon* Ait. plants. Former studies have shown that this bacterial strain is producing the G_q signal transduction inhibitor FR900359 (FR), a member of the non-ribosomal peptide family chromodepsins, under laboratory conditions.

The overall aim of this study was to search for bioactive secondary metabolites, with special emphasize on new FR derivatives, in the genome and the metabolome of *C. vaccinii* MWU205. To shed light on the ecological relevance of FR, its production was investigated under soil-like conditions. Subsequently, its bioactivity on soil organisms, e.g., nematodes was assayed.

Thus, this investigation included the following partial projects:

(i) Bioinformatic analysis of the genome of *C. vaccinii* MWU205 was intended to reveal the BGCs of all relevant secondary metabolites. Afterwards, feature-based molecular networking was to be applied to characterize the metabolome of *C. vaccinii* MWU205 with special emphasis on novel FR derivatives, their isolation, characterization and assessment of bioactivity, i.e., G_q inhibition.

(ii) Within the framework of the research group FOR2372, I aimed to obtain $^{13}C/^{15}N$-labeled FR using labeled precursors for detailed NMR studies of the FR/G_q interaction. Following the metabolome analysis, additional feeding experiments were conducted to investigate the substrate flexibility of the biosynthetic enzymes.

(iii) Soil extracts were utilized to examine whether FR is produced under soil-like conditions and combined with experiments contemplating the excretion of FR to answer whether FR is affecting its surrounding habitat.

(iv) The ecological bioactivity of FR on soil-associated nematodes was aimed to be assessed using *in silico*, *in vitro*, and *in vivo* methods. *In silico* alignments combined with visualization of the changes in the FR binding site were intended to evaluate whether FR binds nematode $G\alpha_q$ proteins, and which

organisms are representatively chosen for further *in vitro* and *in vivo* assays. *In vitro* assays with the $G\alpha_q$ of these selected nematodes were planned to study whether FR acts as nematode $G\alpha_q$ inhibitor. Furthermore, *in vivo* assays with the selected nematodes were designated to unveil whether FR affects selected physiological parameters of nematodes, involving their movement and propagation.

3. Results

3.1. Analysis of the metabolome of *C. vaccinii* MWU205

Prior to the metabolome analysis a bioinformatic investigation of the genome sequence (size: 5,091,536 kilobase pair) of *Chromobacterium vaccinii* MWU205 was conducted via antiSMASH[175], to reveal potential biosynthetic gene clusters (BGCs) of already described and unknown NPs. AntiSMASH translates all protein-encoding genes in a DNA sample and searches these genes with profile hidden markov models to detect BGCs of secondary metabolites and compares them subsequently to known BGCs[176].

Afterwards, the metabolome of *C. vaccinii* MWU205was explored using high performance liquid chromatography (HPLC) combined with high-resolution tandem mass spectrometry (LC/MS^2) to investigate extracts of *C. vaccinii* MWU205grown in different media. The generated MS^2 data were investigated with MZmine 2[177–179] and visualized using the feature-based molecular networking (FBMN) workflow[180] offered by global natural product social molecular networking (GNPS)[181]. A molecular network (MN) is an untargeted analysis tool for MS^2 data, which consists of nodes and connecting edges between nodes. Each node represents one compound with a distinct mass-to-charge (*m/z*) value and a fragmentation pattern, while edges between two nodes indicate similar fragmentation patterns. Depending on the chosen parameters, nodes are detected and connected thereby forming clusters and visualizing the chemical space of extracts. This enables the identification of related compounds as molecular families and therefore guides the detailed MS^2 analysis towards novel compounds or derivatives[181–183]. In case of the FBMN, information of the HPLC retention time of a compound is included for the MN creation[180]. The resulting FBMN was examined in detail for secondary metabolites and their derivatives produced by *C. vaccinii* MWU205, using manual analysis and other tools, i.e., the library search, the DEREPLICATOR tool, and MS2LDA offered by GNPS, or the CANOPUS tool from the SIRIUS platform[184–189].

3.1.1. Prediction of NP BGCs in the genome of *C. vaccinii* MWU205

To investigate the genome of *C. vaccinii* MWU205 for its potential to produce NPs antiSMASH was applied as described in **chapter 5.11**. In total, ten regions were predicted to encode NP biosynthetic pathways, with two regions showing 100 % and further two

regions around 90 % similarity to known NP BGCs (**Figure 4**). Region 1 was identified as BGC of violacein, a NP produced by various members of the genus *Chromobacterium* and known for many different bioactivities (**Figure 1**)[72,75]. Region 9 was identified as genes encoding the biosynthetic enzymes for *N*-acyl homoserine lactone (AHL) production. AHLs are known to regulate genes like the violacein BGC in *C. violaceum* in response to QS[81,190]. Region 7 was found to be the BGC of chromobactin, and region 3 contained a viobactin-related BGC (92 %). Both, viobactin and chromobactin are siderophores with unknown structure, even though their gene clusters and production has been detected for *C. violaceum*[102]. Region 10 was diagnosed to contain the BGC of FR, with 87 % similarity to *frs* from *Cand.* Burkholderia crenata. A closer look into region 10 revealed it to also contain the BGC of cyclic and linear lipopeptides known as valhidepsins, that might function as biosurfactant[129]. Another region with high similarity, i.e., 75 %, was region 6, which was related to the BGC of *Pseudomonas fluorescens* Q2-87 encoding the biosynthesis enzymes of 2,4-diacetylphloroglucinol[191]. Recently, the genus *Chromobacterium* was investigated for its ability to produce 2,4 phloroglucinol and the gene cluster has been identified in eleven strains including *C. vaccinii* MWU205. The study by Johnson et al, 2023 proved the BGC to be functioning, however, the isolation of 2,4-diacetylphloroglucinol was not achieved[126]. The remaining four regions, with predicted BGCs related to terpenes, polyketides, and β-lactones did not have a similarity higher than 50 % to known sequences.

Region	Type	From	To	Most similar known cluster	Similarity
1	Indole	253,547	276,543	Violacein (Alkaloid)	100 %
2	Terpene	561,068	582,795	Surfactin (NRP: Lipopeptide)	8 %
3	NRPS	1,062,077	1,108,786	Viobactin (NRP)	92 %
4	PKS-like, transAT-PKS	1,296,157	1,386,469	Kalimantacin A (NRP + Polyketide: Modular Type 1 + Polyketide: Trans-AT Type 1)	24 %
5	Betalactone	2,006,956	2,029,875	Corynecin I-III (other)	13 %
6	T3PKS	2,198,740	2,239,789	2,4-diacetylphloroglucinol (Polyketide)	75 %
7	NRP-metallophore, NRPS	2,339,076	2,387,612	Chromobactin (NRP)	100 %
8	NRPS, T1PKS, NRPS-like	2,962,778	3,036,404	Oxalomycin B (NRP + Polyketide)	6 %
9	Homoserine lactone cluster	3,195,345	3,215,998		
10	NRPS	4,261,802	4,371,656	FR900359 (NRP: Cyclic depsipeptide)	87 %

Figure 4: Bioinformatical search of the genome of *Chromobacterium vaccinii* MWU205 with antiSMASH version 7 for potential biosynthetic gene clusters of secondary metabolites. PKS = Polyketide synthase, T3 = Type 3, T1 = Type 1. NRP(S) = Nonribosomal peptide (synthetase).

3.1.2. Analysis of *C. vaccinii* MWU205 extracts using FBMN

To explore the metabolome of *C. vaccinii* MWU205, the bacterium was grown in a complex (LB) and a minimal medium (M9) for 7.5 d and extracted with *n*-butanol every 12 h as described in **chapter 5.6.2**. Afterwards the samples were analyzed using LC/MS^2, adding the already existing LC/MS^2 data of the depsipeptide-containing fraction from the leaves of the cultivated plant *A. crenata*[173] to the data set. This allowed the comparison of FR derivatives present in the plant/bacterial symbiont association with those produced by *C. vaccinii* MWU205. The MS^2 data of all sixty-one samples were visualized and compared with each other using the FBMN workflow (version: release_20) from GNPS to include chromatographic information, e.g., retention time, into the analysis and to distinguish isomers as described in **chapter 5.12**[177,178,180,181].

The resulting FBMN (**Figure 5 (A)**) consists of forty clusters and 845 single nodes[1]. Thirty clusters, are exclusively derived from *C. vaccinii* MWU205extracts (clusters harboring only red or/and white nodes, e.g., **Figure 5 (A)** cluster 2). The depsipeptide-containing *A. crenata* fraction yielded five unique clusters (clusters containing only green

nodes, e.g., **Figure 5 (A)**, cluster 15). In total five molecular families of mixed origin have been identified where both, plant and *C. vaccinii* MWU205 extracts, contained either the same (**Figure 5 (A)**, cluster 7) or a different *m/z* (**Figure 5 (A)**, cluster 16) of the family (occurrence of red, white, and green nodes)[1].

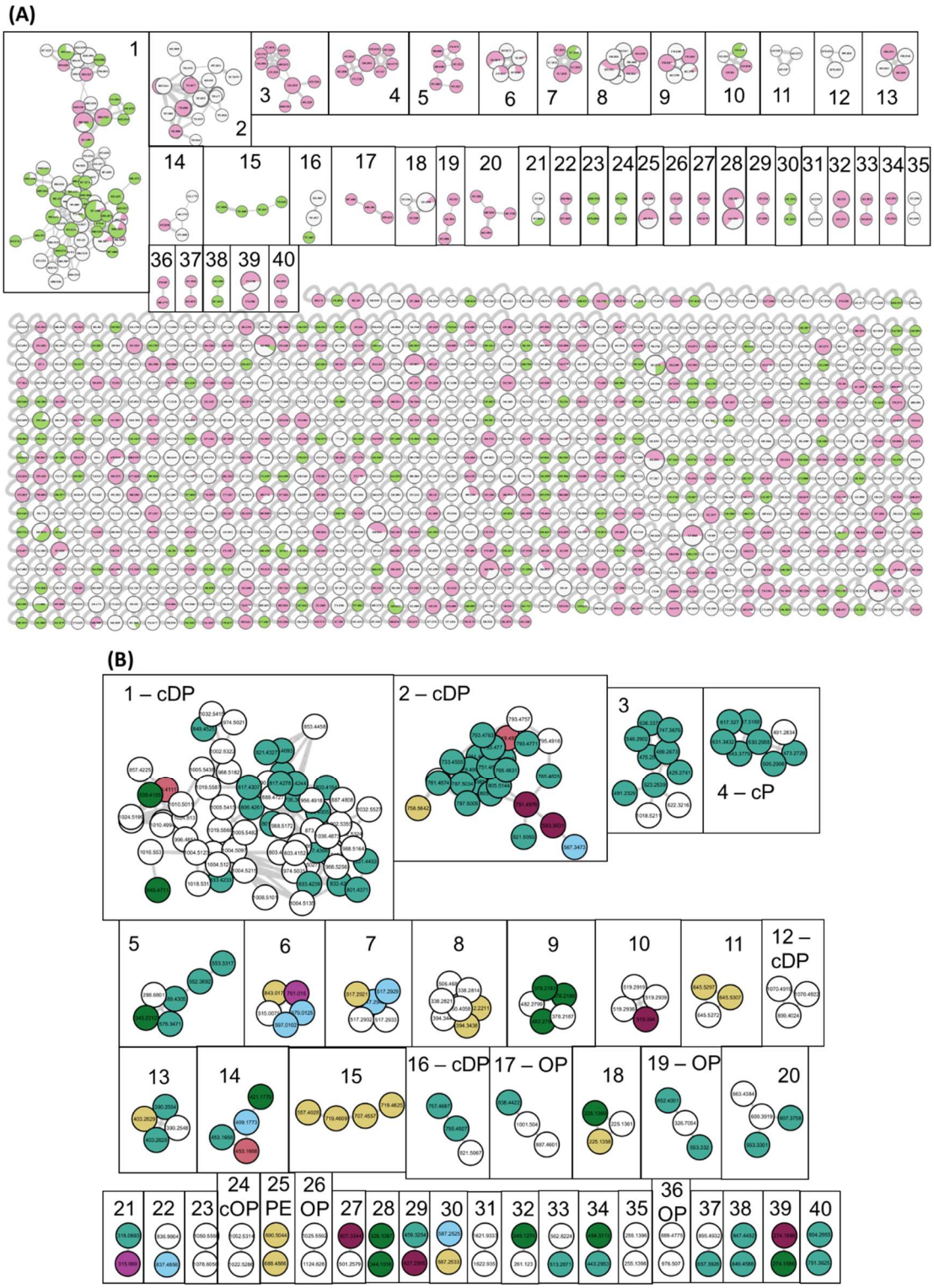

Figure 5: Feature-based molecular network (FBMN) (workflow release_20.0) of the metabolomes of *n*-butanol extracts from *Chromobacterium vaccinii* MWU205 cultivated in LB or M9 medium and the depsipeptide-containing fraction of *Ardisia crenata* leaves. **(A)** shows the complete FBMN, displaying the origin (*C. vaccinii* MWU205 LB medium: red, *C. vaccinii* MWU205 M9 medium: white, *A. crenata*: green) of each node as pie chart. All clusters containing at least two nodes are numbered. **(A)** was adapted and modified from Hanke et al, 2021[1]. **(B)** shows only the clusters of the FBMN that were labeled with their predicted compound classes by global natural product social molecular networking tools (DEREPLICATOR[184,187], MS2LDA[185,186]) and colored according to the predicted compound classes by the CANOPUS tool[188,189]. No compound class = white, amino acids and peptides = light green, fatty acids = yellow,

shikimates/phenylpropanoids = purple, carbohydrates = light blue, alkaloids = dark green, polyketides = red, terpenoids = dark red.

The library search done by GNPS proposed structures for thirteen nodes, with twelve nodes being part of clusters. Seven nodes from cluster 1 were identified as FR, FR-2, and FR-1, revealing this cluster to be the FR molecular family, which is further analyzed in **chapter 3.1.2.1.13.1.2.1**. Furthermore, two nodes from cluster 19 and one node from cluster 26 were predicted to be peptides, while cluster 25 was identified as membrane components (**Table 13**).

Next to the library search, cluster 2 was manually identified to contain the molecular family of valhidepsins, which is analyzed further in **chapter 3.1.2.2**, and cluster 28 was diagnosed manually to be the violacein molecular family analyzed in **chapter 3.1.2.3**.

All clusters were analyzed to find products related to the predicted BGCs by combining two tools available on the GNPS platform, the DEREPLICATOR for the identification of peptidic natural products (PNP), using *in silico* spectra of PNPs from chemical libraries[184,187] and the MS2LDA to annotate molecular substructures[185,186] (**Table 14**). To extent the search for compound classes beyond the PNPs the MS^2 data were investigated with the CANOPUS tool[188] available on the SIRIUS platform[189](**Table 15**). The information of both platforms, GNPS and SIRIUS, were united in **Figure 5 (B)** and revealed compound classes for nearly all clusters or at least one node of a cluster in the network, leaving only four clusters without any prediction. Most nodes were identified as amino acids and peptides, followed by alkaloids and fatty acids. The analyses confirmed the predictions of the library search done by GNPS and additionally classified the cluster of the valhidepsins and violacein correctly. For the remaining regions with predicted BGCs related to terpenes, polyketides, β-lactones, AHLs, or nonribosomal peptides, possible candidates of all NP classes except polyketides were determined. Due to the lack of information regarding the structure of the NPs produced by the predicted BGCs a subsequent analysis using fragmentation patterns was impossible.

In total, thirty-four of the *C. vaccinii* MWU205 clusters were unidentified and underline the potential of *C. vaccinii* MWU205 as source for new NP.

3.1.2.1. Molecular family of FR

Cluster 1 of the FBMN was identified to contain the molecular family of FR, which is represented by fifty-three nodes (**Figure 5**). To focus on unique nodes and to find new FR

derivatives, sodium and ammonium adduct ions were deleted from the network. These deletions condensed the FR molecular family to a core network of thirty-eight nodes, ranging from *m/z* 706 to 1036 (**Figure 6**).

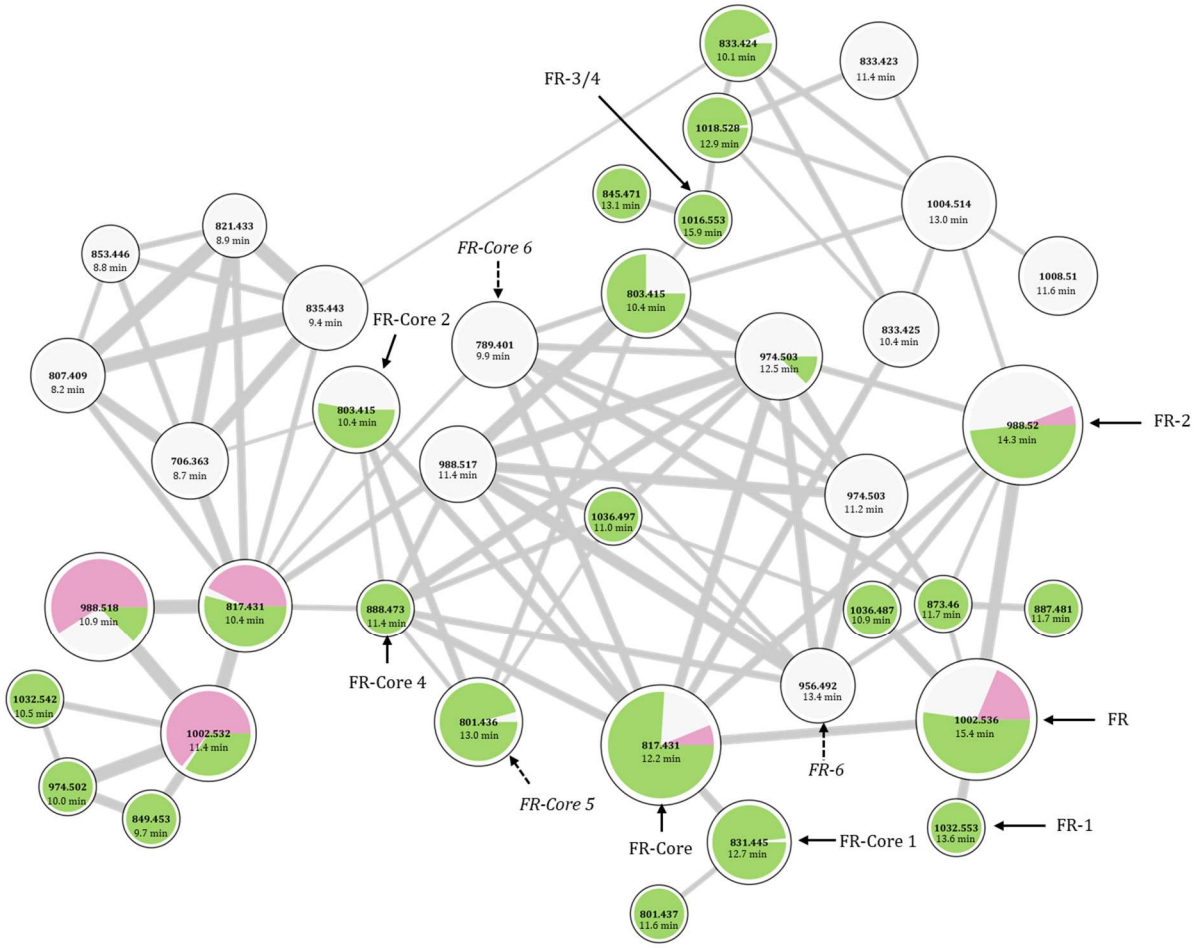

Figure 6: Molecular cluster of FR900359 (FR) (determined by MS^2) from the feature-based molecular network (NH_4^+ and Na^+ adducts were removed). Data pool includes extracts of *Chromobacterium vaccinii* MWU205 cultivated in M9 (white color) and LB medium (red color), and the depsipeptide-containing fraction of *Ardisia crenata* leaves (green color). Nodes display distinct *m/z* features, i.e., parent mass and LC retention time. Their size corresponds to the number of spectra obtained and their color displays the origin. The width of the edges corresponds to the similarity of the fragmentation spectra of the connected nodes. Known and already published FR derivatives (**Figure 3**) are indicated by arrows and named. Newly identified FR derivatives are indicated by dashed arrows and italic names. Figure was adapted and modified from Hanke et al, 2021[1].

All currently known FR derivatives, i.e., FR, FR-1, FR-2, and FR-3/4, and FR-Core derivatives, i.e., FR-Core, FR-Core 2, and FR-Core 4, were identified using LC/MS^2 fragmentation pattern analyses (**Figure 12** and **Figure 44** to **Figure 46**) and retention times of standards (FR, FR-2, and FR-Core) or previously reported LC/MS^2 data[173]. FR-Core 1 was identified as well, and the detailed analysis of the fragmentation pattern was done in **chapter 3.1.2.1.1**.

As described in the accompanying publication, a second peak with the extracted ion chromatogram (EIC) of *m/z* 1002.53 (as FR) and a shorter retention time (11.5 min) was observed, which was interpreted as that of an FR isomer[1] (**Figure 7**). This phenomenon was also noticed for the described FR derivatives FR-2 (*m/z*: 988.518, RT: 10.9 min), FR-1 (*m/z*: 1032.542, RT: 10.5 min), and FR-Core (*m/z*: 817.431, RT: 10.4 min). The comparison of the MS^2 spectra of FR and its isomer by GNPS did not reveal a cosine score above 0.7, leaving them unconnected in the cluster (**Figure 6**). The same was observed for the isomers of FR-1, FR-2, and FR-Core, as well as the isomers of structurally not yet determined FR derivatives (*m/z*: 974.502, RT: 10.0 min and *m/z*: 849.453, RT: 9.7)[1].

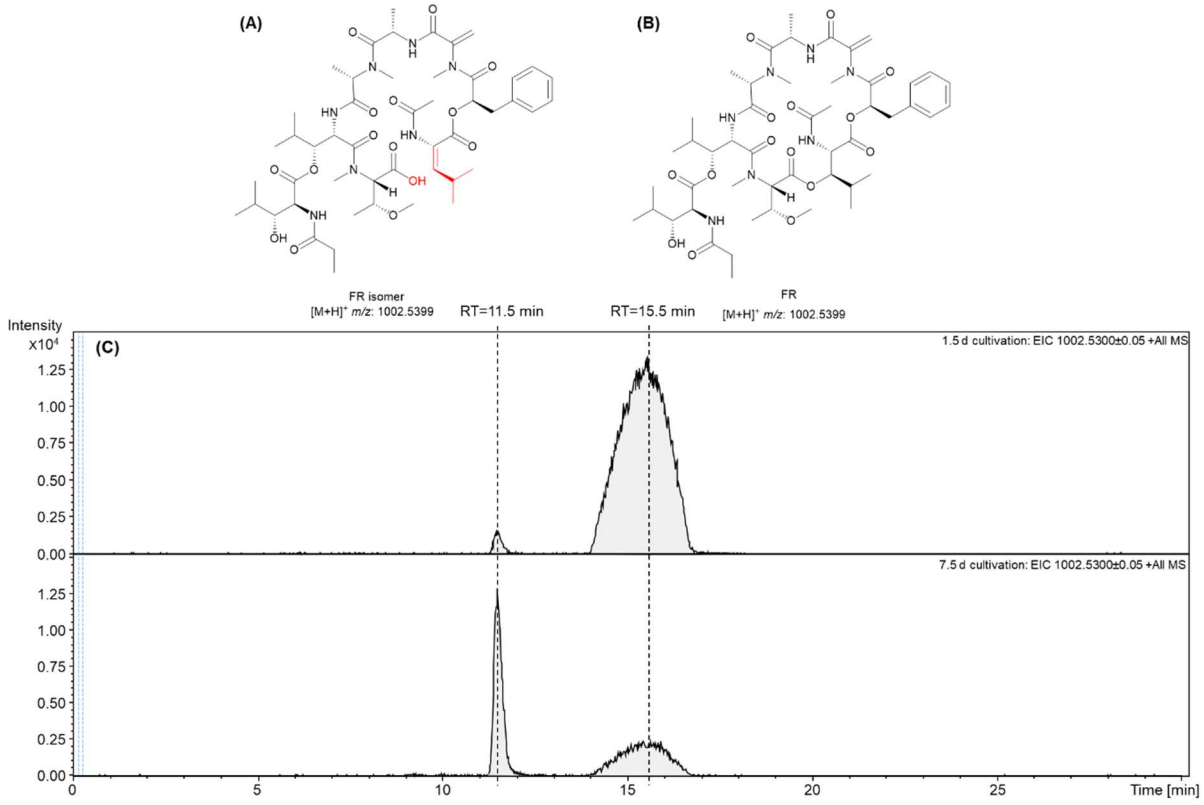

Figure 7: Structures of the isomer of FR900359 (FR)[129] (A) and FR (B), and the extracted ion chromatograms (EIC) (*m/z* 1002.53±0.05) of *Chromobacterium vaccinii* MWU205 extracts grown in LB medium for 1.5 and 7.5 days (C).

The structure of the isomer was revealed to be a linearized FR molecule hydrolyzed between the *N,O*-Me_2-Thr and the *N*-Ac-β-HyLeu, whereby the latter was dehydrated forming *N*-acetyldehydroleucine. In addition, the corresponding isomer of FR-2 was purified and revealed to have the same structural rearrangement[129].

Next to the known molecules, twenty-seven *m/z* ratios (71 %) for unknown compounds were found in the FR cluster. In total, thirteen nodes (34 %) of the FR cluster

originate specifically from *C. vaccinii* MWU205 cultivated in M9 medium (white, **Figure 6**). No unique *m/z* was discovered in LB medium extracts (red, **Figure 6**). Twelve nodes (31 %) were only found in the depsipeptide-containing fraction of *A. crenata* leaves extract (green, **Figure 6**). Thirteen *m/z* values were found in extracts from both plant and bacterium (34 %). This demonstrates, that both bacterial FR producers, i.e., *Cand.* Burkholderia crenata in *A. crenata* and *C. vaccinii* MWU205, synthesize a different spectrum of FR derivatives.

3.1.2.1.1. Identification of new FR derivatives via MS^2 fragmentation analysis

The focus of this study was the investigation of the metabolome of *C. vaccinii* MWU205 and the identification of new FR derivatives unique to *C. vaccinii* MWU205. Therefore, FBMN nodes found only in *C. vaccinii* MWU205 cultures were targeted. Twelve nodes of unexplored metabolites, which were directly connected to a known FR derivative, were selected from the core network (**Figure 6**), i.e., *m/z* 706.363 (RT: 8.7 min), 789.401 (RT: 9.9 min), 801.436 (RT: 13.0 min), 803.415 (RT: 10.4 min), 833.425 (RT: 10.4 min), 956.492 (RT: 13.4 min), 974.503 (RT: 11.2 and 12.5 min), 988.517 (RT: 11.7 min), 1004.514 (RT: 13.0 min), and 1018.528 (RT: 12.9 min), respectively. To investigate the structures of these twelve FR derivatives, their MS^2 data were analyzed in detail, using the characteristic MS fragmentation pathways of FR and FR-Core, as changes in *m/z* values of individual fragments to FR and FR-Core identify structural modifications.

The ions in the fragmentation pattern of FR and FR derivatives are named according to the nomenclature system developed by Ngoka et al[192] based on the Biemanns modifications[193] of Roepstorffs nomenclature[194]. Cyclic depsipeptides like FR and its derivatives linearize due to the breakage of a peptide or ester bond. In case of FR, the most observed breakage occurs between the alanine (A') and hydroxyleucine (L''). Peptides are known to produce different types of fragments, i.e., the b-series consists of acylium ions, the y-series of ammonium ions, and the a-series is like the b-series without a carbon monoxide. In case of FR, mainly b-ions are observed losing one building block after another. Fragment ions are named using the following formula: b_{nJZ}. "n" equals the number of building blocks left in the peptide chain, In the case of FR, "n" can be two to eight. For the orientation of the molecule "J" is naming the building block containing the *N*-terminus and "Z" is the *C*-terminal amino acid residue. In this case, the C-terminus is a

newly formed oxazolone representing the alanine residue of FR. Changes in the fragmentation pattern of derivatives can be used to pinpoint the structural differences, therefore the fragmentation pattern of FR is displayed in **Figure 8**[195].

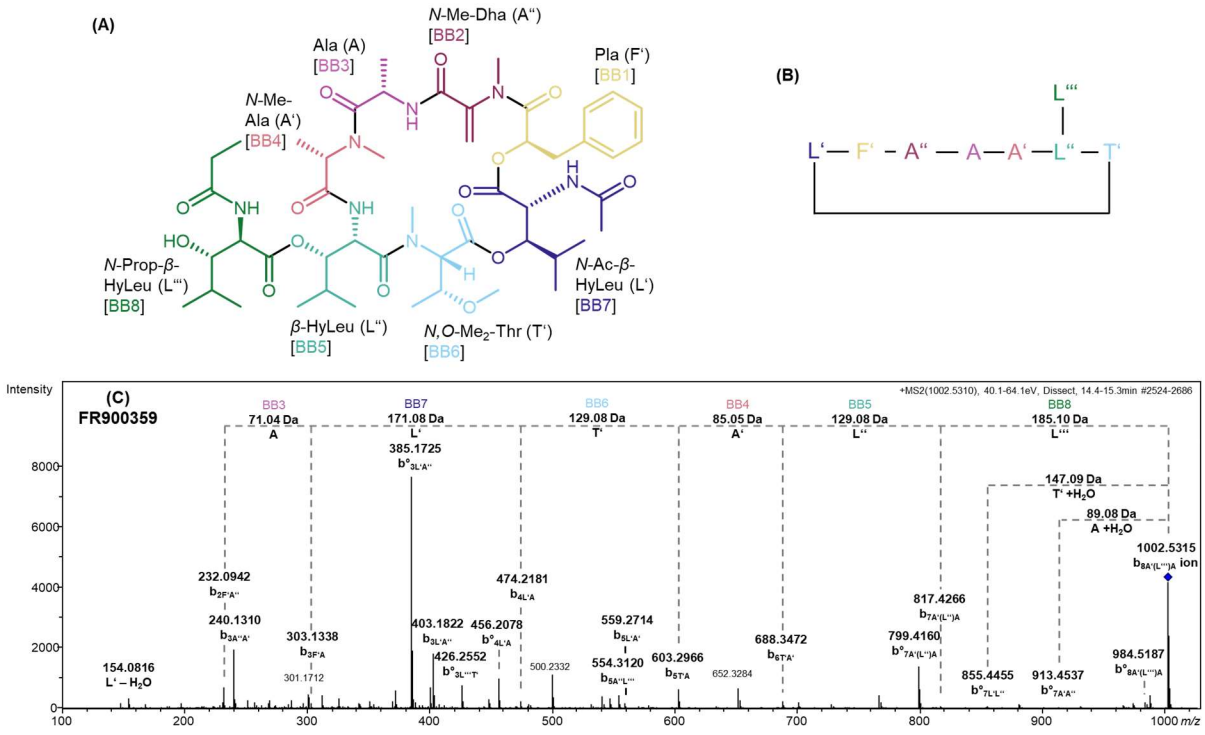

Figure 8: Structure of FR900359 (FR) (A) and schematic version (B) with named and colored building blocks. Fragmentation pattern of *m/z* 1002.5310 named following the nomenclature system by Ngoka[192] based on Biemanns modifications[193] of Roepstorffs nomenclature in one-letter amino acid code[194]. b° = b-ion with loss of water. L' = *N*-Ac-β-HyLeu, A = Ala, A' = *N*-Me-Ala, T' = *N,O*-Me$_2$-Thr, L"' = *N*-Prop-β-HyLeu, L'' = β-HyLeu, F' = Pla, A'' = *N*-Me-Dha.

Apart from the twelve targeted novel *m/z* values, FR-Core 1 was identified to be present in both *C. vaccinii* MWU205 and the plant extract. However, the detailed comparison of the fragmentation patterns from the plant and the bacterium differed significantly (**Figure 9**). For the novel compound unique for *C. vaccinii* MWU205 with *m/z* 831.445, the difference of 14.01 Dalton (Da) compared to FR-Core, most likely a CH_2 group, was pinpointed to the alanine. Two possibilities for the position of the additional CH_2 group are reasonable: (i) The replacement of the alanine by homoalanine as already observed for FR-4, a FR derivative from the plant with a homoalanine in the position of the alanine (**Figure 3**) or (ii) the methylation of nitrogen leading to the presence of two *N*-Me-Ala next to each other.

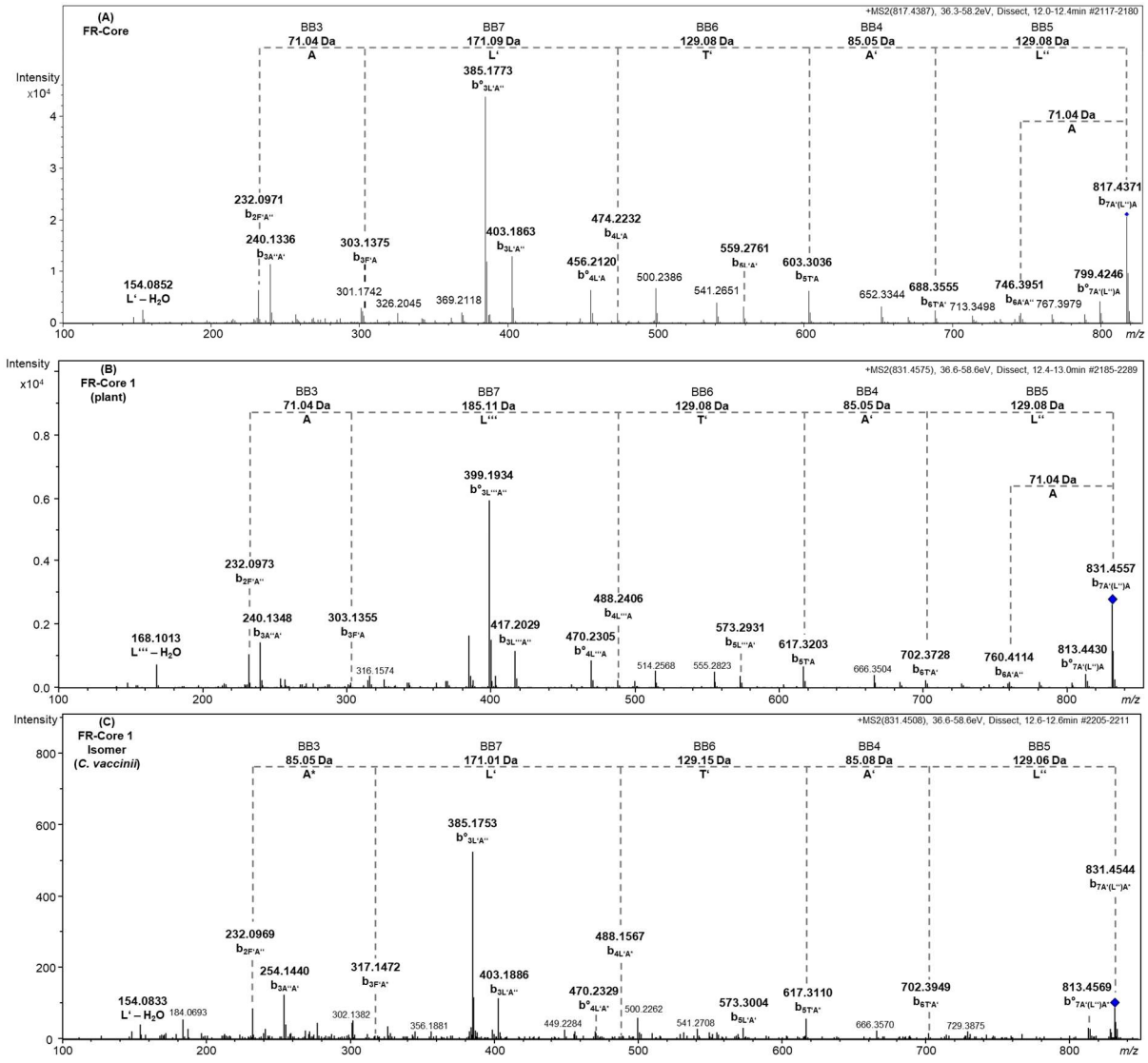

Figure 9: Fragmentation pattern of **(A)** FR-Core (*m/z* 817.4387) from Hanke et al, 2021[1], FR-Core 1 (*m/z* 831.4575), and the isomer of FR-Core 1 (*m/z* 831.4508 **(B)** following the nomenclature system by Ngoka[192] based on Biemanns modifications[193] of Roepstorffs nomenclature in one-letter amino acid code[194]. b° = b-ion with loss of water. L' = *N*-Ac-β-HyLeu, L'' = β-HyLeu, L''' = *N*-Prop-β-HyLeu, A = Ala, A' = *N*-Me-Ala, A* = methylated Ala, T' = *N,O*-Me_2-Thr, F' = Pla, A'' = *N*-Me-Dha.

For the compounds with *m/z* 801.436 and 789.401, a structure close to that of FR-Core (**Figure 10**) was speculated and therefore, their *m/z* and fragmentation pattern was compared to FR-Core. In the case of *m/z* 801.436, a 16.00 Da difference to FR-Core was most likely the outcome of a missing oxygen. The MS^2 spectrum (**Figure 10 (B)**) revealed that the β-HyLeu/L'' was replaced by leucine. This change results in a more hydrophobic derivative now named FR-Core 5, which has a longer retention time in reversed-phase chromatography (RT: 13.0 min) compared to FR-Core (RT: 12.2 min).

The mass difference of the compound giving rise to *m/z* 789.401 and FR-Core (Δ*m/z*: 28.03 Da) suggested the lack of two CH_2 groups for the new derivative. The MS fragmentation pattern (**Figure 10 (C)**) investigation pointed towards the lack of both

methylations of the building block *N,O*-Me_2-Thr, resulting in an unmodified threonine. The missing methyl groups cause a more polar derivative, for which the name FR-Core 6 is suggested, resulting in a much shorter retention time (RT: 9.9 min) as compared to that of FR-Core (RT: 12.2 min).

For both compounds, FR-Core 5 and 6 (**Figure 10**), structure elucidation via LC/MS^2 was unambiguous. In other cases, fragmentation pattern analysis merely identified the building block in which the structural change is located. These metabolites and their respective *m/z* values are described in the following part.

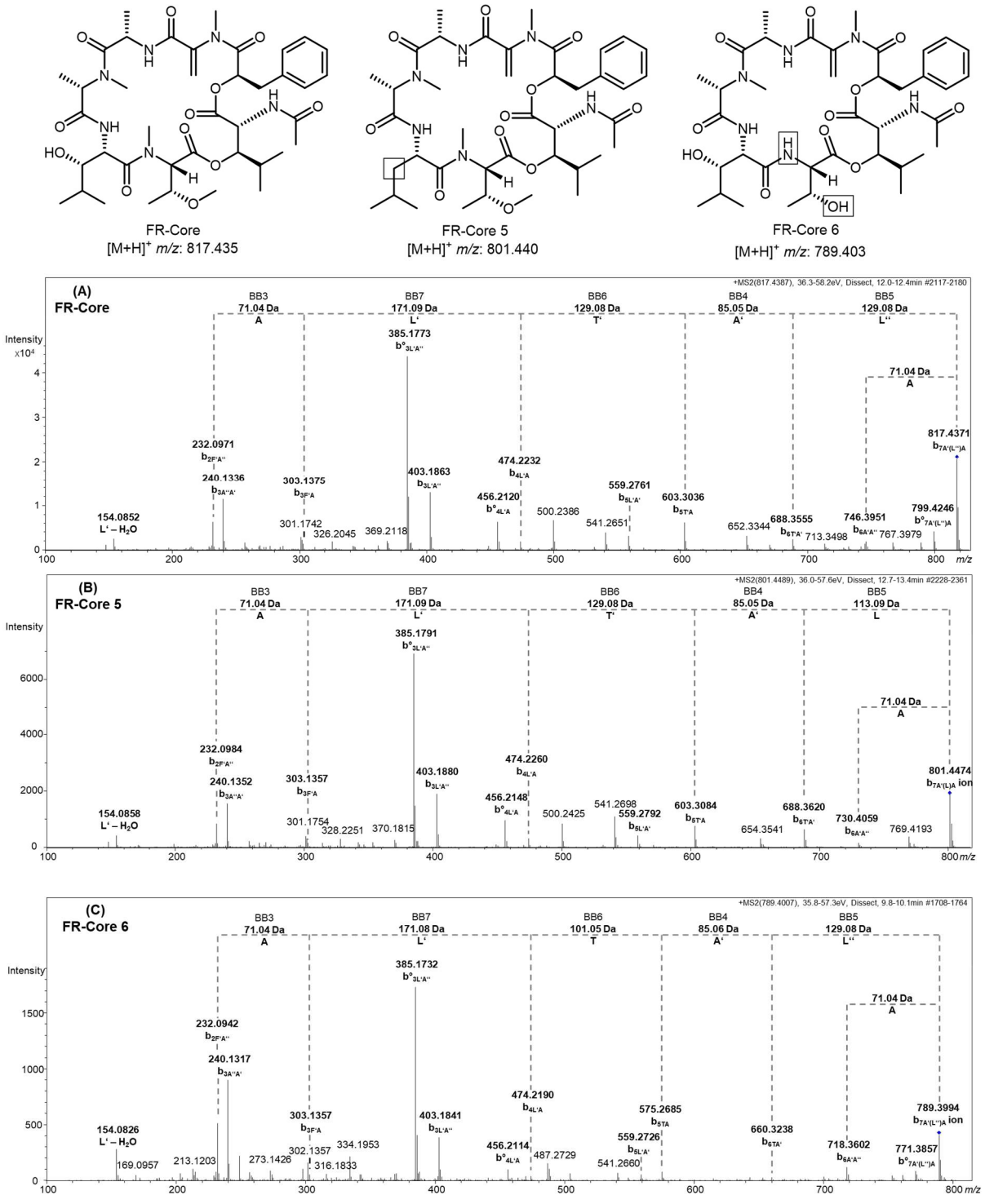

Figure 10: Structure of FR-Core (left) and proposed structures for the new FR-Core derivatives FR-Core 5 (middle) and FR-Core 6 (right) based on MS fragmentation patterns (**(B)**, **(C)**) compared to FR-Core **(A)**. The structural changes compared to FR-Core are highlighted by boxes. Fragmentation ions are named following the nomenclature system by Ngoka[192] based on Biemanns modifications[193] of Roepstorffs nomenclature in one-letter amino acid code[194]. b° = b-ion with loss of water. L' = *N*-Ac-β-HyLeu, A = Ala, A' = *N*-Me-Ala, T' = *N,O*-Me$_2$-Thr, T = Thr, L'' = β-HyLeu, L = Leu, F' = Pla, A'' = *N*-Me-Dha. Figure adapted and modified from Hanke et al, 2021[1].

For the derivative with *m/z* 833.425 (RT: 10.4 min) the mass change of 15.99 Da compared to FR-Core was probably the result of an additional oxygen. Comparison of the

fragmentation spectra with FR-Core revealed a change in the phenyllactic acid (Pla) moiety, where instead of Pla a hydroxylated Pla was added by the biosynthetic machinery (**Figure 11**). The exact position of this hydroxy group could not be determined by MS^2. *In vitro* experiments with the respective biosynthetic enzymes, FrsE and FrsC, did show that 4-hydroxy-phenylpyruvic acid and 4-hydroxy-Pla are incorporated at very low levels[148]. Due to the polar nature of the oxygen the retention time of this FR-Core derivative was shorter compared to FR-Core. The *m/z* values 1004.514 (RT: 13.0 min) and 1018.528 (RT: 12.9 min) probably represent the respective FR and FR-2 analog with a hydroxylated Pla moiety. However, the fragmentation patterns for both *m/z* were not clear enough to draw any conclusions towards their structures.

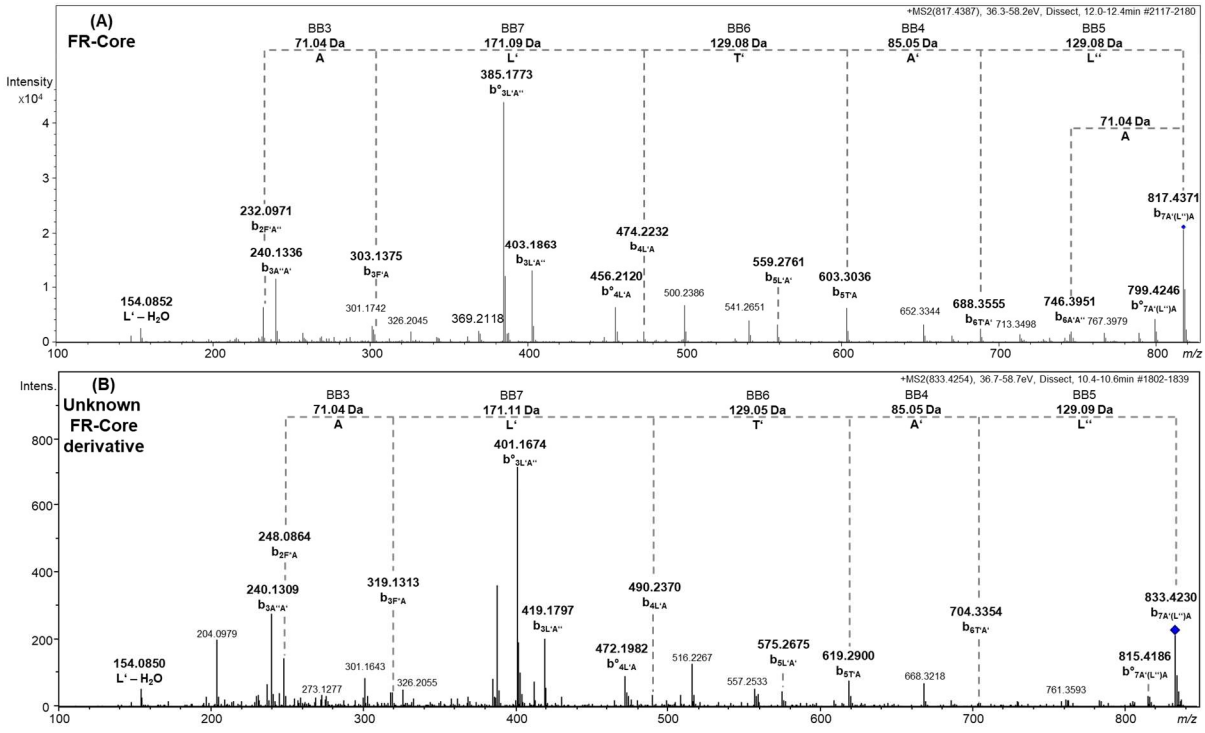

Figure 11: Fragmentation pattern of **(A)** FR-Core (*m/z* 817.4387) from Hanke et al, 2021[1] and **(B)** the new FR-Core derivative (*m/z* 833.4254) named following the nomenclature system by Ngoka[192] based on Biemanns modifications[193] of Roepstorffs nomenclature in one-letter amino acid code[194]. b° = b-ion with loss of water. L' = *N*-Ac-β-HyLeu, A = Ala, A' = *N*-Me-Ala, T' = *N,O*-Me_2-Thr, L'' = β-HyLeu, F' = Pla, F* = HyPla, A'' = *N*-Me-Dha.

Two isomers with the identical *m/z* value of 803.415, were distinguished based on their different retention times, i.e., 10.4 and 12.0 min, respectively. The compound with RT: 12.0 min was identified as FR-Core 2, which lacks one methyl group at the *N*-Me-Ala (A' in **Figure 8**) residue compared to FR-Core (**Figure 12 (B)**). The fragmentation pattern of the other compound with an *m/z* value of 803.415 (RT: 10.4 min) indicated the lack of

a methyl group at the *N,O*-Me$_2$-Thr moiety, i.e., either the *N*- or the *O*-methyl group (**Figure 12 (C)**).

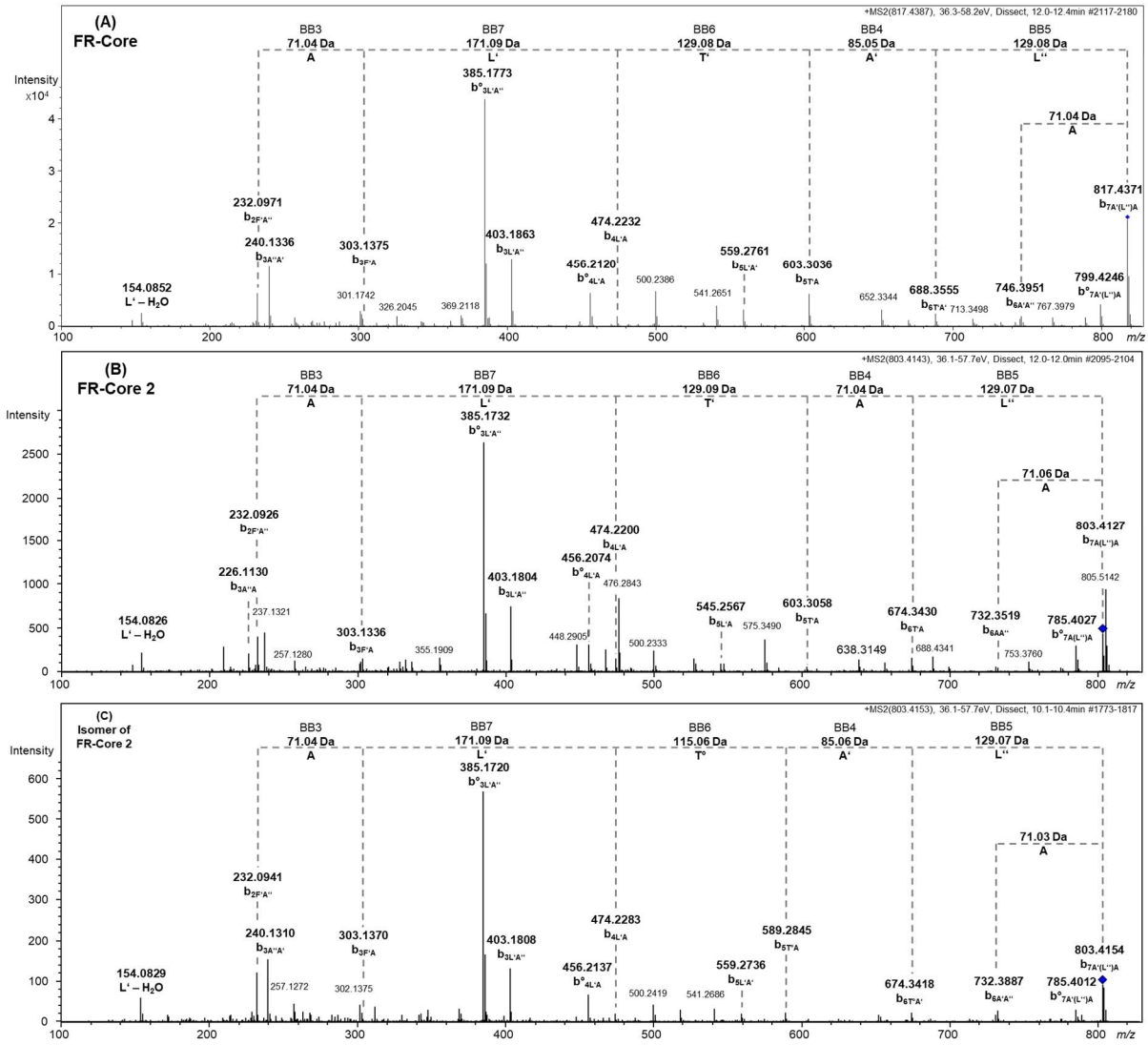

Figure 12: Fragmentation pattern of **(A)** FR-Core (*m/z* 817.4387), **(B)** FR-Core 2 (*m/z* 803.4143) and the isomer of **(C)** FR-Core 2 with an *m/z* of 803.4153 named following the nomenclature system by Ngoka[192] based on Biemanns modifications[193] of Roepstorffs nomenclature in one-letter amino acid code[194]. b° = b-ion with loss of water. L' = *N*-Ac-β-HyLeu, A = Ala, A' = *N*-Me-Ala, T' = *N,O*-Me$_2$-Thr, T° = *N*- or *O*-Me-Thr, L'' = β-HyLeu, F' = Pla, A'' = *N*-Me-Dha. Figure from Hanke et al, 2021[1].

A similar case was observed for two compounds with *m/z* 974.503 appearing at different retention times (RTs: 11.2 min and 12.5 min). For both FR derivatives, the mass difference of 28.03 Da indicated the loss of two CH_2 groups compared to FR. The fragmentation pattern of the more polar compound with an *m/z* 974.503 (RT: 11.2 min) (**Figure 13**) exposed two building blocks lacking one methyl group, the *N,O*-Me$_2$-Thr and the *N*-Prop-β-HyLeu (L''' in **Figure 8**), where instead of the propionic acid moiety, acetic acid most likely is present. As seen for the FR-Core 2 isomer, either the *N*- or the *O*-methyl group could be missing. Unfortunately, the second metabolite with an *m/z* value of

974.503 (RT: 12.5 min) did not have a clear MS fragmentation pattern and thus could not be analyzed further.

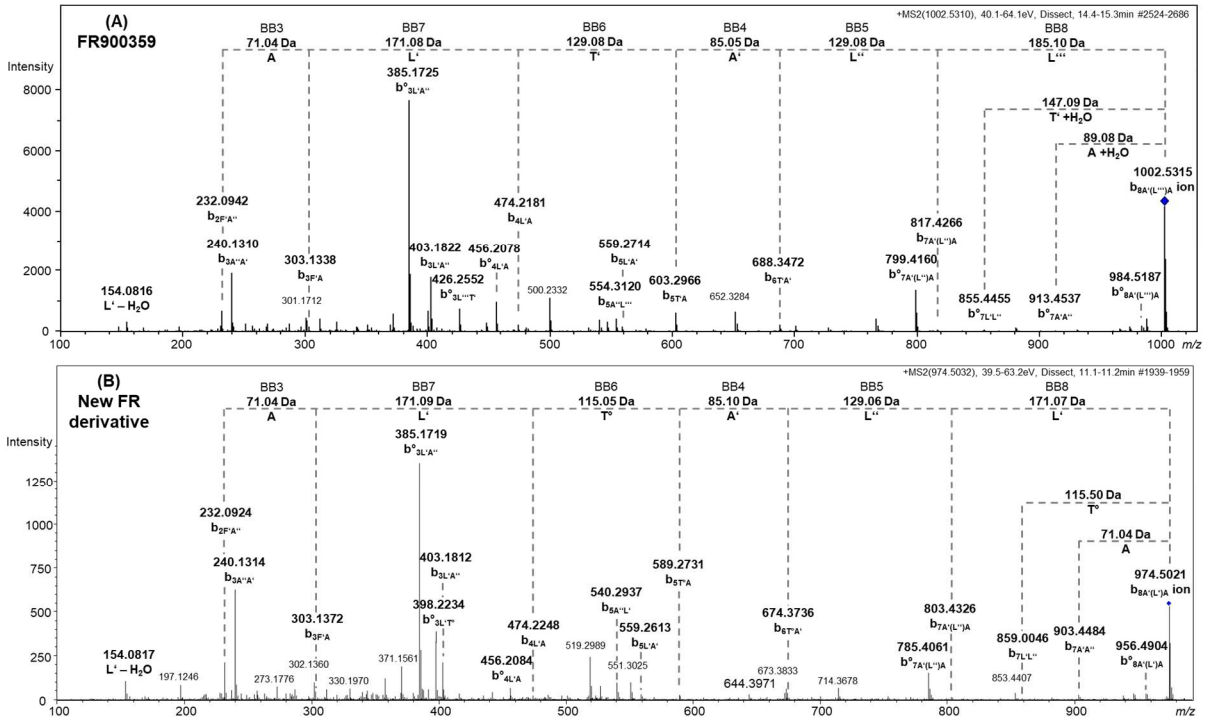

Figure 13: Fragmentation pattern of **(A)** FR900359 (*m/z* 1002.5310) and **(B)** the substance with *m/z* 974.5032 named following the nomenclature system by Ngoka[192] based on Biemanns modifications[193] of Roepstorffs nomenclature in one-letter amino acid code[194]. b° = b-ion with loss of water. L' = *N*-Ac-β-HyLeu, A = Ala, A' = *N*-Me-Ala, T' = *N,O*-Me$_2$-Thr, T° = *N*- or *O*-Me-Thr, L''' = *N*-Prop-β-HyLeu, L'' = β-HyLeu, F' = Pla, A'' = *N*-Me-Dha. Figure from Hanke et al, 2021[1].

FR-Core 5 (RT: 13.0 min) gives rise to *m/z* 801.436 (**Figure 10**). A second remarkably close, but not identical *m/z* value of 801.437 (RT: 11.6 min) was recognized in the extracts of the plant *A. crenata* with a similar fragmentation pattern compared to its neighbor node FR-Core 1 (RT: 12.7 min, Δ*m/z* of 30.01 Da). The comparison to the fragmentation pattern of FR-Core revealed three structural changes (**Figure 14**), i.e., the absence of an oxygen from the β-HyLeu/L'' in **Figure 8** (Δ*m/z* of 15.99 Da); the exchange of acetic acid to propionic acid for the *N*-Ac-β-HyLeu residue in FR-Core (Δ*m/z* of 14.01 Da); and the lack of a methyl group in the *N,O*-Me$_2$-Thr moiety (Δ*m/z* of 14.01 Da). As before, it was not possible to determine which methyl group of the *N,O*-Me$_2$-Thr moiety was missing.

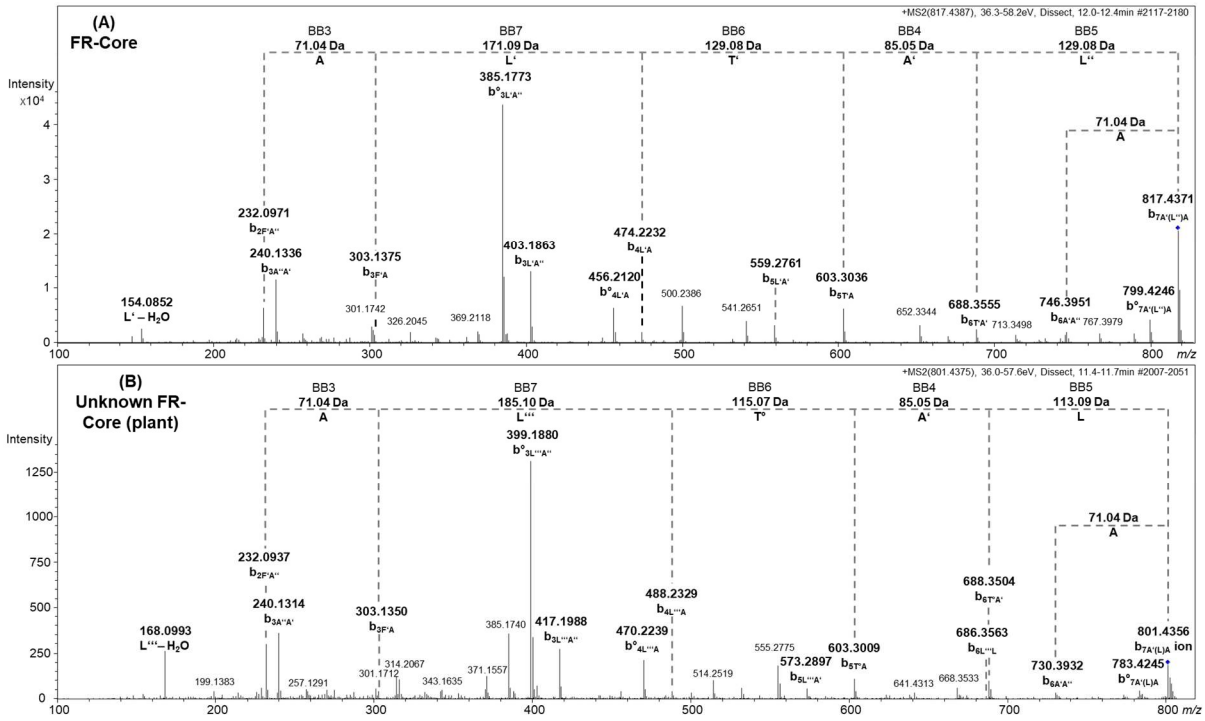

Figure 14: Fragmentation pattern of **(A)** FR-Core (*m/z* 817.4387) and **(B)** the substance with *m/z* 801.4375 named following the nomenclature system by Ngoka[192] based on Biemanns modifications[193] of Roepstorffs nomenclature in one-letter amino acid code[194]. b° = b-ion with loss of water. L' = *N*-Ac-β-HyLeu, A = Ala, A' = *N*-Me-Ala, T' = *N,O*-Me$_2$-Thr, T° = *N*- or *O*-Me-Thr, L''' = *N*-Prop-β-HyLeu, L'' = β-HyLeu, L = Leu, F' = Pla, A'' = *N*-Me-Dha. Figure from Hanke et al, 2021[1].

For the derivative with *m/z* 706.363 (RT: 8.7 min) connected to the compound with *m/z* 835.443 the mass difference of 129.08 Da was proposed to be the lack of the β-HyLeu or the *N,O*-Me$_2$-Thr. According to the mass difference of 18.01 Da between the derivative giving rise to *m/z* value 835.443 (RT: 9.4 min) and the FR-Core isomer (RT: 10.4 min) the addition of water is plausible, resulting in a shorter retention time. The fragmentation pattern strengthened the presence of a linear FR-Core derivative, as it resembled those of the other linear isomers (**Figure 47**). However, the exact building block containing the change could not be determined.

For the *m/z* values 974.503 (RT: 12.5 min) and 988.517 (RT: 11.7 min), both presumably isomers of FR-2 and the compound described above, the fragmentation patterns were not clear enough to draw any conclusion towards their structure.

3.1.2.1.2. FR-6 isolation and bioactivity

To isolate and characterize new FR derivatives, *C. vaccinii* MWU205 was cultivated in 6 L M9 medium as described in **chapter 5.6.1.3**. After several chromatographic separation and purification steps described in **chapter 5.8**, 3 mg of a white compound having an *m/z* value of 956.480 were isolated.

LC/MS^2 analysis of the compound FR-6 (*m/z* 956.480, **Figure 15**) indicated this FR derivative to have the molecular formula $C_{47}H_{69}N_7O_{14}$ (calculated 956.4975 for $[M+H]^+$). The comparison of the MS spectrum of FR-6 to FR (**Figure 15**) revealed a mass difference of 32.03 Da in all fragments containing the *N,O*-Me$_2$-Thr moiety. Additionally, a mass difference of 14.01 Da was observed in all fragments containing the *N*-Prop-β-HyLeu compared to FR.

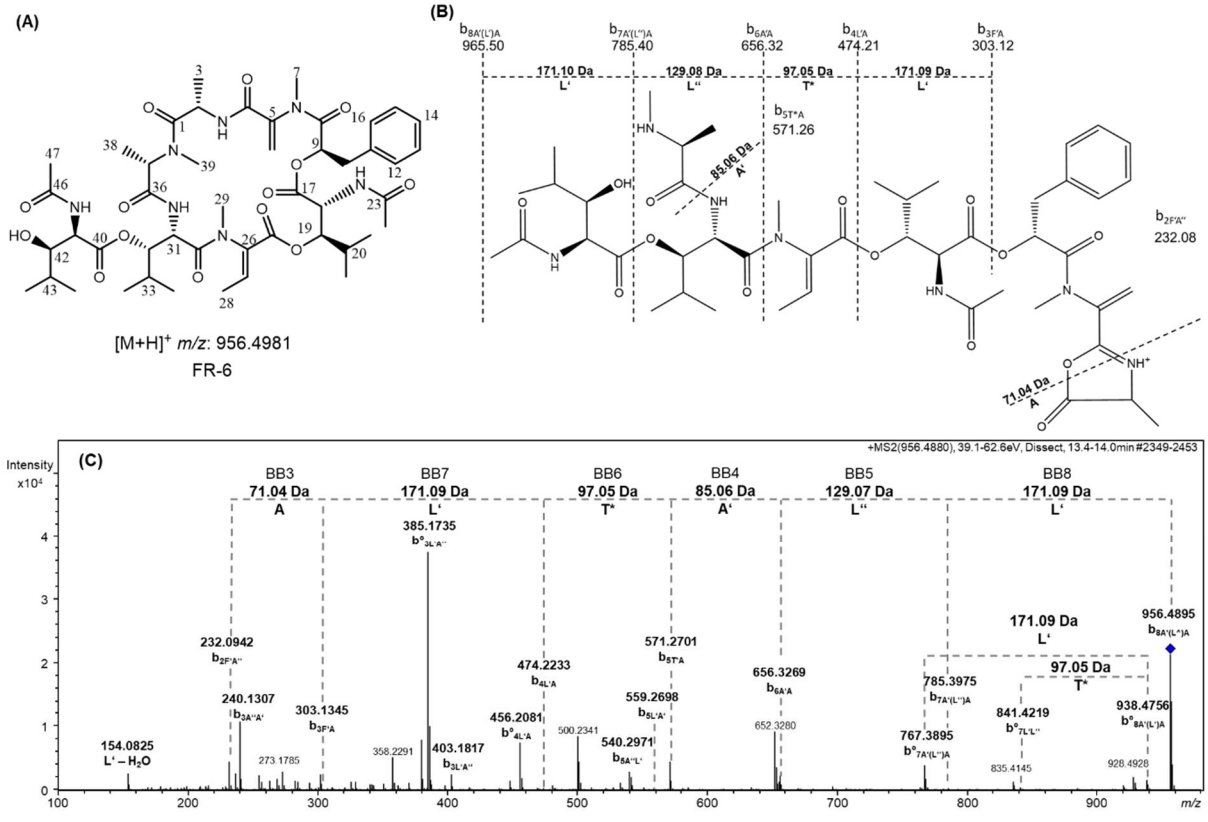

Figure 15: **(A)** Structure of FR-6. **(B)** Fragmentation pathway of FR-6 proton adduct. **(C)** Fragmentation pattern of the substance with an *m/z* of 956.4880 named following the nomenclature system by Ngoka[192] based on Biemanns modifications[193] of Roepstorffs nomenclature in one-letter amino acid code[194]. b° = b-ion with loss of water. L' = *N*-Ac-β-HyLeu, A = Ala, A' = *N*-Me-Ala, T* = 2-methylamino-2-butenoyl, L'' = β-HyLeu, F' = Pla, A'' = *N*-Me-Dha. Figure adapted and modified from Hanke et al, 2021[1].

NMR data analysis of FR-6 (**Table 1**) verified the findings of the fragmentation pattern analysis, as its main difference compared to FR was pinpointed in the *N,O*-Me$_2$-Thr moiety. Thus, in the ^{1}H and ^{13}C NMR spectra of FR-6 three resonances are missing, i.e., the resonance for a methoxy group is missing and the resonances for the respective α and β methine groups. As a substitute, two carbon (C-26, C-27) resonances at δ 132.8 and δ 141.2 indicated the presence of a double bond. Taken together, a 2-methylamino-2-butenoic acid moiety, probably a result from dehydration of a threonine, replaces the originally present threonine moiety in FR-6. Another difference between FR and FR-6 is the exchange of the propionyl residue in *N*-Prop-β-HyLeu (as in FR) by an acetyl group,

which is known for FR-2. Detailed analyses of the 1D and 2D NMR data unambiguously proved the structure of FR-6 (**Table 1**, **Figure 48** to **Figure 53**). Both, FR and FR-6, are products of the same NRPS biosynthetic system, therefore the configuration of FR-6 is suggested to be identical to that of FR. The configuration of the double bond Δ26,27 was determined to be Z due to a ROESY correlation between H3-28 and H3-29.

Table 1: ^{1}H and ^{13}C NMR spectroscopic data of FR-6 in chloroform-*d*$_3$ (^{1}H: 600 MHz; ^{13}C: 150 MHz). Table from Hanke et al, 2021[1].

Residue[a]	No C/H	δ_C, mult	δ_H (*J* [Hz])	COSY	HMBC	ROESY
Ala	1	173.5, C	–			
	2	44.7, CH	5.24 (dq, 10.1, 6.5)	3, 2-NH	1, 3, 4	2-NH, 3, 39
	2-NH	–	7.80 (d, 10.1)	2	2, 4	2, 3, 6a
	3	18.4, CH_3	1.38 (d, 6.5)	3	1, 2	2, 2-NH
***N*-Me-Dha**	4	163.6, C	–			
	5	142.0, C	–			
	6a	123.3, CH_2	a 5.32 (br s)	6b	5	2-NH, 6b
	6b	–	b 3.42 (br s)	6a	5	6a
	7	37.9, CH_3	3.12 (s)		5, 8	
Pla	8	167.6, C	–			
	9	71.0, CH	5.21 (dd, 4.2, 11.2)	10a, 10b	8, 10, 17	10b
	10a	38.8, CH_2	a 3.26 (dd, 11.2, 12.7)	9, 10b	9, 11, 12/16	10b, 12/16
	10b	–	b 2.87 (dd, 4.2, 12.7)	10a	9, 11, 12/16	9, 10a, 12/16
	11	135.8, C	–			
	12/16	130.0, CH	7.08 (d, 7.7)	13/15	10, 14	10a, 10b, 13/15
	13/15	128.5, CH	7.23[d]	12/16	11	12/16
	14	127.1, CH	7.23[d]		12/16	
***N*-Ac-β-HyLeu**	17	167.8, C	–			
	18	53.1, CH	5.33 (dd, 3.1, 10.3)	18-NH, 19	17, 19	18-NH, 19
	18-NH	–	7.32, (d, 10.3)	18	18, 23	18, 20, 24
	19	79.8, CH	5.57 (dd, 3.1, 10.0)	18, 20	20, 25	18, 21, 22
	20	29.7, CH	1.89 (m)	19, 21, 22		21, 22

	21	19.1, CH_3	0.88 (d, 6.6)	20	20, 22	19, 22
	22	18.7, CH_3	1.04 (d, 6.6)	20	20, 21	19, 21
	23	170.2, C	–			
	24	22.5[c], CH_3	2.23 (s)		23	37, 18-NH
Dab	25	162.4, C	–			
	26	132.8, C	–			
	27	141.2, CH	7.13 (q, 7.3)	28	25, 26, 28	28
	28	13.4, CH_3	1.87 (d, 7.3)	27	26, 27	27, 29
	29	37.6, CH_3	3.30 (s)		26, 30	28, 31
β-HyLeu	30	170.9[b], C	–			
	31	48.7, CH	5.08 (d, 8.3)	31-NH, 32	30, 32	31-NH
	31-NH		9.64, (d, 8.3)		31, 36	31, 32, 33
	32	76.4, CH	5.06 (d, 8.8)	31, 33	40	31-NH, 33
	33	30.7, CH	2.02 (m)	32, 34, 35	34, 35	32, 34, 35
	34	18.9, CH_3	1.09 (d, 6.6)	33	32, 33, 35	32, 35
	35	18.5, CH_3	1.00 (d, 6.6)	33	32, 33, 34	32, 34
***N*-Me-Ala**	36	173.2, C	–			
	37	66.8, CH	3.72 (q, 7.3)	38	36, 38	38, 39
	38	16.2, CH_3	1.79 (d, 7.3)	37	35, 36	37
	39	41.5, CH_3	3.32 (s)		1, 37	37
***N*-Ac-β-HyLeu2**	40	170.9[b], C	–			
	41	54.2, CH	4.86 (d, 9.7)	41-NH	40	41-NH, 42, 44, 45
	41-NH	–	8.40 (d, 9.7)	41	41, 46	47
	42	77.9, CH	3.86 (d, 6.0)	43	40, 43	41, 43, 44, 45
	43	32.2, CH	1.84 (m)	42, 44, 45	44, 45	42, 44, 45
	44	20.2, CH_3	1.09 (6.7)	43	42, 43, 45	43, 45
	45	17.8, CH_3	0.99 (6.7)	43	42, 43, 44	43, 44
	46	171.2, C	–			
	47	22.5[c], CH_3	2.15 (s)		46	41-NH

[a] Residues: Ala = alanine, *N*-Me-Dha = *N*-methyldehydroalanine, Pla = 3-phenyllactic acid, *N*-Ac-β-HyLeu= *N*-acetylhydroxyleucine, Dab = 2-methylamino-2-butenoic acid, β-HyLeu = hydroxyleucine, *N*-Me-Ala = *N*-methylalanine, [b], [c], [d] overlapping resonances.

To evaluate the bioactivity of FR-6 as G_q inhibitor, the dynamic mass redistribution (DMR) assay was performed by Dr. Patt (AG Kostenis, Institute for Pharmaceutical Biology, University of Bonn). DMR technology provides phenotypic measures of cellular activity in real-time when cells are exposed to pharmacologically active stimuli[196,197]. HEK 293 cells were genome edited with the clustered regularly interspaced short palindromic repeats/Caspase9 (CRISPR/Cas9) method to be $G\alpha_q$ and $G\alpha_{11}$ deficient (HEK $G_{q/11}$-KO cells). These cells allow re-expression of $G\alpha_q$ and therefore the specific activation of the G_q signaling cascade by an endogenous G_q-linked muscarinic M3 receptor, which is inactive in HEK $G_{q/11}$-KO cells. (**Figure 54**). In this study's specific DMR paradigm, cell activation results from G_q signaling only. As shown in **Figure 16 (A_i)**, **(A_{ii})**, and **(B)**, a robust muscarinic acetylcholine receptor type 3-dependent G_q activation in response to carbachol (Cch) was observed and inhibited by both FR and FR-6. However, FR-6 was less potent (6-fold) as compared to FR, revealing the importance of the methoxy group of the *N,O*-Me_2-Thr for efficient G_q inhibition and the negative impact of the double bound.

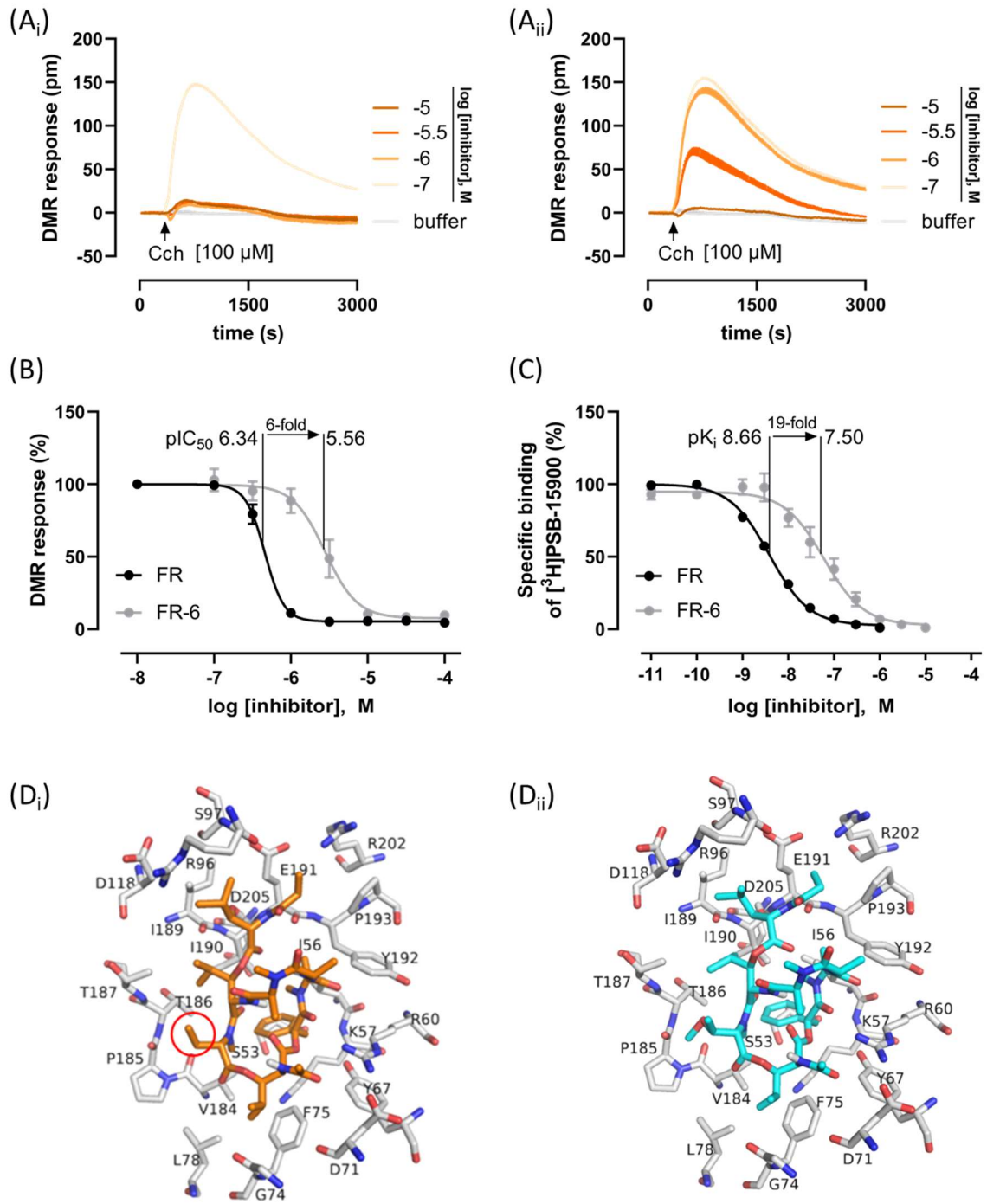

Figure 16: Characterization of FR-6 and FR900359 (FR) for inhibition of and binding to G_q proteins. Concentration-dependent inhibition of cell responses induced with carbachol (Cch) [100 µM] by **(A$_i$)** FR and **(A$_{ii}$)** FR-6 in HEK $G_{q/11}$-KO cells transfected to express wild type $G\alpha_q$. **(B)** Concentration-inhibition relationships for the traces shown in **(A$_i$)** and **(A$_{ii}$)** and quantification. Dynamic mass redistribution (DMR) recordings are representative (mean + Standard error of the mean (SEM)) of at least 5 independent biological replicates conducted in triplicate. Negative logarithms of the half maximal inhibitory concentrations (pIC_{50}) (FR, FR-6) were determined by nonlinear regression from concentration-inhibition relationships. **(C)** Specific binding of the FR-derived radioligand [^{3}H]PSB-15900 (5 nM) to human platelet membrane preparations (25 µg of protein) in the presence of varying concentrations of FR and FR-6. Data points represent means ± SEM of five independent experiments. Binding poses of (**(D$_i$)**, orange) FR-6 and **(D$_{ii}$)**, cyan) FR in the G_q protein (white, PDB code: 3AH8)[198] as suggested by molecular docking. Nearby amino acid residues are depicted as white sticks and are labeled accordingly. Figure from Hanke et al, 2021[1].

To evaluate the affinity of FR-6 towards G_q proteins in human platelet membranes, a competition binding assay, using the radiolabeled FR derivative [^{3}H]PSB-15900 (**Figure 16 (C)**) was conducted by Dr. Voss (AG Müller, PharmaCenter Bonn, Pharmaceutical Institute, Pharmaceutical & Medicinal Chemistry, University of Bonn)[159]. The negative logarithm of the inhibitor constant (pK_i) of FR-6 was calculated to be 7.50 ± 0.16 and revealed a 19-fold reduced affinity towards G_q as compared to FR (pK_i = 8.66).

Molecular docking experiments were performed by Dr. Namasivayam (AG Müller, PharmaCenter Bonn, Pharmaceutical Institute, Pharmaceutical & Medicinal Chemistry, University of Bonn) to compare the poses of FR-6 and FR in their human G_q protein binding sites (**Figure 16** (D_i) and (D_{ii})). The comparison of all crucial inhibitor-protein interactions of FR and FR-6 revealed them to be nearly identical, as only minor rotations around single bonds are predicted, e.g., for the propionate in proximity to E191 or the isopropyl residue near I190. Therefore, the docked pose of FR-6 is predicted to be virtually identical to the docked pose of the parent compound FR. The structural difference between FR and FR-6, i.e., the elimination of methanol of the *N,O*-Me_2-Thr residue of FR, was expected to reduce hydrophobic interactions between the inhibitor and the surrounding amino acids L78, V184, P185, T186, and T187 in the binding pocket. The impact of the double bound in FR-6 was not predictable by the molecular docking experiments. Taken together, the comparison provides an atom-level hypothesis for the affinity decrease of FR-6 observed in the radioligand binding assay. The reduced affinity correlates to the decreased binding affinity and G_q inhibition capacity of FR-6 determined in functional DMR assays.

3.1.2.2. Molecular family of valhidepsins

In *C. vaccinii* MWU205, another NRPS BGC was located directly downstream of the *frs* gene cluster (**Figure 4**). The NRPS encoded by this gene cluster is responsible for the formation of cyclic and linear lipopeptides, known as valhidepsins which mostly consist of valine moieties. Eight of these peptides have recently been described and characterized[128]. In the extracts of *C. vaccinii* MWU205 cultivated in LB and M9 medium six of these peptides were identified (**Figure 17**).

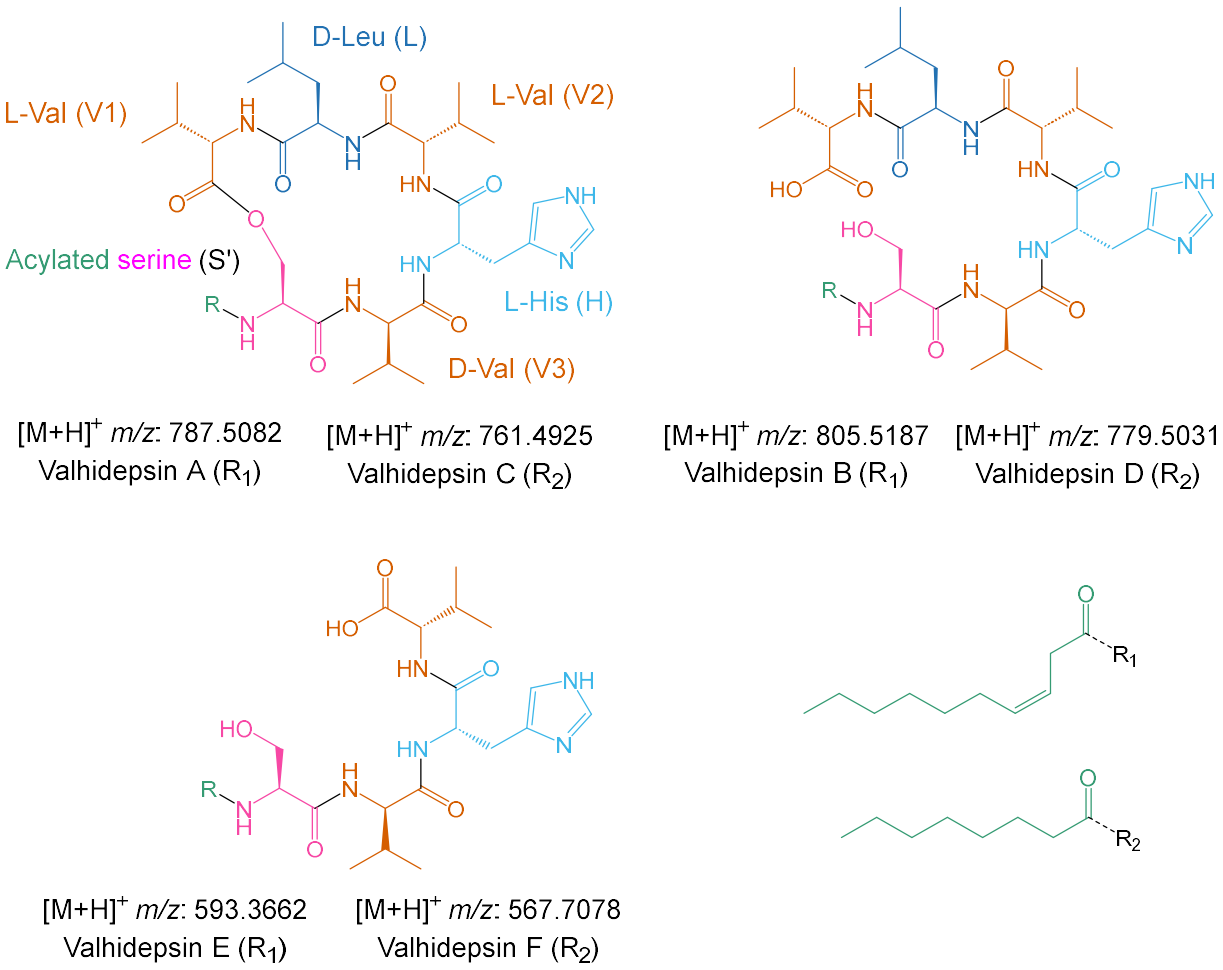

Figure 17: Structures of the six known valhidepsins[128] found in extracts of *Chromobacterium vaccinii* MWU205. Building blocks are colored and named exemplarily for valhidepsin A.

Cluster 2 was revealed to be the molecular family of the valhidepsins, as the *m/z* values 567.347, 593.363, 787.501, 761.487, 779.500, and 805.514 were identified as valhidepsins A-F according to their fragmentation spectra (**Figure 55** to **Figure 59**) which matched the described fragmentation pattern and the corresponding structures[128]. For the *m/z* values 751.468, 761.487, 765.483, 779.500, 787.501, and 805.514 two nodes were detected, one originating from LB medium extracts with a shorter retention time and one from M9 medium extracts with a longer retention time. Comparison of their fragmentation patterns (**Figure 55** to **Figure 58**, **Figure 60**) revealed all of these *m/z* pairs to be identical except for the *m/z* 765.483. As the measurements of the LB extracts were done separately from those of the M9 extracts, retention time shifts due to small variation in the conditions might have occurred. Therefore, five of six pairs were merged into one node in **Figure 18**, as their fragmentation patterns did not differ significantly, while both nodes with *m/z* 765.483 were left separated. In the original network created by the FBMN workflow (release_20), five nodes with *m/z* 793.474-793.477 were detected.

The detailed analysis of the extracted ion chromatograms for the *m/z* 793.476 (±0.01) revealed four peaks (RTs: 8.2 min, 8.5 min, 8.8 min, and 10.0 min). As the preprocessing by MZmine 2 was not able to separate the three early peaks (RTs: 8.2 min, 8.5 min, and 8.8 min) consistently in each sample, the nodes representing the three early peaks were merged into *m/z* 793.476 with a RT of 8.2 min, whereas *m/z* 793.476 with a RT of 9.9 min corresponds to the HPLC peak with a RT of 10.0 min. In total, seventeen valhidepsin analogues were identified, among them eleven unknowns, with one being unique for LB medium and nine unique for M9 medium.

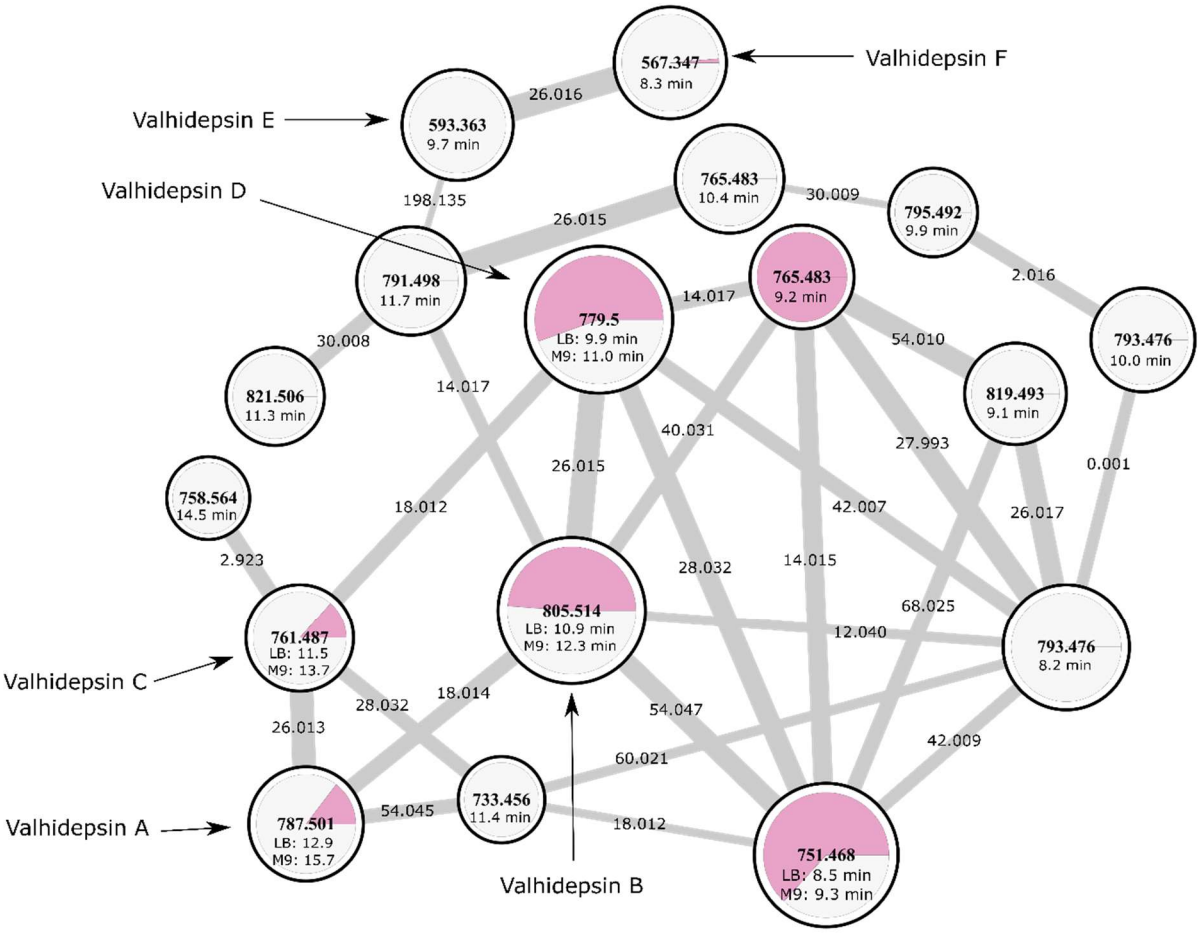

Figure 18: Molecular cluster of cyclic and linear valhidepsin lipopeptides (determined by MS^2) from the feature-based molecular network of *n*-butanol extracts of *Chromobacterium vaccinii* MWU205 cultivated in M9 and LB medium. Nodes display distinct *m/z* features, i.e., their parent mass and liquid chromatography retention time. Their size represents the number of spectra obtained and their color displays their origin (white: *C. vaccinii* MWU205 cultivated in M9 medium; red: *C. vaccinii* MWU205 cultivated in LB medium). The width of the edges corresponds to the similarity of the fragmentation spectra of the connected nodes and the display the mass difference between connected *m/z* values. Known and already published valhidepsins[128] are indicated by arrows and named.

Analyses of the fragmentation patterns of the proton adducts were performed and generated first hints for the structure of seven unknown compounds with *m/z* 733.456, 751.468, 765.483 (RT: 10.4 min), 765.483 (RT: 9.2 min), 791.498, and 793.476 (RT:

8.2 min), and 793.476 (RT: 10.0 min). For the remaining four unknown compounds with *m/z* values 758.566, 795.483, 819.493, and 821.506, the fragmentation patterns were not clear enough to draw any conclusion towards their structure. All cyclic lipopeptides were linearized by breakage of the ester between valine and serine, leading to similar fragmentation pattern for valhidepsin A and B (**Figure 19**) and valhidepsin C and D (**Figure 61**). Afterwards the linear peptide chain sequentially loses amino acids from the carboxy terminus, creating b-ions, their respective a-ions, and b-ions without water (b°).

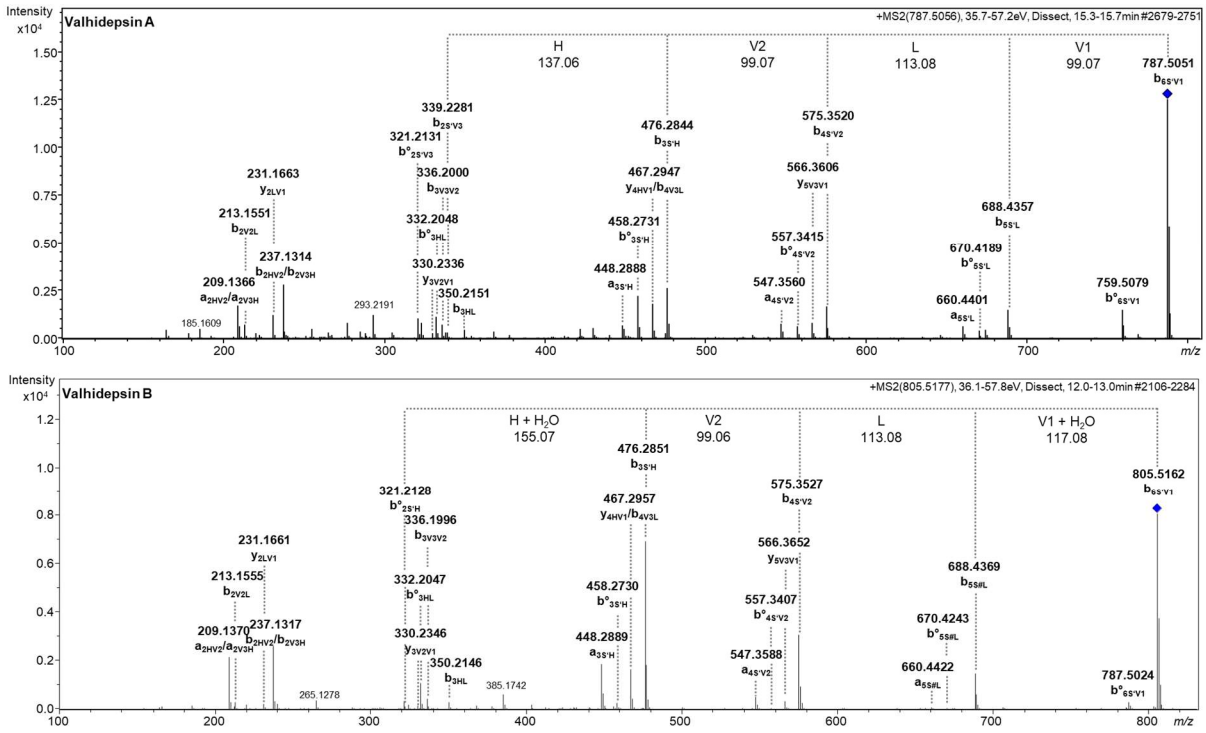

Figure 19: Fragmentation pattern of valhidepsin A (*m/z* 787.501) and valhidepsin B (*m/z* 805.514). Fragment ions were named following the nomenclature system by Ngoka[192] based on Biemanns modifications[193] of Roepstorffs nomenclature in one-letter amino acid code.[194] b° = b-ion with loss of water. S' = acylated serine.

For four compounds with *m/z* values 733.456 (RT: 11.4), 751.468, 793.474 (RT: 8.7), and 765.483 (RT: 9.2 min) structural changes compared to the known lipopeptides were pinpointed to the *N*-acyl-chain, which differed in its length and the presence of a carbon-carbon double bond, as observed for the known lipopeptides. For the derivative with *m/z* 733.456, a mass difference of 28.03 Da compared to valhidepsin C was most likely due to the loss of two CH_2 groups. The same observation was made for the compound giving rise to *m/z* 751.468 compared to valhidepsin D. As both of these *m/z* values for unknown compounds were connected in the network and had a mass difference of 18.01 Da to each other, the derivative with *m/z* 733.456 is most likely the cyclic form of the linear molecule with *m/z* 751.468 (**Figure 20**). In comparison to valhidepsin C and

D, both are hypothesized to have a C_6 acyl chain instead of the C_8 present in valhidepsin C and D. However, both methyl groups also could have been added at different sites of the acylated serine moiety.

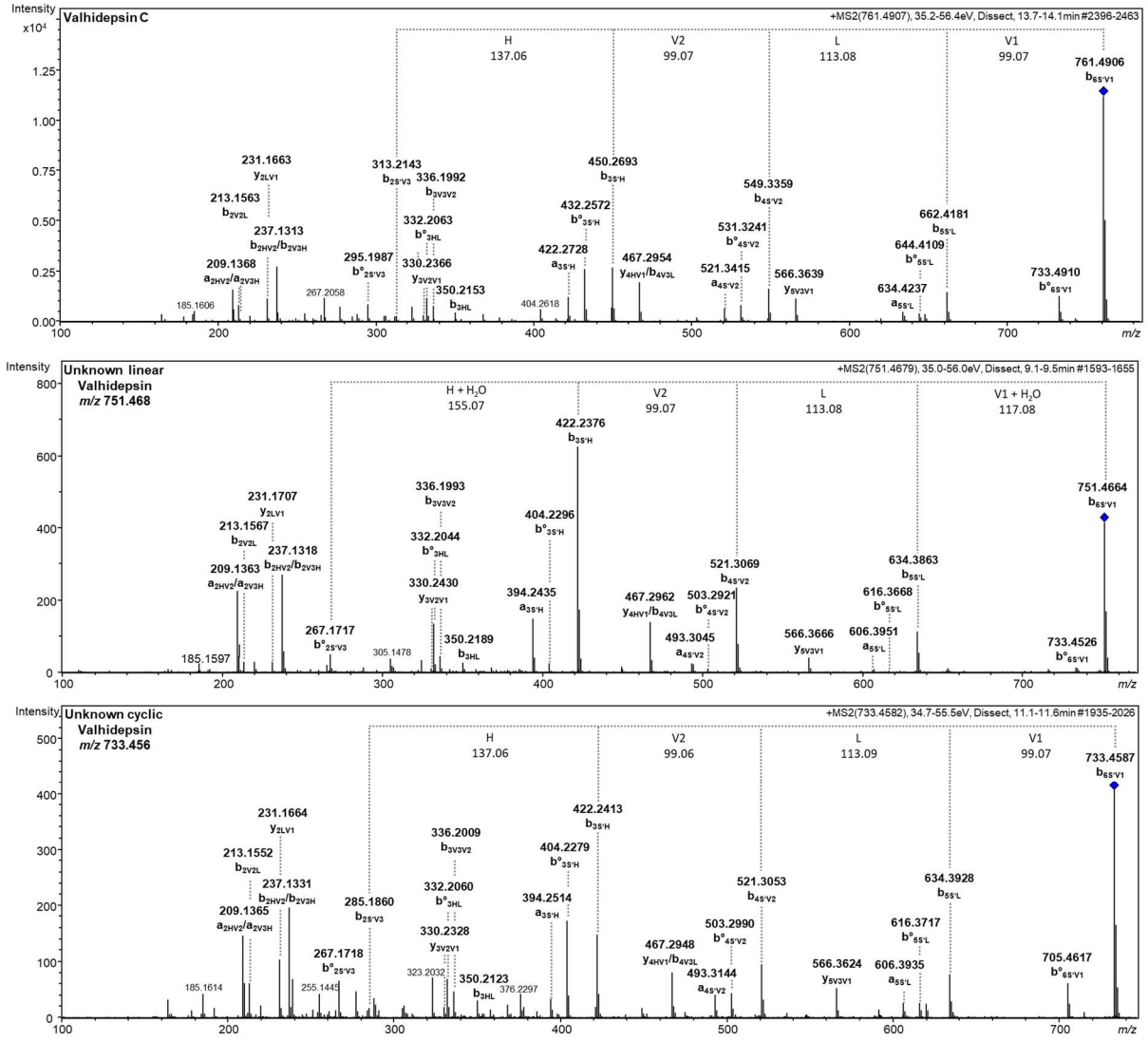

Figure 20: Fragmentation pattern of valhidepsin C (*m/z* 761.493) and the *m/z* values 751.468 and 733.456. Fragment ions were named following the nomenclature system by Ngoka[192] based on Biemanns modifications[193] of Roepstorffs nomenclature in one-letter amino acid code.[194] b° = b-ion with loss of water. S' = acylated serine.

The compound with *m/z* 765.483 (RT: 9.2 min) had a 14.03 Da mass difference compared to valhidepsin D, most likely caused by the loss of a CH_2 group in the valhidepsin acyl chain, as the change was located in the acylated serine. Both compounds giving rise to *m/z* 793.476 but distinguished by different retention times (8.2 min and 10.0 min), showed similar fragmentation patterns, but were not connected to a known valhidepsin. However, the derivative with *m/z* 793.476 (RT: 8.2 min) was related to the compound with *m/z* 765. 483 (RT:9.2 min). As the change of 27.99 Da was located in the

acylated serine, it probably corresponds to two CH_2 groups added to the acyl chain. Therefore, the four isomers found in extracts of *C. vaccinii* MWU205probably differed with regard to the presence of additional CH_2 groups. (**Figure 21**).

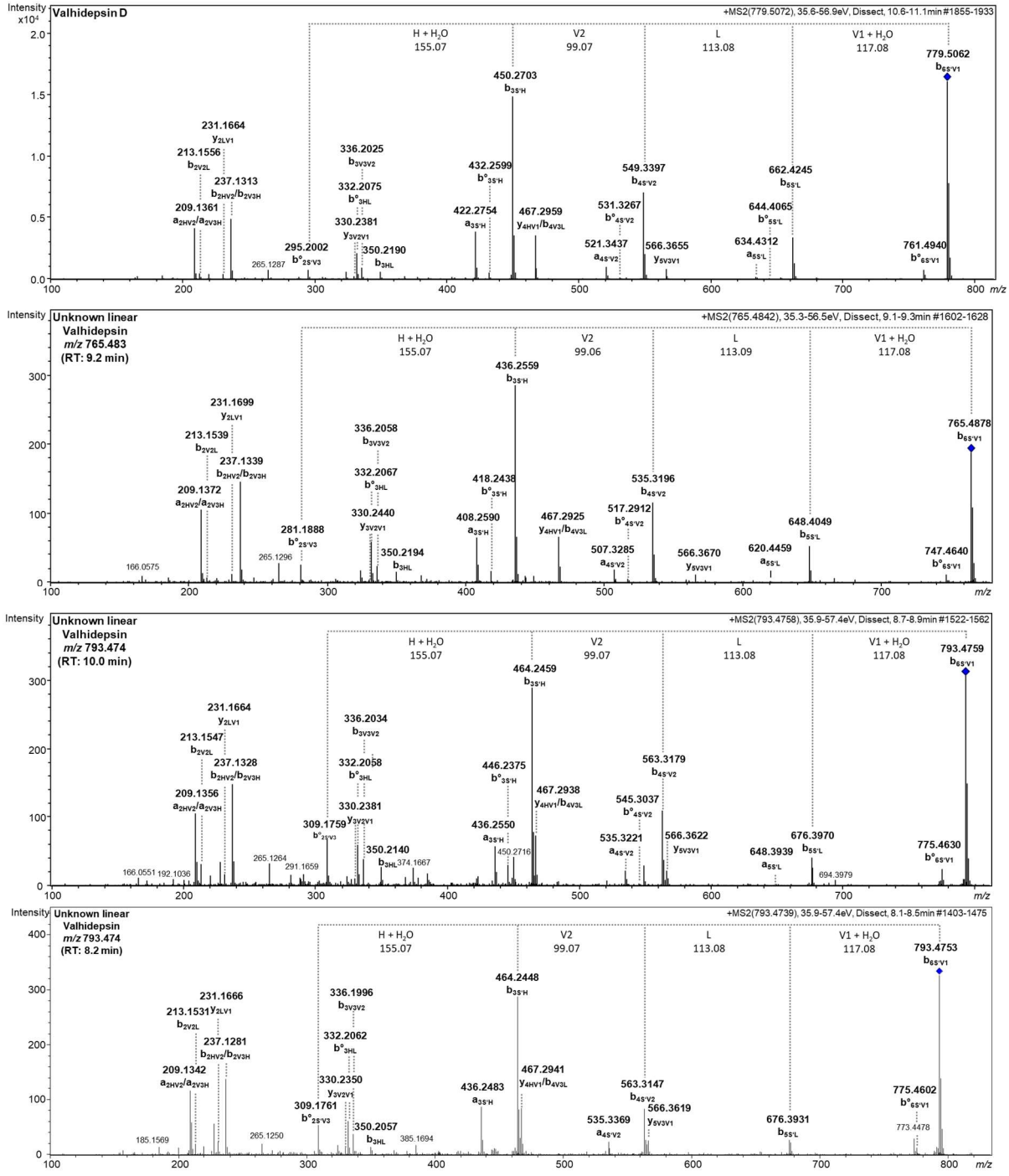

Figure 21: Fragmentation pattern of valhidepsin D (*m/z* 779.503) and the unknown *m/z* values 765.483 (retention time (RT): 9.2 min), and 793.474 (RT: 8.2 min and 10.0 min). Fragment ions were named following the nomenclature system by Ngoka[192] based on Biemanns modifications[193] of Roepstorffs nomenclature in one-letter amino acid code[194]. b° = b-ion with loss of water. S' = acylated serine.

The last two unknown derivatives with *m/z* values 765.483 and 791.498 did not only differ in the acyl chain, but in the peptide part of the molecule. Analysis of the

fragmentation pattern and mass difference of the compound with *m/z* 765.483 (RT: 10.4 min, Δ*m/z*: 14.03) compared to valhidepsin D clearly revealed the loss of a CH_2 group in the leucine moiety (**Figure 22**). As valine is the main building block of the valhidepsins, the replacement of the leucine moiety for a valine moiety is likely. For the molecule giving rise to *m/z* 791.498, connected solely to the derivative with *m/z* 765.483 (RT: 10.4), a similar fragmentation pattern suggested that this compound also contains valine instead of leucine and that the remaining mass difference of 26.02 Da was due to differences in the acyl moiety, indicating the formation of a double bond and addition of two CH_2 groups (**Figure 22**). This could be the same acyl moiety as present in valhidepsins A and B.

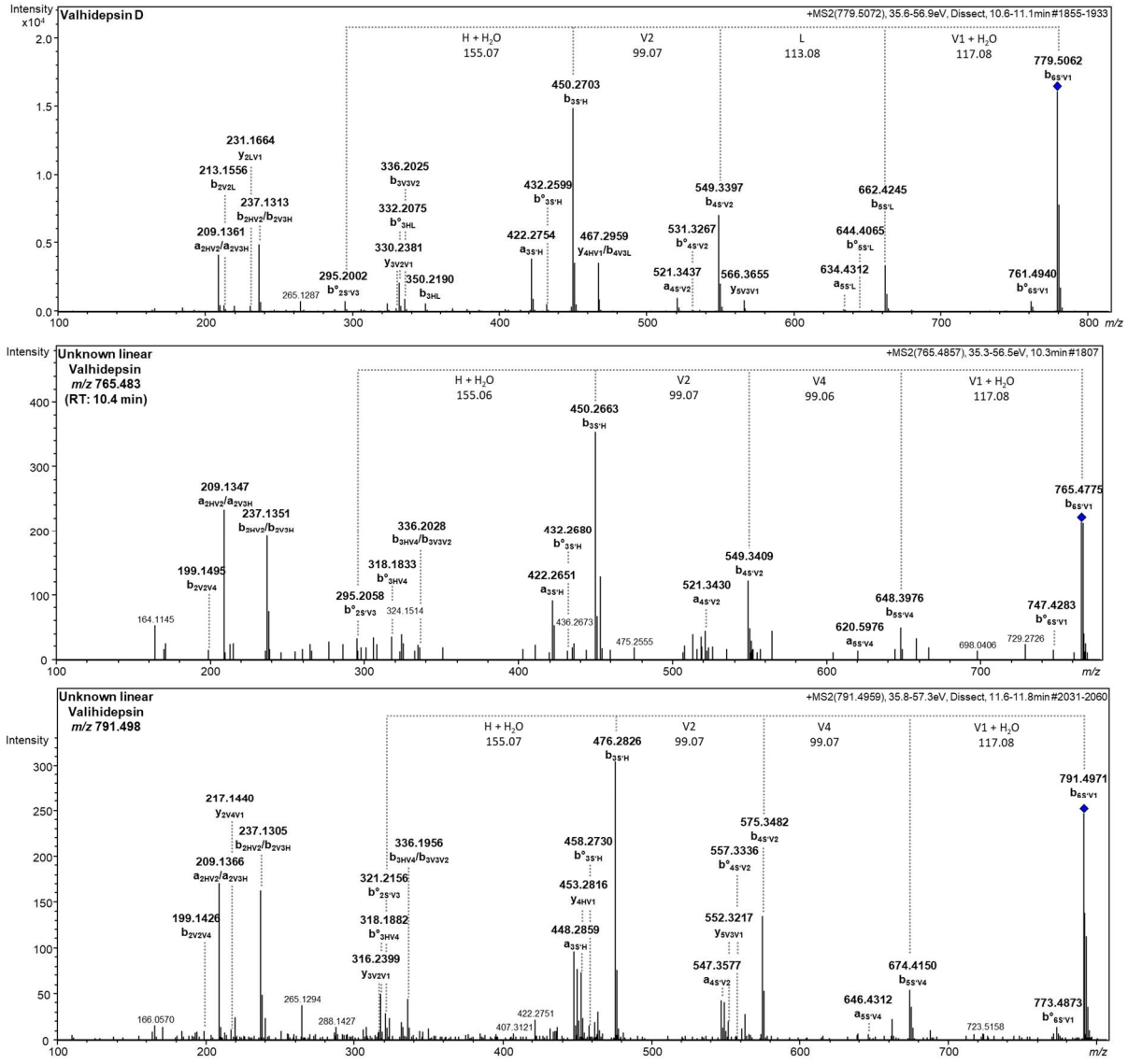

Figure 22: Fragmentation pattern of valhidepsin D (*m/z* 779.503) and the unknown *m/z* values 791.498 and 765.483 (retention time: 10.4 min). Fragment ions were named following the nomenclature system by Ngoka[192] based on Biemanns modifications[193] of Roepstorffs nomenclature in one-letter amino acid code[194]. b° = b-ion with loss of water. S' = acylated serine.

3.1.2.3. Molecular family of violacein

Bacteria of the genus *Chromobacterium* are known producers of the purple pigment violacein and also *C. vaccinii* MWU205 has been reported as violacein-producing bacterium[61]. The molecular family of violacein was identified as cluster 28 in the FBMN (**Figure 5 (A)**) and represents two compounds with *m/z* values 344.102 (RT: 9.6 min) and 328.107 (RT: 11.1 min) (**Figure 23 (A)**). According to the exact mass of violacein (343.0957 Da) and its fragmentation pattern, the compound giving rise to *m/z* 344.107 was identified as proton adduct of violacein (**Figure 23 (B)**)[78]. With a mass difference of 16.00 Da compared to violacein the derivative with *m/z* 328.109 was most likely deoxyviolacein lacking one oxygen. This was further supported by its fragmentation pattern, which revealed the indole moiety as the site of the structural difference (**Figure 23 (C)**).

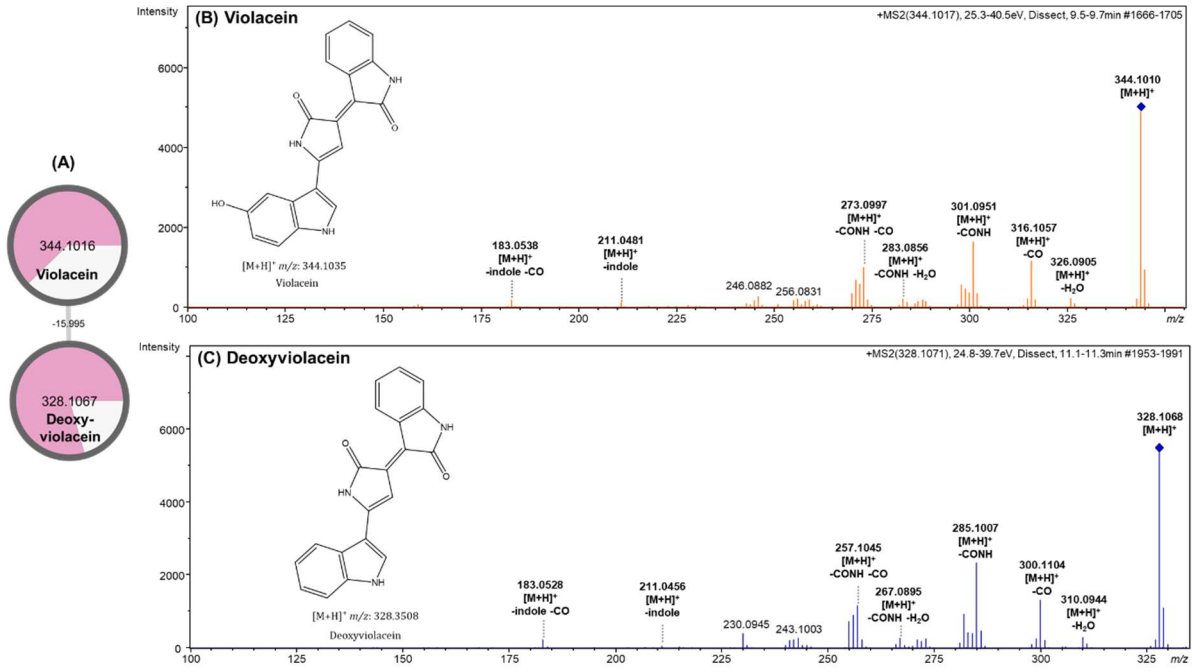

Figure 23: (A) Molecular cluster of violacein (determined by MS^2) from the feature-based molecular network. Data pool includes extracts of *Chromobacterium vaccinii* MWU205 cultivated in M9 and LB medium. Nodes display distinct *m/z* features, representing their parent mass. Their size represents the number of spectra obtained. The width of the edges corresponds to the similarity of the fragmentation spectra of the connected nodes and is labeled according to the mass difference. Node color displays their origin (white: *C. vaccinii* MWU205 cultivated in M9 medium; red: *C. vaccinii* MWU205 cultivated in LB medium). Structures and fragmentation patterns of violacein **(B)** and deoxyviolacein **(C)**[78].

3.1.3. Discussion

The antiSMASH and metabolome analysis of the soil bacterium *C. vaccinii* MWU205 led to the clear identification and subsequent analysis of three molecular families related to FR, valhidepsins, and violacein and their respective BGCs.

The detailed analysis of the molecular family of FR identified thirteen unique FR derivatives in extracts from *C. vaccinii* MWU205, while twelve unique compounds are found in the extracts of *A. crenata* plant leaves containing the bacterial endosymbiont *Cand.* Burkholderia crenata (**Figure 6**). Both FR producers, *C. vaccinii* MWU205 and *Cand.* Burkholderia crenata, were discovered to produce different FR derivatives, which might be explained by the ability of the biosynthetic enzymes to incorporate different building blocks. However, the comparison of *frs* BGCs in *C. vaccinii* MWU205 and *Cand.* Burkholderia crenata revealed that they are close to identical (**Table 16**)[130,199]. The other explanation for this different range of FR derivatives is the presence/absence of certain precursor molecules in the surroundings, which surely affects biosynthesis. For example, FR-1 contains *N*-3-HyProp-β-HyLeu instead of *N*-Ac-β-HyLeu (L') (**Figure 3**), therefore its biosynthesis requires the unusual 3-hydroxypropionate as a precursor. This precursor might not be produced by *C. vaccinii* MWU205 or is not available in the medium. To further investigate the biochemical background of the metabolic differences detected in this study, biosynthetic experiments like feeding experiments and bioinformatic analysis of the bacterial genomes are needed.

With the detailed analysis of the MS^2 fragmentation pattern, the structures of two new FR-Core derivatives were elucidated and named FR-Core 5 and FR-Core 6 (**Figure 10**). Furthermore, the analysis revealed first structural information, i.e., defining the structural change and pinpointing the change to one specific building blocks, on six new FR derivatives, i.e., *m/z* values 706.363 (RT: 8.7 min), 801.436 (RT: 13.0 min), 803.415 (RT:10.4 min), 831.443 (RT: 12.7 min), 833.425 (RT: 10.4 min), 974.503 (RT: 11.2 min). The structure of one new FR derivative, FR-6, was unambiguously established. First, FR-6 was identified by FBMN, then isolated from *C. vaccinii* MWU205 extracts, and the pure compound elucidated via LC/MS^2 and NMR subsequently. Compared to FR, FR-6 contains a *N*-Ac-β-HyLeu as side chain and a Thr moiety without the *O*-Me group but with a double bound, i.e., 2-methylamino-2-butenoic acid (**Figure 15**). FR-6 showed significantly lower inhibition of G_q signaling and lower binding affinity towards G_q compared to FR (**Figure 16**). Molecular docking studies suggested that the absence of the *O*-Me-group in the *N,O*-Me_2-Thr moiety of FR-6 (as compared to FR) reduced hydrophobic interactions with binding pocket residues in $G\alpha_q$. These investigations underline recent findings that almost the whole FR molecule constitutes the pharmacophore essential for binding and inhibition of G_q[200].

The FBMN allowed the analysis of the valhidepsin family of compounds as it connected the known valhidepsins A-F (**Figure 17**) and eleven new derivatives (**Figure 18**). With the help of MS^2 most of the structural changes were pinpointed towards the acylated serine moiety, except one derivative with a change in the leucine moiety. Therefore, the exact structure of these derivatives could not be elucidated using MS^2.

These findings underline the ability of molecular networking combined with the detailed analysis of the fragmentation pattern to investigate minor compounds and isolate new derivatives of known NPs. Nevertheless, the isolation of the pure compounds and subsequent structure elucidation via NMR is indispensable, as mass differences and fragmentation pattern analysis are not sufficient in most cases. For the isolation of compounds a big scale cultivation of *C. vaccinii* MWU205 combined with feeding experiments to enhance the production of minor metabolites can be used, as shown for the three FR derivatives, FR-7, FR-8, and FR-9 (**Figure 3**)[129]. All twelve FR derivatives and the majority of new valhidepsin derivatives were produced by *C. vaccinii* MWU205 in the minimal medium M9 (**Figure 6** and **Figure 18**), making M9 medium the perfect platform to investigate minor and novel derivatives, as shown by the isolation of FR-6 from M9 medium. This was also reported for violacein production in two *Janthinobacterium* strains, where minimal medium enhanced the production. This is further proof that the mimicking of environmental or nutritional stress increases the production of secondary metabolites[201,202]. Therefore, further attempts to isolate the new minor derivatives of both FR and valhidepsins should utilize M9 medium or other minimal media. Additionally, mutation of BGCs of *C. vaccinii* MWU205 might allow the isolation of novel and minor naturally occurring, but also engineered derivatives. One idea is to target specific domains, e.g., the C domain of FrsD, with point mutations that allow the incorporation of other precursors. Another possibility is the deletion of genes, modules, or domains, a method that has been used to isolate FR-Core by deletion of the *frsA* gene[130]. In the case of the FR biosynthesis, the C domain of FrsA and FrsD show high similarity and therefore may be exchangeable, an experiment that could broaden the incorporated building blocks by FrsD and enable the isolation of derivatives like FR-1 (**Figure 3**). These experiments are currently performed by Dr. Richarz and Christoph Ulbricht (AG König/Crüsemann, Institute of Pharmaceutical Biology, University of Bonn).

Apart from the identified clusters and BGCs, thirty-four unknown molecular families were found, and on the genetic level seven regions encoding for BGCs (**Figure 4**) for which no compound could yet be identified were discovered.

The prediction of an AHL BGC in the genome of *C. vaccinii* MWU205 (**Figure 4**, region 9) was expected, as violacein biosynthesis is regulated via QS, a signaling pathway involving AHLs. The production of AHLs was verified and investigated for different *Chromobacterium* strains[81,190,203,204]. However, none of the AHLs found in the other *Chromobacterium* spp. were chemically detected in the metabolome of *C. vaccinii* MWU205[205], which was reasonable, as AHLs are usually extracted using chloroform, dichloromethane, acidified ethyl acetate, and hexane[206], but not with *n*-butanol.

The identification of a BGC for chromobactin and one related to viobactin in the genome of *C. vaccinii* MWU205 (**Figure 4**, regions 3 and 7) showed that the production of these siderophores might not be restricted to *C. violaceum*[102]. Siderophores are iron-binding secondary metabolites, which make iron available for their bacterial producer and other surrounding organisms like plants, thereby promoting their growth. Additionally, the utilization of siderophore-producing bacteria as biofertilizers may inhibit plant pathogens by reducing the amount of available iron for the growth of pathogens[207–210]. Siderophores are divided according to their chemical nature into catecholates and phenolates, hydroxamates, carboxylates, and mixed type siderophores[208]. Viobactin and chromobactin are synthesized by NRPS and belong to the catecholate-type[102] but their exact structure has remained unknown. In order to elucidate these structures, the siderophores of *C. vaccinii* MWU205 may be isolated using iron-deficient media instead of the iron-supplemented M9 and iron-rich LB medium for cultivation[211–213].

The genome analysis predicted a 2,4-diacetylphloroglucinol-related BGC in the genome of *C. vaccinii* MWU205 (**Figure 4**, region 6). 2,4-diacetylphloroglucinol is produced by plant-beneficial *Pseudomonas* spp. and has been shown to suppress plant pathogens thereby controlling soil-borne plant diseases[191,214–216]. Only recently, the presence of the 2,4-diacetylphloroglucinol BGC has been investigated for the genus *Chromobacterium*, including *C. vaccinii* MWU205, and revealed a novel potential ability to promote plant health[126]. Again, as in the case of AHLs, the solvents applied in this study may not dissolve and extract the product produced by the predicted BGC[217,218] and thus was not detected in the metabolome analysis.

For the remaining four BGCs (**Figure 4**), i.e., one related to terpene biosynthesis, one PKS-like system, one NRPS-associated pathway, and one belonging to the β-lactone type, the similarity to known BGCs was too low to draw further conclusions on their products.

The first analysis with the GNPS FBMN workflow was conducted in 2021[1]. Since then, newer versions of the FBMN workflow were released, hence a re-analysis with the current version (release_28.2) from 2023 was performed and the resulting network was very similar to the previous FBMN (**Figure 62**). Clusters for FR, valhidepsins, and violacein, were rediscovered and contained most of the nodes found in the previous molecular families. However, some nodes and connections disappeared in the results obtained with the current version (release_28.2) from 2023, which demonstrates the difficulties of working with external bioinformatic tools. One of the most striking differences between the results from the versions of 2021 and 2023 was the lack of connection between the known valhidepsins, as valhidepsin E and F formed a separate cluster in the network calculated with the version from 2023. The findings in this study verify most of the results from 2021 and underline the importance of a detailed manual analysis to investigate the total spectrum of molecules.

The ecological relevance of *C. vaccinii* MWU205 has been investigated before, as a first draft genome analysis in 2015 revealed *C. vaccinii* MWU205 to possess genes of which the products may be virulence factors towards insect larvae, like violacein, siderophores, hydrogen cyanide, and chitinases[219]. This thesis confirms the production of violacein and further reveals the potential of *C. vaccinii* MWU205 to support plant growth by the detection of BGCs for siderophores and 2,4-diacetylphloroglucinol. The bioinformatic and metabolome analyses underline the potential of *C. vaccinii* MWU205 as source for NPs with ecologically relevant bioactivities. Next steps in order to further investigate the metabolome of *C. vaccinii* MWU205 are the heterologous expression of BGCs of unknown compounds, the cultivation of *C. vaccinii* MWU205 under different conditions allowing the isolation of other NP classes like siderophores, and the utilization of other extraction solvents. To examine the ecological effect of *C. vaccinii* MWU205 in its natural habitat, its secondary metabolites, e.g., FR, valhidepsins, and violacein, should be tested for production under the natural conditions and investigated for bioactivities that affect the natural surrounding organisms. This study focusses on the ecological role of the cyclic depsipeptide FR. For the other secondary metabolites further studies need to be conducted.

3.2. Feeding experiments with *C. vaccinii* MWU205

Complex culture media allow many bacteria to grow without restrictions, but are a limitation if certain precursor molecules, influencing the production of metabolites, shall be added or exchanged. Using minimal media like M9 medium, it is possible to exchange components, e.g., to generate isotope-labeled molecules, or to add certain precursors to investigate their influence on the produced metabolite spectrum. The feeding of isotope-labeled precursors is used to investigate biosynthetic pathways[220,221], to elucidate the structures of target molecules if combined with methods like LC/MS^2 and NMR[222,223], and to generate labeled compounds that may function as internal standards for quantitative LC/MS measurements[224] and also to allow detailed NMR analysis. Feeding precursor molecules to bacterial cultures grown in minimal or even complex medium can shift the spectrum of derivatives produced by a biosynthetic pathway[129,130]. This influence can be used to optimize the production of specific derivatives and to investigate the flexibility and substrate specificity of biosynthetic enzymes.

3.2.1. Generation of completely $^{13}C/^{15}N$-labeled FR

Within the framework of the research group FOR2372, the completely $^{13}C/^{15}N$-labeled FR was crucial for the detailed investigations of the structure of FR using NMR and for the examination of the binding of FR to G_q using solid-state NMR (project of Prof. Glaubitz, Institute for Biophysical Chemistry and Centre for Biomolecular Magnetic Resonance, Goethe University Frankfurt/Main, FOR2372). After establishing the minimal medium M9 as suitable medium for the cultivation of *C. vaccinii* MWU205 and FR production[225], it was now possible to exchange certain components of the minimal media for their labeled counterparts. This was done for the nitrogen source (NH_4Cl), which was exchanged for $^{15}NH_4Cl$, and for the carbon source glucose, which was exchanged for the U-^{13}C-labeled analog, as described in **chapter 5.6.3**. First, a cultivation experiment with 2 L, was performed to test whether the incorporation was successful. After cultivation for 48 h at 25 °C and extraction with *n*-butanol, the extract was separated via flash chromatography as described in **chapter 5.8.1**. According to previous FR isolations, the flash chromatography peak around 60 min was collected and investigated in detail using NMR and LC/MS^2. ^{1}H-NMR and LC/MS^2 measurements confirmed the presence of FR (**Figure 63**, **Figure 24**). The *m/z* value of 1058.684 was detected, which matched the expected *m/z* value for completely $^{13}C/^{15}N$-labeled FR (**Figure 24 (A), (C)**). Further

investigations of the fragmentation pattern verified the complete labeling of all fragments known for the FR fragmentation pattern (**Figure 24 (B), (D)**). However, upscaling of the cultivation to 10 L for the isolation of labeled FR did, after employing the established work-up protocol, only result in 3 mg $^{13}C/^{15}N$-FR and 55 mg $^{13}C/^{15}N$-FR-2.

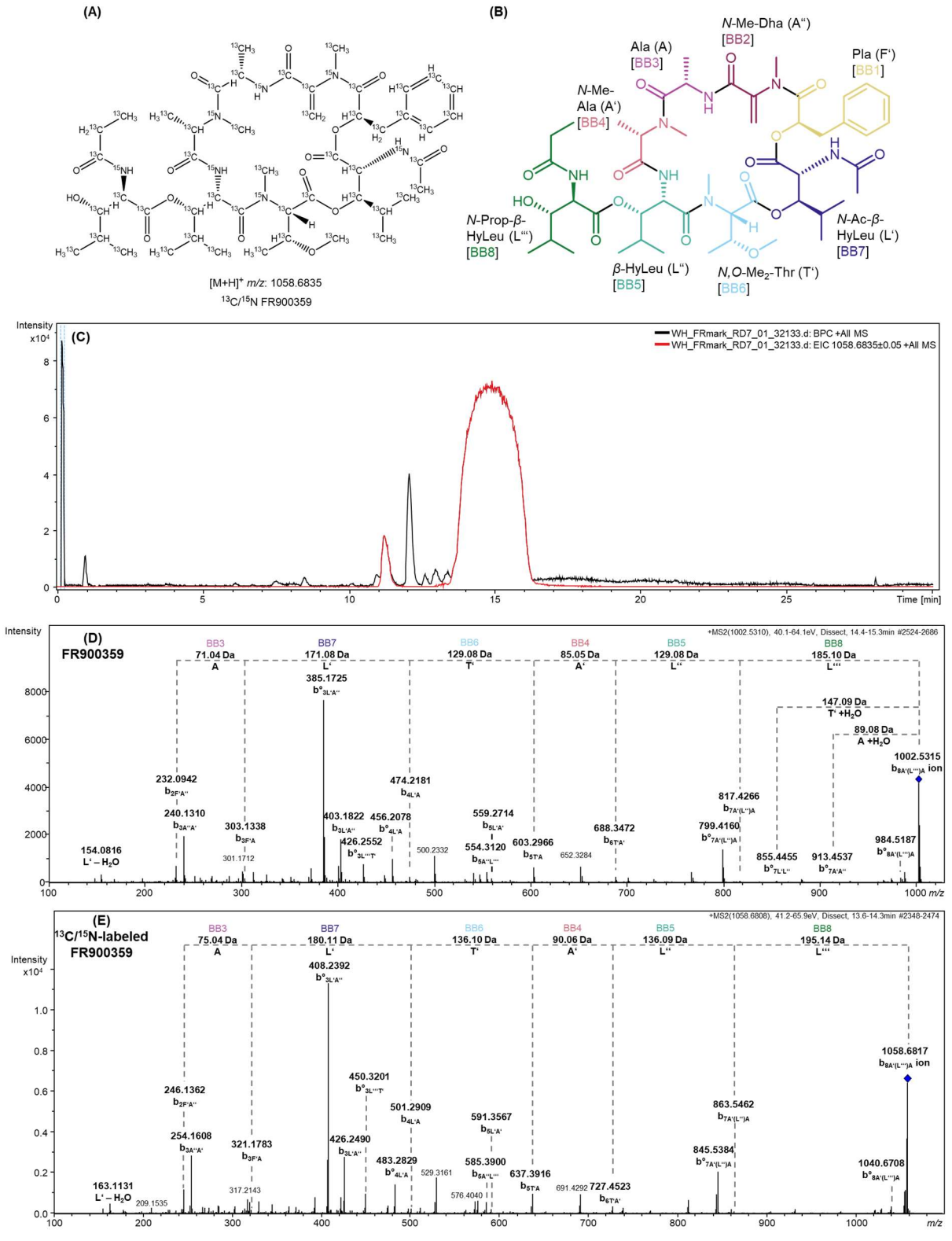

Figure 24: (A) Structure and exact mass of the proton adduct of the completely $^{13}C/^{15}N$-labeled FR900359 (FR). **(B)** Structure of the unlabeled FR with colored and named building blocks. **(C)** LC/MS^2 chromatogram of the FR fraction collected after 60 min and extracted ion chromatogram (EIC) for the *m/z* of the completely labeled FR. Fragmentation pattern of FR **(D)** and completely $^{13}C/^{15}N$-labeled FR **(E)** with fragments labeled following the nomenclature system by Ngoka[192] based on Biemanns modifications[193] of Roepstorffs nomenclature in one-letter amino acid code.[194] b° = b-ion with loss of water. L' = *N*-Ac-β-HyLeu, A = Ala, A' = *N*-Me-Ala, T' = *N,O*-Me_2-Thr, L''' = *N*-Prop-β-HyLeu, L'' = β-HyLeu, F' = Pla, A'' = *N*-Me-Dha.

The shift of the production titers from FR to FR-2 in M9 medium has already been observed during the comparison of the FR production curves by *C. vaccinii* MWU205 grown in M9 and LB medium (**Figure 25 (A)**). In both media, the production peaked after 36 h of cultivation but afterwards the amount of FR decreased in LB medium while its production in M9 medium remained stable over the course of 7.5 days. For FR-2 a similar observation was made, but in M9 medium, the area under the curve (AUC) of the FR peak seemed to be larger compared to FR (**Figure 25 (B)**)[225].

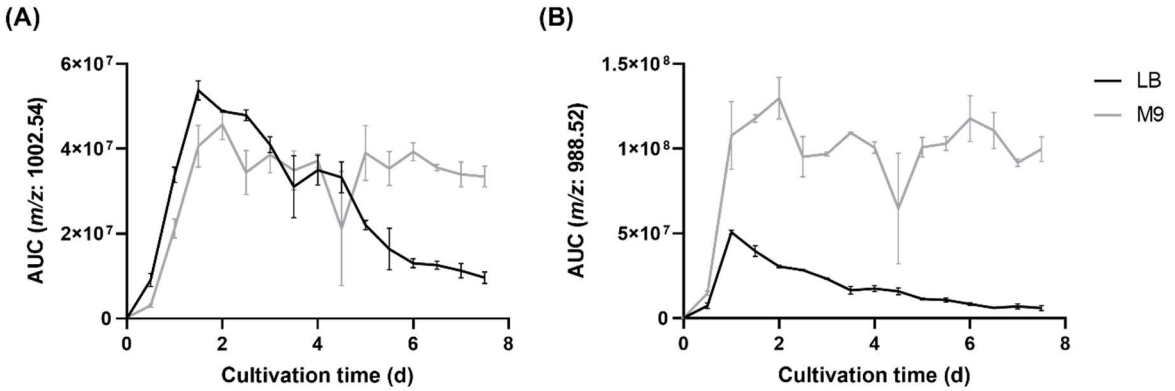

Figure 25: Production of FR900359 measured via LC/MS as area under the curve (AUC) for the *m/z* 1002.54 **(A)** and FR-2 measured as AUC for the *m/z* 988.52 **(B)** by *Chromobacterium vaccinii* MWU205 cultivated in LB medium (black) and M9 medium (grey) over 7.5 d. Error bars show the standard deviation of two repeats. Figures adapted from Hanke, 2018[225].

As FR and FR-2 only differ in the incorporation of acetic acid instead of propionic acid (PA), respectively in the side chain (**Figure 3**) two explanations were possible, i.e., the abundance of PA could be different in the applied media and the pH of the medium might have influenced the FR/FR-2 production. To test the first explanation a small scale experiment with PA fed to *C. vaccinii* MWU205 in M9 medium was conducted as described in **chapter 5.6.4.** The *n*-butanol extracts were analyzed via LC/MS and depicted an increase of the FR *m/z* AUC when PA was fed. Subsequently, the AUC of the *m/z* of FR-2 decreased in presence of PA (**Figure 26**). This result suggested that the production of PA by *C. vaccinii* MWU205 in M9 medium is lower and therefore the precursor is less abundant. This was utilized to enhance the production of completely $^{13}C/^{15}N$-labeled FR by adding ^{13}C-labeled PA to 4.5 L of culture. After purification, 40 mg (8.9 mg/L) of completely $^{13}C/^{15}N$-labeled FR were isolated from 4.5 L.

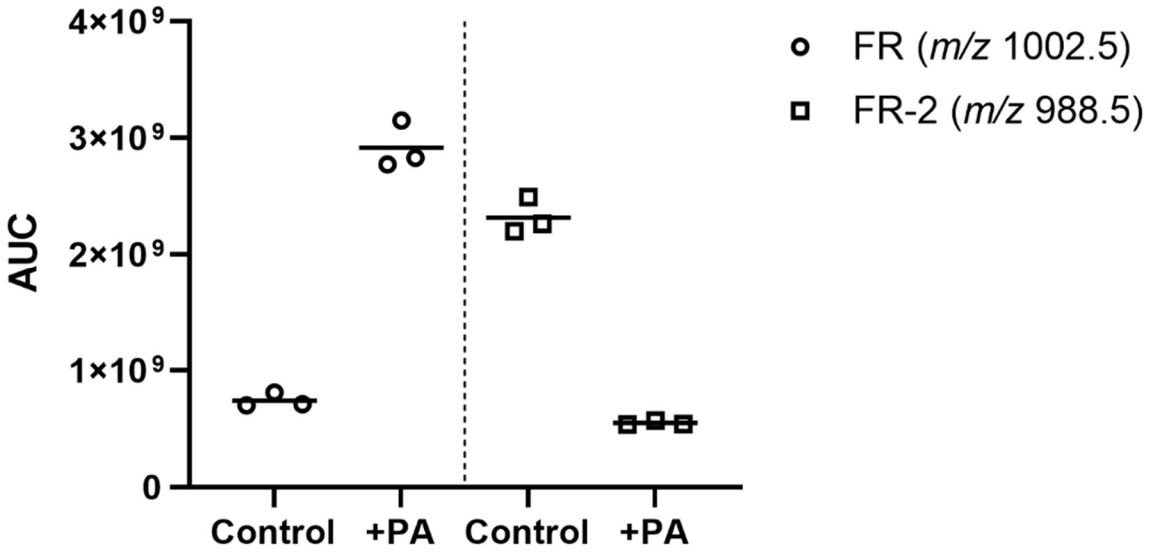

Figure 26: Production of FR900359 (FR) measured via LC/MS as area under the curve (AUC) for *m/z* 1002.54 (circle) and FR-2 measured as AUC for *m/z* 988.52 (rectangle) by *Chromobacterium vaccinii* MWU205 cultivated in LB medium with and without [Control] 5 mM propionic acid [+PA]. All experiments, n = 3.

3.2.2. Non-labeled precursor feeding

The mass spectrometric analyses of the FR molecular family described in **chapter 3.1.2.1** revealed that most FR derivatives produced by *C. vaccinii* MWU205 show their structural changes in certain building blocks, i.e., the three β-HyLeu moieties, the *N,O*-Me_2-Thr, the Pla, and the *N*-Me-Ala moiety. Therefore, feeding experiments were conducted to investigate the substrate flexibility of the FR synthetase towards two of the four moieties, i.e., the β-HyLeu and the Pla moieties.

3.2.2.1. Feeding carboxylic acids to *C. vaccinii* MWU205

In a previous study, feeding butyric acid to *C. vaccinii* MWU205 in LB medium resulted in the formation of FR-5 (**Figure 3**), a derivative with a *N*-butyryl-β-HyLeu side chain[130]. Additionally, most characterized derivatives, e.g., FR-2 and FR-1, differ in the acyl chain of one of the two *N*-acylated-β-HyLeu. Both *N*-Ac-β-HyLeu and *N*-Prop-β-HyLeu are synthesized starting from β-Leu, which is activated by the A domains of FrsA and FrsD and bound to the FrsA/D T domains. Subsequently, the leucine β-hydroxylation by FrsH occurs, followed by *N*-acylation catalyzed by the starter C domains of the respective modules[130,143,150]. These starter C domains seem to have a low substrate specificity, therefore feeding experiments with isobutyric (iBA), valeric (VA) and isovaleric acid (iVA) were conducted to further examine the flexibility *in vivo*. The experimental design is

described in **chapter 5.6.4**. For the experiment with iBA, a new FR derivative with an *m/z* of 1016.56 was expected. As **Figure 27 (A)** shows, the *C. vaccinii* MWU205 wildtype produced a minor compound with the *m/z* 1016.56 with unknown structure (RT: 16.0 min). The production of this ion was increased 6-fold by feeding compared to wildtype extracts. A similar result was observed when feeding iVA and VA for the *m/z* 1030.57 (**Figure 27 (B)**), as a 3-fold increase of the peak occurred. These initial experiments underline the proposed flexible substrate specificity of the C domains of FrsA and FrsD. However, compared to the nearly 50-fold increase detected for the butyric acid feeding done by Dr. Hermes[226], the observed increase was not thought to be enough to isolate the novel compounds.

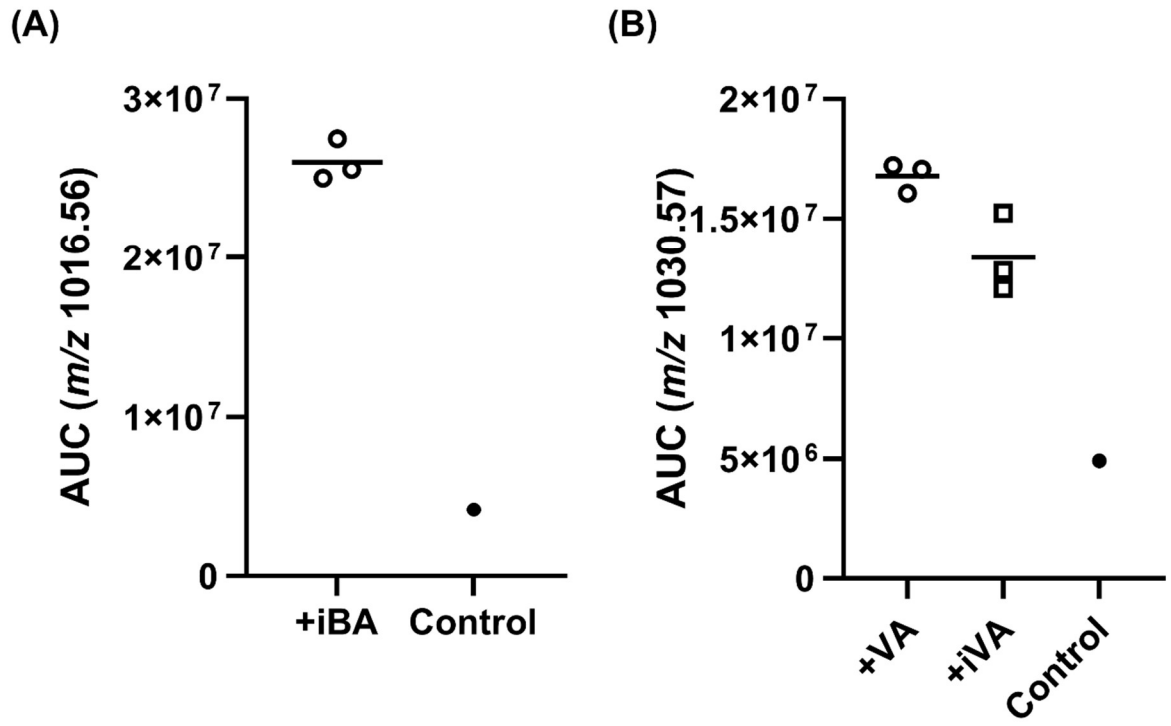

Figure 27: Production of derivatives with *m/z* 1016.56 and *m/z* 1030.57 as area under the curve (AUC) for *n*-butanol extracts of *Chromobacterium vaccinii* MWU205 LB medium cultures fed with **(A)** isobutyric [+iBA], **(B)** valeric [+VA] and **(B)** isovaleric acid [+iVA] compared to *n*-butanol extracts of *C. vaccinii* MWU205 LB medium cultures without feeding [Control]. For the feeding experiments three repeats were performed and measurement was done via LC/MS.

3.2.2.2. Feeding 3-Fluoro-DL-phenylalanine to *C. vaccinii* MWU205

Previous feeding experiments with 3-Fluoro-DL-phenylalanine (*meta*-F-Phe) resulted in the production of a compound with *m/z* 1020.528, with a structural change in the Pla moiety[225]. The precursor phenylpyruvic acid is derived from phenylalanine

metabolism and transformed during the FR biosynthesis by FrsC and FrsE module 3 into D-Pla[148,149]. Three FR derivatives, *m/z* 833.425, 1004.514, 1018.528, were found in the extracts of *C. vaccinii* MWU205 cultivated in M9 medium (**Figure 6**). These compounds were hypothesized to have a hydroxylated D-Pla moiety (**Figure 11**), and thus changes at the benzyl ring of the Pla moiety seem to be tolerated by FrsE and the subsequent domains of FR biosynthesis enzymes.

To verify and optimize the production of the desired fluorinated FR derivative, the experiment with the *meta*-F-Phe was repeated in M9 medium as described in **chapter 5.6.4**. However, *C. vaccinii* MWU205 did not grow in M9 medium supplemented with *meta*-F-Phe and therefore no peak was observed in the EIC for *m/z* 1020.5 (**Figure 28**). Fluorinated amino acid analogs have been reported as growth inhibiting and toxic for organisms like bacteria, which might explain the lack of growth observed[227–230]. In an attempt to avoid the possible toxic effects of the fluorinated Phe the precursor was added after 20 h of cultivation, using an LIS system as described in **chapter 5.6.4**. This allowed growth of *C. vaccinii* MWU205 but did not yield any increased AUC for *m/z* 1020.5 compared to the control (**Figure 64**).

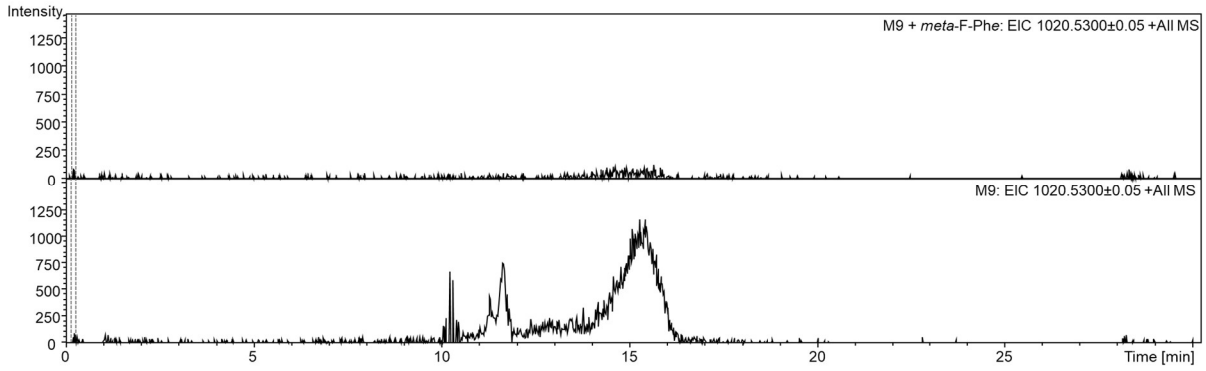

Figure 28: Comparison of the extracted ion chromatograms measured via LC/MS for the *m/z* 1020.53 in *n*-butanol extracts of *Chromobacterium vaccinii* MWU205 cultivated in M9 medium for 36 h with or without the addition of *meta*-F-Phe.

To investigate whether the *C. vaccinii* MWU205 mutant lacking the violacein production (*C. vaccinii* Δ*vioA*) does accept *meta*-F-Phe, feeding experiments were performed by master student Goran Grujičić under my supervision as described in **chapter 5.6.4**. As shown in **Figure 29 (A)** the AUC of the *m/z* 1020.5 increased 9-fold and verified the incorporation of *meta*-F-Phe. As fluorinated pharmaceuticals represent 20 % of all drugs on the market, the isolation from a big scale cultivation, i.e., 4.5 L, of *C. vaccinii* Δ*vioA* fed with *meta*-F-Phe was pursued. The subsequent flash chromatography was performed as described in **chapter 5.8.1** did not show two distinct peaks for FR and the

meta-F-FR derivatives, as the LC/MS analysis of fraction 2 and 3 revealed both fractions to contain mostly FR and the compound with an *m/z* of 1020.5 (**Figure 65**). Nevertheless, the incorporation worked and the purification of the fraction via HPLC is the next step.

To test if the position of the additional fluorine at the ring is important, feeding of 4-fluoro-DL-phenylalanine (*para*-F-Phe) and 2-fluoro-DL-phenylalanine (*ortho*-F-Phe) was tested. **Figure 29 (B)** shows that the phenylalanine containing fluorine at the *ortho*-position was incorporated, as a 29-fold increase of the AUC for the *m/z* 1020.5 was observed, while an exchange at the *para*-position was not accepted. Taken all findings together, changes in the *meta*- and *ortho*-position of the Pla moiety are accepted, while changes in the *para*-position are not.

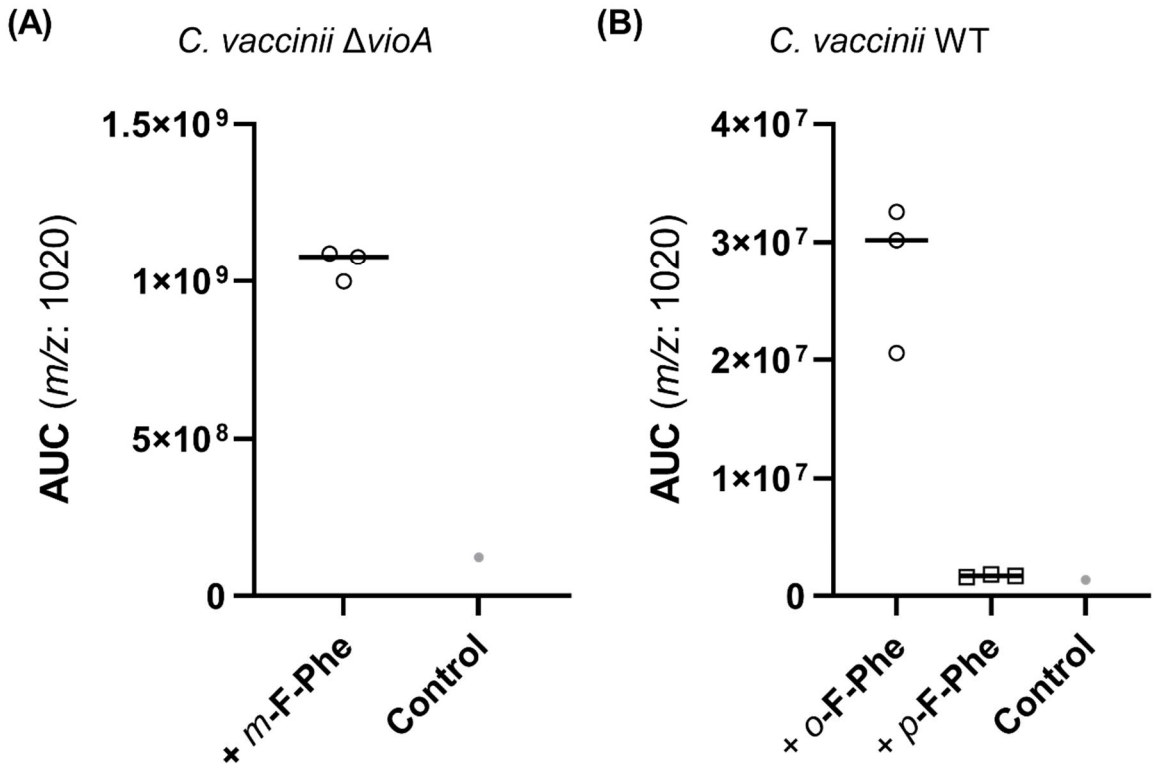

Figure 29: (A) Production of derivatives with *m/z* 1020.5 displayed as area under the curve (AUC) in *n*-butanol extracts of *Chromobacterium vaccinii* MWU205 Δ*vioA* cultivated in LB medium for 36 h at 25 °C fed with *meta*-F-Phe compared to *n*-butanol extracts of *C. vaccinii* MWU205 cultures without feeding [Control]. **(B)** Production of derivatives with *m/z* 1020.5 displayed as area under the curve (AUC) in *n*-butanol extracts of *C. vaccinii* MWU205 wildtype (WT) cultivated in LB medium for 36 h at 25°C fed with *ortho*-F-Phe and *para*-F-Phe compared to *n*-butanol extracts of *C. vaccinii* MWU205 cultures without feeding [Control]. For the feeding experiments three repeats were performed and measurement was done via LC/MS.

3.2.3. Discussion

M9 medium is a minimal and chemically defined medium, thereby offering two advantages compared to LB medium; (i) it mirrors in some ways the nutritional stress in a natural environment and (ii) it simplifies the generation of completely $^{13}C/^{15}N$-labeled compounds, as its nitrogen or carbon sources are defined and thus exchangeable for the isotope-labeled ones. The disadvantage that the FR biosynthesis in M9 medium produces more FR-2 than FR was overcome in this study by shifting the production to FR with PA. Cultivation of *C. vaccinii* MWU205 in M9 medium with labeled precursors enabled the complete ^{13}C and ^{15}N labeling of FR (**Figure 24**), which was isolated in pure form for analysis and further application. The completely $^{13}C/^{15}N$ labeled FR isolated in this study was used for intensive NMR analysis, i.e., the structure elucidation of FR via NMR using natural solvents like water or buffer instead of organic solvents, and the investigation of the binding to G_q with solid state NMR. These investigations were done by Christian Bonifer (AK Glaubitz, Institute for Biophysical Chemistry and Centre for Biomolecular Magnetic Resonance, Goethe University Frankfurt/Main) and will soon be published (correspondence with Christian Bonifer). Furthermore, the completely $^{13}C/^{15}N$-labeled FR can be utilized as internal standard for LC/MS measurements to quantify FR, e.g., in soil samples.

Adding isobutyric, valeric, and isovaleric acid to culture media in feeding experiments did increase the AUC of the expected *m/z*, i.e., 1016.56 and 1030.57, pointing towards an incorporation (**Figure 27**). Thus, an FR derivative with an *N*-isobutyryl-β-HyLeu (*m/z* 1016.56), one with *N*-valeryl-β-HyLeu (*m/z* 1030.57), and one FR derivative with *N*-isovaleryl-β-HyLeu (*m/z* 1030.57) were probably formed. However, LC/MS^2 measurements are necessary to verify this structural proposal by fragmentation pattern analysis. If these measurements verify the incorporation of isobutyric, valeric, and isovaleric acid in the side chain of FR, it will confirm the higher substrate flexibility of the C domain of FrsA compared to the C domain of FrsD observed in *in vitro* assays[130]. Different precursor concentrations, the use of other media like M9 medium, and the feeding of the precursor to *C. vaccinii* MWU205 mutant strains like Δ*vioA* may enable the production of higher amounts and should be tested. Following the observed incorporation even longer acids may be fed to test the limits of the substrate flexibility. Apart from the natural acceptance of precursors, the exchange of the FrsD C domain with the highly similar but not identical FrsA C domain[130], either completely or with point mutations,

should be performed to test whether the substrate flexibility of FrsD could be increased. Natural minor derivatives like FR-3 (**Figure 3**), also known as sameuramide A may be produced in higher amounts as a result.

The addition of different monofluorinated phenylalanines to cultures of *C. vaccinii* MWU205 confirmed that FrsE, responsible for the incorporation of the Pla moiety, which is biosynthetically derived from phenylalanine, tolerated changes in *meta*- and *ortho*-position, but not in the *para*-position (**Figure 28**). Investigations with 4-hydroxy-phenylpyruvic acid and 4-hydroxy-phenyllactic acid, both hydroxy groups at the *para*-position, showed low incorporation rates for the A domain of FrsE and FrsC *in vitro*, which is in line with the lack of incorporation of *para*-F-Phe[148]. The acceptance of *meta*- and *ortho*- but not *para*-substituted precursors has been observed for the synthesis of pyrophen produced by *Aspergillus niger*[231] and alamethicin F50 and trichokonin VI isolated from *Trichoderma* spp.[232]. For the novel compounds (*m/z* 833.425, 1004.514, and 1018.528), which were hypothesized in **chapter 3.1.2.1.1** to contain a hydroxylated Pla moiety, it is reasonable to suspect the hydroxy group in either *meta*- or *ortho*-position. To test this hypothesis the feeding of *meta*- and *ortho*-tyrosine should be tested.

While fluorine is only found in a small number of organic compounds in nature, 20 % of all pharmaceuticals are fluoro-pharmaceuticals. There are several reasons for the use of fluorine in pharmaceuticals; (i) it is best suited to replace hydrogen without changing structures drastically, (ii) the C-F bond often increases the metabolic stability of a drug, (iii) F induces bond polarity due to its electronegativity, that may alter lipophilicity and pK_a values, and (iv) it can be used as a bioisostere of the hydroxyl group[233]. Therefore, the generation of a fluorinated FR might be interesting for its further development as drug candidate. Regarding the isolation of the fluorinated FR derivatives the purification via HPLC might be difficult due to its similar retention time as FR (RT: 14.7 min) and the compound with *m/z* 1020.5 (RT: 15.4 min) observed in the LC/MS and was therefore not completed in this study. Nevertheless, the separation via HPLC should be further pursued.

Taken together, feeding experiments allowed the generation of isotope-labeled FR. They allowed the optimization of the FR production in M9 medium by influencing the FR/FR-2 ratio. Furthermore, feeding experiments revealed new insights regarding the substrate specificity of the biosynthetic enzymes, e.g., FrsA and FrsE. The knowledge obtained from the metabolome analysis of *C. vaccinii* MWU205 in **chapter 3.1.2.1** helped to select specific precursors for feeding experiments and thus proved to be a successful

method to influence the secondary metabolite production of *C. vaccinii* MWU205. Further "targeted feeding experiments" could be performed focusing the *N,O*-Me_2-Thr and the *N*-Me-Ala moiety.

3.3. Cultivation experiments using soil-like conditions

The functional assessment of single members of the soil microbiome, e.g., *C. vaccinii* MWU205, is extremely difficult for mainly three reasons: (i) Only a small percentage of soil bacteria can be cultivated in the laboratory[3,234], (ii) their interactions and secondary metabolite production under natural conditions are mostly unknown[235], and (iii) the ecological function of NPs is often not understood. *C. vaccinii* MWU205 has only been shown to produce FR under standard laboratory conditions[130], therefore it is not clear whether secondary metabolite production also occurs under natural or at least close to natural conditions.

The natural environment of *C. vaccinii* MWU205 are the soil and roots of wild cranberry plants (*Vaccinium macrocarpon* Ait.) in the Cape Cod National Seashore in Truro and Provincetown, and commercial cranberry plants in Wareham, Massachusetts[61]. Most of the bogs in this region are peat bogs, which were formed when the glaciers of the Ice Age melted. Peat bogs require a year-round water saturation, with water that is poor in nutrients and oxygen, acidic, and cool. These conditions, that can be found in kettle-hole peat deposits in Massachusetts, do only allow a slow decomposition of plants resulting in the formation of peat. For commercial cranberries, the peat is covered every two to five years with a thin layer of sand, leading to alternating layers of sand and organic matter with peat at the bottom[236,237].

As the natural bog soil was not available, a soil sample was collected in Germany (location described in **chapter 5.3**) for cultivation experiments with *C. vaccinii* MWU205. In a first attempt the collected soil was used directly as culture, i.e., the soil sample was mixed with agar to test the growth of *C. vaccinii* MWU205 on the respective plates at different cultivation temperatures (described in **chapter 5.4.7**), but did not yield any colonies. To test, whether FR is produced by *C. vaccinii* MWU205 under soil-like conditions, soil extracts which included nutrients present in soil, were thought to be suitable. Therefore, experiments were conducted to test different soil extracts as media to cultivate *C. vaccinii* MWU205 and in order to find soil-like conditions that allow

production of FR. Additionally, the excretion of FR from the bacterial producer cells was investigated, to speculate on the impact of FR on the surrounding environment.

3.3.1. Cultivation of *C. vaccinii* MWU205 in different soil extracts

To investigate FR production under soil-like conditions, topsoil was sampled as described in **chapter 5.3**. Afterwards, the soil was extracted using four different methods and solvents generating four soil extracts; (i) New soil extract (NSE)[238], which uses methanol for extraction, (ii) water extract (WE)[239], (iii) NaOH extract (NE)[240], and (iv) soil-extracted solubilized organic matter (SESOM)[241], which uses water and 3-(*N*-morpholino) propanesulfonic acid (MOPS) buffer for extraction as described in **chapter 5.4.6**. These extracts were used for cultivation of *C. vaccinii* MWU205 for 5 days and compared to a control, which was extracted directly after inoculation. Comparison of the FR concentration determined by the calibration curve shown in **Figure 30 (A)** revealed that SESOM led to the highest production of FR by *C. vaccinii* MWU205 in one of three samples (**Figure 30 (B)**). As only a small increase was observed in cultivations of *C. vaccinii* MWU205 in the water extract and no FR was noticed in the NaOH and NSE experiments, these conditions were not thought to be suitable. Therefore, SESOM was chosen as soil extracts for further experiments.

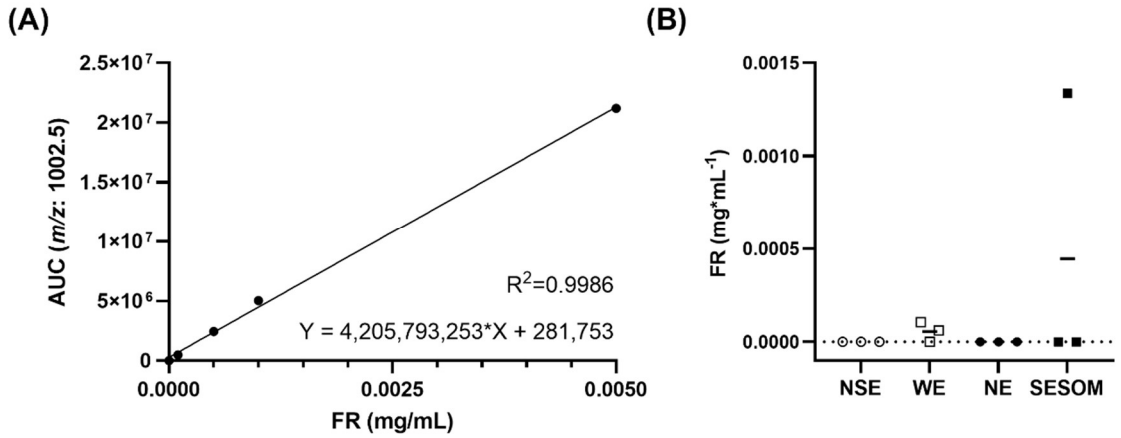

Figure 30: (A) Calibration curve of FR900359 (FR) with the area under the curve (AUC) for FR (*m/z* 1002.5) determined by LC/MS for five concentrations (0; 0.0001, 0.0005, 0.001, and 0.005 mg/mL FR). Equations given in the figures were calculated using Prism (Vers. 9.5.1) **(B)** Concentration of FR in *n*-butanol extracts of *Chromobacterium vaccinii* MWU205 cultures grown in soil extracts for 5 d. NSE=New soil extract[238] (empty circle), WE = water extract[239] (empty square), NE = NaOH extracts[240] (filled circle), and SESOM = soil-extracted solubilized organic matter[241] (filled square).

3.3.2. Cultivation experiments with SESOM and SESOM+

SESOM applies MOPS buffer for soil extraction. The resulting extract can be used for bacterial cultivations[241]. As the production did not seem to be stable, the preculture preparations were optimized as described in **chapter 5.6.6.1**. In short, preparation of the preculture in SESOM was replaced by one in LB medium to generate a big inoculum, which was harvested by centrifugation. Subsequent washing steps helped to remove the complex LB medium. Results calculated as described in **chapters 5.6.6.2** and **5.6.6.3**, using the latter preculture preparation, showed a significant 18-fold increase (unpaired t-test: P<0.0001) of FR in extracts from *C. vaccinii* MWU205 cultures cultivated for 5 days in SESOM (**Figure 31 (B)**). The FR concentration was determined from the AUC for the *m/z* 1002.5 signal, using the calibration curve shown in **Figure 31 (A)**. Furthermore, the naturally occurring soil polymer chitin was added to SESOM (SESOM+), as it is a possible natural nitrogen and carbon source. *C. vaccinii* MWU205 was reported to harbor genes encoding chitinases, which, if active, would make chitin accessible for the bacterium. FR production was proven in the presence of chitin showing a significant 3-fold increase (unpaired t-test: P=0.0007) in FR concentration after 5 days of cultivation (**Figure 31 (C)**). However, no enhancement of the FR concentration in SESOM+ compared to SESOM was observed.

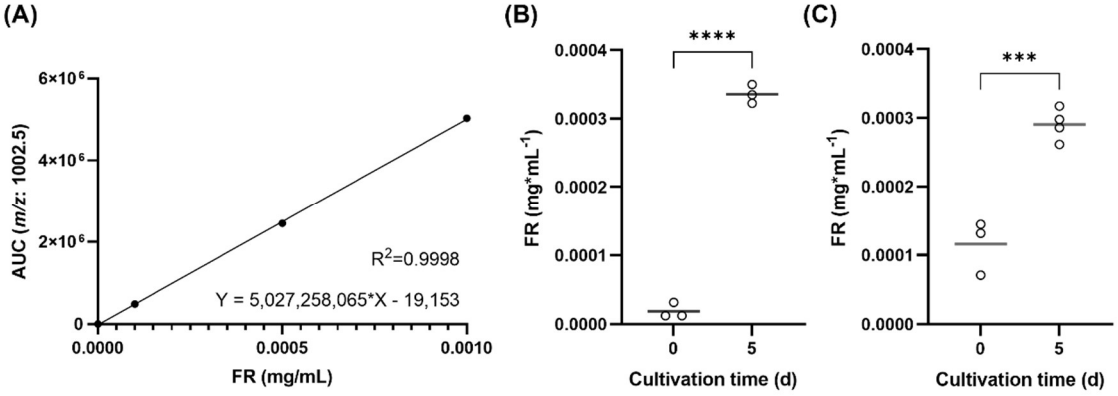

Figure 31: (A) Calibration curve of FR900359 (FR) with the area under the curve (AUC) for FR (*m/z* 1002.5) determined by LC/MS for eight concentrations (0; 0.0001, 0.0005, 0.001, 0.005, 0.01, 0.05, and 0.1 mg/L FR). Equations given in the figures were calculated using Prism (Vers. 9.5.1)**.** FR concentration in *n*-butanol extracts of *Chromobacterium vaccinii* MWU205 cultivated in **(B)** SESOM or**(C)** SESOM supplemented with chitin (SESOM+) for five days or extracted after inoculation [0 days]. FR concentration was evaluated using LC/MS For both experiments n=3. The significance was determined using a two-tailed unpaired t-test. P>0.05=ns, P<0.05=*, P<0.01=**, P<0.001=***, P<0.0001=****. **(A)** was adapted from Hanke et al, 2023 and raw data of the figure can be found in the supplementary of the publication[2].

3.3.3. FR excretion from *C. vaccinii* MWU205 cells

Following the proof of FR production under soil-like conditions, it was studied, whether FR is excreted by *C. vaccinii* MWU205. This was thought to be an important question to answer, in order to examine the environmental impact of FR. As a higher FR production was more suited to observe differences in the FR concentration between the bacterial pellet and the supernatant, LB medium was chosen instead of SESOM. Following the cultivation of *C. vaccinii* MWU205 in LB, the FR content in both the pellet and the supernatant was separately measured and calculated using the FR calibration curve (**Figure 32 (A)**). The supernatant contained a significantly (paired t-test: P<0.0001) higher FR concentration than the pellet (**Figure 32 (B)**).

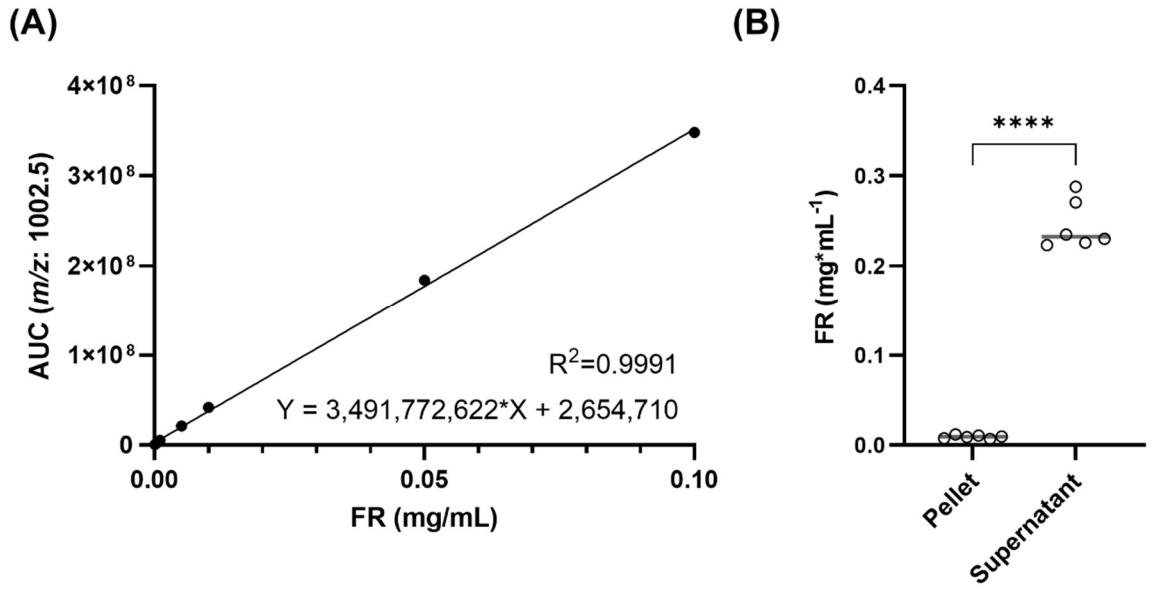

Figure 32: (A) Calibration curve of FR900359 (FR) with the area under the curve (AUC) for FR (*m/z* 1002.5) determined by LC/MS for eight concentrations (0; 0.0001, 0.0005, 0.001, 0.005, 0.01, 0.05, and 0.1 mg/L FR). Equations given in the figures were calculated using Prism (Vers. 9.5.1)**. (B)** Concentration of FR (mg/mL) in supernatant and pellet of *Chromobacterium vaccinii* MWU205 liquid culture. *C. vaccinii* MWU205 was cultivated for 43 h in LB medium and centrifuged afterwards, resulting in pellet and supernatant, which were extracted separately with *n*-butanol. Six repeats were performed. The significance was determined using a paired t-test. P>0.05=ns, P<0.05=*, P<0.01=**, P<0.001=***, P<0.0001=****. Figure was adapted from Hanke et al, 2023 and raw data of the figure can be found in the supplementary of the publication[2].

It is thus concluded, that under soil-like conditions the measured FR concentration is around 0.0003 mg/mL. Furthermore, FR is excreted by *C. vaccinii* MWU205, suggesting the presence of FR in soil inhabited by *C. vaccinii* MWU205.

3.3.4. Discussion

As shown in **Figure 31**, *C. vaccinii* MWU205 is producing FR in soil-derived liquid media, i.e., SESOM from garden soil with concentrations around 0.0003 mg/mL. It has been shown for antibiotics derived from soil bacteria that NPs can affect surrounding organisms at low concentrations, i.e., subinhibitory concentrations of antibiotics may mediate species interactions, a phenomenon called hormesis[235,242,243]. This could also apply to FR. However, it must be mentioned that the FR concentrations found in our experiments are very low, probably caused by insufficient mimicking of natural conditions. *C. vaccinii* MWU205 was originally isolated from bog soil[61] near the root of cranberries (*Vaccinium macrocarpon* Ait.). Commercial bog soil in Massachusetts consists of alternating layers of sand and organic matter supposedly with other nutrients than garden soil[236]. *C. vaccinii* MWU205 might also be part of the rhizosphere of cranberry plants and therefore provided with root exudates, which are missing in SESOM. As multiple organisms are present in soil, their interactions may induce or inhibit the production of metabolites. The dynamic interplay between organisms is difficult to simulate, but likely to influence FR production.

The addition of chitin to SESOM as a naturally occurring nutrient was a first attempt to mirror natural conditions more closely and confirmed FR production. However, it did not enhance it further (**Figure 31**), even though a first genome analysis of the draft genome of *C. vaccinii* MWU205 has revealed it to have the potential to produce chitinases[219]. However, chitin degradation is a complex process[244], and some explanations for the lack of FR enhancement under the tested conditions can be named. Maybe the reported chitinase genes are not transcribed or translated, even if present, they may not able to degrade chitin, or chitin degradation happens, but the resulting nutrients do not influence FR biosynthesis. To verify any of these explanations the transcriptome or proteome of *C. vaccinii* MWU205 should be investigated, the chitinases could also be heterologously expressed and examined for their enzymatic activity, and lastly chitin degradation products could be fed to cultures of *C. vaccinii* MWU205 to test if they enhance the FR production. Additionally, labeled molecules may directly prove the incorporation of the chitin degradation metabolites into FR biosynthesis.

It is reasonable to suggest that mimicking of the factors mentioned above, e.g., nutrients in bog soil and exudates from cranberry, when cultivating *C. vaccinii* MWU205

would lead to a higher FR production. Indeed cultivation of *C. vaccinii* MWU205 in LB medium has revealed its potential to produce much higher amounts of FR, as 2.5 mg of pure FR were isolated from *C. vaccinii* MWU205 cultivated in one liter LB medium[130]. Furthermore, one of the extracts in the preliminary experiments (**Figure 30**) had an FR concentration well-above 0.001 mg/mL, which could, however, not be reached again in the following experiments.

To quantify FR production in the environment directly, an *in situ* approach, in which a suitable adsorber resin is placed into the soil to extract FR from the respective surroundings[245–247], would be of interest. An additional possibility would be to use a droplet-based system to cultivate *C. vaccinii* MWU205 and to simulate the soil bacterial community *in situ.* This would allow to investigate the influence of different factors, e.g., cocultivation with other bacteria isolated from cranberry bog soil, on the growth of *C. vaccinii* MWU205[248,249]. In addition, a metagenomic analysis of various environmental soil DNAs for the *frs* BGC[250] could generate new insights into the overall presence and frequency of potential FR producers.

Still, though limited, the experiments in this study clearly indicate the ability of *C. vaccinii* MWU205 to produce FR in soil.

3.4. Bioactivity of FR against soil-associated nematodes

The phylum Nematoda is ubiquitously distributed in soil[35,36] and many nematodes feed on bacteria. Therefore, it is conceivable that soil bacteria like *C. vaccinii* MWU205 produce NPs like FR as a defense *inter alia* against nematodes[130,153]. The phylum Nematoda also contains members known as dreaded plant pathogens, which may be similarly affected by FR. This is quite plausible, since G_q proteins are highly conserved in most eukaryotes [251,252].

To assess the bioactivity of FR against soil-associated nematodes, the following chapter summarizes the results gained from *in silico*, *in vitro*, and *in vivo* analyses.

3.4.1. *In silico* analysis of FR binding to nematode $G\alpha_q$ proteins

This is the first analysis judging the sensitivity of nematode G_q proteins to FR. Therefore, initially, the basic local alignment search tool (BLAST)[253,254] was used to identify $G\alpha_q$ protein sequences from nematodes. Subsequently, the respective presumed

FR binding sites were aligned and the impact of differences between the human $G\alpha_q$ and the nematode $G\alpha_q$ proteins on FR binding was estimated using PyMOL™ 2.5.4. *In silico* analyses were assumed to be very insightful, due to the detailed knowledge on the binding site of the FR related YM to the human G_q protein, which is in parts confirmed for FR via mutagenesis and binding studies[158,255]. Additionally, G_q proteins are highly conserved in metazoa and essential for their life[251,252], making the findings on the effects of FR on the human G_q translatable to nematode G_q proteins.

3.4.1.1. BLAST search for nematode $G\alpha_q$ proteins

Caenorhabditis elegans is a bacteria-feeding nematode and a well-studied model organism[256–258]. The cDNA of the $G\alpha_q$ ortholog expressed by *C. elegans* has 82 % amino acid sequence identity to the murine $G\alpha_q$ cDNA. Comparable to the impact of the human $G\alpha_q$, *C. elegans* $G\alpha_q$ plays a crucial role in nematode physiology, e.g., egg-laying, locomotion, pharyngeal activity, and axon regeneration[259]. The protein named Egl-30 (UniProt: G5EGU1) is encoded by *egl-30* and was taken as query to search for other nematode $G\alpha_q$ sequences with BLAST[253,254], restricting the organism group to the taxon Nematoda. In total, sixteen sequences were chosen from the resulting output (one hundred sequences) as most sequences belonged to parasitic nematodes known to infect humans and mammals with no direct connection to soil.

Nine sequences of *Caenorhabditis* spp. were chosen for the alignment to fully represent the genus *Caenorhabditis*, which is divided into two supergroups, i.e., *Elegans* and *Drosophilae*, and additionally a basal group. All three clades have *egl-30* orthologs , which were detected by the BLAST search and included in the alignment (**Figure 34**), e.g., *C. elegans*, *C. latens*, *C. nigoni*, *C. tropicalis*, *C. briggsae*, *C. remanei*, *C. japonica* belonging to the *Elegans* supergroup, *C. angaria* and *C. bovis* to the *Drosophilae* supergroup, and *C. auriculariae* to the basal group[260]. These *Caenorhabditis* spp. were found on insects[260–268], invertebrates[268], rotten material[268] or in an entomopathogenic relationship with bacteria[269].

The other seven sequences selected for the alignment were soil or soil-associated nematodes (**Figure 34**). *Pristionchus pacificus* and *C. elegans* shared their last common ancestor about 200–300 million years ago[270] and *P. pacificus* is known as satellite model organism associated with scarab beetles, with which it has a necromenic relationship[271]. *Aphelenchus avenae* is recognized as a fungivorous nematode found commonly in soil[272].

Bursaphelenchus okinawaensis has been isolated from the longhorn beetle *Monochamus maruokai*. The genus *Bursaphelenchus* feeds on plants and fungi and is phoretically associated with insects[273]. All other selected nematodes are plant parasitic. *Ditylenchus destructor* is the potato cyst nematode and used as model organism for plant parasitism[274]. *Meloidogyne graminicola* and *Meloidogyne enterolobii* (syn *Meloidogyne mayaguensis*) are plant parasitic root-knot nematodes, with *Meloidogyne graminicola* targeting rice plants as sedentary endoparasite[275] and *Meloidogyne enterolobii* harming vegetables in China, Vietnam, and America[276]. The last plant parasitic nematode is the foliar *Aphelenchoides besseyi*, which feeds as ecto- and endoparasite on above-ground plant parts causing, e.g., the 'white tip' disease on rice[43].

Another representative, the plant parasitic cyst nematode *Heterodera schachtii*, is known as pest of the sugar beet[277]. After sequencing its genome and transcriptome[278] a search for probable $G\alpha_q$ orthologs revealed an messenger ribonucleic acid encoding of 353 amino acids, which was used for the alignment (Access to the sequences was provided to us by Dr Sebastian-Eves-van den Akker).

In total, eighteen nematode $G\alpha_q$ sequences (**Table 11**) were selected from the BLAST search and compared to the human $G\alpha_q$.

3.4.1.2. Alignment of nematode $G\alpha_q$ proteins

A literature survey showed that the FR binding site was investigated by multiple studies, starting with the identification of the binding site of the FR-related depsipeptide YM (**Figure 3**) in a heterotrimeric human $G_{i/q}$ chimeric protein by X-ray crystallography[198]. Based on this structure, further binding and mutagenesis studies have investigated the FR and YM binding site[158,255]. In summary, these studies show that FR attaches to human G_q in the interdomain cleft between the helical (H) and GTPase domain (G) by connecting to linker I and switch I (linker 2) (**Figure 33**)[158]. Hydrophobic interactions, more specifically the eight following positions in the human $G\alpha_q$ according to the common Gα numbering system, were reported to be crucial for FR binding[279]: $V182^{G.hfs2.1}$ and $V184^{G.hfs2.3}$, $I190^{G.S2.2}$, $E191^{G.S2.3}$, and $P193^{G.S2.5}$, followed by, $G74^{H.HA.6}$, $F75^{H.HA.7}$, and $L78^{H.HA.10}$. In addition, hydrogen bonds with $R60^{H.H1.9}$, which are relying on the salt-bridge formation between the polar aspartate $D71^{H.HA.3}$ and the mentioned arginine[158,198,255] stabilize FR binding. Aside from these amino acid residues, eight others

were revealed by the crystal structure to directly or indirectly interact with YM and thus may also be relevant for FR binding[198].

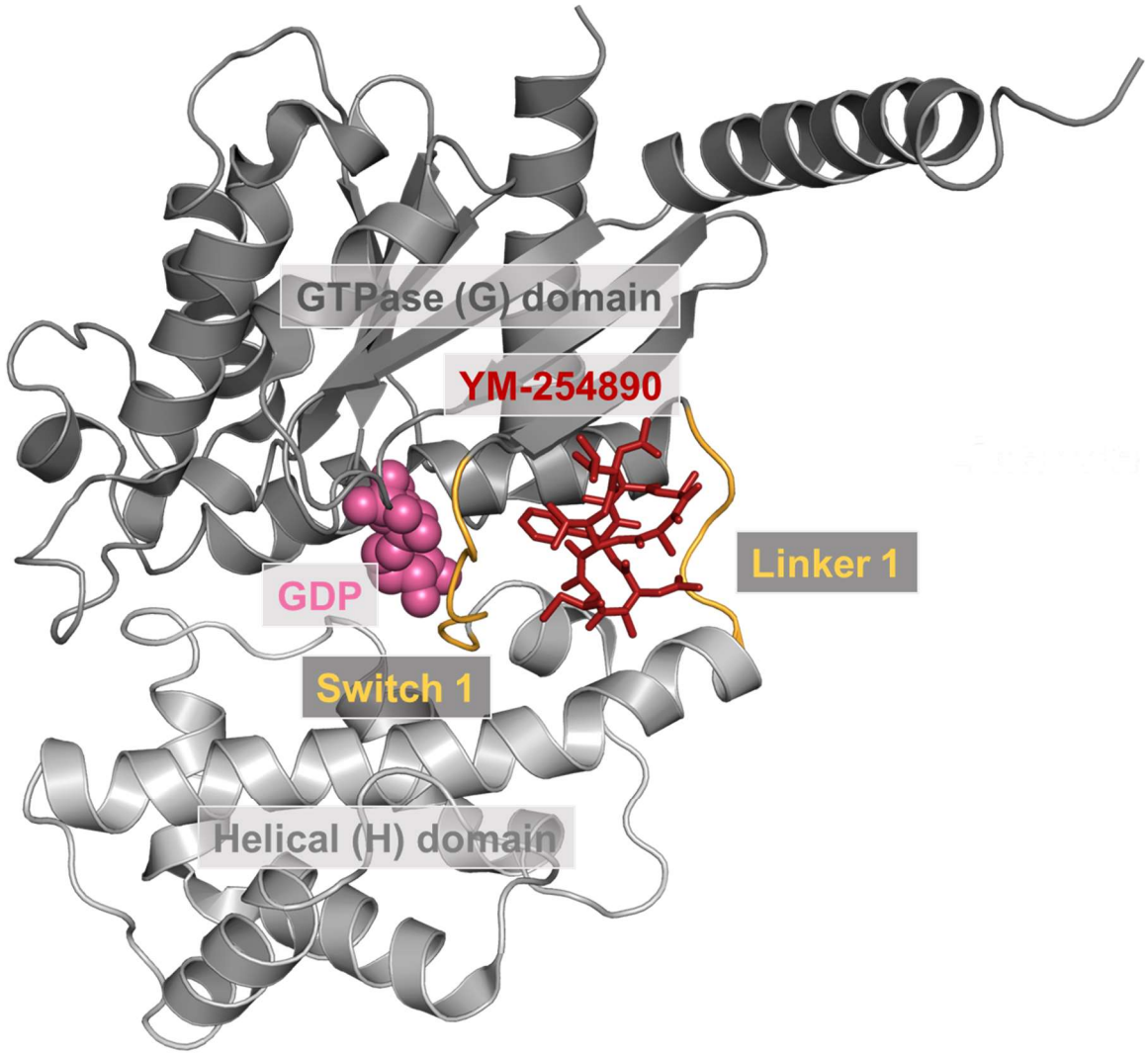

Figure 33: $G\alpha_{i/q}\beta\gamma$ heterotrimer (grey) in complex with YM-254890 (red, sticks) and guanosine diphosphate (spheres, rose) (Protein data bank code: 3AH8). Linker 1 and switch I (linker 2) are shown in orange. The figure was taken from Hanke et al, 2023[2].

To compare the assumed FR binding region, i.e., forty-two amino acid residues of the human $G\alpha_q$ protein, to the corresponding sequences in eighteen nematode $G\alpha_q$ proteins an alignment was performed as described in **chapter 5.13.2** (**Figure 34**). The hereby identified differences were visualized via PyMOL™ 2.5.4 using the inhibitor binding the YM-$G_{q/i}$ crystal structure (Protein data bank code: 3AH8) to estimate the importance of each difference (**Figure 35**)[198].

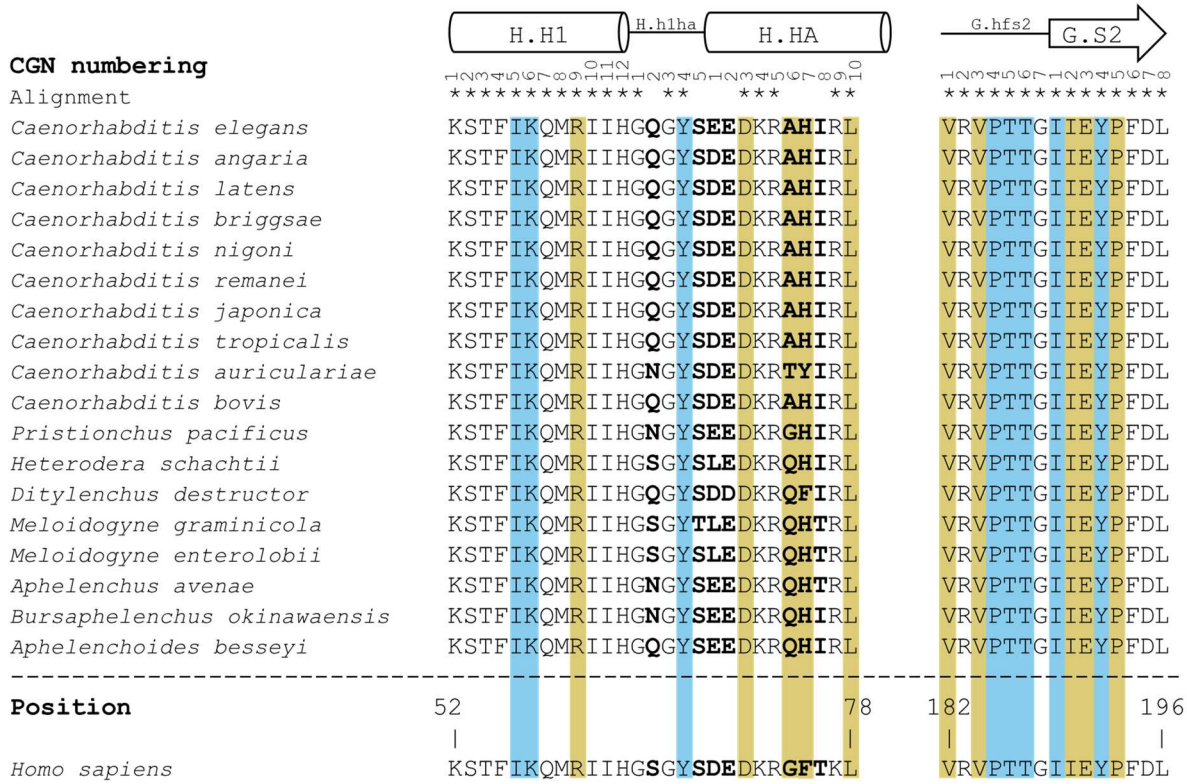

Figure 34: FR900359 (FR) and YM-254890 (YM) binding sites in $G\alpha_q$ proteins of nematodes. Sequences (**Table 11**) were aligned using the Clustal W algorithm and compared to the human $G\alpha_q$ protein (UniProtKB: P50148). Identical positions within the binding sites are marked with asterisks and positions shown in bold are divergent. Positions predicted to be important for FR and YM binding are highlighted in blue, and positions confirmed via mutagenesis studies highlighted in yellow[158,198,255]. The common Gα numbering system was used and secondary structures were indicated with symbols (cylinder=α-helix; arrow=β-sheet)[279]. The figure was adapted from Hanke et al, 2023[2].

The comparison identified seven positions of the forty-two amino acid residues investigated which differ between the $G\alpha_q$ sequences of nematodes and the FR-sensitive human $G\alpha_q$ protein: position G.h1ha.2, G.h1ha.5, H.HA.1-2, and H.HA.6-8 (**Figure 34**). The visualization revealed that five positions are unlikely to influence FR or YM binding due to two reasons: The distance between the amino acid residue and the inhibitor is too big and therefore a change is improbable to affect the inhibitor binding as observed for $S65^{G.h1ha.2}$, which has a distance of >6.9 Å to the inhibitor. Also, if the amino acid side chain points away from the inhibitor this residue is unlikely to have an impact on inhibitor binding. This is the case for the positions $S68^{G.h1ha.5}$, $D69^{H.HA.1}$, $E70^{H.HA.2}$, and $T76^{H.HA.8}$ as depicted in **Figure 35 (A)**. These findings are in line with published studies[198].

The other two positions, $G74^{H.HA.6}$ and $F75^{H.HA.7}$, were predicted to have a more profound influence on FR and YM binding. Three different amino acids are found at position H.HA.6, i.e., glycine for the human $G\alpha_q$ protein and alanine or glutamine for the

nematode $G\alpha_q$ proteins. As the distance between the glycine in the heterotrimeric human $G_{i/q}$ chimeric protein and YM is 3.8 Å, the change to bigger residues might influence FR and YM binding (**Figure 35 (B)**). Binding experiments support this assumption, as exchanging glycine to the bigger residue valine at this position leads to a faster dissociation of an FR-based radioligand [^{3}H]PSB-15900-FR[158].

A direct interaction of F75$^{H.HA.7}$ with YM is predicted by Nishimura et al.[198] and further supported for FR itself[158], as phenylalanine is part of a hydrophobic network important to stabilize FR and YM binding. Additionally, F75$^{H.HA.7}$ has approximately 4.1 Å distance to YM as predicted from the crystal structure (**Figure 35 (C)**). The alignment unveiled that 89 % of all nematode sequences contain a histidine at H.HA.7, and all sequences of nematodes (**Figure 34**) contain aromatic amino acids, e.g., tyrosine, histidine or phenylalanine. This change is not considered to severely impact FR binding, as these amino acids do not disrupt the hydrophobic network.

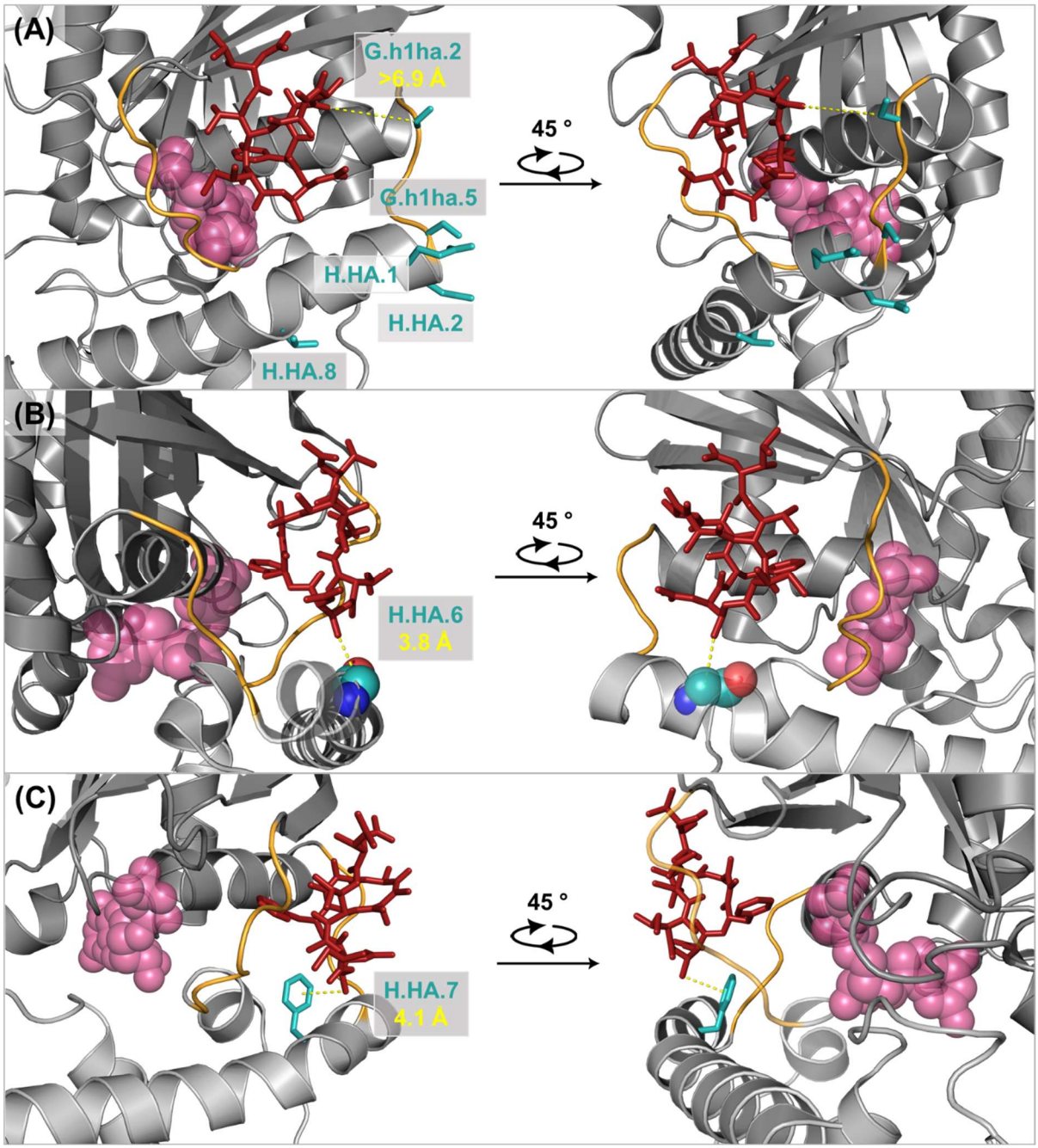

Figure 35: $G\alpha_{i/q}\beta\gamma$ heterotrimer (grey) in complex with YM-254890 (YM) (red, sticks) and guanosine diphosphate (spheres, rose) (Protein data bank code: 3AH8). Linker 1 and switch I (linker 2) are shown in orange. Representation of human residues at positions with differing nematode amino acids in the $G\alpha_q$ sequence alignment $S65^{G.h1ha.2}$, $S68^{G.h1ha.5}$, $D69^{H.HA.1}$, $E70^{H.HA.2}$, and $T76^{H.HA.8}$ in **(A)** as turquoise sticks; $G74^{H.HA.6}$ in **(B)** as spheres; $F75^{H.HA.7}$ in **(C)** as turquoise sticks. Each position was rotated once by 45° along the z-axis. Measured distances between the amino acids and YM are shown as dashed yellow lines. Visualization and measurement were done using PyMOL™ 2.5.4. Figure taken from Hanke et al, 2023[2].

The other investigated regions, i.e., G.hfs2 and G.s2 of all $G\alpha_q$ proteins (**Figure 34**), are clearly involved in YM and FR binding[158,198,255] and identical for all sequences.

Taken together, *in silico* analyses revealed that the $G\alpha_q$ proteins of nematodes are likely to be inhibited by FR and YM. Two positions in $G\alpha_q$ proteins of nematodes were identified to differ from human $G\alpha_q$ and possibly influence the binding of FR. To

substantiate this further, *in vitro* experiments were conducted with the $G\alpha_q$ of the nematode model organism *C. elegans* and the plant parasitic *H. schachtii*.

A pairwise alignment to compare both full length $G\alpha_q$ amino acid sequences of *H. schachtii* and *C. elegans* revealed 90 % identity, while the investigated FR binding region of these two nematodes (**Figure 34**) differed only at three positions, G.h1ha.2, H.HA.1, and H.HA.6. As revealed above the first two positions, G.h1ha.2 and H.HA.1, are unlikely to be required for the interaction with FR/YM (**Figure 35 (A)**). The difference at position H.HA.6 is seemingly of interest as nematodes belonging to the *Caenorhabditis* group have a less spacious residue with alanine compared to the glutamine present in plant parasitic nematodes like *H. schachtii*. The influence of these changes on binding and activity of FR is difficult to predict and therefore inhibition of FR on nematode $G\alpha_q$ was tested *in vitro*.

3.4.2. *In vitro* analysis of FR inhibition of heterologously expressed nematode $G\alpha_q$ proteins

Both, *H. schachtii* as plant pathogenic nematode and *C. elegans* as bacteria-feeding nematode and well-characterized model organism, were chosen to investigate the sensitivity of their $G\alpha_q$ isoforms to FR *in vitro*. Using the CRISPR/Cas9 technology, endogenous G_q and G_{11} proteins were knocked out in HEK293 cells (HEK $G_{q/11}$-KO cells) to avoid signal confounding. Afterwards the $G\alpha_q$ protein of *H. schachtii* and *C. elegans* were transiently introduced. For the *in vitro* investigation the inositol monophosphate (IP_1) and the calcium mobilization assay were chosen as functional G_q readout. $G\alpha_q$ triggers the β-isoform of the phospholipase C (β-PLC) to cleave phosphatidylinositol bisphosphate (PIP_2) into inositol 1,4,5-triphosphate (IP_3) and diacylglycerol (DAG), leading to calcium mobilization[157]. Therefore, measurement of calcium and IP_1, which is a degradation product of IP_3, are suitable readouts for G_q signaling[280–285]. These experiments were conducted by Judith Alenfelder (AG Kostenis, Institute for Pharmaceutical Biology, University of Bonn).

3.4.2.1. IP_1 assay with heterologously expressed nematode $G\alpha_q$ proteins

First experiments with different carbachol concentrations up to 100 µM testing the functional expression of the $G\alpha_q$ of *H. schachtii* in HEK293 together with endogenously expressed muscarinic acetylcholine receptor type 3 (M3) did not increase the level of IP_1

level over vector control. Under the same conditions, heterologously expressed murine G_q resulted in increased IP_1 accumulation. Various explanations for the lack of signal were considered, ranging from improper protein folding or location to the absence of additional proteins necessary for *H. schachtii* G_q signaling. One of these proteins, the resistance to inhibitors of cholinesterase 8A (RIC-8A) was first identified as a crucial part of G_q signaling in the nematode *C. elegans*[286]. Further studies revealed RIC-8A to increase G protein expression[287] by facilitating folding, act as guanine-nucleotide exchange factor[288], and has been used to amplify signaling of other insect G proteins[289]. Based on this, a co-expression of RIC-8A with *H. schachtii* $G\alpha_q$ was tested, but also did not result in a measurable response of the $G\alpha_q$ protein to carbachol. Furthermore, the M3 receptor for G protein activation was over-expressed, but did not lead to an increase in IP_1 accumulation over vector control (**Figure 36**). Finally, when combining RIC-8A expression and M3 over-expression, a concentration-dependent IP_1 accumulation upon carbachol addition was observed (**Figure 37 (A)**). As is evident from **Figure 37 (C)**, *C. elegans* $G\alpha_q$ (*egl-30*) can be functionally expressed in HEK $G_{q/11}$-KO cells if M3 is over- and RIC-8A is expressed. Furthermore, the activation behavior of *C. elegans* $G\alpha_q$ is similar to that of *H. schachtii* $G\alpha_q$, regarding the shapes of their dose response curves and their negative logarithms of the half maximal effective concentration (pEC_{50}) values.

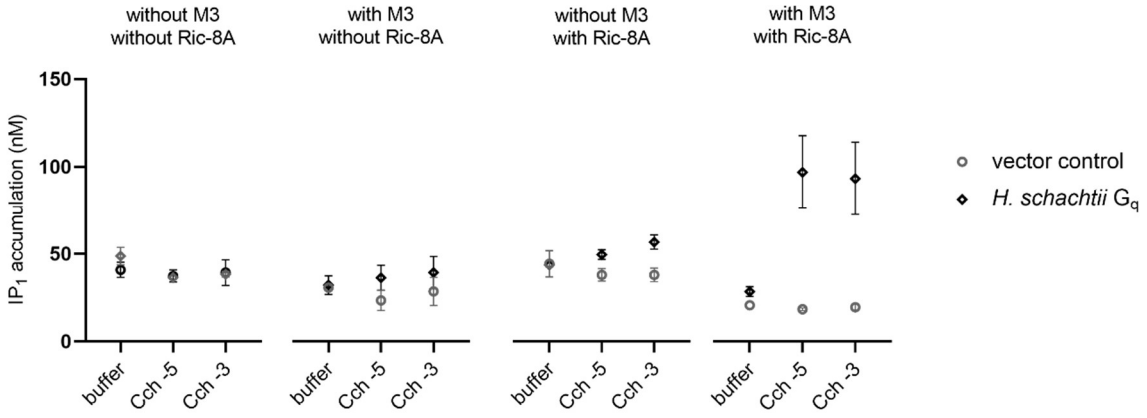

Figure 36: myo-Inositol 1 phosphate (IP_1) accumulation after stimulation without and with 1 mM and 10 µM carbachol (Cch) of HEK $G_{q/11}$-KO cells transfected to express only *H. schachtii* $G\alpha_q$ isoform; *H. schachtii* $G\alpha_q$ isoform with muscarinic acetylcholine receptor type 3 (M3) overexpression; with the resistance to inhibitors of cholinesterase 8A (RIC-8A) expression; or with both M3 overexpression and RIC-8A expression. Mean ± Standard error of the mean, 3 biological replicates performed in triplicate. Figure was adapted from Hanke et al, 2023 and raw data of the figure can be found in the supplementary material of the publication[2].

After these experiments, the FR sensitivity of *H. schachtii* $G\alpha_q$ and *C. elegans* $G\alpha_q$ were investigated by pre-incubating cells with varying concentrations of the inhibitor and

stimulating with the carbachol concentration that elicits the highest response (10 µM). In line with the predictions from the *in silico* analyses, both nematode $G\alpha_q$ proteins are clearly FR-sensitive, as FR was able to completely blunt *H. schachtii* and *C. elegans* G_q signaling with low micromolar potency (**Figure 37 (B)**, **(D)**).

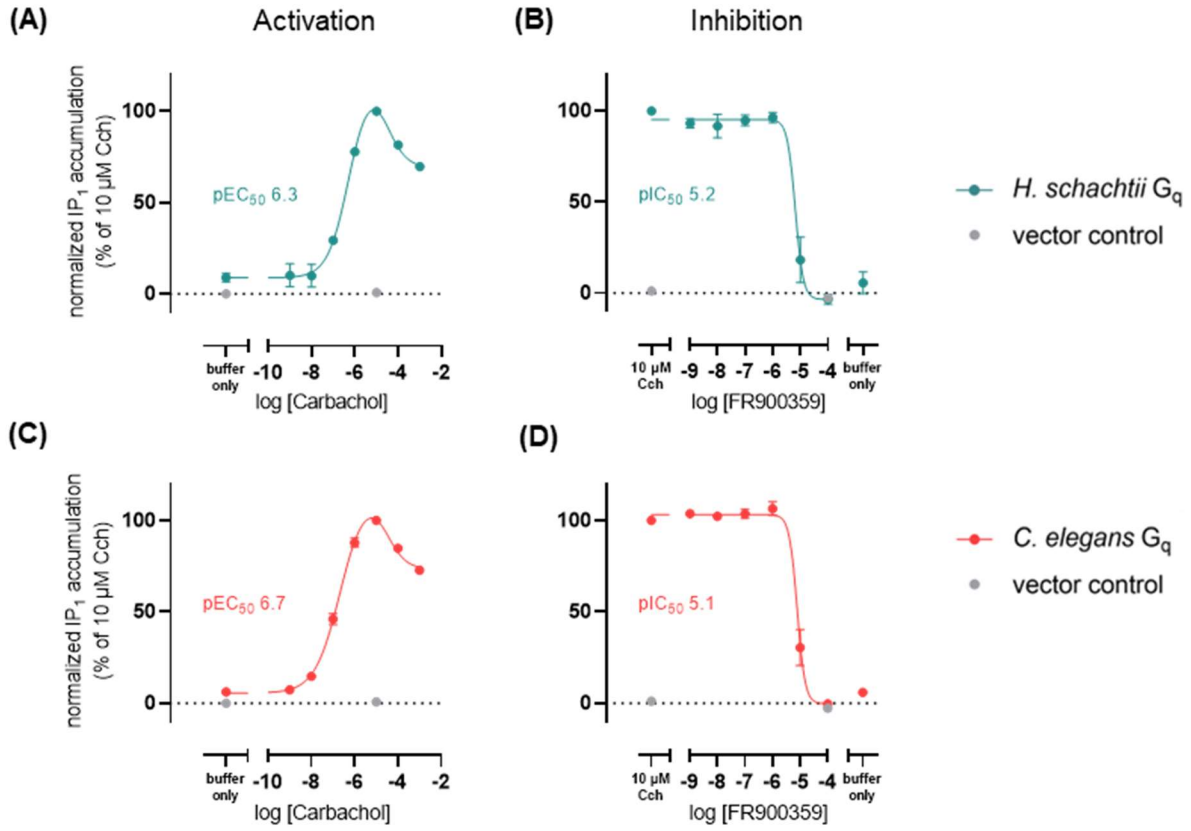

Figure 37: Functional expression of nematode $G\alpha_q$ proteins and inhibition by FR900359. **(A)**, **(C)** Concentration-dependent IP_1 accumulation after stimulation of HEK $G_{q/11}$-KO cells transfected to express **(A)** *Heterodera schachtii* and **(C)** *Caenorhabditis elegans* $G\alpha_q$ isoforms with carbachol. **(B)**, **(D)** Concentration-inhibition curves of FR on *H. schachtii* **(B)** and *C. elegans* **(D)** $G\alpha_q$ proteins normalized to the IP_1 accumulation evoked by 10 µM carbachol (Cch). Mean ± standard error of the mean, at least 3 biological replicates performed in triplicate. Figure was adapted from Hanke et al, 2023 and raw data of the figure can be found in the supplementary of the publication[2].

3.4.2.2. Ca^{2+} mobilization assay with heterologously expressed nematode $G\alpha_q$ proteins

Due to the plethora of established experimental methods known for *C. elegans*, the effects of FR may be studied more easily in this organism. Therefore, the calcium assay was chosen as additional read-out[157] and conducted with *C. elegans* $G\alpha_q$ to corroborate the functional expression of the nematode $G\alpha_q$ and its inhibition by FR observed in the IP_1 accumulation assay. As before, activation and inhibition experiments were carried out measuring the increase of intracellular calcium concentrations as consequence of G_q

activation. Again, *C. elegans* $G\alpha_q$ was functionally expressed (**Figure 38 (A)**) and inhibited by FR (**Figure 38 (B)**). Curiously, the resulting dose-response curve was shifted to the left to a high nanomolar potency, revealing a more moderate steepness of the curve compared to the IP_1 accumulation assay. These results confirmed the conclusions from the IP_1 assay data in that FR was able to inhibit *C. elegans* $G\alpha_q$. Therefore, a calcium assay with *H. schachtii* $G\alpha_q$ was not expected to reveal new insight and deemed unnecessary.

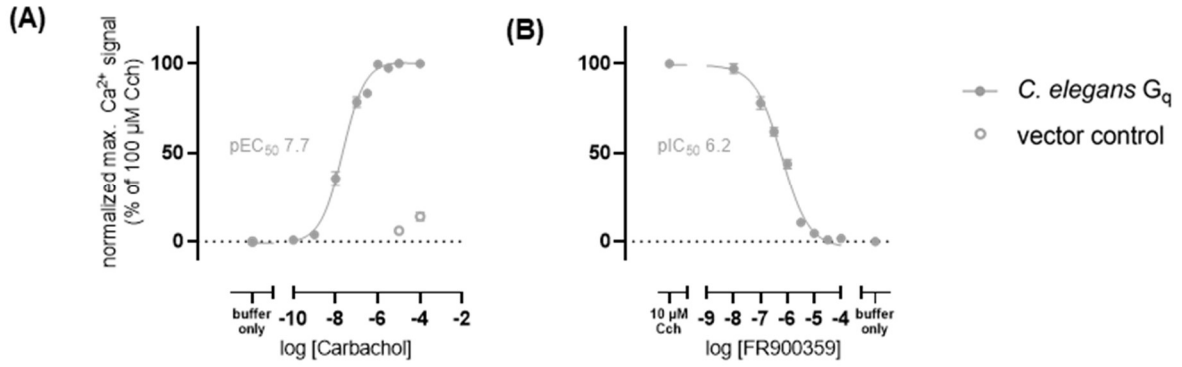

Figure 38: Functional expression of nematode $G\alpha_q$ proteins and inhibition by FR900359 (FR). **(A)** Concentration-dependent calcium signal after stimulation of HEK $G_{q/11}$-KO cells transfected to express *Caenorhabditis elegans* $G\alpha_q$ isoforms with carbachol (Cch). **(B)** Concentration-inhibition curves of FR on *C. elegans* $G\alpha_q$ proteins normalized to the calcium signal evoked by 100 µM Cch. Mean ± standard error of mean, at least 3 biological replicates performed in triplicate. Figure was adapted from Hanke et al, 2023 and raw data of the figure can be found in the supplementary material of the publication[2].

Taken together, both $G\alpha_q$ proteins of *H. schachtii* and *C. elegans* were functionally expressed in cell cultures and inhibited by FR. Interestingly, the potency of inhibition was similar for *H. schachtii* and *C. elegans* $G\alpha_q$ in the IP_1 assay. This implies that the difference in the FR binding site between both proteins observed in the *in silico* analyses is not interfering with FR activity. The variance at position H.HA.6 might not influence FR binding because alanine and glutamine both face away from the inhibitor. These promising *in vitro* results made *in vivo* effects very likely, which were thus examined in the next experiments.

3.4.3. *In vivo* assays with soil-associated nematodes

To investigate the effect of FR on soil-associated nematodes like *C. elegans* and plant pathogenic nematodes like *H. schachtii*, different *in vivo* assays focusing on movement and propagation were chosen. As Egl-30 is known to be involved in locomotion and egg-laying of *C. elegans*, tracking experiments and egg-laying assays were selected to study the effect of FR on these physiological mechanisms[259]. Subsequently, the effects of FR on the activity of juvenile stage 2 (J2) *H. schachtii* and the hatching of J2's from the cyst were examined.

Experiments with *C. elegans* were conducted with the help of Dr. Liu and Dr. Scholz (Neural Information Flow, Max Planck Institute for Neurobiology of Behavior – CAESAR, Bonn), while experiments with *H. schachtii* were done together with Dr. Gutbrod (Molecular Biotechnology/Biochemistry Department, Institute of Molecular Physiology and Biotechnology of Plants, University of Bonn). The results of these experiments are summarized in this chapter.

3.4.3.1. *In vivo* experiments with *C. elegans* and FR

In the following assays, *C. elegans* wildtype N2 and five different *C. elegans* mutant strains were examined to investigate the effect of FR. Three strains with different *egl-30* mutations demonstrate different G_q loss-of-function phenotypes, i.e., one severe egg-laying phenotype, which it is nearly paralyzed and bloated with eggs, also called "strong mutant" (*egl-30*(*ad805*), and two hypomorphic mutants, *egl-30*(*n686*), and *egl-30*(*ad806*), which are both less bloated with eggs and sluggish (*egl-30*(*ad806*)) to very sluggish (*egl-30*(*n686*)), but never paralyzed, and termed "weak mutants" in this study[259]. To investigate the opposing phenotype, two G_q signaling suppressor mutants were included as well. One suppressor mutant, *dgk-1*(*sy428*), encodes a loss-of-function diacylglycerol kinase (Dgk-1)[290]. The kinase is known to function as a negative regulator of G_q signaling by phosphorylating the second messenger diacylglycerol (DAG)[291]. The second suppressor mutant, *eat-16*(*sa609*), is a missense loss-of-function mutant with an amino acid exchange (R396C) of *eat-16*, encoding a negative regulator of G protein signaling. This negative regulator belongs to the family of GTPase activating proteins, which turn G proteins into their inactive state by the hydrolysis of GTP[292]. Both suppressor mutants are described to be hyperactive due to their movements and rapid egg-laying[292].

3.4.3.1.1. Investigation of the effect of FR on movement and spatial distribution of *C. elegans*

As $G\alpha_q$ is important for the locomotion of *C. elegans*[259], tracking experiments on agar plates as explained in **chapter 5.15.2** were performed. In short, a spot of *Escherichia coli* OP50 bacteria was placed in the center of the agar plate thereby creating the bacterial lawn on which the nematodes feed. This setup allowed the analysis of three parameters, i.e., the velocity of nematodes, the spatial distribution of nematodes outside or in the bacterial lawn, and the number of border crossings. For each of the six genotypes (*C. elegans* N2, *egl-30*(*ad805*), *egl-30*(*n686*), *egl-30*(*ad806*), *dgk-1*(*sy428*), *eat-16*(*sa609*))

three repeats were conducted and the results are depicted in **Figure 39**, **Figure 40**, and **Table 2**. Pictures summarizing the nematodes movement of each tracking are depicted in **Figure 66** to **Figure 71**.

Comparing the velocity of each genotype control in **Figure 39**, i.e., without FR treatment, revealed a clear ranking: Both suppressor mutants, i.e., *dgk-1*(*sy428*) and *eat-16*(*sa609*), were the fastest moving genotypes, followed by the wildtype N2. The slowest genotypes were the *egl-30* mutants, i.e., *egl-30*(*n686*), *egl-30*(*ad806*), and *egl-30*(*ad805*). Previous reports have shown similar results[259,292].

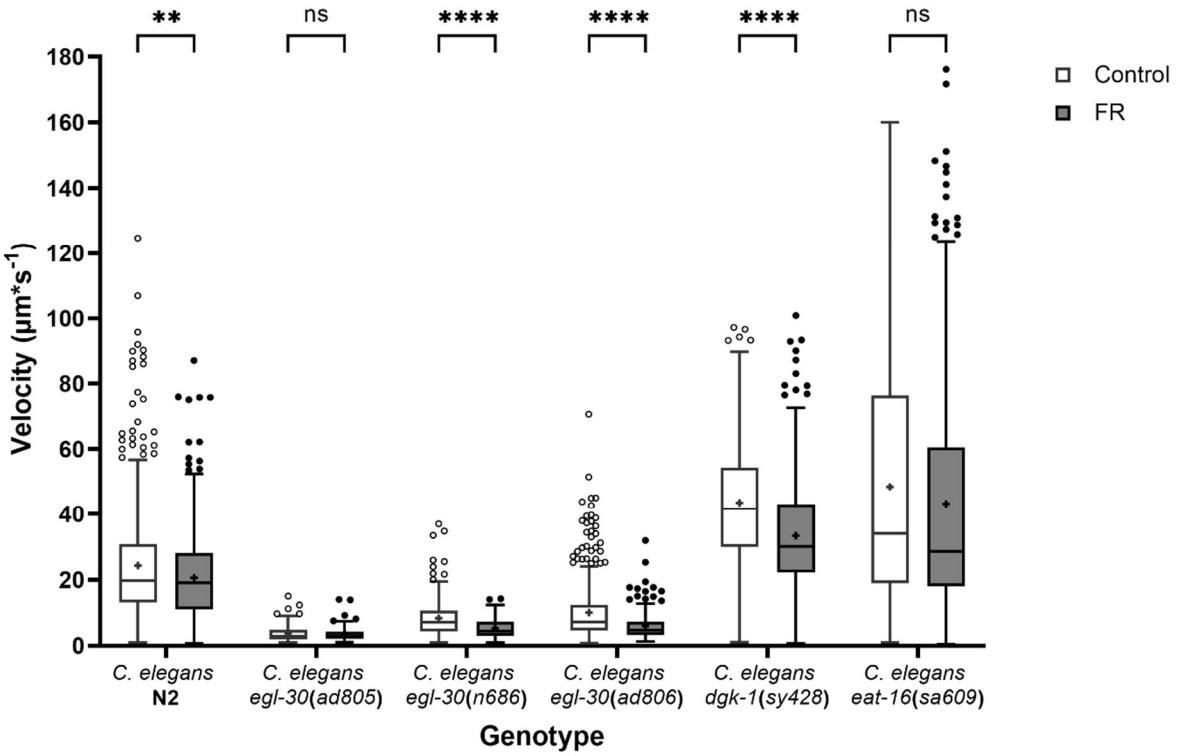

Figure 39: Effect of FR900359 (FR) on the velocity of six *Caenorhabditis elegans* genotypes (N2, *egl-30*(*ad805*), *egl-30*(*n686*), *egl-30*(*ad806*), *dgk-1*(*sy428*), *eat-16*(*sa609*)). All nematodes were fed with *Escherichia coli* OP50, placed as lawn in the middle of the nematode growth medium plate and mixed with 1 % dimethyl sulfoxide (Control). In the FR group 2.5 mM FR were added to the food. The movement of adult nematodes in and around the lawn was recorded and analyzed. Velocities are displayed as box plot with tukey whiskers (Quartile ± 1.5*inter-quartile distance), and the mean is displayed as +. Results summarize the data from three repeats. Velocities of *C. elegans* N2, *dgk-1*(*sy428*), and *eat-16*(*sa609*) were compared (FR versus control) using the Mann-Whitney test and velocity of *egl-30* mutants were compared using the unpaired t-test. P>0.05=ns, P<0.05=*, P<0.01=**, P<0.001=***, P<0.0001=****. Figure was adapted from Hanke et al, 2023 and raw data of the figure can be found in the supplementary material of the publication[2].

Regarding the wildtype N2, nematodes moved with a significantly lower average velocity in the presence of FR (Multiple Mann-Whitney tests: P=0.0076) (**Figure 39**). The spatial distribution of *C. elegans* N2 was also influenced by FR, as the number of worms in the lawn was significantly reduced, i.e., 92.2 % without FR compared to 83.8 % with FR

(Modified two sample binomial test (MBT): P=0.0021) (**Figure 40**). These results comply with the expected outcome of G_q inhibition.

FR did not influence the mean velocity (Unpaired t-test: P=0.9876) of the strong mutant *egl-30*(*ad805*) (**Figure 39**) or its spatial distribution (MBT: P=0.6818) (**Figure 40**). It must be mentioned that only two repeats were included in the analysis of the spatial distribution, as the bacterial lawn of the third repeat was enlarged unevenly as evident in **Figure 67 (B)** and therefore excluded. The strong mutant *egl-30*(*ad805*) was not expected to be affected by the G_q inhibition of FR, as it already has a severely impaired G_q signaling. Therefore, the results were as expected.

Both weak *egl-30* mutants, *egl-30*(*n686*) and *egl-30*(*ad806*), moved significantly slower on average in the presence of FR (Unpaired t-test: both P<0.0001) (**Figure 39**). Comparison of the control experiments of both genotypes revealed that *egl-30*(*ad806*) had a significantly higher velocity than *egl-30*(*n686*) in the control experiment (unpaired t-test: P=0.0168), which agreed with previous reports[259]. For the weak *egl-30* mutants, significantly more worms were observed outside of the FR-containing lawn compared to the control (*egl-30*(*n686*) MBT: P<0.0001, *egl-30*(*ad806*) MBT: P=0.0003) (**Figure 40**). As the inhibition of G_q by FR increased the impairment of *egl-30*(*n686*) and *egl-30*(*ad806*), similar phenotypes as observed for *egl-30*(*ad805*) were expected and confirmed.

The suppressor mutant *dgk-1*(*sy428*) showed a significantly reduced velocity in the FR-containing lawn (Mann-Whitney tests: P<0.0001) (**Figure 39**), which was expected as the G_q hyperactivity caused by the mutation of *dgk-1* should be reduced by FR. Compared to N2 grown in FR-containing lawn, *dgk-1*(*sy428*) worms moved significantly faster in presence of FR (Mann-Whitney test: P<0.0001) revealing that *dgk-1*(*sy428*) was able to rescue the velocity decrease by FR. The spatial distribution was significantly affected by FR, as the number of worms in the lawn was significantly reduced, i.e., 84.4 % without FR compared to 59.6 % with FR (MBT: P<0.0001) (**Figure 40**).

For the other suppressor mutant *eat-16*(*sa609*) the average velocity was reduced by FR; however, the reduction was not significant (Multiple Mann-Whitney tests: P=0.0534). Compared to *dgk-1*(*sy428*) a greater span of velocities was discovered for *eat-16*(*sa609*), which might explain the lack of significance. Nevertheless, *eat-16*(*sa609*) grown on FR-containing lawn was able to rescue the velocity decrease of N2 grown in presence of FR (Mann-Whitney test: P<0.0001) as expected (**Figure 39**). As observed for the other

suppressor mutant *dgk-1*(*sy428*), the number of *eat-16*(*sa609*) inside the lawn was significantly decreased in the FR-containing lawn (MBT: P<0.0001) (**Figure 40**).

All *C. elegans* genotypes, except the strong *egl-30*(*ad805*) mutant, appeared to avoid the presence of FR (**Figure 40**), as the number of nematodes was always significantly lower in the bacterial lawn with FR compared to the control. One explanation is the detection of FR by *C. elegans* via its sensory system, which subsequently initiates lawn avoidance, as described for serrawettin W2, a cyclic depsipeptide and biosurfactant produced by *Serratia marcescens* Db10[293]. In this case it is likely that FR-Core would be detected similarly, but experiments with FR-Core did not influence the spatial distribution of *C. elegans* N2 (**Table 26**). This suggests that the inhibitory effect of FR results in the observed avoidance and the fact that G_q signaling plays an antagonistic role in olfactory adaption to amphid wing "C" cells-sensed odorants[294] might be an explanation. Therefore, the G_q inhibition by FR might accelerate the adaptation of nematodes resulting in avoidance. Nevertheless, the effect of FR is probably not solely connected to the G_q inhibition, as avoidance has been observed for all genotypes, except the strong mutant *egl-30*(*ad805*).

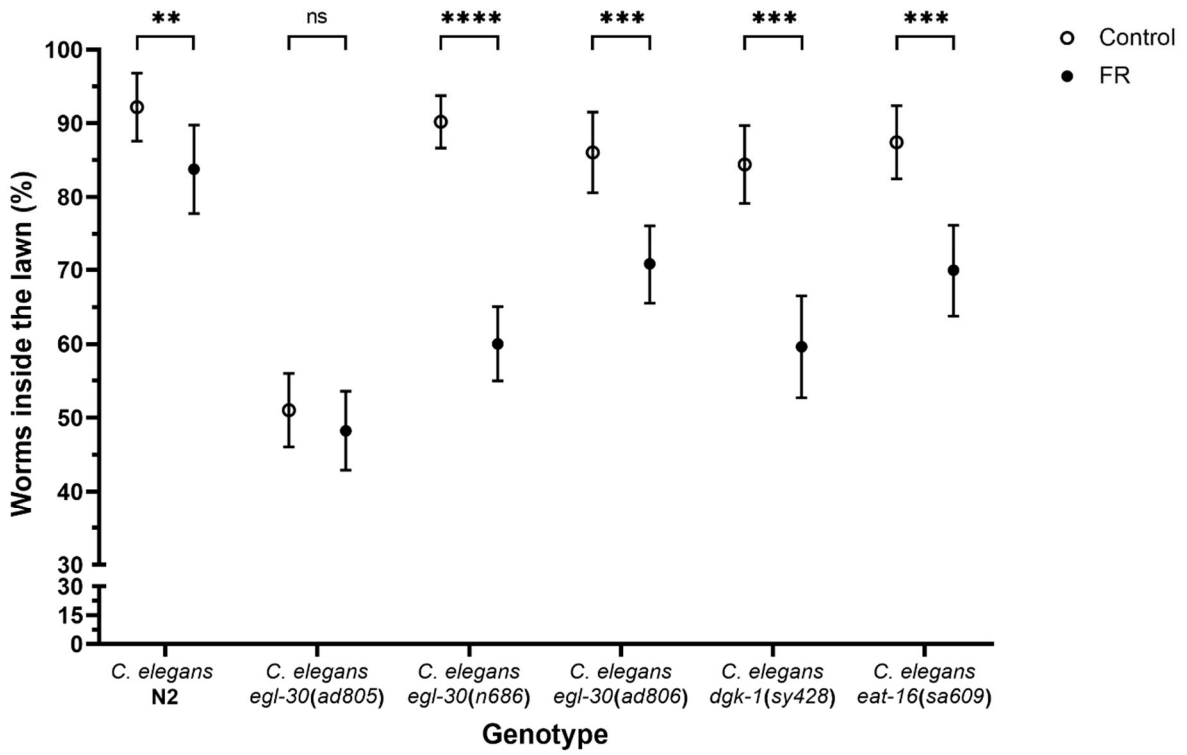

Figure 40: Effect of FR900359 (FR) on the spatial distribution of six *Caenorhabditis. elegans* genotypes (N2, *egl-30*(*ad805*), *egl-30*(*n686*), *egl-30*(*ad806*), *dgk-1*(*sy428*), *eat-16*(*sa609*)). All nematodes were fed with *Escherichia coli* OP50, placed as lawn in the middle of the nematode growth medium plate

and mixed with 1 % dimethyl sulfoxide (Control). In the FR group 2.5 mM FR were added to the food. The movement of adult nematodes in and around the lawn was recorded and analyzed. All experiments except spatial distribution experiments for *egl-30*(*ad805*) (two repeats) were done in three repeats. The spatial distribution of nematodes in the lawn was compared using the modified two sample binomial test[295] and the empirical standard deviation was presented as error bars. P>0.05=ns, P<0.05=*, P<0.01=**, P<0.001=***, P<0.0001=****. Figure was adapted from Hanke et al, 2023 and raw data of the figure can be found in the supplementary material of the publication[2].

The counting of border crossings was thought to further support the avoidance of FR, as more nematodes were expected to leave the lawn, thereby crossing its border. This is in line with the behavior of *C. elegans* N2 and both suppressor mutants *dgk-1*(*sy428*) and *eat-16*(*sa609*), as they showed an increase of border crossings (**Table 2**). Next to the repellent effect of FR increasing the number of border crossings, an opposing effect was observed for the locomotion impaired *egl-30* mutants. In the cases of both weak mutants, *egl-30*(*n686*) and *egl-30*(*ad806*), the presence of FR led to a smaller number of border crossings (**Table 2**). This effect can be explained by the inhibition of locomotion in presence of FR, which prevented the crossing of the lawn border. The difference between both weak mutants is in line with their average velocity, as the slower mutant *egl-30*(*n686*) did only cross borders in the control twice, while no crosses were observed in the presence of FR. The more mobile *egl-30*(*ad806*) crossed the borders of the lawn nineteen times in the control, but only twice in the presence of FR. In the case of the strong mutant, the paralyzed phenotype did not allow border crossings.

Table 2: Effect of FR900359 (FR) on the total number of border crossings of six *Caenorhabditis. elegans* genotypes (N2, *egl-30*(*ad805*), *egl-30*(*n686*), *egl-30*(*ad806*), *dgk-1*(*sy428*), *eat-16*(*sa609*)). All nematodes were fed with *Escherichia coli* OP50, placed as lawn in the middle of the nematode growth medium plate and mixed with 1 % dimethyl sulfoxide (Control). In the FR group 2.5 mM FR were added to the food. The movement of adult nematodes in and around the lawn was recorded and analyzed.

	C. elegans					
	N2	***egl-30*(*ad805*)**	***egl-30*(*n686*)**	***egl-30*(*ad806*)**	***dgk-1*(*sy428*)**	***eat-16*(*sa609*)**
Control	8	0	2	19	28	37
FR	28	0	0	2	35	41

In summary, FR reduces the velocity of *C. elegans* by G_q inhibition. Additionally, nematodes seemed to evade the presence of FR, as more nematodes are found outside of the FR-containing lawn. The mechanism behind this effect is unknown thus further studies investigating a learned avoidance of FR by *C. elegans* might reveal new insights into the interaction of FR targets and FR producers.

3.4.3.1.2. Investigation of the effect of FR on egg-laying of *C. elegans*

$G\alpha_q$ malfunction is associated with defective egg-laying (i.e., egl) by *C. elegans*[259], therefore the effect of FR on egg-laying was examined. For these experiments, the strong *C. elegans egl-30*(*ad805*) mutant was excluded, as time extended tracking experiments already revealed, as expected, that this mutant was close to being unable to lay eggs (**Figure 72**). The remaining five genotypes (*C. elegans* N2, *C. elegans egl-30*(*n686*), *C. elegans egl-30*(*ad806*), *C. elegans dgk-1*(*sy428*), *C. elegans eat-16*(*sa609*)) were investigated regarding their egg-laying rate and raised as described in **chapter 5.15**. In short, twelve egg-laying adults per genotype and for each condition (i.e., with and without FR) were picked and placed on a new plate with the same condition (i.e., with or without FR). Nematodes were removed after two hours and eggs counted.

The results shown in **Figure 41** confirmed that an adult hermaphrodite *C. elegans* lays between four to ten eggs per hour[296] as the wildtype N2 laid an average of five eggs per hour. Surprisingly, N2 laid significantly more eggs per hour in the presence of FR (Unpaired t-test: P=0.0350), possibly because of more eggs retained as worms without hermaphrodite specific motor neurons accumulate eggs, due to a longer inactive state[297], and subsequently lay multiple eggs in their active state[297].

Both weak *egl-30* mutants *egl-30*(*n686*) and *egl-30*(*ad806*) laid fewer eggs compared to the wildtype and therefore verified that the mutation of *egl-30* results in egg-laying malfunction[259]. FR treatment further reduced the egg-laying rate significantly for both weak *egl-30* mutants, and in the case of *egl-30*(*n686*), no eggs were laid (Unpaired t-tests: P<0.0001, P=0.0005) (**Figure 41**). These results comply with the expected outcome, considering the influence of G_q on egg-laying.

For both suppressor mutants *dgk-1*(*sy428*) and *eat-16*(*sa609*), reduced egg-laying compared to N2 was observed, which might be caused by the lack of egg production[292]. However, both suppressor mutants were unaffected by FR treatment (Unpaired t-tests: P=0.3542, P=0.0618) (**Figure 41**).

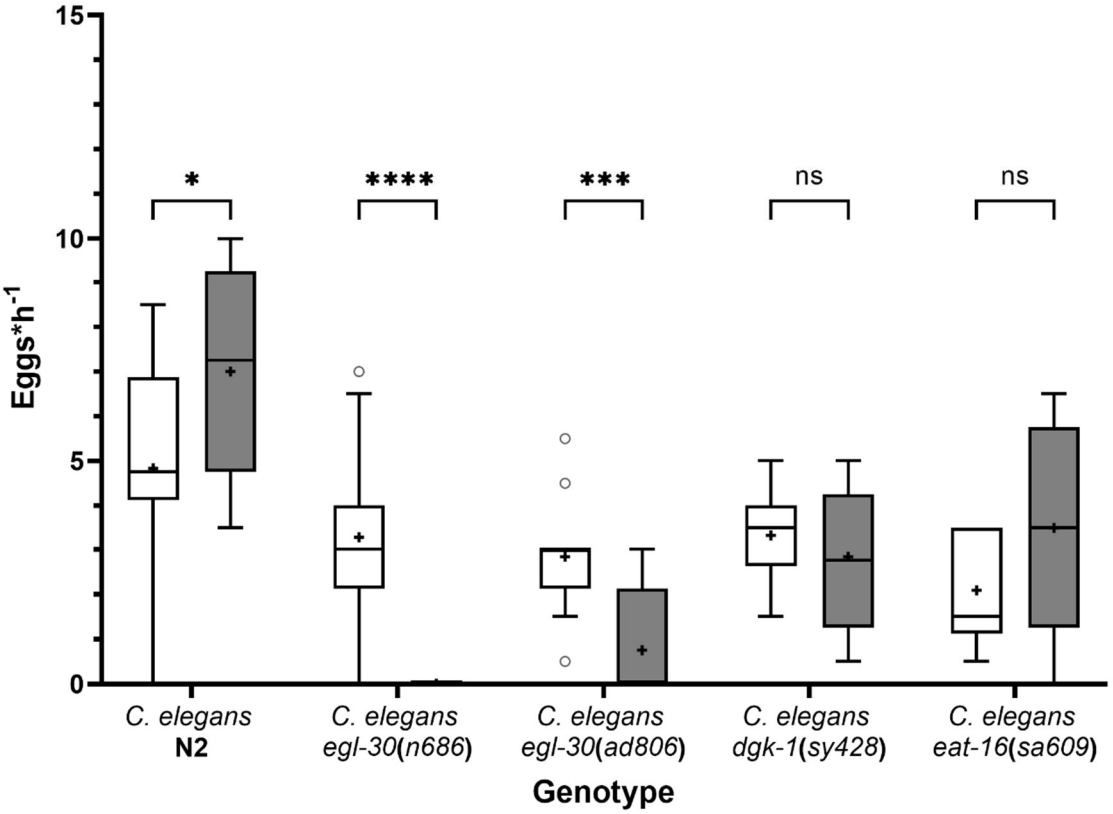

Figure 41: FR900359 (FR) inhibits egg-laying of *Caenorhabditis elegans*. Egg-laying rate for different *C. elegans* strains (N2, *egl-30*(*n686*), *egl-30*(*ad806*), *dgk-1*(*sy428*), and *eat-16*(*sa609*)) in presence (grey) or absence of FR (control, white). Both groups were grown until egg-laying adult stage on nematode growth medium plates covered with *Escherichia coli* OP50 as food source mixed with 1 % dimethyl sulfoxide, and FR for the FR group. Twelve nematodes per group were analyzed individually for their egg-laying (Worms on FR were analyzed in presence of FR and similar for control). Data are presented as box and tukey whiskers (Quartile ± 1.5*inter-quartile distance) plot. The significance was evaluated using uncorrected multiple t-tests. P>0.05=ns, P<0.05=*, P<0.01=**, P<0.001=***, P<0.0001=****. Figure was adapted from Hanke et al, 2023 and raw data of the figure can be found in the supplementary material of the publication[2].

Another read-out to investigate egg-laying and a more common approach is to count the numbers of eggs in the uterus, also known as retained eggs. The retained eggs assay was performed to disentangle the effects on egg-laying versus egg production, reasoning that the more eggs are still in the uterus, the lower must be the egg-laying rate. The number of mutants investigated was reduced by excluding both weak *egl-30* mutants, *egl-30*(*n686*) and *egl-30*(*ad806*), due to the clear and unequivocal result in the egg-laying assay (**Figure 41**). In short, twenty egg-laying adults per condition (i.e., with and without FR) and genotype (*C. elegans* N2, *C. elegans dgk-1*(*sy428*), *C. elegans eat-16*(*sa609*)) were sampled, dissolved in bleach solution, and their remaining eggs counted as described in **chapter 5.15.3.2**.

FR treatment led to significantly more eggs in the uterus of wildtype N2 nematodes, as the mean increased from eleven to twenty-two eggs (**Figure 42**) (Unpaired t-test:

P<0.0001). This strengthened the proposed explanation for the observed increase of the egg-laying rate of *C. elegans* N2 in the presence of FR (**Figure 41**). In the absence of FR, *eat-16*(*sa609*) and *dgk-1*(*sy428*) showed less eggs in their uterus, compared to prior reports. However, the results in the report were achieved using a different timing schedule[292]. In the presence of FR, the number of retained eggs increased in both suppressor mutants *dgk-1*(*sy428*) (Mann-Whitney test: P=0.0012) and *eat-16*(*sa609*) (Unpaired t-test: P=0.0005) as well (**Figure 42**). The results for the wildtype and the suppressor mutants, witnessed in the retained eggs assay, were expected as G_q inhibition by FR led to higher numbers of eggs in the uterus due to egg-laying inhibition. Furthermore, in presence of FR, the number of eggs in the uterus was significantly decreased by *dgk-1*(*sy428*) (Mann-Whitney test: P<0.0001) and *eat-16*(*sa609*) (unpaired t-test: P=0.0001) compared to N2, showing that the suppressor mutants rescue *C. elegans* N2.

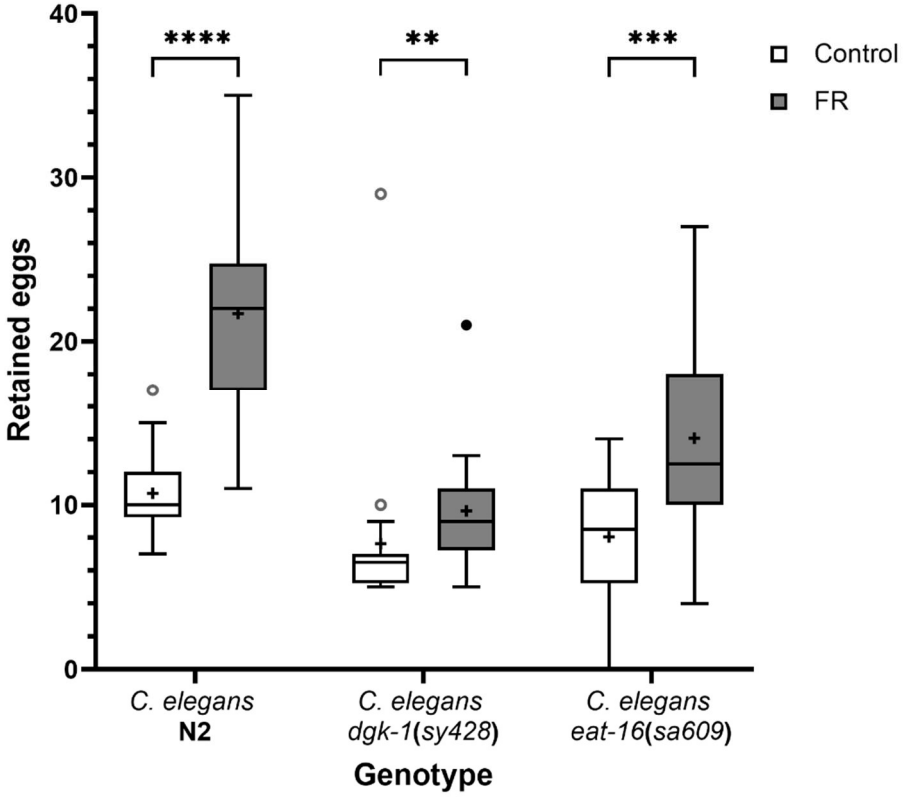

Figure 42: FR900359 (FR) inhibits egg-laying of *Caenorhabditis elegans*. Retained egg assay was performed with *C. elegans* N2, *dgk-1*(*sy428*), and *eat-16*(*sa609*). Both groups were grown until egg-laying adult stage on nematode growth medium plates covered with *Escherichia coli* OP50 as food source and 1 % dimethyl sulfoxide. For the FR group 2.5 mM FR were added to the food source. Twenty nematodes per group were bleached and eggs were counted. Data are presented as box and tukey whiskers (Quartile ± 1.5*inter-quartile distance) plot. The significance was evaluated using uncorrected multiple t-tests for *C. elegans* N2 and *eat-16*(*sa609*), while *dgk-1*(*sy428*) was evaluated using Mann-Whitney test. P>0.05=ns,

P<0.05=*, P<0.01=**, P<0.001=***, P<0.0001=****. Figure was adapted from Hanke et al, 2023 and raw data of the figure can be found in the supplementary material of the publication[2].

Taken together, FR reduced velocity and inhibited egg-laying of *C. elegans*. Furthermore, FR targets the $G\alpha_q$ ortholog of *C. elegans* and leads to phenotypes as observed for *egl-30* deficient mutants.

3.4.3.2. *In vivo* assays with *H. schachtii* and FR

As representative for plant pathogenic nematodes, *H. schachtii* was chosen to assess the effects of FR. As unhatched juvenile stage 2 worms (J2) can survive in the cyst for a long time, parasitic cyst nematodes, e.g., *Globodera* and *Heterodera* spp., are difficult to erase from soil and present a challenge for agriculture. After hatching from their cyst, J2 worms explore the soil for the root of a plant which they enter by piercing the cell wall, migrate into, and form a syncytium by modifying plant cells. Until reaching juvenile stage 4 for males and adult stage for females, they stay at the plant and feed on the syncytium. Then, the male fertilizes females, which develop into the cysts. Only two stages, i.e., the cyst and the J2 stage of *H. schachtii*, are detached from the host plant during the life cycle of *H. schachtii* and therefore may be influenced by soil compounds[277,298–300].

For the activity assay, J2 *H. schachtii* were exposed to FR and active versus inactive J2 were determined by their body shape and compared. Additionally, the effect of octopamine was tested, which is used to stimulate feeding, leading to an oral uptake of xenobiotic compounds from surrounding media[301]. This resulted in four different conditions that were tested, the control without FR and without octopamine (OA), the experiment with OA, the experiment with FR, and the one with FR and OA (**Figure 43 (A)**). Compared to the control, FR (without OA) significantly raised the number of inactive worms from 70 % to 83 % (One-way analysis of variance (ANOVA): P=0.0009). This effect was stronger in the presence of octopamine as only 9 % were inactive nematodes in the control and 92 % were inactive in the presence of FR (One-way ANOVA: P<0.0001). Therefore, FR inhibition of G_q resulted in a decrease of *H. schachtii* J2 activity. However, the physiology behind this is unknown. As **Figure 43 (B)** illustrates, the number of inactive nematodes at the J2 stage is increasing in a FR concentration-dependent manner.

Comparing both experiments without FR, OA was revealed to significantly lower the number of inactive nematodes in the control experiment from 70 % to 9 % (One-way ANOVA: P<0.0001). Furthermore, octopamine increased the number of inactive nematodes significantly in presence of FR from 83 % to 92 % (One-way ANOVA:

P=0.0262) (**Figure 43 (A)**). These effects were expected, as octopamine enhanced the intake of xenobiotic compounds, i.e., FR[301], and significantly reduced the number of inactive worms in the experiment with OA but without FR, due to its influence on movement[302] and quiescence[303,304].

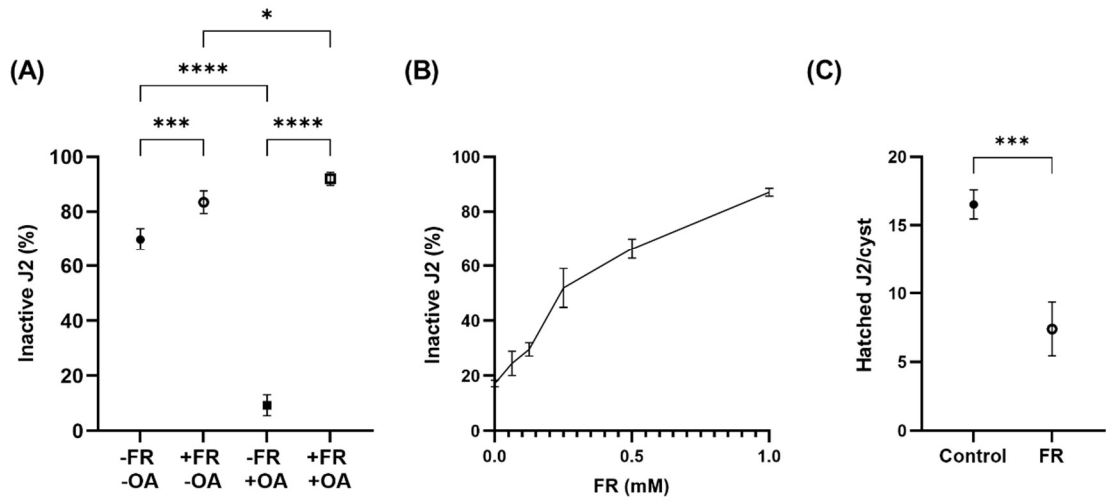

Figure 43: Effects of FR900359 (FR) on movement **(A)**, **(B)** and hatching **(C)** of *Heterodera schachtii* juvenile stage 2 (J2). **(A)** After incubation of *H. schachtii* J2 for four days in the presence of FR (1 mM) mixed with 1 % dimethyl sulfoxide (DMSO) [+FR] or 1 % DMSO [-FR] either with [+OA] or without octopamine (OA) [-OA] the number of inactive (not bend or moving) and active worms was counted. The relative amount is depicted on the y-axis. The significance was evaluated using ordinary one-way analysis of variance with Tukey's multiple comparisons test. **(B)** After incubation of *H. schachtii* J2 for four days in presence of six different FR concentrations (0, 0.0625, 0.125, 0.25, 0.5, 1 mM) mixed with 1 % DMSO the number of inactive (not bend or moving) and active worms was counted. The relative amount is depicted on the y-axis. **(C)** Comparison of hatched *H. schachtii* juveniles per cyst with 1 mM FR disolved in 1 % DMSO [FR] or 1 % DMSO [Control] after seven days of incubation. The significance was evaluated using unpaired t-test. All experiments, n = 4. P>0.05=ns, P<0.05=*, P<0.01=**, P<0.001=***, P<0.0001=****. Figure was adapted from Hanke et al, 2023 and raw data of the figure can be found in the supplementary material of the publication[2].

Next, the cysts of *H. schachtii* were exposed to FR during the cyst assay for 7 days. Afterwards, the number of hatched juveniles in comparison to not treated cysts was counted (**Figure 43 (C)**) and the ratio hatched juveniles per cyst calculated. FR inhibited hatching of J2, as the number of hatched J2 per cyst was significantly decreased in the presence of FR from 17 ± 1 to 7 ± 1 hatched J2 per cyst (Unpaired t-test: P=0.0002).

In summary, inhibition of G_q by FR impairs J2's hatching from the cysts of *H. schachtii*. As hatching from cysts involves movement of the juvenile worms[305], the inhibition of activity by FR may result in J2 that are unable to hatch. Alternative explanations are also possible, e.g., an effect of FR on the development of *H. schachtii* stages or the inhibition of signaling cascades involved in hatching.

3.4.4. Discussion

The following discussion is taken from Hanke et al, 2023[2]: "FR is an inhibitor of G_q proteins involved in signal transduction of GPCRs and shown to have the potential to protect plants from insects[143] and mammals[164,171] *in vitro* and *in vivo*. Our *in silico* analysis of the putative FR binding sites of various nematodic G_q proteins strongly indicated the possibility of FR binding and inhibition of these proteins. (**Figure 34** and **Figure 35**). *In vitro* expression of *egl-30* (i.e., G_q) of *C. elegans* and the here newly identified $G\alpha_q$ ortholog of *H. schachtii* in HEK $G_{q/11}$-KO cells, together with overexpression of RIC-8A and M3, enabled functional expression and characterization of the proteins (**Figure 37** and **Figure 38**). *In vitro*, FR inhibited both, *C. elegans* and *H. schachtii* $G\alpha_q$ signaling, as IP_1 accumulation and calcium increase were blocked.

In vivo, FR affects the nematode *C. elegans* by significantly decreasing their velocity (**Figure 39**) and inhibiting egg-laying (**Figure 41** and **Figure 42**). Considering that *C. elegans* is feeding on bacteria, these effects suggest that *C. vaccinii* MWU205 produces FR to reduce the activity and abundance of predators. *H. schachtii* is a pathogen feared in agricultural cultivation of crops belonging to the family Brassicaceae or Amaranthaceae, especially sugar beets (*Beta vulgaris*)[306], as the cysts persist in soil and are difficult to erase[300]. *In vivo* experiments (**Figure 43**) demonstrate an inhibitory effect of FR on the activity of J2 *H. schachtii* and revealed FR to suppress hatching of J2.

It must be noted, however, that the low concentrations of FR observed in SESOM could hardly lead to similar *in vivo* effects on *C. elegans* and *H. schachtii*. Chronic exposure to FR in soil and exponential effects[307,308] as conceivable by reduced egg-laying or hatching, could work together in a synergistic fashion. Also, a higher production of FR by *C. vaccinii* MWU205 in soil compared to SESOM is reasonable. The presence of other potent metabolites from *C. vaccinii* MWU205, e.g., valhidepsins, for which a surfactant effect has been shown[128], and violacein[61], which is reported to have also nematocidal and antibacterial activity[78] also has to be taken into account."[2]

The results concerning the biological activity of FR, as described in this chapter, provide a compelling example for the ecological importance of bacteria like *C. vaccinii* MWU205 and their excreted metabolome in the soil. The bacterial community may well contribute to an ecological homeostasis, being a requirement for the fruitful growth and sustainable cultivation of plants.

4. Conclusion and Outlook

This study focusses on *Chromobacterium vaccinii* MWU205 and one of its most prominent secondary metabolites, i.e., FR. The bacterium was found to be part of the soil microbiome[61] and to secret FR (**Figure 32**). The conducted investigations aimed to shed light on the possible role of *C. vaccinii* MWU205 and FR in its natural environment in the context of plant health, focusing on soil-associated nematodes. The examination of the function of single members of the microbiome, i.e., here *C. vaccinii* MWU205, may reveal new insights into complex interactions.

The microbiome was defined by Berg et al in 2020 as a characteristic microbial community in a defined habitat, which encompasses a theatre of activity thereby forming a dynamic and interactive micro-ecosystem integrated in macro-ecosystems, for whose health and function they are crucial[309]. Therefore, it has been the subject of science for more than fifty years[310], with a tremendous increase over the last twenty years until today, as the number of publications on the platform PubMed® for the keyword "microbiome" reached its maximum in 2022 with nearly 30,000 publications (5th September 2023). This development underlines the enormous and growing importance of research on microbiomes, whether it's the microbiome of humans[311–314], animals[315–317], plants[11,318–320], or soil[6,8,13]. Recently, even holistic approaches were pursued looking at the connection between all microbiomes in regard to their impact on "One health"[8]. Efforts to influence the microbiome of an organism to benefit the host are known under the term microbiome breeding and currently microbiome therapeutics, e.g., fecal microbiota transplantation, probiotics, are developed for humans[321–323]. In 2022, the Federal Drug Administration approved Rebyota™ as first fecal microbiota product for the prevention of recurrence of *Clostridioides difficile* infection in adults[324]. As stated by Peixoto et al, 2021, "Host-associated microbiomes contribute in many ways to the homeostasis of the metaorganism"[315]. This is not only true for animals, but also transferable to soil, as soil itself functions like a metaorganism and its homeostasis is supported by its microbiome.

Soil Health is the ability of soil to function as a vital living ecosystem that sustains plants, animals, and humans[325]. Challenges like climate change and the increasing demand of food underline the need for a healthy soil for sustainable agriculture[9,326]. As the soil microbiome functions as the backbone of sustainable agriculture[327] and "[…] innovations with the use of microbiomes represent the future of sustainable agriculture."[328], further

research on this topic is indispensable[329]. Over the past years intensive investigations of the soil microbiome have been conducted using different approaches like metagenomics, metatranscriptomics, metaproteomics, and metabolomics that are united by the soil metaphenome, which combines the expressed functions encoded in the metagenome with the resources and spatial, biotic and abiotic constraints of the environment[3,14,326]. However, the elucidation of the microbiome's function is difficult due to its heterogeneity and complexity[326], thus studies to elucidate the microbiome are becoming more complex like the review published by Saleem et al in 2019 that used "[…] biodiversity–ecosystem functioning relationships as an overarching framework that combines molecular interactions with community ecology, thereby linking microbiome taxonomic and functional diversity or composition to plant growth and soil health."[327].

The herein investigated *C. vaccinii* MWU205 is a member of the soil microbiome, as it was isolated from wild cranberry bogs in 2013[61]. Previous investigations of the strain have revealed it to produce the NPs violacein[61], valhidepsins[128], and FR[130,151]. Furthermore, *C. vaccinii* MWU205 possesses insecticidal activities probably due to FR and violacein[113,330], carries genes for virulence factors, e.g., siderophores, hydrogen cyanide, and secreted chitinases[219], and produces volatile organic compounds that inhibit the growth of fungal isolates from cranberry bogs[331]. Recently, the BGC of 2,4-diacetylphloroglucinol was detected in the genomes of eleven *Chromobacterium* strains. Additionally, the BGC of FR was discovered in all *C. vaccinii* strains[126]. All of these traits make *C. vaccinii* MWU205 a soil bacterium with the ability to affect soil health and influence organisms associated to soil.

In this study this trait was further investigated, as *C. vaccinii* MWU205 was revealed to carry the BGCs for two siderophores and one 2,4-phloroglucinol-related compound (**Figure 4**), which might have plant-growth promoting bioactivities. Furthermore, several novel derivatives of FR and valhidepsins have been identified via mass spectrometric approaches in **chapter 3.1.2**.

In the ecological context it is important to note, that this study provides the first evidence that the biosynthesis of FR by *C. vaccinii* MWU205 is possible in soil extracts (**Figure 31**), and taken together with the here shown excretion of FR from the bacterial cell into the surrounding (**Figure 32**), FR can be suspected to be present in soil. As a consequence, and based on former studies, FR might inhibit or even kill insects in soil[113,143,330]. The experiments conducted in this project could show that FR affects soil-

associated nematodes in *in vivo* experiments, as it reduces the velocity (**Figure 39**) and inhibits the egg-laying of *C. elegans* (**Figure 41** and **Figure 42**), and suppresses the activity and the hatching of *H. schachtii* juveniles (**Figure 43**). In general, it is most likely that FR affects all $G\alpha_q$-containing organisms in soil and therefore might play a crucial role in sustaining the ecological equilibrium and homeostasis of soil.

As this study has revealed the potential impact of FR on soil organisms, the question "how widespread is the ability to produce FR in soil and specifically in the species *C. vaccinii*?" needs to be answered in future. Using a combination of 'omics' technologies, i.e., metagenomics, metatranscriptomics, metaproteomics, and metabolomics[326], soil samples may be systematically scanned for the presence of FR/FR-related BGCs or other potential FR producers in soil.

Recently, Johnson et al, 2023, proposed that genomes of all *C. vaccinii* strains carry the BGC for FR. However, the authors did neither provide the respective sequences, nor any data base entries of them. These sequences would enable a detailed comparison of all FR gene clusters and allow investigations of its evolution. Furthermore, a comparison of the spectrum of FR derivatives produced by each strain may be conducted using molecular networking to identify novel FR derivatives. As *C. vaccinii* was found on North and South America, and the European continent, further studies examining the diversity of the species *C. vaccinii* may find new strains.

The ecological role and function of *C. vaccinii* MWU205 is still a complex puzzle, therefore the identification of compounds encoded by the predicted BGCs, their isolation, and the investigation of their bioactivity will help to further characterize the abilities of *C. vaccinii* MWU205. One example are the siderophores viobactin and chromobactin, the exact structure of which are not known[102]. Johnson et al., 2023 have proven the activity of the 2,4-diacetylphloroglucinol-related BGC by conversion experiments of 2,4-phloroglucinol to 2-acetylphloroglucinol and phloroglucinol, however, they were not able to isolate the product of this cluster[126].

Another current research gap are the synergistic effects of the produced secondary metabolites, i.e., valhidepsins, violacein, and FR. Furthermore, the plant-growth promoting effect of *C. vaccinii* MWU205 itself needs to be investigated. Pot experiments[332,333] or novel methods like "ASURE"[334] may be utilized to investigate the

effect of *C. vaccinii* MWU205 and different mutants of *C. vaccinii* MWU205 on the growth and health of plants.

In essence, this study reveals the impact of the secondary metabolite FR produced by *C. vaccinii* MWU205 on soil-associated organisms and supports the hypothesis that *C. vaccinii* MWU205 and the excreted FR in soil might contribute to an ecological equilibrium, maintaining and establishing the successful growth of plants.

5. Material and Methods

5.1. Chemicals

All chemicals were bought from Sigma-Aldrich®, Fisher Chemical®, Carl Roth®, Sarstedt®, Labsolute® and Cambridge Isotope Laboratories if not otherwise mentioned.

5.2. Organisms

"Cultivation of *Ardisia crenata* was performed by the Botanical Garden Bonn of the University of Bonn, after *A. crenata* was purchased commercially (Herbarium specimens' location: Institute for Pharmaceutical Biology of the University of Bonn). The specimens were dried at 25 °C until extraction."[1]

"*Chromobacterium vaccinii* MWU205 (DSM 25150, ATCC BAA 2314) was purchased from the German Collection of Microorganisms and Cell Cultures, DSMZ."[1] Mutantes (Δ*frsC*, Δ*vioA*, Δ*frsGvioA*) were generated by René Richarz. *H. schachtii* was kindly contributed by Philipp Gutbrod. "*C. elegans* strains N2, *egl-30(n686)*, *egl-30(ad806)*, *egl-30(ad805)*, *dgk-1(sy428)*, *eat-16(sa609)* and *Escherichia coli* strain OP50 were provided by the Caenorhabditis Genetics Center, which is funded by the NIH Office for Research Infrastructure Programs (P40 OD010440)*."*[2]

5.3. Soil sample

"Topsoil was collected in a garden on the 2nd of April 2019 (Dortmund Eichlinghofen, North Rhine-Westphalia: 51°28'35.0"N 7°24'22.1"E) and air-dried on paper for one week at room temperature."[2] It was stored at 4 °C and sieved before usage to separate it from plant debris and rocks.

5.4. Media and buffers

The following media, LB and M9, were prepared as described below and supplemented with the antibiotic carbenicillin disodium salt (final concentration: 50 µg/mL) except media used in the context of SESOM experiments.

5.4.1. LB medium

The components of **Table 3** were solved in distilled water (dH_2O) and the medium's pH was adjusted to 7.5 using 5 M NaOH, and autoclaved.

Table 3: Components of LB medium, solved in dH_2O. The pH was adjusted to 7.5 with 5 M sodium hydroxide.

Component	Final concentration
NaCl	10 g/L
Tryptone	10 g/L
Yeast extract	5 g/L

For agar plates 16 g of agar was added for 1 L of medium before autoclaving.

5.4.2. M9 medium

M9 medium was prepared according to the protocol of the Helmholtz Zentrum München summarized in **Table 4** with biotin and thiamin for molecular networking and without both supplements for later cultivations.

Table 4: M9 medium composition for 1 L. EDTA = Ethylenediaminetetraacetic acid.

Volume	Component	Final concentration
100 mL	M9 salt solution (10x) pH 7.2 (with 5 M NaOH) autoclaved	Na_2HPO_4: 33.7 mM KH_2PO_4: 22 mM NaCl: 8.55 mM NH_4CL: 9.35
20 mL	20 % Glucose autoclaved	0.4 %
1 mL	1 M $MgSO_4$ autoclave	1 mM
0.3 mL	1 M $CaCl_2$ autoclave	0.3 mM
1 mL / -	Biotin (1 mg/mL) sterile filtration	1 µg/mL
1 mL / -	Thiamin (1 mg/mL) sterile filtration	1 µg/mL
10 mL or 1 mL*	Tracer elements solution (100x or 1000x) Solve EDTA (pH 7.5 with 5 M NaOH) + others sterile filtration	EDTA: 0,134 mM $FeCl_3$: 0,031 mM $ZnCl_2$: 6,2 µM $CoCl_2$: 0,76 µM CoCl: 0,42 µM, H_3BO_3: 1,62 µM $MgCl_2$: 0,081 µM
867 mL/876 mL*: +biotin & thiamin	Autoclaved dH_2O	-

869 mL/878 mL*: -biotin & thiamin

5.4.3. Nematode growth medium (NGM)

NGM agar plates were used to work with *C. elegans*. NGM was prepared using the components listed in **Table 5**.

Table 5: Recipe for 1 L of NGM agar.

Component	Amount
NaCl	3 g
Agar	17 g
Peptone	2.5 g
Cholesterol	1 mL (5 mg/mL in 95 % EtOH)
dH_2O	975 ml

After autoclaving, sterile solutions (autoclaved) as described in **Table 6** were added.

Table 6: Components added to autoclaved NGM agar before plating. *to avoid precipitation, mix between the addition of $MgSO_4$ and potassium phosphate

Component	Volume
1 M $CaCl_2$	1 mL
1 M $MgSO_4$	1 mL
1 M potassium phosphate (pH 6)*	25 mL

NGM agar plates were prepared with 1 mL for 3.5 cm plates, 10 mL for 6 cm plates, and 20 mL for 10 cm plates. The smallest size was used for egg-laying experiments, while 6 cm was used for the tracking experiments. Both bigger sizes were used for maintenance.

5.4.4. M9 buffer

For synchronization and collection of *C. elegans* M9 buffer was prepared as described in **Table 7** and below.

Table 7: Recipe for 1 L M9 buffer.

Component	Amount
KH_2PO_4	3 g
Na_2HPO_4	6 g

NaCl	5 g

After dissolving all components, dH_2O was added to 1 L and autoclaved. 1 mL autoclaved 1 M $MgSO_4$ was added to cool solution.

5.4.5. MOPS buffer

MOPS buffer was prepared as summarized in **Table 8**, its pH adjusted to 7 at 40°C, and used to extract SESOM.

Table 8: Recipe for MOPS buffer.

Component	Concentration
MOPS	2.093 g/L
Sodium acetate	0.205 g/L
Na_2EDTA	0.186 g/L

5.4.6. Soil extracts

For the NSE[238] 500 g of dry soil were mixed with 1.3 L of 80 % methanol in dH_2O and shaken at 160 rpm overnight at 21 °C. The supernatant was collected after 30 min of sedimentation and transferred to a new flask. Then 1.3 L of 80 % methanol was added to the soil and shaken at 160 rpm for 3 h at 21 °C. The two supernatants were combined and filtered through paper (folded filter paper, qualitative No. 40, Labsolute). The extract was evaporated followed by adjustment to a final volume of 200 mL with dH_2O, subsequently sterile filtered (0.2 µm polyether sulfone membrane) using a vacuum pump, and stored at 4 °C.

For the WE, also known as DSMZ medium 12[239], 100 g were mixed with 250 mL tap water for 1 h at 120 °C. After sedimentation and cooling for 1.5 h the extract was centrifuged at 14,500 rpm to collect the supernatant (pH=6.9). Subsequently, the extract was sterile filtered (0.2 µm polyether sulfone membrane) using a vacuum pump, and stored at 4 °C.

The NE extract was generated following the previous protocol[240]: 125 g of soil were mixed with 250 mL of 50 mM NaOH and shaken over night at 160 rpm and 21 °C. After 30 min of sedimentation the mixture was centrifuged at 14,500 rpm to collect the

supernatant. Subsequently, the extract was sterile filtered (0.2 µm polyether sulfone membrane) using a vacuum pump, and stored at 4 °C.

SESOM was extracted from soil according to the previous protocol[241]: 100 mg sieved soil was extracted with 0.5 L MOPS buffer at 160 rpm for 2 h. Afterwards the extract was filtered two times over paper filter (folded filter paper, qualitative No. 40, Labsolute) followed by vacuum filtration with 5 µm and subsequently 0.45 µm polyvinylidene fluoride. The pH was determined (7.1-7.3) and the whole extract was subsequently sterile filtered (0.2 µm polyether sulfone membrane). For SESOM+, chitin was autoclaved in the flask, which was afterwards used for sterile filtration of the final SESOM (final chitin concentration: 1 g/L).

All soil extracts were tested for sterility by inoculation of a LB plate and incubating it at 37 °C for 24 h.

5.4.7. Soil agar

The protocol was adapted from a method to grow *Streptopmyces* soil (Version Sept 2021) provided by Jana Schniete. 50 g sieved soil were mixed with 0.6 % autoclaved agarose (prepared with dH_2O) in a sterile glass plate. After it solidified, the soil agar was inoculated with 40 µL of *C. vaccinii* MWU205 precultures prepared as described in **chapter 5.6.6.1** and cultivate for 5 days at 4 °C, 25 °C, and 37 °C.

5.5. Cultivation of *E. coli* OP50

E. coli OP50 was utilized as food source for *C. elegans* in all *C. elegans* experiments, if not mentioned otherwise. An overnight culture of *E. coli* OP50 was prepared by picking a single colony from an LB plate (stored at 4 °C) using a sterile tip and place 200 mL LB medium. The culture was shaken at >150 rpm overnight at 37 °C.

Afterwards 100 µL of *E. coli* OP50 culture were added to NGM plates, swirled to distribute, and dried overnight on the bench. Plates were stored for three weeks in the cold room.

5.6. Cultivation of *C. vaccinii* MWU205

5.6.1. General protocols

5.6.1.1. Generation of a cryo culture

To generate cryo cultures for storage at -80 °C, 500 µL glycerol were mixed with 1 mL *C. vaccinii* MWU205 culture and stored at -80 °C.

5.6.1.2. Production of a preculture

30 µL of a cryo culture were used to inoculate an LB agar plate with or without ampicillin (final concentration: 200 µg/mL) and incubated for 2-4 days at 25 °C or 30 °C. Afterwards between 10-30 mL medium (LB or M9 medium - depending on to the main culture) were inoculated from the LB agar plate. Precultures were incubated for 15-36 h at 180 rpm and 25 °C.

5.6.1.3. Cultivation of main cultures

Except for soil experiments, 0.1 % of the main culture volume was taken as volume of preculture used for inoculation. The main culture was incubated between 36 to 48 h at 25 °C and 180-200 rpm if not mentioned otherwise. For the isolation of FR-6, 6 L M9 medium were used for cultivation, for FR varying volumes between 2 and 6 L were chosen, and for the completely $^{13}C/^{15}N$-labeled FR 2 L, 4.5 L, and 10 L were cultivated.

5.6.2. *C. vaccinii* MWU205 sample generation for FBMN

For cultivation in LB medium, sixteen 300 mL flasks were filled with 130 mL LB medium, inoculated, and cultivated for 7.5 days. Two measurement series were performed. Therefore, two flasks were treated in parallel each day, with two samples each with 40 mL, one in the morning and one 12 h later, being taken from one flask and extracted with *n*-butanol for 24 h followed by centrifugation at 4,000 rpm for 15 min to harvest and evaporate the upper phase.

For cultivation in M9 medium, 50 mL M9 medium were filled in thirty 100 mL flasks, inoculated, and cultivated for 7.5 days. Two measurement series were performed and on each day two flasks, one in the morning and one 12 h later, per measurement row were extracted with *n*-butanol for 23 h followed by centrifugation at 4,000 rpm for 15 min to harvest and evaporate the upper phase.

For evaluation of the FR and FR-2 production in **Figure 25** the AUC of *m/z* 1002.54 (FR) and 988.52 (FR-2) were calculated and multiplied with their crude extract weight resulting in the modified AUCs shown in **Table 17** and **Table 18**.

5.6.3. Feeding experiments with labeled precursors

To generate completely $^{13}C/^{15}N$-labeled FR glucose and ammonium chloride were exchanged by their labeled analogs (U-^{13}C-glucose and $^{15}NH_4Cl$) in all steps of cultivation. In a second big scale experiment completely ^{13}C-labeled PA (5 mM final concentration) was added to the cultivation.

5.6.4. Feeding experiments with non-labeled precursors

To change the FR derivative produced by *C. vaccinii* MWU205 different carbon acids and monofluorinated phenylalanines were added to LB or M9 medium with final concentrations stated in **Table 9**. All precursors were solved in their respective medium, and the pH was adjusted to approximately 7.

Table 9: Final concentrations of precursor carbon acids.

Carbon acid	**Final concentration**
Propionic acid	5 mM
U-^{13}C-propionic acid	5 mM
Isovaleric acid	20 mM
Isobutyric acid	20 mM
Valeric acid	20 mM
meta-F-Phe	2 mM
ortho-F-Phe	20 mM
para-F-Phe	20 mM

For PA, three repeats (50 mL M9 medium) with and without PA and three blanks (M9 medium, Carbenicillin, PA) were examined. The average AUC of the three blanks for *m/z* 1002.5 and *m/z* 988.5 were deducted from the respective AUC of the control and the experiment with PA resulting in the modified AUC in **Table 19**. These values were used for **Figure 26**.

For each carbon acid, except PA, one blank with 25 mL LB medium, carbenicillin and one of the carbon acids was prepared. For the experiment, three repeats with 35 mL LB

medium and one of the carbon acids were prepared. One control without any carbon acid was prepared as well. For the evaluation the blank AUC (*m/z* of the expected FR derivative) was deducted from the AUC of the control and the feeding experiments, resulting in the modified AUCs in **Table 20** and **Table 21**.

For the *meta*-F-Phe feeding in M9 medium, 50 mL of medium were cultivated and supplemented at the beginning with *meta*-F-Phe, with one control in M9 medium without feeding. Another experiment with M9 medium was conducted with the LIS system from scientific bioprospecting (formally known as aquila biolabs), which injected a single shot of *meta*-F-Phe, two repeats, or M9 medium for the control after 20 h of cultivation. Using *C. vaccinii* MWU205 Δ*vioA*, three 40 mL LB cultures fed with *meta*-F-Phe at the beginning, one control without feeding, and one medium blank were cultivated (**Table 22**). For the big scale experiment, 4.5 L were prepared and fed with *meta*-F-Phe.

To examine the impact of the location of the fluorine, *ortho*-F-Phe and *para*-F-Phe were fed using higher concentrations plus one blank with 40 mL LB medium, carbenicillin and *ortho*-F-Phe was prepared. For the experiment, three repeats with 35 mL LB medium and either *ortho*-F-Phe and *para*-F-Phe were prepared. One control without any phenylalanine was prepared as well. For the evaluation the blank AUC (*m/z* of the expected FR derivative) was deducted from the AUC of the control and the feeding experiments, resulting in the modified AUCs in **Table 22**.

5.6.5. Cultivation in soil extracts

For each of the four soil extracts, 35 mL were filled in four flasks. One of the flasks was directly extracted with *n*-butanol and represented the negative control, which AUC was later deducted from the inoculated samples. Three flasks represented the experiment and were inoculated using two *C. vaccinii* MWU205 colonies grown on LB plates. Afterwards the flasks were cultivated for 5 days as RT and subsequently extracted with *n*-butanol. For the generation of **Figure 30** the AUC for *m/z* 1002.5 of each extract blank was subtracted from the AUC for *m/z* 1002.5 of the samples (**Table 23**). The resulting AUCs were used to calculate the FR concentration, using the calibration curve in **Figure 30**.

5.6.6. Cultivation in SESOM

5.6.6.1. Preculture preparation

Precultures in LB medium were prepared without carbenicillin as described in **chapter 5.6.1.2**. Afterwards they were centrifuged at 5,000 rpm and 15 °C for 5 min. The pellet was washed two times with 0.9 % sodium chloride solution and resuspended afterwards. Next, colony-forming units (CFU) were determined using a dilution series, which was plated onto LB agar plates. After 2-4 days at 25 °C they were evaluated.

5.6.6.2. SESOM

For SESOM two main cultures à 80 mL were inoculated using $3.2*10^4$ CFU/µL. "One culture was separated at the start (0 days) into three samples à 25 mL, which were directly extracted. The second culture was separated similarly after 5 days of cultivation at 25 °C and 180 rpm. One blank was prepared using only SESOM. Extraction (1:1) was performed for 6 h at 180 rpm using *n*-butanol. Afterwards the whole extract was centrifuged for 15 min at 4,000 rpm and the upper phase was evaporated."[2]

For the generation of **Figure 31** the AUC for *m/z* 1002.5 of the blank (41,991) was subtracted from the AUC for *m/z* 1002.5 of the samples (**Table 24**). The resulting AUCs were used to calculate the FR concentration, using the calibration curve in **Figure 31**. Afterwards the concentration was multiplied with the weight of the raw extract in **Table 24**.

5.6.6.3. SESOM+

For SESOM+ eight 50 mL flasks with 30 mg chitin were sterilized and subsequently filled with SESOM. A blank was generated by extracting one flask without inoculation. Seven flasks were inoculated with $5.2*10^6$ CFU/µL and three of these flasks were extracted afterwards (0 days). Four flasks were cultivated (25°C and 180 rpm) and extracted after five days. For analysis via LC/MS 2 mg/mL solutions were prepared using LC/MS grade methanol.

For the generation of **Figure 31** the AUC for *m/z* 1002.5 of the blank (20,448) was subtracted from the AUC for *m/z* 1002.5 of each sample (**Table 25**). The resulting AUCs were used to calculate the FR concentration, using the calibration curve in **Figure 31**. Afterwards the concentration was divided by two and multiplied with the weight of the crude extract in **Table 25**.

5.7. Extraction protocols

5.7.1. General

Extractions were performed 1:1 with *n*-butanol over night at 180 rpm. Afterwards, the upper phase was collected using centrifugation at 4,000 rpm for 10-15 min followed by evaporation. The extract was weighed. If not mentioned otherwise, the concentration of samples diluted with LC/MS grade methanol was 1 mg/mL for measurement with LC/MS and LC/MS^2.

5.7.2. Separation into pellet and supernatant and extraction

Main cultures of *C. vaccinii* MWU205 grown in LB medium were prepared as described in **chapter 5.6.15.6.1.3** with a cultivation time of 43 h. All six LB medium cultures were centrifuged for 5 min at 5,000 rpm. The pellet was washed two times with 2.5 mL of 0.9 % sodium chloride solution. All three supernatants were united and extracted with 30 mL *n*-butanol as described above. The pellets were extracted with *n*-butanol, shortly treated with ultrasonic, and finally further extracted as described above. Samples with a concentration of 2 mg/mL were evaluated using LC/MS. The AUC at *m/z* 1002.5 of each sample was used for the calculation of the FR concentration with the calibration curve in **Figure 32** and divided by two and multiplied with the crude extract weight.

5.7.3. Extraction and isolation of *A. crenata* leaves

"LC/MS extracts of *A. crenata* were prepared using plant material from the green house of the Botanical Garden Bonn. After grounding 200 g of dried plant leaves and extracting them with methanol, the MeOH extract was extracted with n-butanol/water. Afterward the butanolic phase was fractionated by RP_{18} vacuum liquid chromatography (column: 11 x 7 cm, Polygoprep 60–50 C_{18}, Macherey-Nagel, Düren, Germany) using gradient elution from 70/30 H_2O/MeOH to 100 % MeOH to yield eight fractions (each 200 mL). Fraction 8 (100 % MeOH) was further purified using Sephadex LH-20 size exclusion chromatography (column: 60 x 3 cm) using MeOH as eluent. After sample loading and discarding the first 150 mL, a fraction of 30 mL was collected for LC/MS measurement."[1].

5.8. Isolation of pure compounds

FR-Core was isolated as described by Hermes et al, 2021[130].

5.8.1. Flash chromatography

For the isolation of FR, FR-6 and completely $^{13}C/^{15}N$-labeled FR crude extracts were fractionated using a Reveleris® C_{18} flash column (220 g, 40 µm) following the protocol in **Table 10**.

Table 10: Fractionation run to isolate FR derivates on a Reveleris® C_{18} flash column (220 g, 40 µm).

Duration	dH2O (%)	Methanol (%)
13 min	50	50
1 min	30	70
13 min	30	70
1 min	25	75
15-25 min	25	75
1 min	20	80
13 min	20	80
1 min	15	85
15-25 min	15	85
1 min	0	100
10 min	0	100

According to the measured evaporative light scattering detector and ultraviolet signals at 220 nm, a FR-6 containing fraction was collected at 60 min and FR as well as $^{13}C/^{15}N$-labeled FR containing fractions were collected at 70 min.

5.8.2. HPLC

Final purification was done by HPLC with a semi-preparative Macherey-Nagel Nucleodur C_{18} column (250 x 8 mm, 5 µm) using an isocratic elution with 20/8 H_2O/MeOH (flow 2.0 mL/min) for FR and $^{13}C/^{15}N$-labeled FR (RT: 20 min) and 19/81 H_2O/MeOH (flow 2.0 mL/min) for FR-6. Pure FR-6 was isolated as a white powder (FR-6: RT: 13 min, 3 mg).

5.9. Investigation of pure compounds and extracts

5.9.1. LC/MS

"High-performance liquid chromatography mass spectrometry (HPLC/MS) data were recorded on a Waters 2695 separation module, which was coupled to a Waters 996 photodiode array detector, and a Waters QDa detector with electrospray ionization source. For separation a gradient elution with mobile phases A (acetonitrile/water 5/95 with 5 mM ammonium acetate and 40 µL acetic acid per Liter) and B (acetonitrile/water 95/5 with 5 mM ammonium acetate and 40 µL acetic acid per liter) on a Waters X Bridge Shield RP_{18} column (100 x 2.1 mm; 3.5 µm) at 25 °C were used (flow of 0.3 mL/min, 80/20 A/B to 0/100 A/B within 20 min and hold for 10 min). MS data were collected in positive and negative mode in the range between *m/z* 140-1250 and additionally in the positive single ion mode for the mass trace of FR (*m/z* 1002.5; $M+H^+$). HPLC was carried out either using a Waters HPLC system, controlled by Waters Millenium software, consisting of a 600E pump, a 996 PDA detector, and a 717 plus autosampler or on a Waters Breeze HPLC system equipped with a 1525µ dual pump, a 2998 photodiode array detector, and a Rheodyne 7725i injection system."[2].

5.9.2. LC/MS^2

The measurements via HPLC combined with high resolution MS were done as described by Hanke et al, 2021: "LC/MS data were recorded on a micrOTOF-QII mass spectrometer (Bruker) with ESI-source coupled with a HPLC Dionex Ultimate 3000 (Thermo Scientific) using an EC10/2 Nucleoshell C_{18} 2.7 µm column (Macherey-Nagel). The column temperature was 25 °C. MS data were acquired over a range from 100-3,000 *m/z* in positive mode. Auto MS/MS fragmentation was achieved with rising collision energy (35-50 keV over a gradient from *m/z* 500-2,000) with a frequency of 4 Hz for all ions over a threshold of 100. HPLC begins with 90 % H_2O containing 0.1 % AcOH. The gradient starts after 1 min to 100 % acetonitrile (0.1 % AcOH) in 20 min. A 5 µL amount of a 1 mg/mL sample solution (MeOH) was injected to a flow of 0.3 mL/min. Data analysis was performed using Bruker Compass DataAnalysis Version 4.2 (Build: 383.1)."[1].

5.9.3. NMR

NMR spectra were recorded on a Bruker Avance 300 DPX spectrometer performing at 300 MHz (^1H) and a Bruker Ascend 600 NMR spectrometer operating at 600 MHz (^1H)

and 150 MHz (^{13}C) using $CDCl_3$ as solvent (Deutero GmbH; 99.8 % D). Spectra were referenced to residual solvent signals with resonances at δH/C 7.26/ 77.0 (CDCl3). NMR spectra were processed using Bruker Topspin Version 1.3 or MestReNova 8.0.1 software.

5.9.4. Further measurements

"Optical rotations were measured with a Jasco P-2000 polarimeter. UV and IR spectra were obtained using Perkin-Elmer Lambda 40 and Perkin-Elmer Spectrum BX instruments."[1].

5.10. Calibration curve for FR

Eight different FR concentrations (0; 0.0001; 0.0005; 0.001; 0.005; 0.01; 0.05; 0.1 mM FR) were prepared using highly purified FR (purity >90 %) solved in LC/MS grade methanol and measured via LC/MS. The measured AUC for the *m/z* of FR, 1002.5, was used to calculate a calibration curve for FR. Three calibration curves, one with the four smallest concentrations, one with the five smallest concentrations, and one with all concentrations, were calculated using Prism 9.5.1 (733). The blank was subtracted from the AUC of *m/z* 1002.5 measured by LC/MS and this value was used to determine the FR concentration in 1 or 2 mg of crude extract. Subsequently, the FR concentration in the total crude extract was determined and used to create the graphs in **Figure 30** to **Figure 32**.

5.11. Bioinformatic analysis with antiSMASH

For the analysis the bacterial version of antiSMASH[175] was started with the *C. vaccinii* MWU205 genome sequence as input. Default parameters were selected, and all extra features were turned on.

5.12. Molecular networking

5.12.1. MZmine 2 data preprocessing

The preprocessing was done as described by Hanke et al, 2021: LC/MS^2 files were exported to the .mgf and .mzXML format with Bruker Compass DataAnalysis Version 4.2 (Build: 383.1) and further processed using an ad hoc-written Perl5 script[1]. The resulting .mzXML files were processed using the MZmine 2.53[177,178]. For mass detection (MS^1), the noise level was kept at 1.0 x 10^3 and for MS^2 the noise level was kept at 1.0 x 10^2. For chromatogram building the ADAP chromatogram builder[335] was applied sorting

all data points by their intensity and creating an EIC for the highest intense data point when there are 8 scans of continuous data points above the noise level of 5.0^2 each. Other data points within an *m/z* range of 0.01 (or 20 ppm) will be added to the EIC. If a data point does not fit in the *m/z* range of another EIC but fulfills the other criteria it will become a new EIC. Next the chromatogram is smoothed using a filter width of 5. The chromatogram deconvolution baseline cut-off algorithm was used with the following settings: A peak min. height of 1.0^3, a max. peak duration of 0.1 to 3.5 min and a baseline level of 2.0^2. The *m/z* range for MS^2 pairing (Da) was fixed at 0.02, the RT range for MS^2 pairing (min) was fixed at 0.15. Chromatograms were deisotoped using the isotopic peaks grouper algorithm with an *m/z* tolerance of 0.01 (or 20 ppm) and a RT tolerance of 0.7 min. Maximum charge was set on 2 and the most intense isotope was chosen as representative isotope. Peak alignment was performed using the join aligner method, where a match score is formed based on mass (*m/z* weight: 0.75) and retention time (RT weight: 0.25) of each peak with a given tolerance (*m/z* tolerance: 0.01 or 20 ppm; RT tolerance: 0.7 min). Finally, the peak list was filtered using the feature list row filter keeping only peaks with MS^2. The peak list was searched for sodium, potassium, ammonium, and magnesium adducts with a retention time tolerance of 0.7 min and an *m/z* tolerance of 0.01 (or 20 ppm). The maximum height of the adduct peak was set to 50 % of the main peak[1].

5.12.2. FBMN

After MZmine 2 preprocessing as described above the peak list was exported merging the MS/MS data and filter rows, which have no MS^2. The MS/MS data was merged across the sample, with the *m/z* values being merged using the weighted average and their intensities getting summed up. The expected mass deviation was set to 0.01 (or 20 ppm). The cosine threshold was set to 70 %. Peaks only occurring in 20 % of the merged spectra were excluded. The isolation window was defined by an offset of 0 *m/z* and a width of 3 *m/z*. After exporting the data set via the "Export/Import to GNPS-FBMN" function the Feature Networking tool of GNPS (release_20 and release_28.2 for the reanalysis) was used[180,181]. "The .mgf and .csv file were uploaded to CCMS (ccms.ucsd.edu). For the network creation, a parent mass tolerance of 0.02 Da and a fragment ion tolerance of 0.02 Da were applied. Edges were filtered to have a cosine score above 0.7 and more than six matched peaks. If each of the nodes appeared in each other's respective top 10 most similar nodes further edges between two nodes were kept in the network. The spectra in

the network were searched against GNPS' spectral libraries. The library spectra were filtered in the same manner as the input data. All matches kept between network spectra and library spectra were required to have a score above 0.7 and at least six matched peaks. Additionally, 100 Da was decided to be the maximum difference between the precursor ion mass of the searched MS/MS spectrum and the library MS/MS spectra."[1].

Cytoscape 3.8.2 (www.cytoscape.org) was utilized to visualize the networks using the solid style layout.

5.12.3. Further tools

The DEREPLICATOR tool (version 1.2.8) from the GNPS platform was utilized to analyze the FBMN generated with the old (release_20) and the new (release_28.2) FBMN workflow using default parameters except for the maximal isotopic shift, which was set to 2 and the additional search for sodium and potassium adducts. Additionally, the VarQuest search was activated with default parameters[184,187].

The MS2LDA tool (release_31.1) was used as advanced tool to investigate both networks generated with the old (release_20) and the new (release_28.2) FBMN workflow with default parameters[185,186].

The MolNetEnhancer (release_22) is offered by GNPS to combine tools like MS2LDA and DEREPLICATOR and applied with default parameters to unite the information from the either the old (release_20) FBMN with its respective DEREPLICATOR and MS2LDA analysis or the new (release_28.2) FBMN using default parameters[1].

The MZmine 2 data was analyzed on the SIRIUS platform (Version 5.6.3)[188,189] with the tools CANOPUS[336,337], CSI:Finger ID set to $[M+Na]^+$ and $[M+H]^+$ for fallback adducts, and non *in silico* databanks, ZODIAC, and SIRIUS set to all data banks and $[M+Na]^+$ and $[M+H]^+$ as possible ionization.

5.13. Comparison of $G\alpha_q$ amino acid sequences of nematodes

BLAST search, alignment, and visualization were done as described by Hanke et al, 2023[2].

5.13.1. BLAST

"The Basic Local Alignment Search Tool (BLAST)[253,254] was utilized using the amino acid sequence of the $G\alpha_q$ isoform a of *C. elegans* (UniProt: G5EGU1) as query. Standard

databases (non-redundant protein sequences) were selected as search set but restricted to the organisms belonging to Nematoda. The blastp algorithm was used with default parameters."[2].

5.13.2. Alignment

Alignment of sequences named in **Table 11** were aligned using the Clustal W alignment tool in MEGA 11 (Version 11.0.11). "For the pairwise alignment, a penalty of 10 for gap opening and 0.1 for gap extension were selected. For the multiple alignment, the penalty for gap opening was the same, but gap extension was punished with 0.2. Gonnet was chosen as protein weight matrix, and residue-specific and hydrophilic penalties were switched on. Concerning gap separation, a matrix of four and no end were selected. No negative matrix was used, and the delay divergent cutoff was set at 30 %."[2].

Table 11: Sequence accession numbers, corresponding organisms from **Figure 34** and their description.

Sequence accession No. or Origin	Organisms	Type and Origin (Clade for *Caenorhabditis* spp. [260])
G5EGU1 (UniProtKB)	*Caenorhabditis elegans*	*Elegans* supergroup
B6VBV2 (UniProtKB)	*Caenorhabditis angaria*	*Drosophilae* supergroup, ectophoretic associate of *Metamasius hemipterus* [261]
A0A261B5L1 (UniProtKB)	*Caenorhabditis latens*	*Elegans* supergroup, strain from Jiangsu and Wuhan City in China [262,263]
Q4VT45 (UniProtKB)	*Caenorhabditis briggsae*	*Elegans* supergroup, entomopathogenic strain associated with *Serratia* sp [269]
A0A2G5VU95 (UniProtKB)	*Caenorhabditis nigoni*	*Elegans* supergroup, isolated in south India and Congo from rotting flowers [263,338]
E3LXV8 (UniProtKB)	*Caenorhabditis remanei*	*Elegans* supergroup, isolated from isopods obtained from compost heaps [264]
A0A1I7UE77 (UniProtKB)	*Caenorhabditis tropicalis*	*Elegans* supergroup, isolated in La Réunion and French Guiana from rotting flowers [263,338]
A0A8R1DI86 (UniProtKB)	*Caenorhabditis japonica*	*Elegans* supergroup, associated with *Parastrachia japonensis* [265]
A0A8S1GU46 (UniProtKB)	*Caenorhabditis auriculariae*	Basal group, isolated from fruiting bodies of *Auricularia polytricha* [339]
A0A8S1F2E0 (UniProtKB)	*Caenorhabditis bovis*	*Drosophilae* supergroup, associated with *Chrysomya bezziana* [340]
KAF8367701.1 (Genbank)	*Pristionchus pacificus*	Satellite model organism associated with scarab beetles [271]
KAI1707081.1 (Genbank)	*Ditylenchus destructor*	Plant parasitic potato root nematode [274]

A0A8S9ZE38 (UniProtKB)	*Meloidogyne graminicola*	Plant parasitic root-knot nematodes [275]
A0A6V7U1D6 (UniProtKB)	*Meloidogyne enterolobii*	Plant parasitic root-knot nematodes [276]
KAH7721960.1 (Genbank)	*Aphelenchus avenae*	Fungivorous soil nematode [272]
A0A811JUE8 (UniProtKB)	*Bursaphelenchus okinawaensis*	Associated with longhorn beetle *Monochamus maruokai* [273]
KAI6178527.1 (Genbank)	*Aphelenchoides besseyi*	Foliar plant parasitic nematode [43]
WormBase ParaSite - BioProject PRJNA722882: Transcript of Hsc_gene_6303 (Hsc_gene_6303.t1)	*Heterodera schachtii*	Plant pathogenic cyst nematodes [277]
P50148 (UniProtKB)	*Homo sapiens*	-

5.13.3. Visualization

"Depictions of YM in complex with a chimeric $G_{i1/q}$ protein were created with PyMOL™ 2.5.4 (Schrodinger) from PDB ID 3AH8[198]."[2].

5.14. *In vitro* assays and molecular docking

5.14.1. Cell Culture and transient transfection

Cell culture materials were purchased from Invitrogen (Carlsbad, CA, USA). Generation of genetically engineered HEK293 cells using CRISPR/Cas9 technology to knockout the subunits of $G\alpha_q$ and $G\alpha_{11}$ (HEK $G_{q/11}$-KO cells) is described elsewhere[131]. Cells were maintained in Dulbecco's modified Eagle's medium supplemented with 10 % (v/v) fetal calf serum (PAN biotech, Germany), penicillin (100 units/mL), and streptomycin (0.1 mg/mL), and cultured at 37 °C in a humidified atmosphere of 95 % air and 5 % CO_2. All cell lines were screened by polymerase chain reaction monthly for mycoplasma contamination and were tested negative.[1,2]

HEK $G_{q/11}$-KO cells were transfected in suspension 48 h prior to the experiments using polyethylenimine (PEI, 1 mg/mL, Polyscience) following the manufacturer's protocol. A total amount of 8 µg plasmid (3 µg, 0.6 µg, 2 µg of expression plasmids containing human influenza hemagglutinin-tagged $G\alpha_q$ isoforms, muscarinic acetylcholine M3 receptor, and RIC-8A, respectively, filled up with pcDNA3.1(+)) and 24 µL PEI solution were added to 2.8 x 10^6 cells plated in 10 cm dishes.[2]

5.14.2. Label-free DMR Assay

„At 48 h post transfection with the $G\alpha_q$ subunit, real-time whole-cell DMR measurements were conducted as previously described in detail[196,197] using the Epic DMR

reader (Corning, NY, USA) together with the Cybi-SELMA semi-automated electronic pipetting system (Analytik Jena AG, Jena, Germany). Briefly, 24 h after transfection, HEK293 cells were counted and seeded at a density of 17 000 cells per well on 384-well fibronectin-coated biosensor plates. On the next day, cells were washed twice with Hanks' buffered salt solution containing 20 mM HEPES (HBSS+HEPES) and incubated for 1 h at 37 °C in the EPIC reader. FR and FR-6 were added 1 h before the measurement in HBSS+HEPES. The sensor plate was scanned for a baseline optical read (no change in basal DMR) of about 3 min and after agonist addition, DMR alterations were monitored for 3,000 s at 37 °C. All data were analyzed using GraphPad Prism 8.0.0 (GraphPad Inc, La Jolla, CA, USA). Quantification of DMR signals was performed by calculation of the maximum responses. Data points from inhibition curves of individual functional experiments were fitted to a four-parameter logistic function:

$$Y = bottom + \frac{(top - bottom)}{1 + 10^{(logEC_{50} - x)slope}}$$

Concentration-inhibition curves represented in **Figure 54** were normalized by setting each experimental maximal effect as 100 % response. All data are expressed as mean + or ± standard error of the mean (SEM) of at least three independent experiments performed in technical triplicates.“[1].

5.14.3. IP_1 accumulation assay

“The IP_1 accumulation was measured using homogeneous time resolved fluorescence (HTRF) technology (Cisbio) following the manufacturer’s instructions.”[2] For this, transfected HEK $G_{q/11}$-KO cells were detached and washed in phosphate-buffered saline. “After resuspension in LiCl-containing assay buffer stopping breakdown of IP_1, cells were seeded into white 384-well plates with 50,000 cells per well. Carbachol and FR were added simultaneously, followed by 40 minutes of incubation at 37 °C. Subsequently, cells were lysed and incubated with d2-labeled and cryptate-labeled IP_1 antibodies for a minimum of 60 min at room temperature. The HTRF ratio values measured with a Mithras LB 940 multimode plate reader (Berthold Technologies) were converted to IP_1 concentrations in nM using an IP_1 (unlabeled) standard curve.”[2].

5.14.4. Calcium mobilization assay

“Calcium^{2+} mobilization was measured using FLIPR Calcium 5 assay kit using the Flex Station 3 MultiMode Benchtop reader (both Molecular Devices), as described

elsewhere[283] with slight modifications."[2] Briefly, 24 h after transfection HEK $G_{q/11}$-KO cells transferred to flat-bottom 96-well cell culture plates at a density of 60,000 cells per well. "On the day of the assay, cells were incubated in Calcium 5 dye for 45 min at 37 °C before 1 to 3 dilutions with HBSS+HEPES. For preincubation with inhibitor, FR was added to the dye in the appropriate concentrations. Kinetic fluorescence measurements (baseline read and addition of agonist or buffer after 20 s) were performed to assess calcium^{2+} release from intracellular stores."[2].

5.14.5. Competition binding assay

„Competition binding assays were conducted as previously described[159]. In short, competition binding assays of FR-6 versus the radiolabeled FR derivative [^{3}H]PSB-15900 were performed at human platelet membrane preparations that natively express a high quantity of G_q proteins. The experiments were conducted in 50 mM Tris-HCl buffer, pH 7.4, in a final assay volume of 200 µL. Each assay tube contained 25 µg of protein of a human platelet membrane preparation, a final concentration of 5 nM [^{3}H]PSB-15900, and 5 µL of competitor (FR-6 or FR) in 10 different concentrations (dissolved in dimethyl sulfoxide (DMSO)). Non-specific binding was determined in the presence of 5 µM FR (dissolved in DMSO), and total binding was determined in the presence of DMSO without inhibitor. The incubation was started by the addition of the human platelet membrane preparation and lasted for 90 min at 37 °C with gentle shaking of the samples in a water bath. The incubation was terminated by rapid filtration through GF/C glass fiber filters using a Brandel 48-sample harvester. Filters were dried, punched out, transferred to scintillation vials, and incubated for at least 6 h in scintillation cocktail (2.5 ml ProSafe FC+®, Meridian Biotechnologies Ltd, UK) prior to scintillation measurement in a liquid scintillation counter at an efficiency of 53 %. Data were evaluated using GraphPad Prism 8 (GraphPad Inc., San Diego, CA, USA), and K_i values were determined by the "One site – Fit log K_i"-equation. Results were normalized to the controls, i.e., total binding (100 %) and non-specific binding (0 %)."[1].

5.14.6. Molecular Docking

"Molecular docking was performed based on the structure of the heterotrimeric G protein ($G\alpha_{i/q}\beta\gamma$) co-crystallized with the selective G_q inhibitor YM-254890 (3AH8.pdb, resolution 2.9 Å).[198] The structure was downloaded from the Protein Data Bank and prepared by the structure preparation tool implemented in Molecular Operating

Environment (MOE 2019.01; Chemical Computing Group, Montreal, Quebec, Canada, 2019). Subsequently, hydrogen atoms were assigned by means of the Protonate-3D module in MOE 2019.01. FR-6 and FR were docked into the inhibitor binding site of the G_q protein using Autodock 4.2[341]. Atomic partial charges were added using AutoDockTools,[341,342] and three-dimensional energy scoring grids of 60 × 60 × 60 points with a spacing of 0.375 Å were computed. The energy grids were centered based on the co-crystallized ligand YM. During docking simulations, the ligands FR and FR-6 were fully flexible while receptor residues were kept rigid. Fifty independent docking calculations using the varCPSO-ls algorithm from PSO@Autodock implemented in AutoDock4.2 were performed and terminated after 500,000 evaluation steps.[343] Parameters of the varCPSO-ls algorithm, the cognitive and social coefficients c1 and c2, were set at 6.05 with 60 individual particles as swarm size. All the other parameters of the algorithm were set at their default values. A plausible binding mode of FR and FR-6 was selected based on the lowest binding energy and based on visual inspection of the interactions."[1].

5.15. *In vivo* experiments with *C. elegans*

"*C. elegans* was cultivated at 20 °C using standard cultivation methods."[2].

5.15.1. Synchronization of *C. elegans*

"The investigated pathway directly impacts developmental timings of the worm. To compare animals at the same age, we measured the developmental time from egg to adulthood for all strains. We found 6 h delay for all mutants for adulthood. For the locomotion experiments the animals were offset to allow delayed mutants to develop until the correct age. As checks for egg-laying during the locomotion experiments revealed the suppressor mutants, *dgk-1*(*sy428*) and *eat-16*(*sa609*), to be slower their delay was lengthened to 10 h for the subsequent egg-laying experiments."[2] Synchronization of *C. elegans* (N2, *egl-30*(*ad806*), *egl-30*(*ad805*), *egl-30*(*n686*) *dgk-1*(*sy428*), and *eat-16*(*sa609*)) was performed using bleaching solution, prepared as described in **Table 12**, M9 buffer and *C. elegans* grown for 3-4 days on a 10 cm NGM plate at 20 °C. "Nematodes were washed off with M9 buffer. After centrifugation and removal of 900 µL, 1 mL of bleaching solution was added to the pellet. The sample was mixed for 2 minutes and centrifuged afterwards. This step was repeated a second time. Afterwards the pellet was washed three times with M9. Finally, eggs were counted, and concentration was adjusted

to a maximum of 5 eggs/µL, if necessary, and rotated overnight to synchronize to larval stage 1 (L1)."[2].

Table 12: Recipe of bleaching solution

Component	Volume (mL)
5 % sodium hypochlorite	2.0
5 M KOH	1.5
dH_2O	6.5

5.15.2. Tracking experiments with *C. elegans* und FR

"Approximately 100 synchronized *C. elegans* N2, *egl-30*(*ad805*), *egl-30*(*n686*), *egl-30*(*ad806*), *dgk-1*(*sy428*), *eat-16*(*sa609*) L1 were grown on NGM with a spot (40 µL) *E. coli* [.] mixed with FR (2.5 mM) in 1 % DMSO or just 1 % DMSO as control. After approx. 55 h (N2) plus above-mentioned offset for mutant worms were imaged. Imaging of worms was performed using a commercial upright epifluorescence microscope (Axio Zoom V16; Zeiss) equipped with a 1x objective (PlanNeoFluar Z 1.0x/N.A. 0.25). Brightfield image was performed and imaged on camera (BASLER; acA3088-57um) using a camera adapter with an additional 0.5x magnification (60N-C ⅔ 0.5x; Zeiss) resulting into an effective magnification on camera of 0.35x. Animals were imaged at 15 fps for 5 min unless otherwise indicated.

Animals were tracked using the tracking package trackpy[344] with a custom detection script in Python based on the pharaglow package[345]. The animal speed was calculated from the resulting center-of-mass coordinates as follows: The trajectories (x, y, t) were sub-sampled from 14 fps to 2.8 fps and the speed was calculated as $v(t_2) = \sqrt{\frac{(x_{t2}-x_{t1})^2+(y_{t2}-y_{t1})^2}{dt}}$ with $dt = \frac{1}{2.8}s$.

The animals' spatial distribution was evaluated by counting nematodes inside the lawn and outside the lawn, where outside the lawn meant that no part of the worm touched the lawn. Border crossings were counted in a similar way as the recorded tracks were evaluated and each crossing independent of the direction (leaving or entering) was counted."[2].

5.15.3. Egg-laying assays with *C. elegans* and FR

5.15.3.1. Egg-laying rate assay

“Approx. 50 synchronized *egl-30*(*ad806*), *egl-30*(*n686*), *dgk-1*(*sy428*), *eat-16*(*sa609*), and N2 L1 were grown on NGM plates completely covered with *E. coli* [.] mixed with FR (2.5 mg/mL) in 1 % DMSO or 1 % DMSO as control for 72 h (N2), 78 h (*egl-30*(*ad806*), *egl-30*(*n686*)), and 81 h (*dgk-1*(*sy428*), *eat-16*(*sa609*)). Afterwards 12 worms per genotype were picked and put separately on plates completely covered with the mixtures described before. After two hours the nematode was erased from the plate and eggs were counted.“[2]

5.15.3.2. Retained eggs assay

“Approx. 100 synchronized *dgk-1*(*sy428*), *eat-16*(*sa609*), and N2 L1 were grown on NGM plates completely covered as described for the egg-laying experiment. After 72 h (N2) and 81 h (mutants) 20 worms were picked and put separately in 10 µL drops of 6 % bleaching solution (5 % sodium hypochlorite solution solved in dH_2O) for 15 minutes.”[2]

5.16. Experiments with *H. schachtii*

5.16.1. General cultivation of *H. schachtii*

„*H. schachtii* was cocultivated with *Sinapis alba* to generate cysts and J2 used for the activity and cyst assay[346].“[2].

5.16.2. Activity assay with J2 *H. schachtii* and FR

“Approx. 100 J2 were added to 500 µL volume containing 1 % DMSO mixed with or without 1 mM FR. Additionally one experiment was conducted by adding 50 µL octopamine to control and FR. After 4 d the number of active J2 was determined by microscopic observation of their shape (active: coiled or wavy-like, inactive: straight or slightly curved line). For the concentration-dependency experiment different concentration of FR (0.0624 mM, 0.125 mM, 0.25 mM, 0.5 mM) were added and counted after 4 d[347].“[2].

5.16.3. Hatching assay with cysts of *H. schachtii* and FR

„Approx. 20 cysts were added to 500 µL volume containing 1 % DMSO mixed with or without 0.01 mg/mL FR. Each experiment was replicated 4 times and cultivated for 7

d at room temperature. Afterwards the number of J2 was counted per experiment and divided by the number of cysts in the well."[2].

5.17. Statistical analyses

Statistical analyses were done as described by Hanke et al, 2023 and raw data can be found in the publication and its supplement[2]: „Data and statistical analyses were performed using GraphPad Prism version 9.5.0 as described in detail below. To evaluate the spatial distribution of *C. elegans* a *modified two sample binomial test* [295] was performed using Microsoft Excel. Raw data for all statistical tests performed is summarized in Online Resource 2.

SESOM, SESOM with chitin, and the secretion experiment were tested for normality using the *Shapiro-Wilk test*, which stated them to be normally distributed. Afterwards the *unpaired t-test* for both SESOM experiments and the *paired t-test* for the secretion experiment were utilized. Summarized data represent the data of three technical replicates for SESOM, three or four replicated for SESOM with chitin, and six replicates for the secretion experiment. For the FR calibration curve for SESOM the fours smallest concentrations were picked and for the secretion experiment all eight concentrations were chosen and used to calculate a simple linear regression using Prism 9.5.0.

C. elegans experiments concerning velocity, egg-laying rate, and retained eggs were tested for normality or lognormality using *D'Agostino & Pearson test*. For velocity all three *egl-30* mutants, *egl-30*(*ad805*), *egl-30*(*n686*), and *egl-30*(*ad806*) were found to have a log-normal distribution while N2, *dgk-1*(*sy428*), and *eat-16*(*sa609*) were not normally distributed. Subsequently, the *Mann-Whitney test* was performed for N2, *dgk-1*(*sy428*), and *eat-16*(*sa609*) and the *unpaired t-test* was performed for all three *egl-30* mutants to compare control against FR. For the egg-laying rate, all five genotypes (N2, *egl-30*(*n686*), *egl-30*(*ad806*), *dgk-1*(*sy428*), and *eat-16*(*sa609*)) were found to be normally distributed. Subsequently the *unpaired t-test* was chosen for the comparison of Control versus FR. For the retained eggs assay, *C. elegans* N2 and *eat-16*(*sa609*) displayed normally distributed data, while *dgk-1*(*sy428*) was not normally distributed. Accordingly, *unpaired t-tests* were performed to compare Control vs. FR for *C. elegans* N2 and *eat-16*(*sa609*), while the *Mann-Whitney test* was used for *dgk-1*(*sy428*).

Regarding *H. schachtii*, experiments evaluating the effect of FR and octopamine on the activity of nematodes, *One-Way-ANOVA* with *Tukey's multiple comparisons test* was

performed as data passed the *Shapiro-Wilk test* for normality. To investigate the effect of FR on hatching of J2 *H. schachtii*, the *unpaired t-test* was performed as data passed the *Shapiro-Wilk test* for normality. Summarized data represent the data of four technical replicates.“[2]

6. Appendix

6.1. Appendix for chapter 3.1

Table 13: GNPS library hits detected in extracts of *C. vaccinii* MWU205 and *A. crenata* leaves.

***m/z* value**	**Proposed compound**	***m/z* of proposed compound**	**Cosine**	**Cluster**
1002.54	FR900359	1002.54	0.95	1
1002.53	FR900359	1002.54	0.94	1
1019.56	FR900359 (NH_4^+ adduct)	1019.56	0.71	1
988.52	FR-2	988.52	0.71	1
988.53	FR-2	988.52	0.75	1
988.52	FR-2	988.52	0.70	1
1032.55	FR-1	1032.55	0.81	1
1025.56	Peptide with possible PPQVV seq. Possibly media derived	1025.57	0.91	26
690.50	PE (16:0_16:1) (2-aminoethoxy)[2-[hexadec-9-enoyloxy]-3-(hexadecanoyloxy)propoxy]phosphinic acid	690.51	0.87	25
688.49	Spectral Match to 1,2-Dipalmitoleoyl-sn-glycero-3-phosphoethanolamine from NIST14	688.48	0.88	25
652.40	val-leu-pro-val-pro-gln	652.40	0.81	19
326.71	val-leu-pro-val-pro-gln	652.40	0.83	19
205.09	Spectral Match to Prostaglandin A1 ethyl ester from NIST14	205.09	0.95	singleton

Table 14: Classification of compounds, displayed as *m/z*, found in extracts of *Chromobacterium vaccinii* MWU205 cultivated in M9 and LB medium and one depsipeptide-containing fraction of *A. crenata* according to their MS^2 data analyzed by MS2LDA[185,186] and DEREPLICATOR[184,187].

m/z	RT (min)	CF Dparent	CF Dparent score
839.4	10.4	Cyclic depsipeptides	0.20
779.5	11.0	Cyclic depsipeptides	0.08
1018.5	12.9	Cyclic depsipeptides	0.20
1032.6	13.6	Cyclic depsipeptides	0.20
988.5	14.5	Cyclic depsipeptides	0.20
1022.5	11.0	Cyclic depsipeptides	0.50
821.5	11.3	Cyclic depsipeptides	0.08
1070.5	10.3	Cyclic depsipeptides	0.33
806.4	9.9	Cyclic depsipeptides	0.20
1036.5	11.0	Cyclic depsipeptides	0.20
803.4	10.4	Cyclic depsipeptides	0.20
887.5	12.4	Cyclic depsipeptides	0.20
761.5	11.5	Cyclic depsipeptides	0.08
795.5	10.6	Cyclic depsipeptides	0.33
765.5	10.4	Cyclic depsipeptides	0.08
974.5	11.2	Cyclic depsipeptides	0.20
801.4	13.0	Cyclic depsipeptides	0.20
805.5	10.9	Cyclic depsipeptides	0.08
1032.5	10.5	Cyclic depsipeptides	0.20
787.5	12.9	Cyclic depsipeptides	0.08
819.5	9.1	Cyclic depsipeptides	0.08
1036.5	10.9	Cyclic depsipeptides	0.20
817.4	10.4	Cyclic depsipeptides	0.20
1019.6	15.2	Cyclic depsipeptides	0.20
988.5	14.3	Cyclic depsipeptides	0.20
1024.5	15.2	Cyclic depsipeptides	0.20
857.4	9.4	Cyclic depsipeptides	0.20
805.5	12.3	Cyclic depsipeptides	0.08
1024.5	15.4	Cyclic depsipeptides	0.20
974.5	12.5	Cyclic depsipeptides	0.20
817.4	12.2	Cyclic depsipeptides	0.20

821.5	11.6	Cyclic depsipeptides	0.33
996.5	12.6	Cyclic depsipeptides	0.20
567.3	8.3	Cyclic depsipeptides	0.08
793.5	8.2	Cyclic depsipeptides	0.08
1016.6	15.9	Cyclic depsipeptides	0.20
833.4	10.1	Cyclic depsipeptides	0.20
956.5	13.4	Cyclic depsipeptides	0.20
821.4	9.0	Cyclic depsipeptides	0.20
1010.5	10.8	Cyclic depsipeptides	0.20
899.4	9.9	Cyclic depsipeptides	0.33
833.4	11.3	Cyclic depsipeptides	0.20
751.5	8.5	Cyclic depsipeptides	0.08
831.4	12.7	Cyclic depsipeptides	0.20
803.4	10.3	Cyclic depsipeptides	0.20
803.4	12.0	Cyclic depsipeptides	0.20
793.5	8.8	Cyclic depsipeptides	0.08
1010.5	13.9	Cyclic depsipeptides	0.20
1008.5	11.6	Cyclic depsipeptides	0.20
1005.5	13.6	Cyclic depsipeptides	0.20
988.5	10.9	Cyclic depsipeptides	0.20
751.5	9.3	Cyclic depsipeptides	0.08
793.5	8.6	Cyclic depsipeptides	0.08
821.4	8.9	Cyclic depsipeptides	0.20
974.5	10.0	Cyclic depsipeptides	0.20
765.5	9.2	Cyclic depsipeptides	0.08
757.5	11.0	Cyclic depsipeptides	0.33
779.5	9.9	Cyclic depsipeptides	0.08
835.4	9.4	Cyclic depsipeptides	0.20
795.5	9.9	Cyclic depsipeptides	0.08
1002.5	15.3	Cyclic depsipeptides	0.20
833.4	10.4	Cyclic depsipeptides	0.20
890.5	11.7	Cyclic depsipeptides	0.20
1004.5	12.9	Cyclic depsipeptides	0.20
1024.5	11.5	Cyclic depsipeptides	0.20

988.5	13.1	Cyclic depsipeptides	0.20
873.5	11.7	Cyclic depsipeptides	0.20
1018.5	12.7	Cyclic depsipeptides	0.20
733.5	11.4	Cyclic depsipeptides	0.08
1004.5	13.0	Cyclic depsipeptides	0.20
1010.5	13.2	Cyclic depsipeptides	0.20
839.4	12.1	Cyclic depsipeptides	0.20
849.5	9.6	Cyclic depsipeptides	0.20
787.5	15.7	Cyclic depsipeptides	0.08
791.5	11.7	Cyclic depsipeptides	0.08
1002.5	15.4	Cyclic depsipeptides	0.20
845.5	13.1	Cyclic depsipeptides	0.20
1002.5	11.4	Cyclic depsipeptides	0.20
1070.5	11.7	Cyclic depsipeptides	0.33
793.5	10.0	Cyclic depsipeptides	0.08
888.5	11.4	Cyclic depsipeptides	0.20
817.4	10.6	Cyclic depsipeptides	0.20
761.5	13.7	Cyclic depsipeptides	0.08
1004.5	11.7	Cyclic depsipeptides	0.20
1004.5	12.6	Cyclic depsipeptides	0.20
1052.5	10.4	Cyclic depsipeptides	0.50
758.6	14.5	Cyclic depsipeptides	0.08
807.4	8.2	Cyclic depsipeptides	0.20
789.4	9.9	Cyclic depsipeptides	0.20
1005.5	10.7	Cyclic depsipeptides	0.20
706.4	8.7	Cyclic depsipeptides	0.20
1019.6	11.5	Cyclic depsipeptides	0.20
853.4	8.8	Cyclic depsipeptides	0.20
801.4	11.6	Cyclic depsipeptides	0.20
988.5	11.7	Cyclic depsipeptides	0.20
793.5	9.4	Cyclic depsipeptides	0.08
1004.5	11.9	Cyclic depsipeptides	0.20
593.4	9.7	Cyclic depsipeptides	0.08
1005.5	12.5	Cyclic depsipeptides	0.20

617.3	5.4	Cyclic peptides	0.13
631.3	5.4	Cyclic peptides	0.13
530.3	6.0	Cyclic peptides	0.13
587.3	5.7	Cyclic peptides	0.13
491.3	4.7	Cyclic peptides	0.13
473.3	5.8	Cyclic peptides	0.13
505.3	5.3	Cyclic peptides	0.13
643.4	7.1	Cyclic peptides	0.13
813.5	10.6	Hybrid peptides	1.00

Table 15: CANOPUS prediction of natural products pathways and superclasses for compounds, displayed as *m/z*, found in *Chromobacterium vaccinii* MWU205 and *A. crenata* extracts processed by MZmine2[188,189].

m/z	**RT**	**cluster**	**NPC Pathway**		**NPC Superclass**	
225.1	5.9	18	Alkaloids	0.22	Small peptides	0.53
225.1	6.2	18	Fatty acids	0.97	Fatty acyl glycosides	0.36
245.1	6.1	32	Alkaloids	0.53	Small peptides	0.11
261.1	3.7	32	Alkaloids	0.92	Pseudoalkaloids	0.59
274.2	17.0	39	Alkaloids	0.95	Pseudoalkaloids	0.32
274.2	17.5	39	Terpenoids	0.40	Phloroglucinols	0.54
282.2	19.4	8	Fatty acids	0.97	Fatty acyls	0.96
315.1	1.8	21	Amino acids and Peptides	0.56	Aminosugars and aminoglycosides	0.16
315.1	1.1	21	Shikimates and Phenylpropanoids	0.83	Phenolic acids (C6-C1)	0.54
328.1	11.1	28	Alkaloids	1.00	Tryptophan alkaloids	0.99
344.1	9.6	28	Alkaloids	1.00	Tryptophan alkaloids	0.99
345.2	5.9	5	Alkaloids	0.84	Small peptides	0.61
378.2	19.7	9	Alkaloids	0.94	Anthranilic acid alkaloids	0.41
378.2	19.3	9	Alkaloids	0.98	Anthranilic acid alkaloids	0.42
378.2	18.9	9	Alkaloids	0.83	Tryptophan alkaloids	0.21
390.3	9.9	13	Amino acids and Peptides	0.11	Ornithine alkaloids	0.29
394.3	23.6	8	Fatty acids	0.77	Fatty Acids and Conjugates	0.45
403.3	12.3	13	Amino acids and Peptides	0.77	Small peptides	0.89
403.3	10.9	13	Fatty acids	0.20	Sphingolipids	0.10

409.2	11.0	14	Carbohydrates	0.72	Aminosugars and aminoglycosides	0.83
421.2	11.6	14	Alkaloids	0.89	Flavonoids	0.23
425.3	4.4	3	Amino acids and Peptides	0.95	Small peptides	0.75
427.3	5.7	29	Terpenoids	0.95	Steroids	0.47
443.3	5.0	34	Amino acids and Peptides	0.98	Small peptides	1.00
450.4	25.5	8	Fatty acids	0.94	Glycerophospholipids	0.15
453.2	10.9	14	Amino acids and Peptides	0.56	Small peptides	0.55
453.2	10.1	14	Polyketides	0.32	Tryptophan alkaloids	0.28
454.3	5.3	34	Alkaloids	0.04	Fatty amides	0.42
459.3	4.9	29	Amino acids and Peptides	0.90	Small peptides	0.99
473.3	5.8	4	Amino acids and Peptides	1.00	Small peptides	1.00
475.3	3.7	3	Amino acids and Peptides	1.00	Small peptides	0.99
482.3	20.9	9	Alkaloids	0.99	Nicotinic acid alkaloids	0.39
489.3	4.5	3	Amino acids and Peptides	1.00	Small peptides	1.00
491.2	5.5	3	Amino acids and Peptides	1.00	Small peptides	0.97
501.3	6.1	27	Alkaloids	0.48	Ornithine alkaloids	0.17
505.3	5.3	4	Amino acids and Peptides	1.00	Small peptides	0.96
513.3	6.3	33	Amino acids and Peptides	0.97	Small peptides	0.98
517.3	20.8	7	Carbohydrates	1.00	Polyols	0.68
517.3	26.3	7	Carbohydrates	1.00	Polyols	0.70
517.3	27.4	7	Fatty acids	0.88	Ornithine alkaloids	0.56
519.3	20.8	10	Terpenoids	0.99	Steroids	0.61
523.3	5.5	3	Amino acids and Peptides	1.00	Small peptides	1.00
530.3	6.0	4	Amino acids and Peptides	1.00	Small peptides	0.92
546.3	4.1	3	Amino acids and Peptides	0.62	Oligopeptides	0.50
552.4	6.6	5	Amino acids and Peptides	0.98	Oligopeptides	0.74

553.3	3.6	19	Amino acids and Peptides	0.99	Oligopeptides	0.77
553.3	5.1	20	Amino acids and Peptides	0.99	Oligopeptides	0.76
553.3	4.5	5	Amino acids and Peptides	1.00	Oligopeptides	0.94
557.4	15.5	15	Fatty acids	0.99	Glycerolipids	0.91
567.4	8.3	2	Carbohydrates	0.61	Small peptides	0.16
576.4	4.4	5	Amino acids and Peptides	0.80	Oligopeptides	0.48
587.3	4.5	30	Carbohydrates	0.31	Saccharides	0.51
587.3	4.9	30	Fatty acids	0.29	Fatty acyl glycosides	0.32
587.3	5.7	4	Amino acids and Peptides	0.89	Oligopeptides	0.59
593.4	9.7	2	Terpenoids	0.79	Triterpenoids	0.28
597.0	0.9	6	Carbohydrates	0.68	Nucleosides	0.26
604.3	3.8	40	Amino acids and Peptides	1.00	Small peptides	0.95
607.3	6.8	27	Terpenoids	0.99	Carotenoids (C40)	0.98
607.4	8.5	20	Amino acids and Peptides	0.71	Small peptides	0.46
617.3	5.4	4	Amino acids and Peptides	1.00	Small peptides	0.78
631.3	5.4	4	Amino acids and Peptides	0.97	Oligopeptides	0.63
636.3	5.9	3	Amino acids and Peptides	0.94	Oligopeptides	0.73
643.4	7.1	4	Amino acids and Peptides	0.89	Oligopeptides	0.67
645.5	28.0	11	Fatty acids	1.00	Glycerolipids	0.99
645.5	14.4	11	Fatty acids	1.00	Sphingolipids	1.00
652.4	4.3	19	Amino acids and Peptides	0.99	Oligopeptides	0.80
657.4	6.1	37	Amino acids and Peptides	0.99	Oligopeptides	0.89
679.0	0.9	6	Carbohydrates	0.74	Nucleosides	0.90
688.5	18.4	25	Fatty acids	1.00	Glycerophospholipids	1.00
689.4	5.8	5	Amino acids and Peptides	0.96	Oligopeptides	0.70
690.5	28.0	25	Fatty acids	1.00	Glycerophospholipids	1.00

706.4	8.7	1	Amino acids and Peptides	0.98	Oligopeptides	0.73
707.5	15.0	15	Fatty acids	1.00	Glycerolipids	0.87
719.5	14.3	15	Fatty acids	0.96	Glycerolipids	0.73
719.5	14.9	15	Fatty acids	0.53	Oligopeptides	0.38
733.5	11.5	2	Amino acids and Peptides	1.00	Small peptides	0.96
747.4	8.0	3	Amino acids and Peptides	1.00	Small peptides	0.99
751.4	5.7	40	Amino acids and Peptides	1.00	Small peptides	0.96
751.5	8.5	2	Amino acids and Peptides	0.98	Oligopeptides	0.86
751.5	9.3	2	Amino acids and Peptides	0.95	Oligopeptides	0.86
757.5	11.0	16	Amino acids and Peptides	1.00	Small peptides	0.77
758.6	14.5	2	Fatty acids	1.00	Glycerophospholipids	1.00
761.0	0.9	6	Shikimates and Phenylpropanoids	1.00	Flavonoids	0.99
761.5	13.7	2	Amino acids and Peptides	0.98	Oligopeptides	0.89
765.5	9.2	2	Amino acids and Peptides	0.97	Oligopeptides	0.55
765.5	10.4	2	Amino acids and Peptides	0.96	Oligopeptides	0.89
779.5	9.9	2	Amino acids and Peptides	1.00	Oligopeptides	0.93
779.5	11.0	2	Amino acids and Peptides	0.90	Oligopeptides	0.78
787.5	12.9	2	Amino acids and Peptides	0.99	Oligopeptides	0.62
787.5	15.7	2	Amino acids and Peptides	1.00	Oligopeptides	0.94
789.4	9.9	1	Amino acids and Peptides	1.00	Oligopeptides	0.73
791.5	11.7	2	Terpenoids	0.68	Macrolides	0.56
793.5	8.8	2	Amino acids and Peptides	0.99	Oligopeptides	0.91
793.5	8.6	2	Amino acids and Peptides	0.82	Oligopeptides	0.22

793.5	8.2	2	Amino acids and Peptides	0.84	Oligopeptides	0.22
793.5	9.4	2	Amino acids and Peptides	0.97	Oligopeptides	0.98
795.5	10.6	16	Amino acids and Peptides	1.00	Oligopeptides	0.62
801.4	13.0	1	Amino acids and Peptides	0.95	Oligopeptides	0.30
801.4	11.6	1	Amino acids and Peptides	1.00	Oligopeptides	0.60
803.4	12.0	1	Amino acids and Peptides	1.00	Small peptides	0.81
805.5	10.9	2	Amino acids and Peptides	0.93	Oligopeptides	0.90
805.5	12.3	2	Amino acids and Peptides	0.97	Oligopeptides	0.85
806.4	9.9	1	Amino acids and Peptides	0.99	Oligopeptides	0.63
807.4	8.2	1	Amino acids and Peptides	0.99	Oligopeptides	0.69
817.4	12.2	1	Amino acids and Peptides	0.99	Small peptides	0.60
817.4	10.4	1	Amino acids and Peptides	0.97	Oligopeptides	0.71
817.4	10.6	1	Amino acids and Peptides	0.89	Oligopeptides	0.63
819.5	9.1	2	Polyketides	0.70	Macrolides	0.13
821.4	9.0	1	Amino acids and Peptides	0.96	Oligopeptides	0.60
821.4	8.9	1	Amino acids and Peptides	0.84	Oligopeptides	0.17
821.5	11.3	2	Amino acids and Peptides	0.96	Oligopeptides	0.76
831.5	12.7	1	Amino acids and Peptides	0.96	Oligopeptides	0.83
833.4	10.1	1	Amino acids and Peptides	0.97	Oligopeptides	0.58
833.4	10.4	1	Amino acids and Peptides	0.87	Small peptides	0.46
833.4	11.4	1	Amino acids and Peptides	0.84	Oligopeptides	0.69
835.4	9.4	1	Amino acids and Peptides	1.00	Oligopeptides	0.68

837.0	9.4	22	Carbohydrates	0.99	Nucleosides	0.99
838.4	5.4	17	Amino acids and Peptides	1.00	Small peptides	0.79
839.4	10.4	1	Alkaloids	0.76	Pseudoalkaloids	0.32
839.4	12.1	1	Polyketides	0.92	Macrolides	0.70
843.0	0.9	6	Fatty acids	0.98	Fatty esters	1.00
845.5	13.1	1	Alkaloids	0.99	Tryptophan alkaloids	0.54
847.5	11.4	38	Amino acids and Peptides	0.95	Oligopeptides	0.96
849.5	9.7	1	Amino acids and Peptides	0.99	Oligopeptides	0.64
849.5	11.2	38	Amino acids and Peptides	0.93	Small peptides	0.33

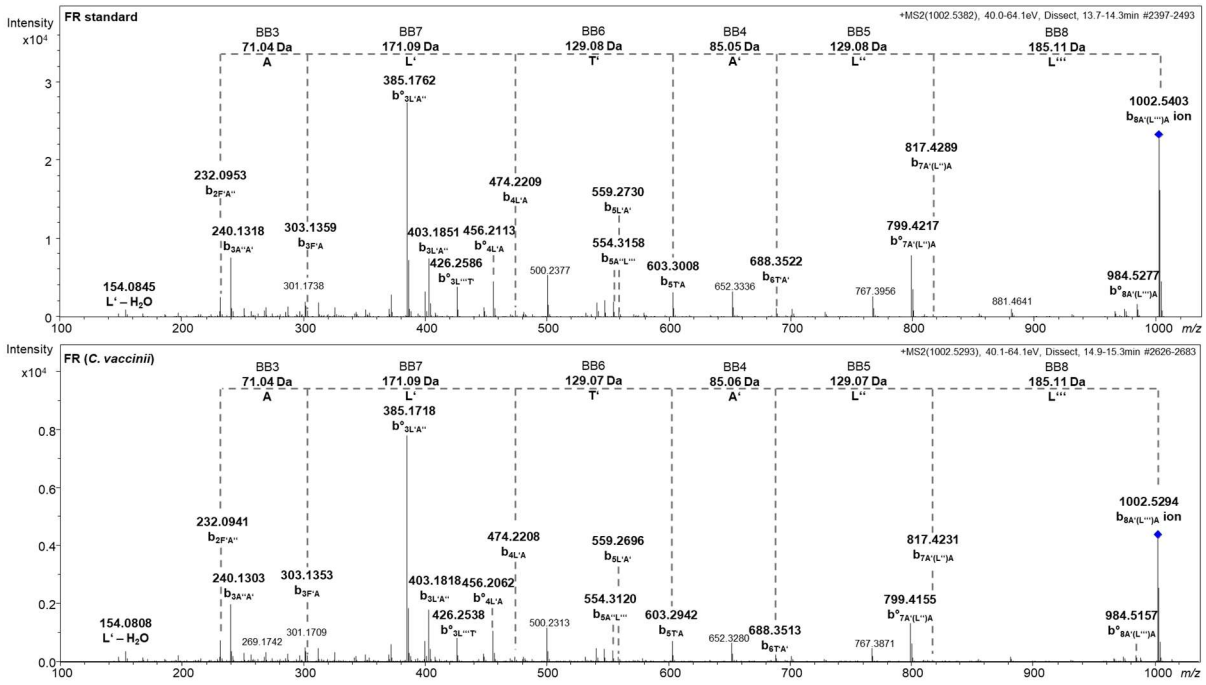

Figure 44: Fragmentation spectra of purified FR900359 (FR) as standard compared to the compound with *m/z* 1002.5293 found in extracts of *Chromobacterium vaccinii* MWU205. Building blocks were named following the nomenclature system by Ngoka[192] based on Biemanns modifications[193] of Roepstorffs nomenclature in one-letter amino acid code[194]. b° = b-ion with loss of water. L' = *N*-Ac-β-HyLeu, A = Ala, A' = *N*-Me-Ala, T' = *N,O*-Me_2-Thr, L''' = *N*-Prop-β-HyLeu, L'' = β-HyLeu, F' = Pla, A'' = *N*-Me-Dha.

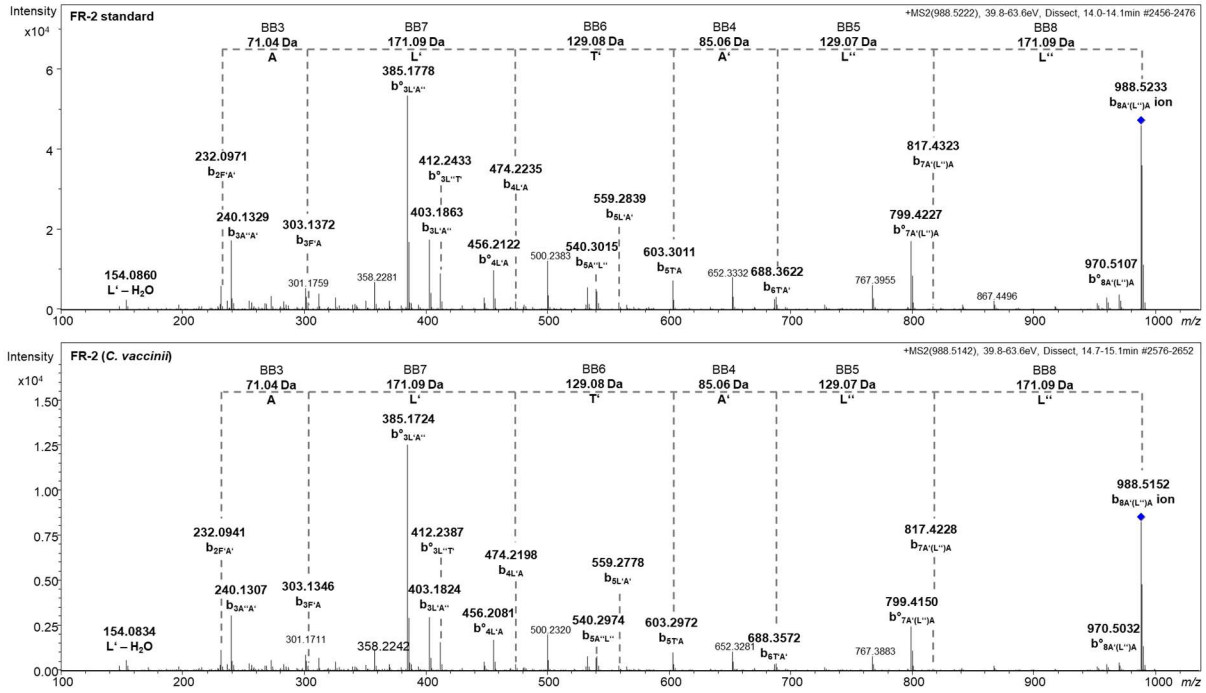

Figure 45: Fragmentation spectra of purified FR-2 as standard compared to the compound with *m/z* 988.5142 found in extracts of *Chromobacterium vaccinii* MWU205. Building blocks were named following the nomenclature system by Ngoka[192] based on Biemanns modifications[193] of Roepstorffs nomenclature in one-letter amino acid code[194]. b° = b-ion with loss of water. L' = *N*-Ac-β-HyLeu, A = Ala, A' = *N*-Me-Ala, T' = *N,O*-Me$_2$-Thr, L'' = β-HyLeu, F' = Pla, A'' = *N*-Me-Dha.

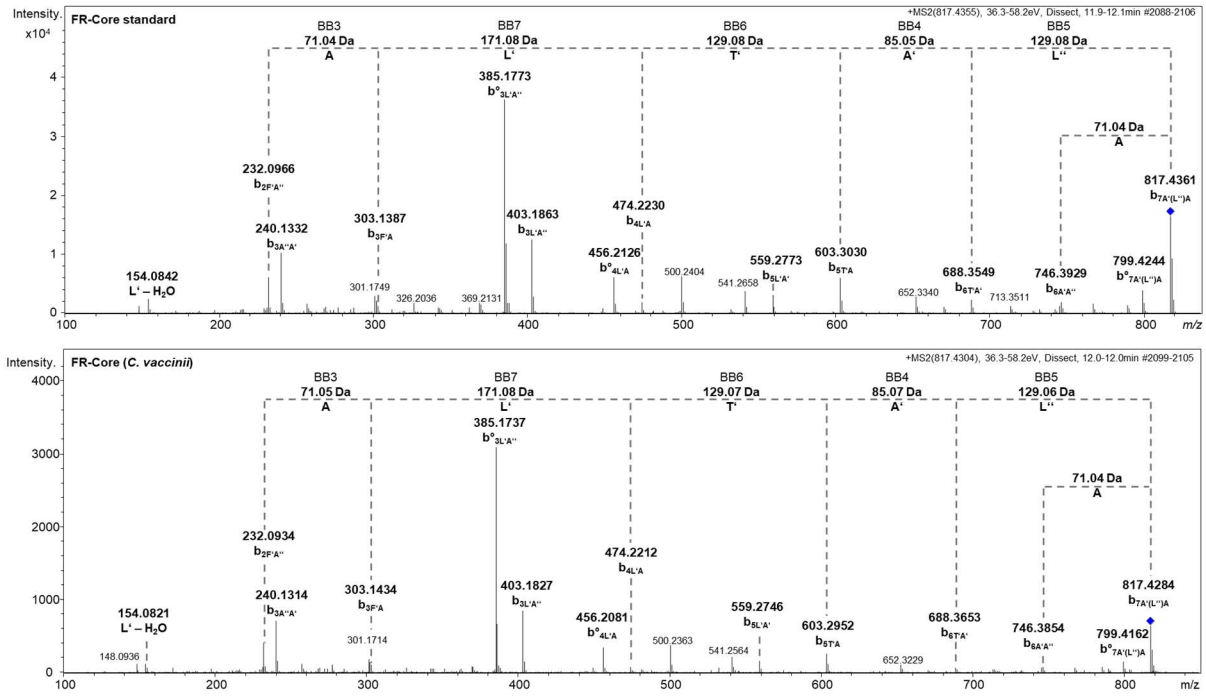

Figure 46: Fragmentation spectra of purified FR-Core as standard compared to the compound with *m/z* 817.4304 found in extracts of *Chromobacterium vaccinii* MWU205. Building blocks were named following the nomenclature system by Ngoka[192] based on Biemanns modifications[193] of Roepstorffs nomenclature in one-letter amino acid code[194]. b° = b-ion with loss of water. L' = *N*-Ac-β-HyLeu, A = Ala, A' = *N*-Me-Ala, T' = *N,O*-Me$_2$-Thr, L'' = β-HyLeu, F' = Pla, A'' = *N*-Me-Dha.

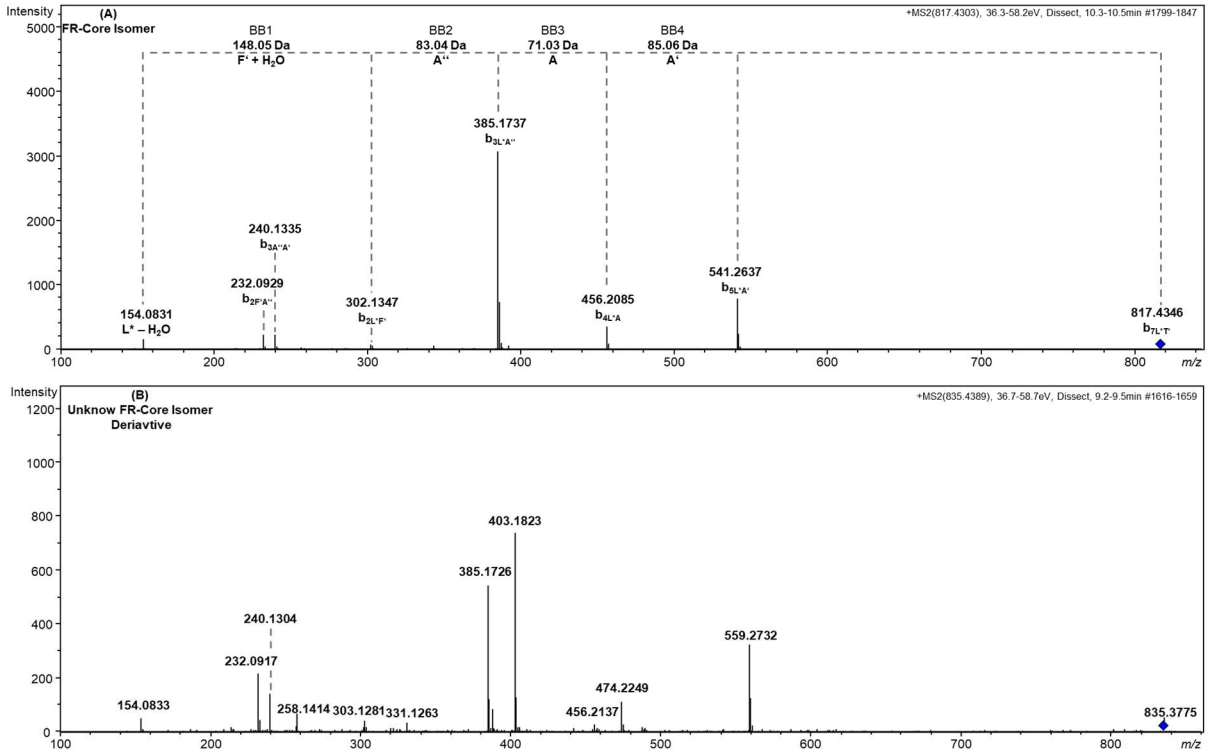

Figure 47: Fragmentation pattern of the FR-Core isomer (A) (*m/z* 817.4303) and the *m/z* value 835.4389 (B) following the nomenclature system by Ngoka[192] based on Biemanns modifications[193] of Roepstorffs nomenclature in one-letter amino acid code[194]. L' = *N*-Ac-β-HyLeu, L'' = β-HyLeu, L''' = *N*-Prop-β-HyLeu, A = Ala, A' = *N*-Me-Ala, T' = *N,O*-Me$_2$-Thr, F' = Pla, A'' = *N*-Me-Dha.

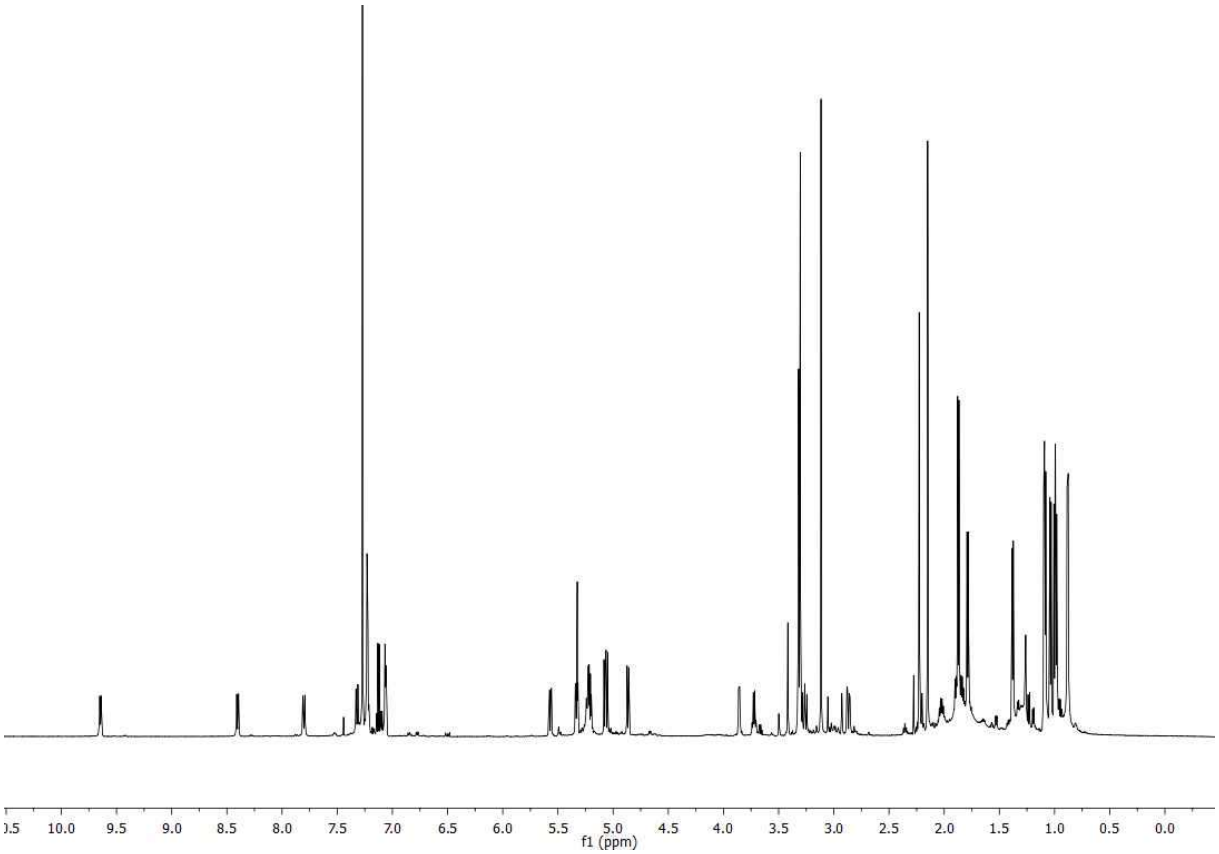

Figure 48: ^{1}H-Nuclear magnetic resonance spectrum (600 MHz, CDCl3) of FR-6.

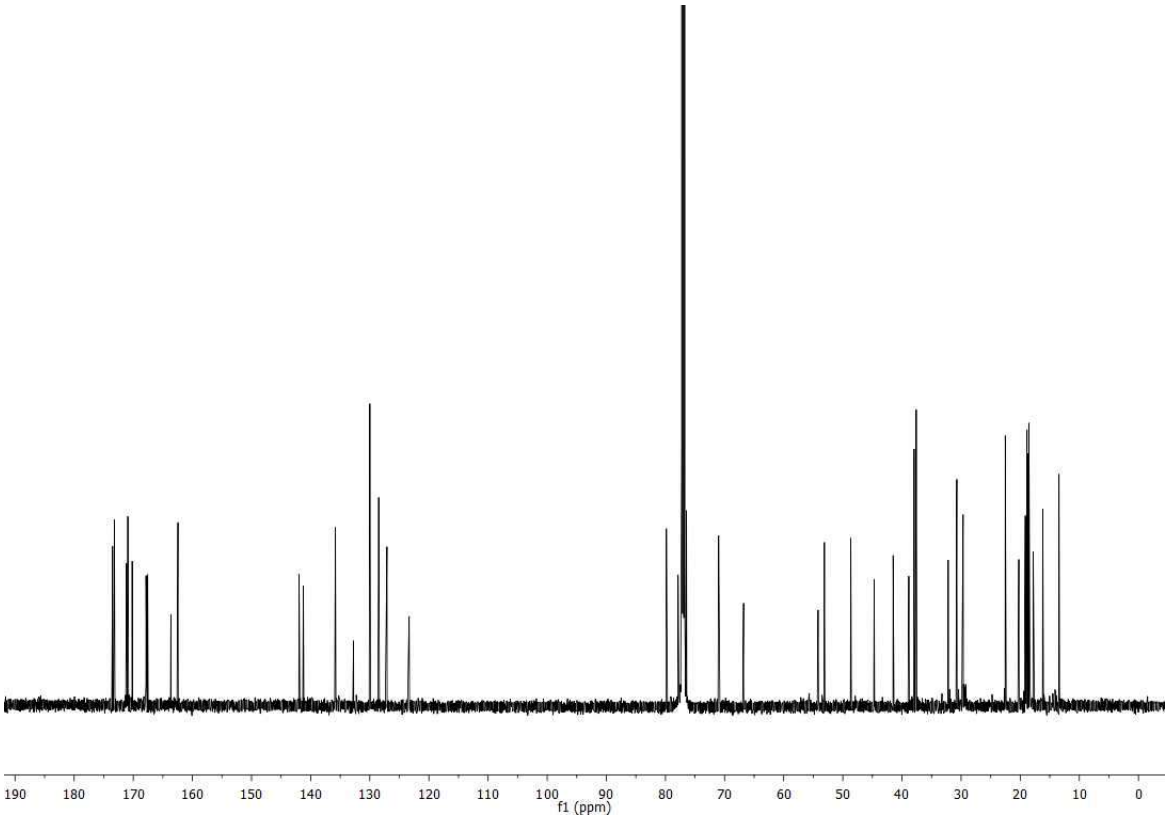

Figure 49: ^{13}C-Nuclear magnetic resonance spectrum (150 MHz, $CDCl_3$) of FR-6.

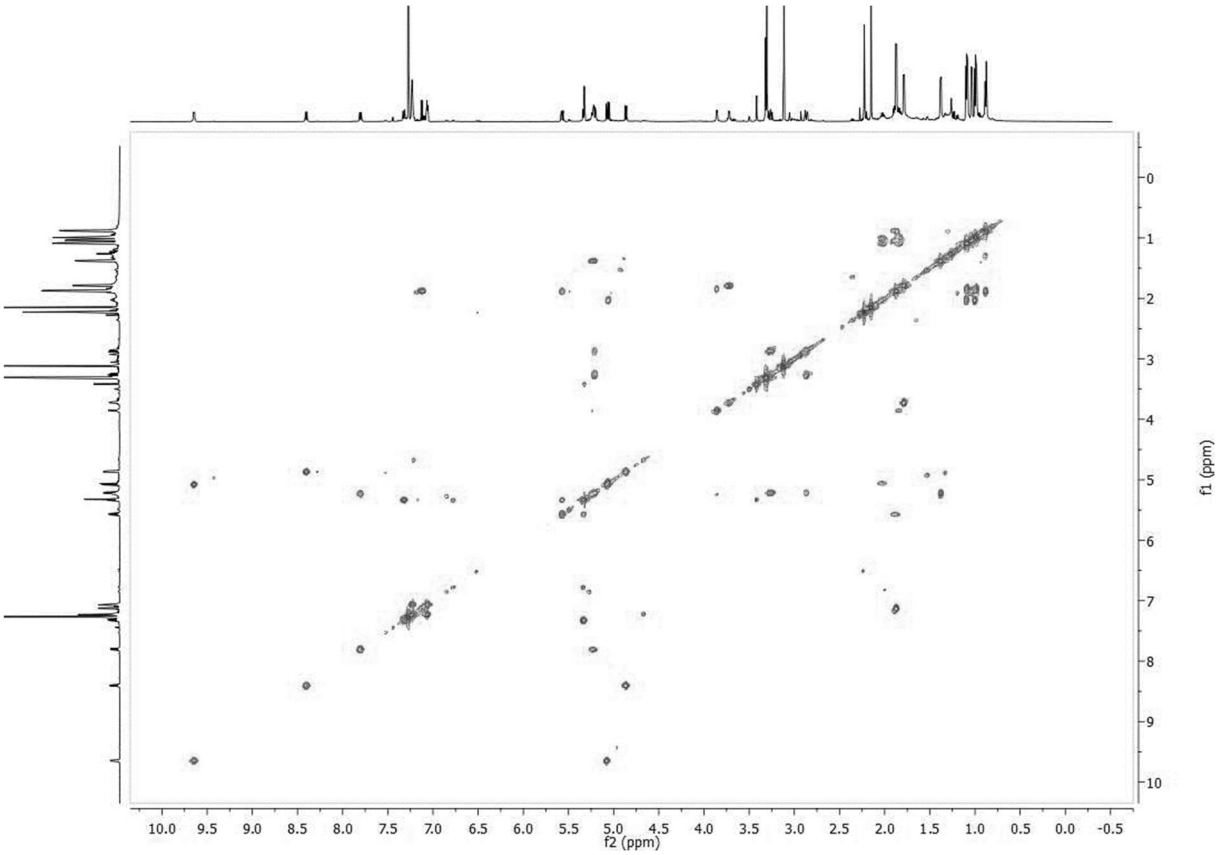

Figure 50: ^{1}H-^{1}H- Correlated Spectroscopy (COSY) nuclear magnetic resonance spectrum (600 MHz, $CDCl_3$) of FR-6.

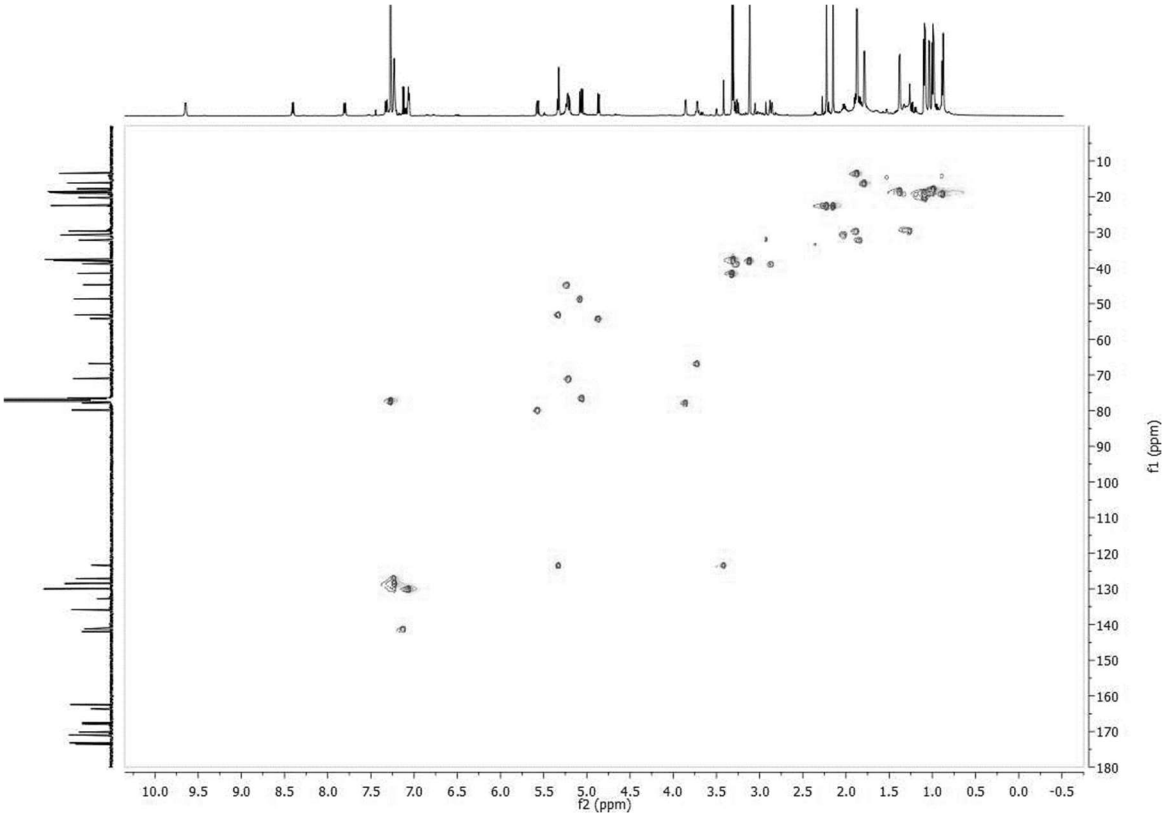

Figure 51: ^{1}H-^{13}C Heteronuclear single quantum coherence (HSQC)nuclear magnetic resonance spectrum (600 MHz, $CDCl_3$) of FR-6.

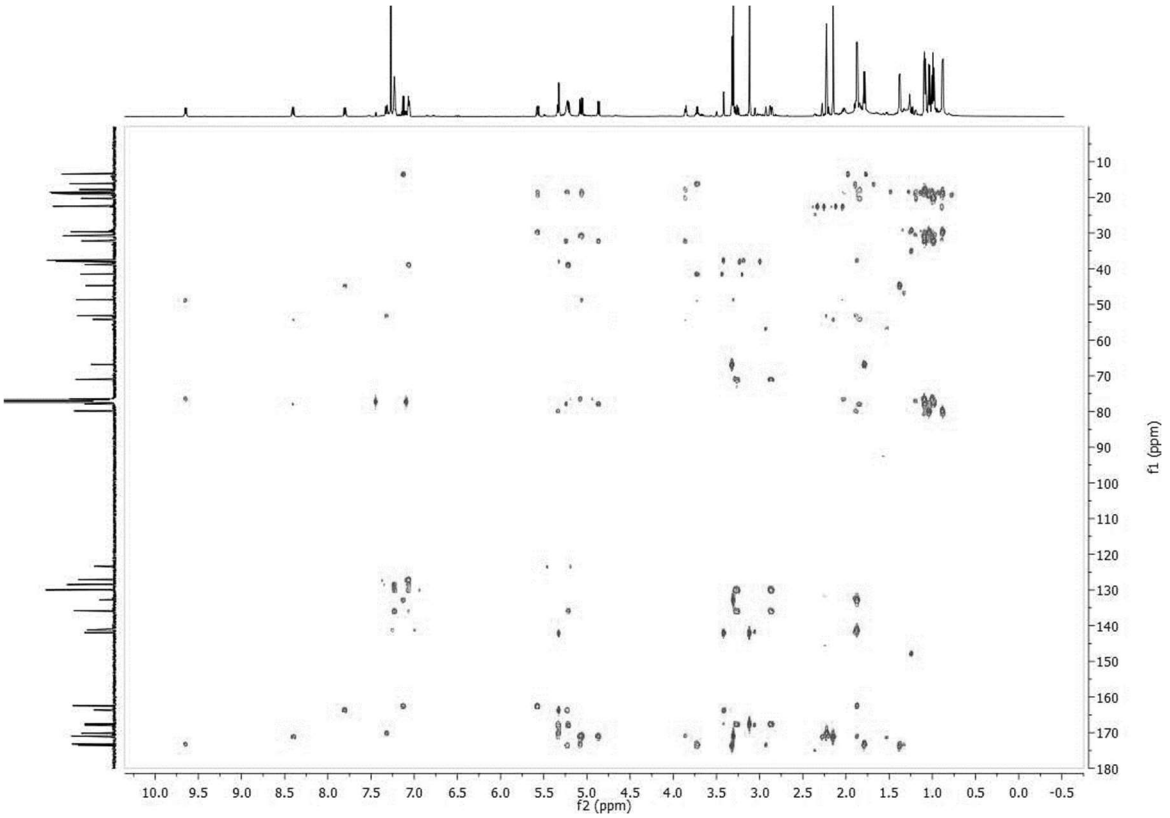

Figure 52: ^{1}H-^{13}C Heteronuclear multiple bond correlation (HMBC) nuclear magnetic resonance spectrum (600 MHz, $CDCl_3$) of FR-6.

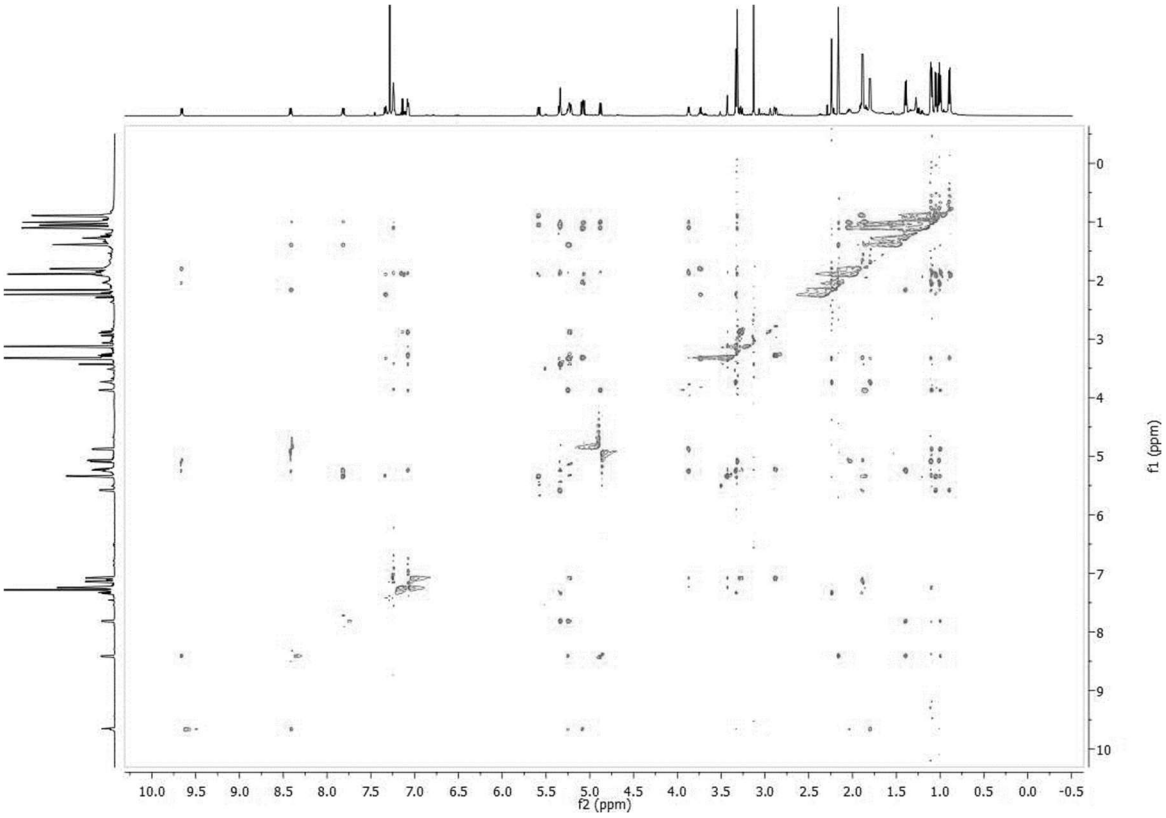

Figure 53: ^{1}H-^{1}H Rotating frame overhauser enhancement spectroscopy (ROESY) nuclear magnetic resonance spectrum (600 MHz, $CDCl_3$) of FR-6.

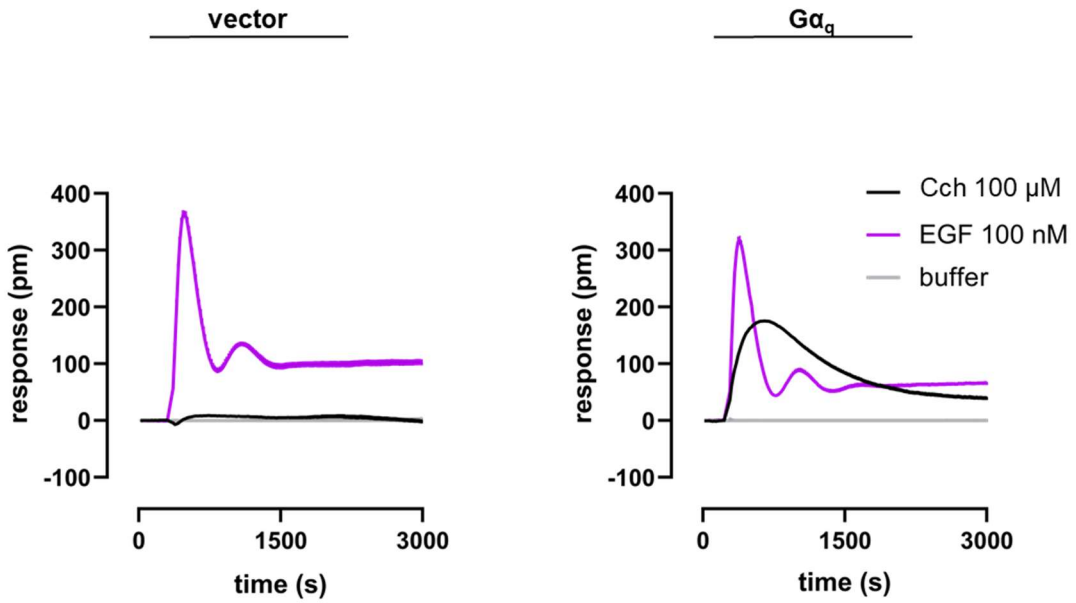

Figure 54: Clustered regularly interspaced short palindromic repeats/Caspase 9 edited HEK $G_{q/11}$-KO cells respond to carbachol (Cch) only after re-expression of $G\alpha_q$. Dynamic mass redistribution (DMR) analysis of whole cell responses evoked by epidermal growth factor (as the cell viability control) and Cch, which activates $G\alpha_q$-sensitive endogenous muscarinic acetylcholine receptor type 3 receptors, at the indicated concentrations in HEK293 cells genome-edited by CRISPR-Cas9 to lack all functional alleles for $G\alpha_q$ and $G\alpha_{11}$. HEK-$\Delta G\alpha_{q/11}$ cells respond to epidermal growth factor with robust alteration of DMR profiles but require the presence of $G\alpha_q$ to respond to Cch. Shown are real-time measurements (mean + Standard error of the mean, technical triplicates) representative of three such experiments.

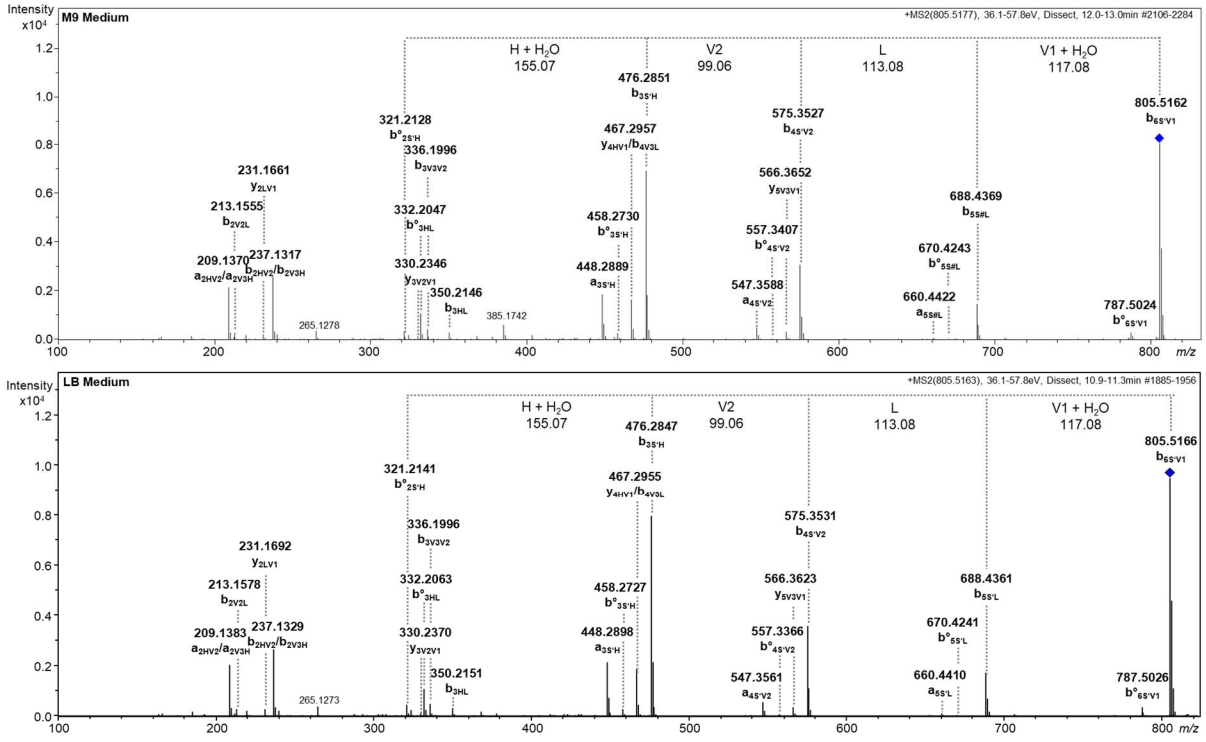

Figure 55: Comparison of the fragmentation pattern of valhidepsin B (*m/z*: 805.519) found in *n*-butanol extracts of *Chromobacterium vaccinii* MWU205 grown in M9 medium and LB medium. Fragments were labeled following the nomenclature system by Ngoka[192] based on Biemanns modifications[193] of Roepstorffs nomenclature in one-letter amino acid code.[194] b° = b-ion with loss of water. *S'* = acylated serine.

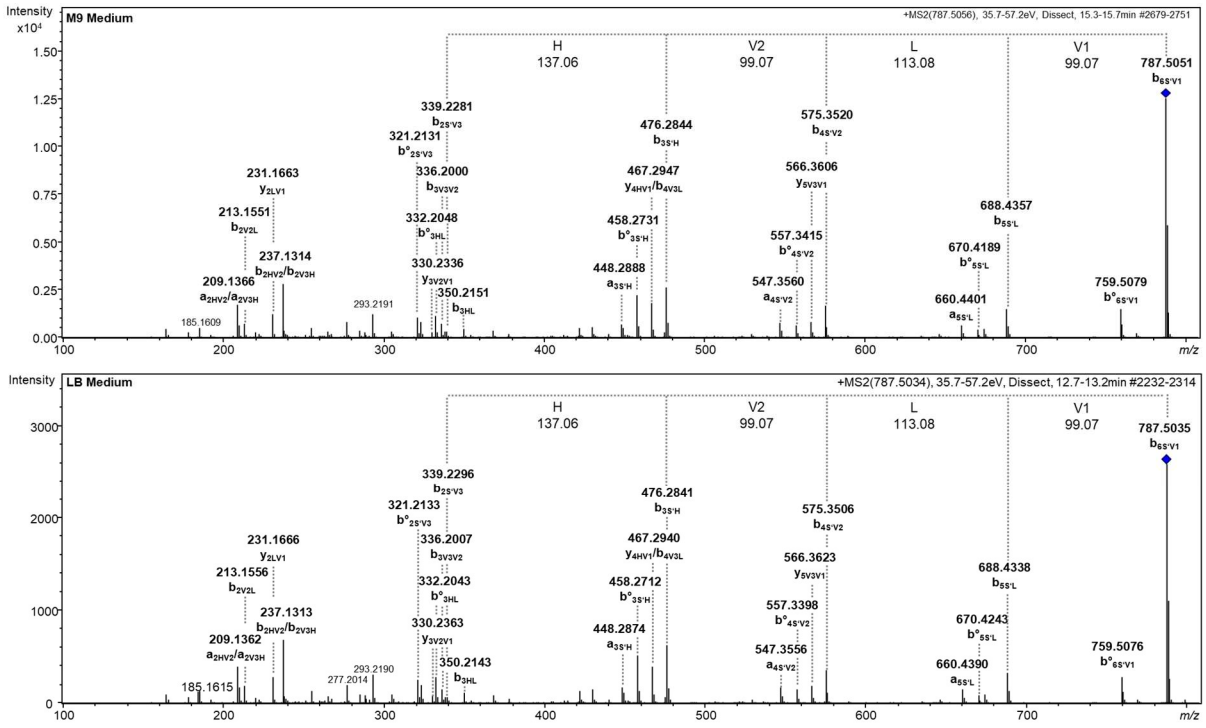

Figure 56: Comparison of the fragmentation pattern of valhidepsin A (*m/z*: 787.508) found in *n*-butanol extracts of *Chromobacterium vaccinii* MWU205 grown in M9 medium and LB medium. Fragments were labeled following the nomenclature system by Ngoka[192] based on Biemanns modifications[193] of Roepstorffs nomenclature in one-letter amino acid code.[194] b° = b-ion with loss of water. *S'* = acylated serine.

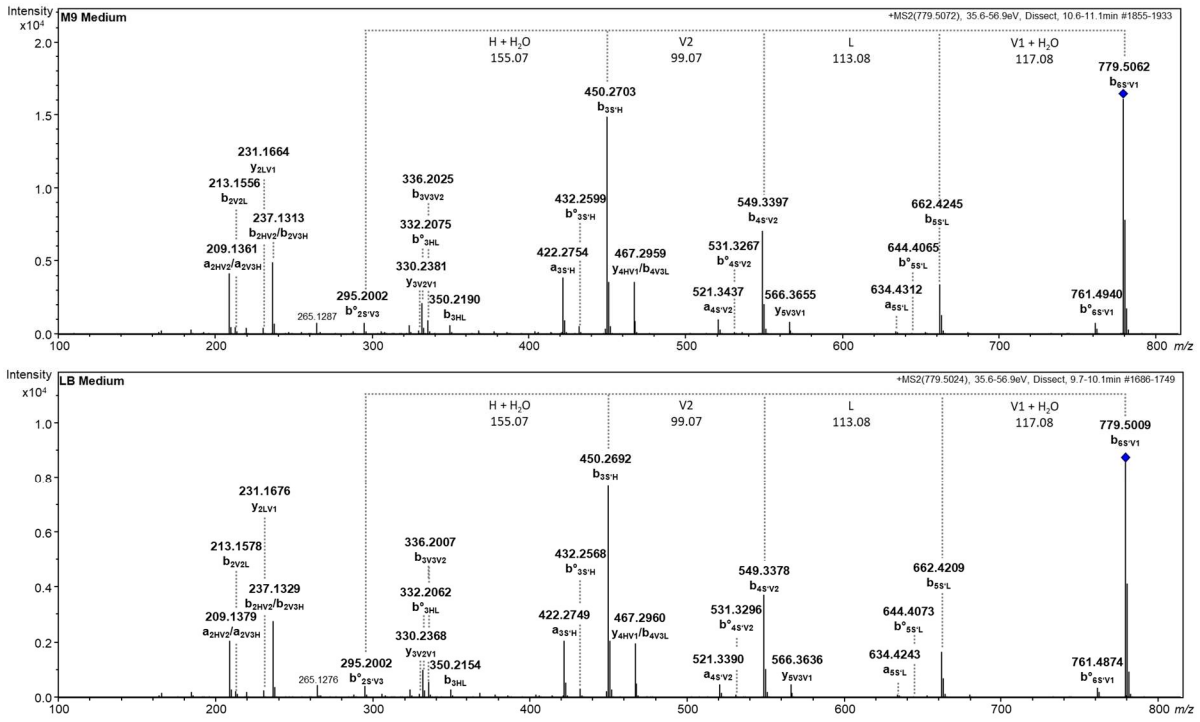

Figure 57: Comparison of the fragmentation pattern of valhidepsin D (*m/z*: 779.503) found in *n*-butanol extracts of *Chromobacterium vaccinii* MWU205 grown in M9 medium and LB medium. Fragments were labeled following the nomenclature system by Ngoka[192] based on Biemanns modifications[193] of Roepstorffs nomenclature in one-letter amino acid code.[194] b° = b-ion with loss of water. S' = acylated serine.

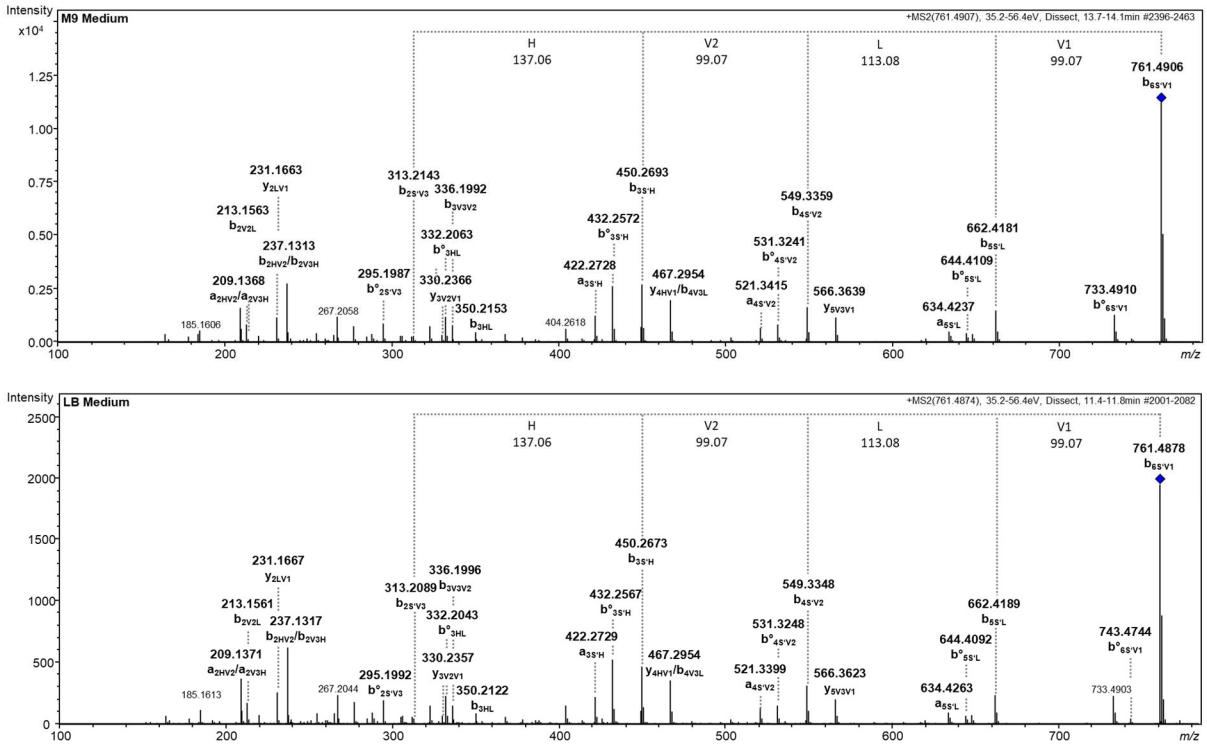

Figure 58: Comparison of the fragmentation pattern of valhidepsin C (*m/z*: 761.493) found in *n*-butanol extracts of *Chromobacterium vaccinii* MWU205 grown in M9 medium and LB medium. Fragments were labeled following the nomenclature system by Ngoka[192] based on Biemanns modifications[193] of Roepstorffs nomenclature in one-letter amino acid code.[194] b° = b-ion with loss of water. S' = acylated serine.

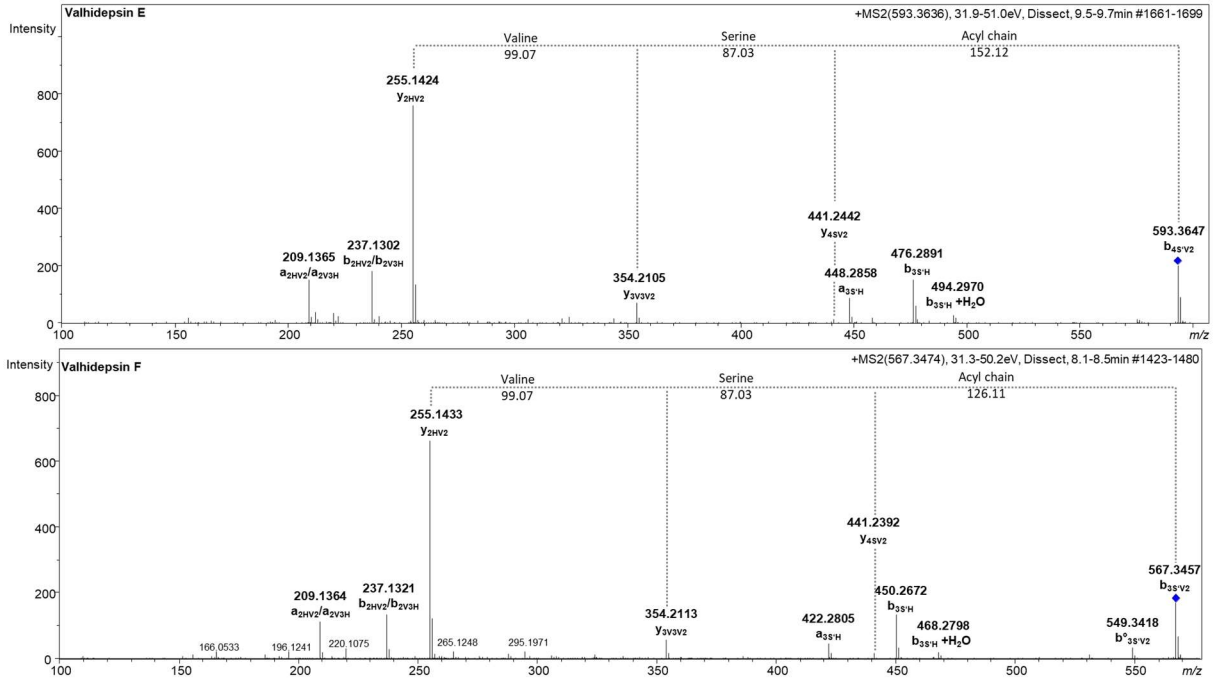

Figure 59: Fragmentation pattern of valhidepsin E (*m/z*: 593.3636) and Valhidepsin F (*m/z*: 567.3474) found in *n*-butanol extracts of *Chromobacterium vaccinii* MWU205 grown in M9 medium. Fragments were labeled following the nomenclature system by Ngoka[192] based on Biemanns modifications[193] of Roepstorffs nomenclature in one-letter amino acid code.[194] b° = b-ion with loss of water. S' = acylated serine.

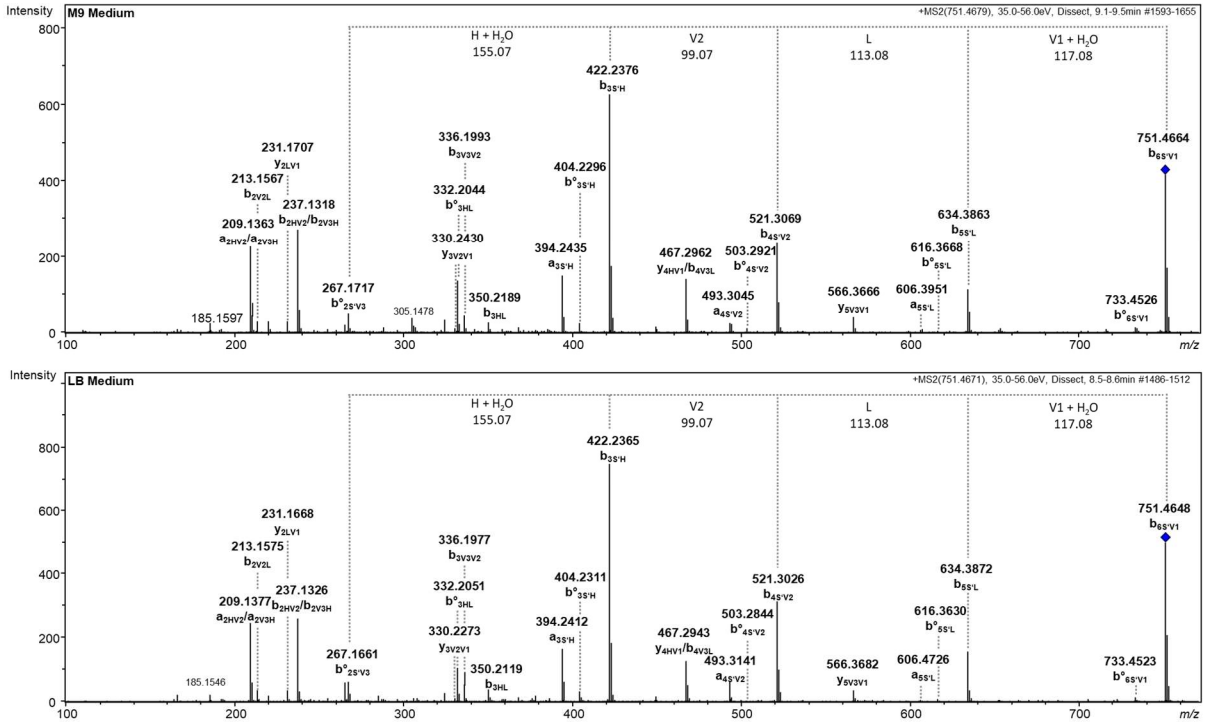

Figure 60: Comparison of the fragmentation pattern of the unknown valhidepsin with an *m/z* of 751.468 found in *n*-butanol extracts of *Chromobacterium vaccinii* MWU205grown in M9 medium and LB medium. Fragments were labeled following the nomenclature system by Ngoka[192] based on Biemanns modifications[193] of Roepstorffs nomenclature in one-letter amino acid code.[194] b° = b-ion with loss of water. S' = acylated serine.

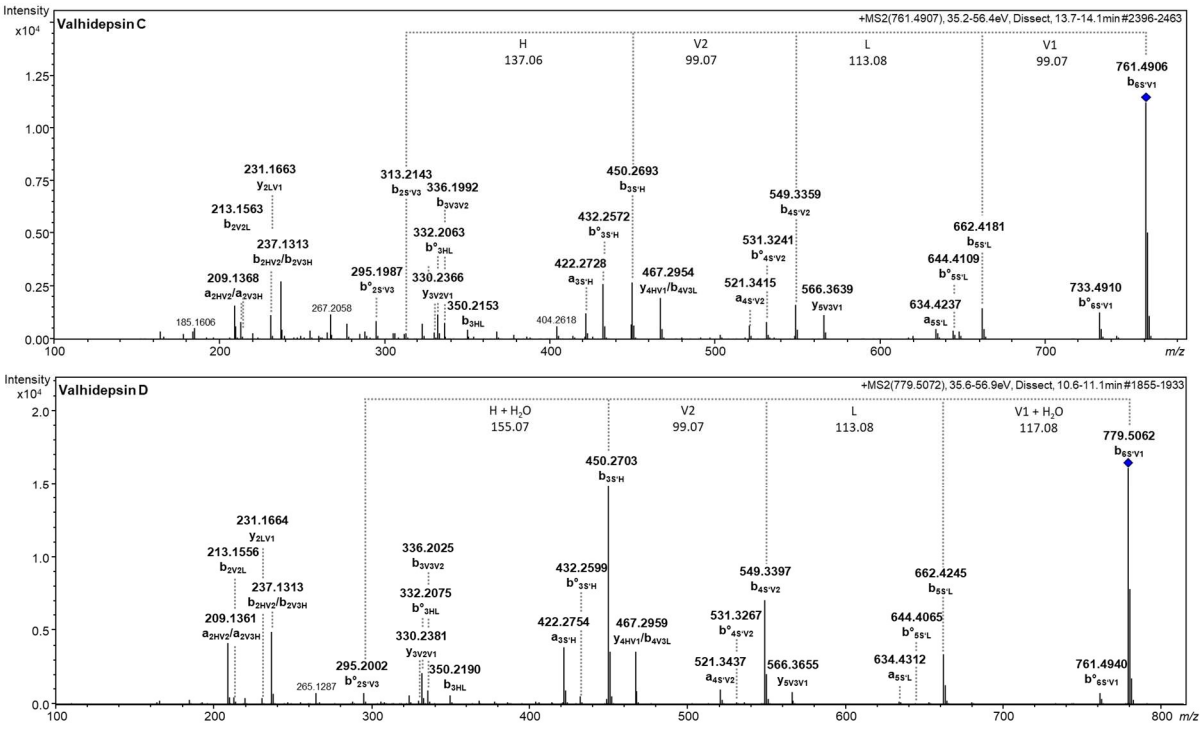

Figure 61: Fragmentation pattern of valhidepsin C (*m/z* 761.487) and valhidepsin D (*m/z* 779.500). Fragment ions were named following the nomenclature system by Ngoka[192] based on Biemanns modifications[193] of Roepstorffs nomenclature in one-letter amino acid code.[194] b° = b-ion with loss of water. S' = acylated serine.

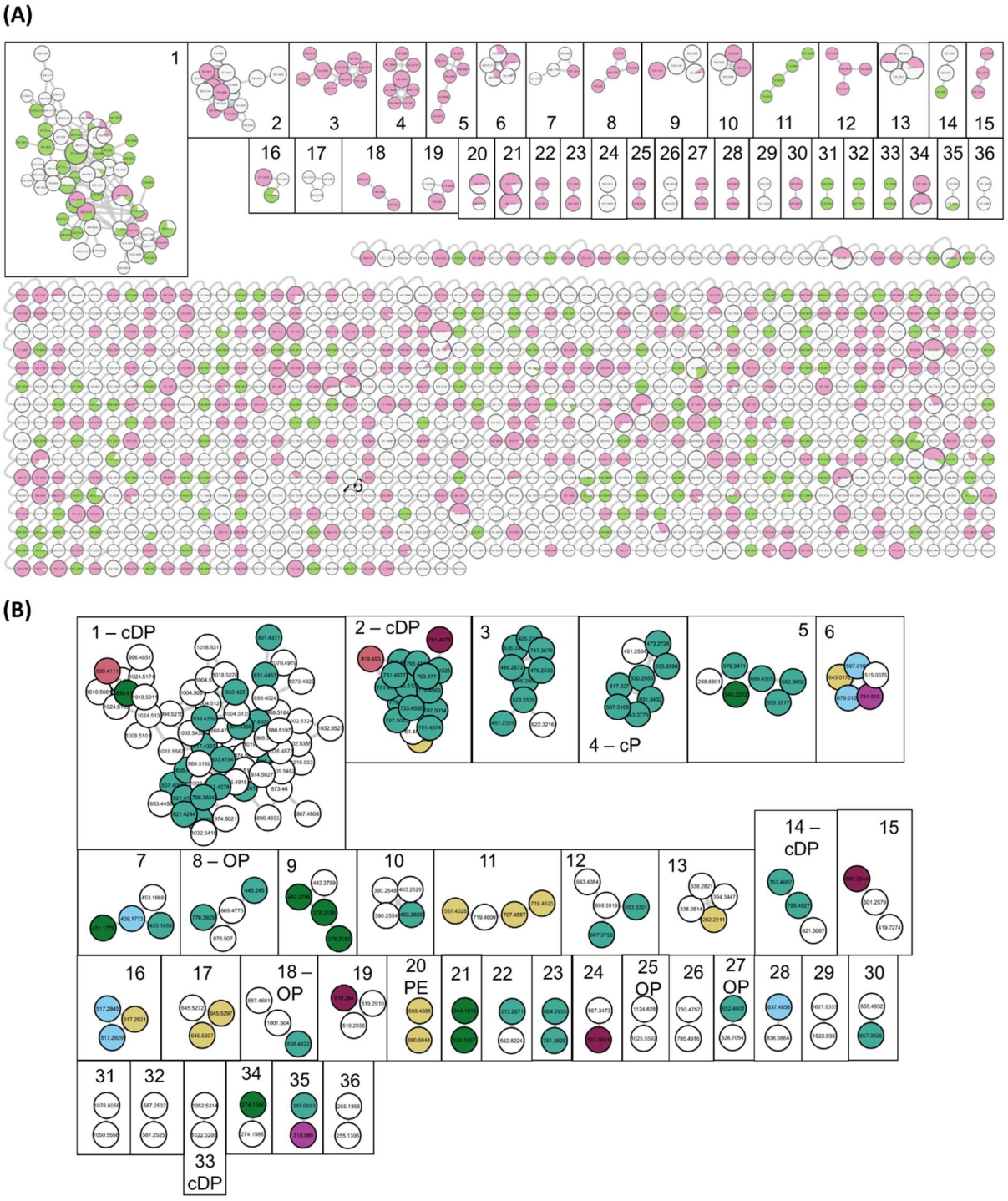

Figure 62: Feature-based molecular network (FBMN) (workflow version: release_28.2) of the metabolomes of *n*-butanolic extracts from *Chromobacterium vaccinii* MWU205 cultivated in LB or M9 medium and the depsipeptide-containing fraction of *Ardisia crenata* leaves. **(A)** shows the complete FBMN, displaying the origin (*C. vaccinii* MWU205 LB medium: red, *C. vaccinii* MWU205 M9 medium: white, *A. crenata*: green) of each node as pie chart. All clusters containing at least two nodes are numbered. **(B)** shows only the clusters, which were labeled with their predicted compound classes by Global natural product social molecular networking tools (DEREPLICATOR[184,187], MS2LDA[185,186]) and colored according to the predicted compound classes by the CANOPUS tool[188,189]. No compound class = white, amino acids and peptides = light green, fatty acids = yellow, shikimates/phenylpropanoids = purple, carbohydrates = light blue, alkaloids = dark green, polyketides = red, terpenoids = dark red.

Table 16: Stachelhaus Code for the adenylation domains from the *frs* biosynthesis gene clusters from both FR900359 producers. The table was taken from the PhD thesis of Cornelia Hermes[226].

	***Candidatus* Burkholderia crenata**[199]	***Chromobacterium vaccinii* MWU205**
FrsA	DAMLVGA**V**CK	DAMLVGA**A**CK
FrsD	DAMLVGA**V**CK	DAMLVGA**A**CK
FrsE	GAFVMAGVCK	GAFVMAGVCK
FrsE	DVWHLSLVDK	DVWHLSLVDK
FrsF	DVFSVAIVYK	DVFSVAIVYK
FrsF	DVFSVAIVYK	DVFSVAIVYK
FrsG	DAMLVGA**V**CK	DAMLVGA**A**CK
FrsG	DFWN**I**GMVHK	DFWN**V**GMVHK

6.2. Appendix for chapter 3.2

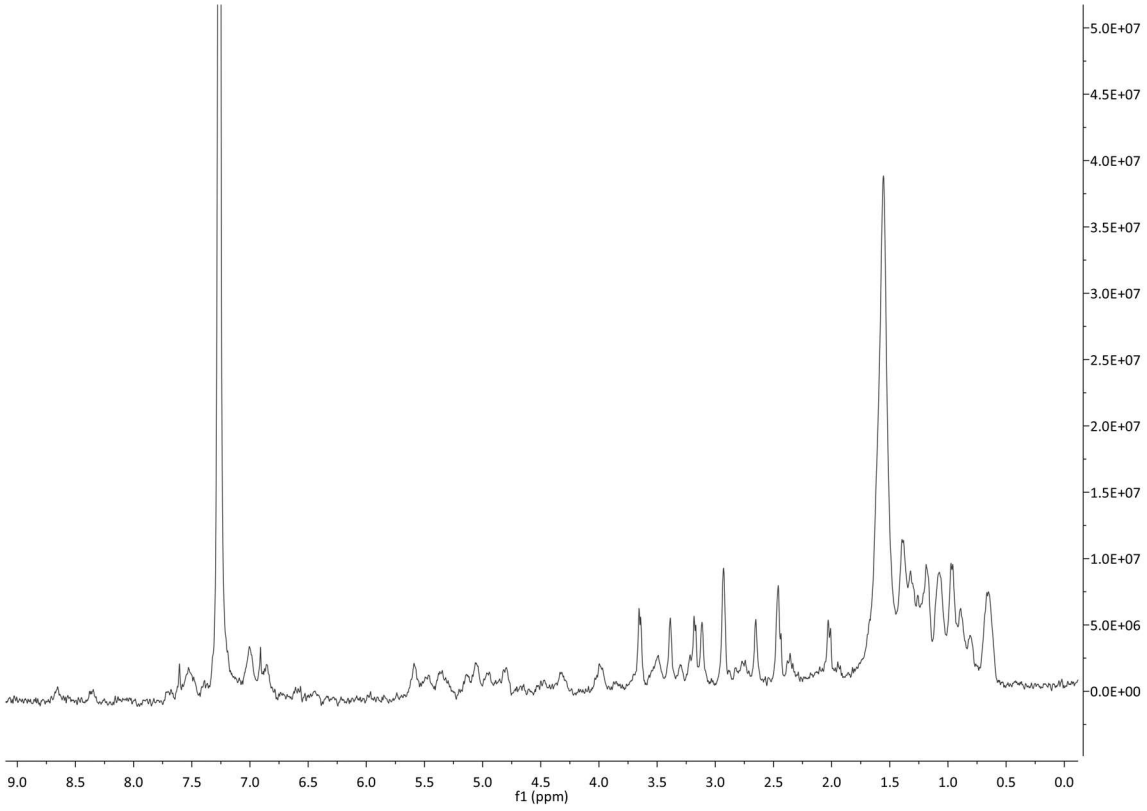

Figure 63: ^{1}H-Nuclear magnetic resonance spectrum (300 MHz $CDCl_3$) of completely ^{13}C/^{15}N-labeled FR900359.

Table 17: Area under the curve (AUC) for *m/z* 1002.54 to determine the production of FR in *n*-butanol extracts of *Chromobacterium vaccinii* MWU205 grown in LB and M9 medium for 7.5 days with samples taken every 12 h and two measurements rows per medium.

Cultivation time (days)	AUC (*m/z* 1002.54) LB		AUC (*m/z* 1002.54) M9	
0	0	0	241,371	227,513
0.5	7,519,130	10,616,213	2,720,170	3,404,664
1	35,743,832	32,055,368	18,991,986	23,501,066
1.5	56,019,635	51,508,369	45,556,060	35,717,250
2	49,075,656	48,677,517	42,229,239	49,249,340
2.5	46,682,611	49,178,507	29,224,041	39,618,579
3	39,058,414	42,847,565	42,946,363	34,287,397
3.5	23,759,953	38,419,891	39,563,206	30,331,536
4	31,474,599	38,479,764	38,791,987	35,586,138
4.5	29,621,228	36,910,804	7,797,342	34,687,692
5	20,884,773	23,131,656	45,505,750	32,580,980
5.5	21,314,881	11,456,827	39,412,278	31,353,241
6	14,077,116	11,968,603	37,239,799	41,442,114
6.5	11,617,081	13,511,536	34,821,581	36,316,559
7	9,560,195	13,021,883	36,907,170	31,021,623
7.5	8,297,424	10,958,613	35,934,914	31,038,120

Table 18: Area under the curve (AUC) for *m/z* 988.52 to determine the production of FR-2 in *n*-butanol extracts of *Chromobacterium vaccinii* MWU205 grown in LB and M9 medium for 7.5 days with samples taken every 12 h and two measurements rows per medium.

Cultivation time (days)	AUC (*m/z* 988.52) LB		AUC (*m/z* 988.52) M9	
0	410,582	338,180	523,589	148,889
0.5	5,803,813	9,058,580	13,612,779	16,114,464
1	51,935,790	49,592,605	87,732,855	127,815,599
1.5	42,845,652	36,474,107	120,109,411	115,448,325
2	31,306,245	29,864,806	117,480,743	142,120,500
2.5	28,053,256	28,799,485	83,414,596	107,318,487
3	23,793,054	22,927,409	95,750,694	98,224,921
3.5	14,266,675	18,878,568	109,944,655	109,027,602
4	15,776,963	19,383,737	104,058,994	97,294,316
4.5	13,972,982	18,009,468	32,144,261	97,420,973
5	11,947,273	10,989,577	106,689,027	95,241,582

5.5	12,116,158	9,453,762	107,208,458	99,020,699
6	7,744,026	9235,571	104,269,348	131,447,043
6.5	6,283,590	6,154,142	100,214,372	121,440,998
7	5,484,727	8,546,726	94,012,690	89,512,115
7.5	4,509,234	7,557,471	107,045,954	92,517,525

Table 19: Raw data of **Figure 26** showing the modified area under the curve (AUC) of *m/z* 1002.5 and *m/z* 988.5 in *n*-butanol extracts of *Chromobacterium vaccinii* MWU205 cultures grown in M9 Medium with [+PA] and without 5 mM propionic acid (PA) [Control].

Sample	**AUC (*m/z* 1002.5)**	**AUC (*m/z* 988.5)**
Control repeat 1	712,181,106	2,201,575,293
Control repeat 2	701,829,824	2,263,831,105
Control repeat 3	812,685,684	2,493,656,318
+PA repeat 1	3,149,348,881	571,559,310
+PA repeat 2	2,826,151,378	539,985,728
+PA repeat 3	2,776,633,968	540,788,459

Table 20: Raw data of **Figure 27** showing the modified area under the curve (AUC) of *m/z* 1016.56 in *n*-butanol extracts of *Chromobacterium vaccinii* MWU205 cultures grown in LB Medium with [+iBA] and without isobutyric acid (iBA) [Control].

Sample	**AUC (*m/z* 1016.56)**
Control	4,176,166
+iBA repeat 1	27,498,848
+iBA repeat 2	25,004,632
+iBA repeat 3	25,563,982

Table 21: Raw data of **Figure 27** showing the modified area under the curve (AUC) of *m/z* 1030.57 in *n*-butanol extracts of *Chromobacterium vaccinii* cultures grown in LB Medium with valeric acid [+VA], with isovaleric acid [+iVa] and without feeding [Control].

Sample	**AUC (*m/z* 1030.57)**
Control	4,920,980

+VA repeat 1	17,228,390
+VA repeat 2	16,076,034
+VA repeat 3	17,076,754
+iVA repeat 1	15,245,129
+iVA repeat 2	12,831,949
+iVA repeat 3	12,070,318

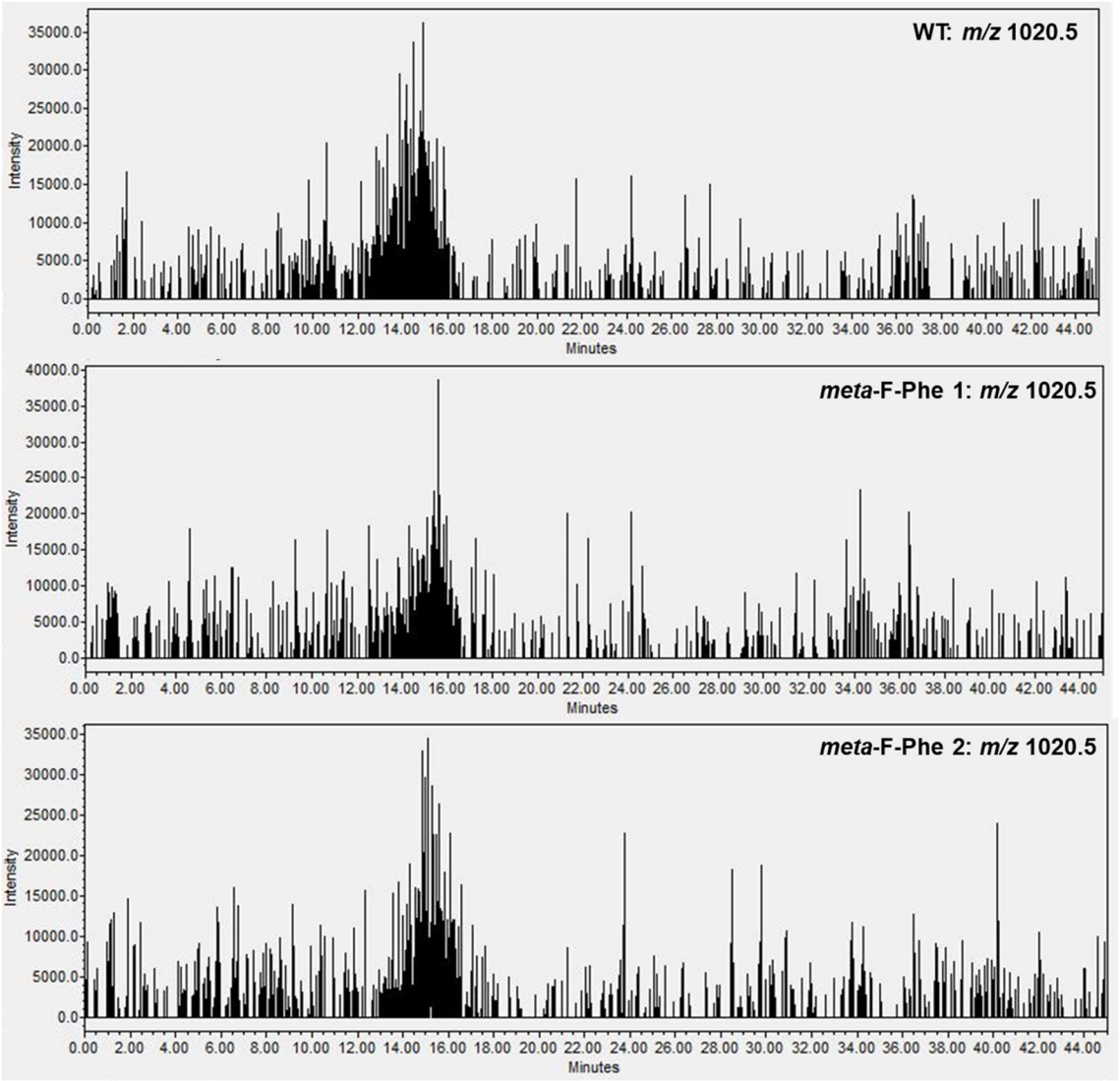

Figure 64: Extracted ion chromatograms of *m/z* 1020.5 of *n*-butanol extracts from *Chromobacterium vaccinii* MWU205 cultures cultivated in M9 medium with and without feeding of *meta*-F-Phe after 20 h.

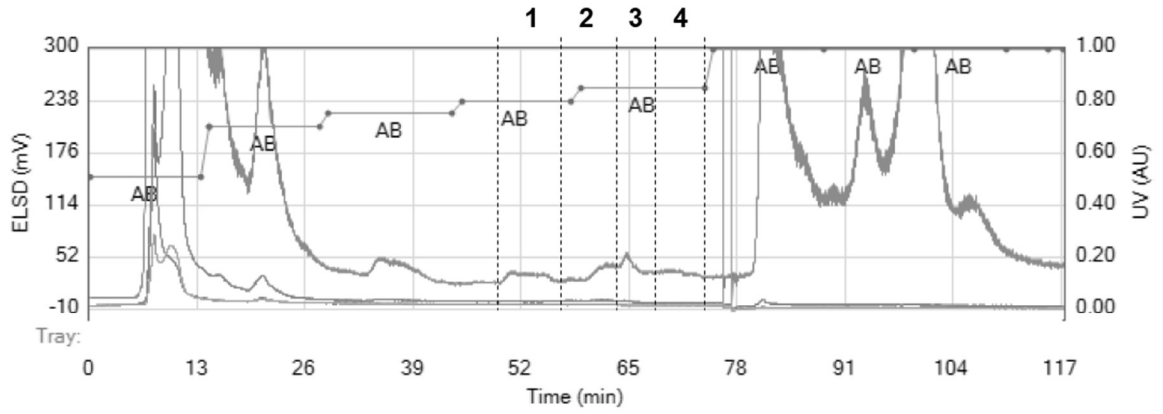

	Fraction 1	Fraction 2	Fraction 3	Fraction 4
***m/z* 1002.5 (FR)**	$1.3*10^7$	$1.0*10^9$	$3.1*10^8$	$1.9*10^7$
***m/z* 1020.5**	$4.0*10^6$	$4.9*10^8$	$4.1*10^8$	$1.3*10^7$

Figure 65: Flash chromatography of the *n*-butanol extract of 4.5 L *Chromobacterium vaccinii* MWU205 Δ*vioA* cultivated in LB medium fed with *meta*-F-Phe. Collected fractions are numbered and their area under the curve for *m/z* 1002.5 (FR900359) and *m/z* 1020.5 was calculated.

Table 22: Area under the curve (AUC) of *m/z* 1020.5 in *n*-butanol extracts of *Chromobacterium vaccinii* MWU205 Δ*vioA* without feeding [Control (A)] and with feeding of *meta*-F-phenylalanine (*m*-F-Phe) displayed in **Figure 29 (A)**. AUC of *m/z* 1020.5 in *n*-butanol extracts of *C. vaccinii* MWU205 without feeding [Control (B)] and with feeding of *ortho*-F-Phe or *para*-F-Phe displayed in **Figure 29 (B)**.

Sample	AUC (*m/z* 1020.5)
Control (A)	4,920,980
+*m*-F-Phe repeat 1	1078089248
+*m*-F-Phe repeat 2	998944543
+*m*-F-Phe repeat 3	1089278350
Control (B)	43928679
+*o*-F-Phe repeat 1	1029597994
+*o*-F-Phe repeat 2	1464634768
+*o*-F-Phe repeat 3	1348126437
+*p*-F-Phe repeat 1	80749641

+*p*-F-Phe repeat 2	63699040
+*p*-F-Phe repeat 3	69945061

6.3. Appendix for chapter 3.3

Table 23: Area under the curve (AUC) of m/z 1002.5 in *n*-butanol extracts of *Chromobacterium vaccinii* MWU205 cultures grown in soil extracts for 5 d and blanks without inoculation. NSE = New soil extract[238], WE = water extract[239], NE = NaOH extracts[240], and SESOM = soil-extracted solubilized organic matter[241].

Sample	AUC (*m/z* 1002.5)
NSE blank	233,660
NSE repeat 1	37,040
NSE repeat 2	114,986
NSE repeat 3	199,460
WE blank	169,942
WE repeat 1	297181
WE repeat 2	126,899
WE repeat 3	167,055
NE blank	0
NE repeat 1	0
NE repeat 2	0
NE repeat 3	0
SESOM blank	125,571
SESOM repeat 1	149,484
SESOM repeat 2	107,492
SESOM repeat 3	1,437,699

Table 24: Crude extract weight in mg and area under the curve (AUC) of *m/z* 1002.5 of all six *n*-butanol extracts of *Chromobacterium vaccinii* MWU205 cultivated in SESOM for 0 or 5 days.

Sample	Crude extract (mg)	AUC (*m/z* 1002.5)
0 days, repeat 1	2.8	117,598
0 days, repeat 2	2.6	84,445
0 days, repeat 3	3.1	81,145
5 days, repeat 1	3.9	492,642

5 days, repeat 2	2.8	640,038
5 days, repeat 3	3.2	610,946

Table 25: Crude extract weight in mg and area under the curve (AUC) of *m/z* 1002.5 of all seven *n*-butanol extracts of *Chromobacterium vaccinii* MWU205 cultivated in SESOM for 0 or 5 days.

Sample	**Crude extract (mg)**	**AUC (*m/z* 1002.5)**
0 days, repeat 1	3.1	466,318
0 days, repeat 2	2.3	349,851
0 days, repeat 3	2.7	578,250
5 days, repeat 1	4.7	717,770
5 days, repeat 2	3.5	860,838
5 days, repeat 3	3.8	731,828
5 days, repeat 4	4.7	676,437

6.4. Appendix for chapter 3.4

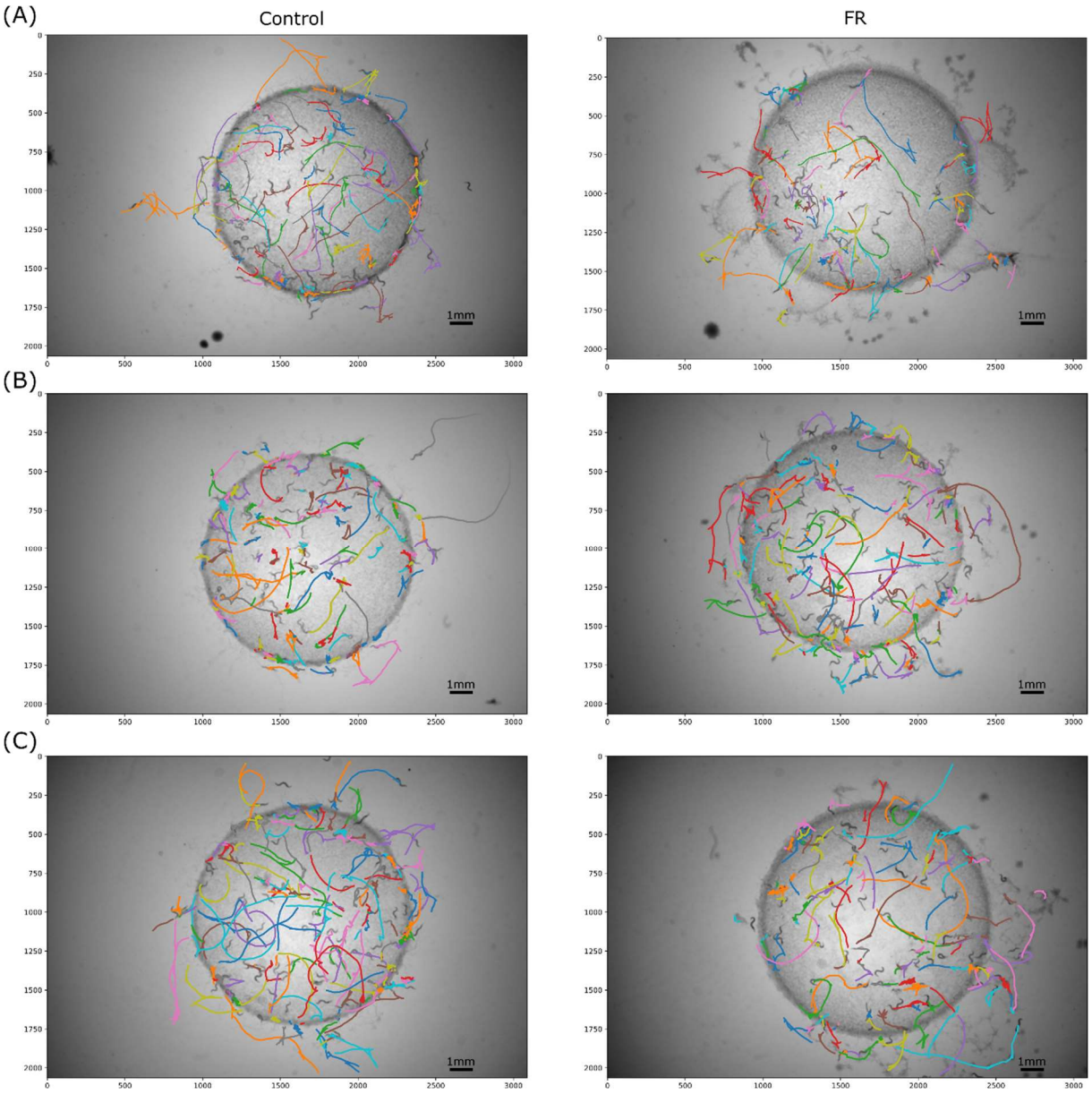

Figure 66: Tracking patterns of *Caenorhabditis elegans* N2 with and without FR900359 (FR). Adult nematodes synchronized using bleach were recorded for five minutes on nematode growth medium with a control (1 % dimethyl sulfoxide (DMSO) mixed with *Escherichia coli* OP50) or FR (2.5 mM FR/1 % DMSO mixed with *E. coli* OP50) spot. All experiments were done in three repeats **(A)-(C)**. Figure adapted from Hanke et al, 2023[2].

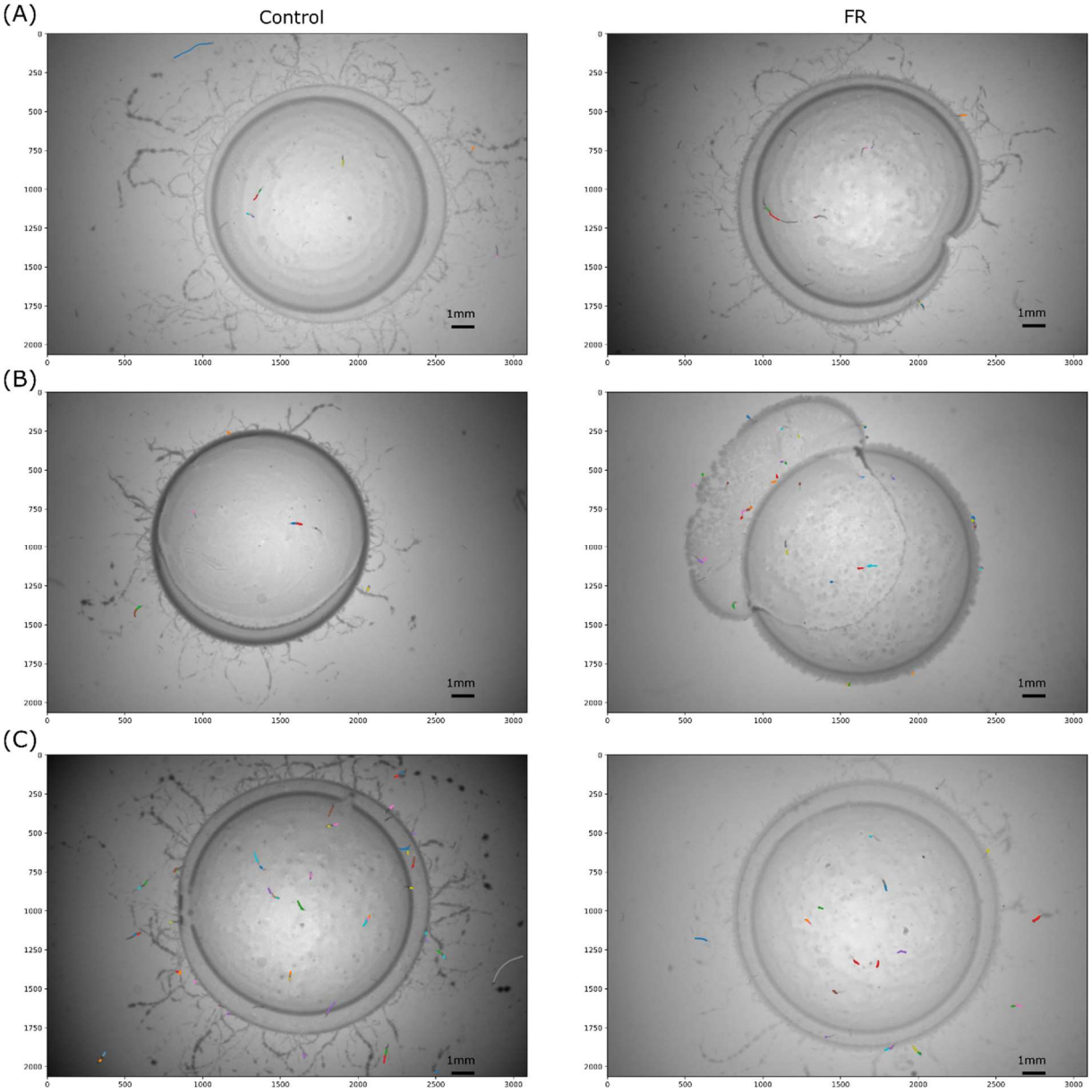

Figure 67: Tracking patterns of *Caenorhabditis elegans egl-30*(*ad805*) with and without FR900359 (FR). Adult nematodes synchronized using bleach were recorded for five minutes on nematode growth medium with a control (1 % dimethyl sulfoxide (DMSO) mixed with *Escherichia coli* OP50) or FR (2.5 mM FR/1 % DMSO mixed with *E. coli* OP50) spot. All experiments were done in three repeats **(A)**-**(C)**. Figure adapted from Hanke et al, 2023[2].

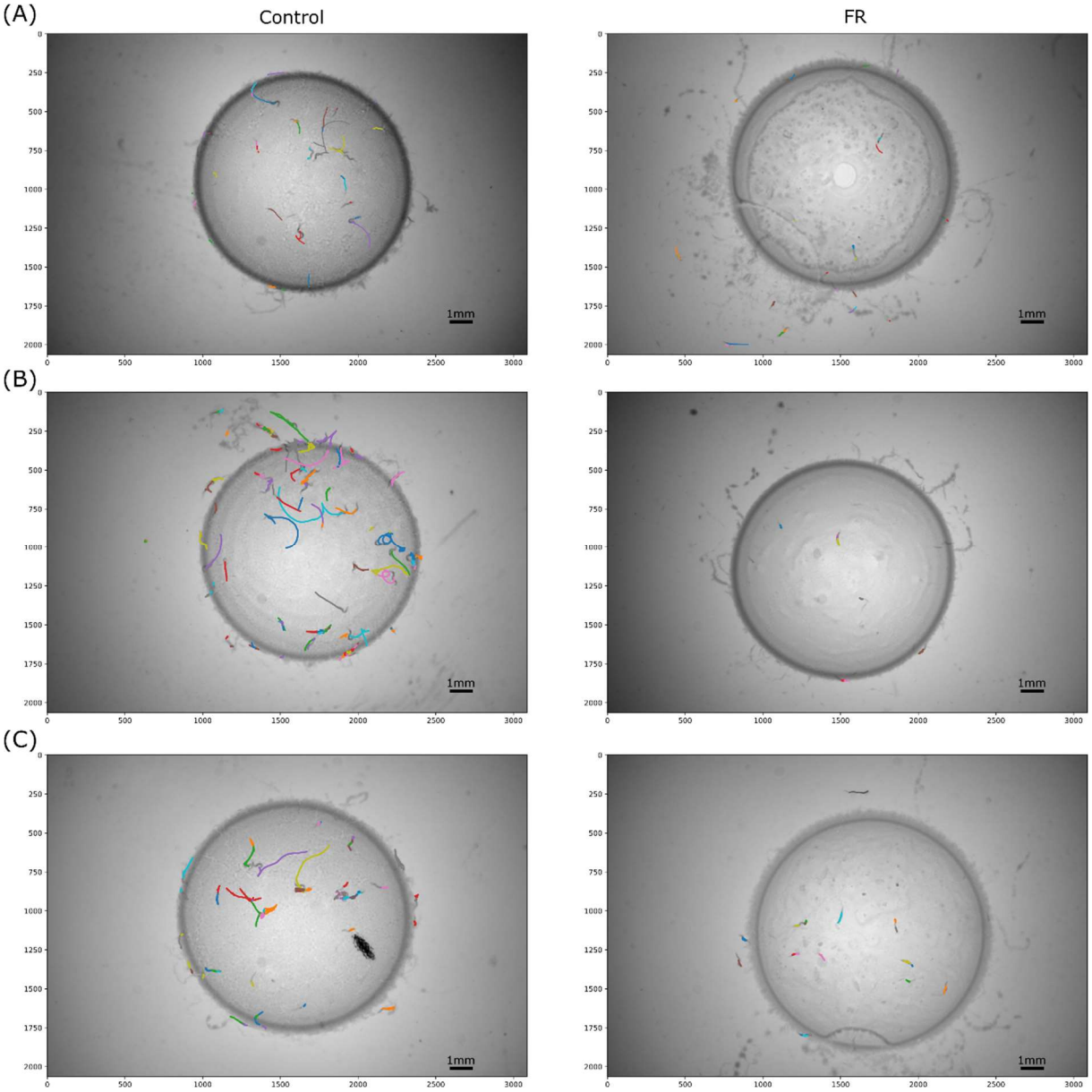

Figure 68: Tracking patterns of *Caenorhabditis elegans egl-30*(*n686*) with and without FR900359 (FR). Adult nematodes synchronized using bleach were recorded for five minutes on nematode growth medium with a control (1 % dimethyl sulfoxide (DMSO) mixed with *Escherichia coli* OP50) or FR (2.5 mM FR/1 % DMSO mixed with *E. coli* OP50) spot. All experiments were done in three repeats **(A)**-**(C)**. Figure adapted from Hanke et al, 2023[2].

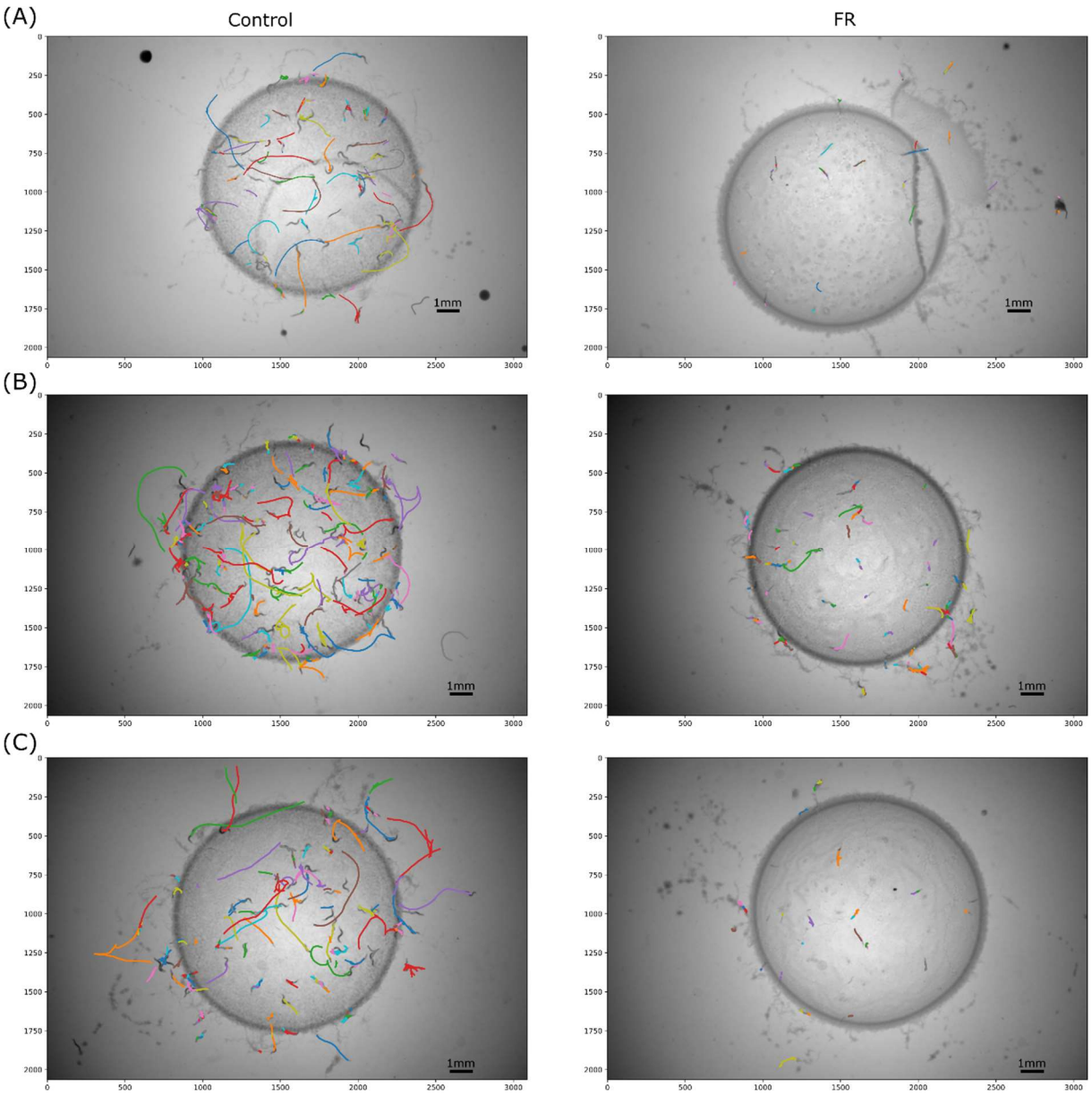

Figure 69: Tracking patterns of *Caenorhabditis elegans egl-30*(*ad806*) with and without FR900359 (FR). Adult nematodes synchronized using bleach were recorded for five minutes on nematode growth medium with a control (1 % dimethyl sulfoxide (DMSO) mixed with *Escherichia coli* OP50) or FR (2.5 mM FR/1 % DMSO mixed with *E. coli* OP50) spot. All experiments were done in three repeats **(A)**-**(C)**. Figure adapted from Hanke et al, 2023[2].

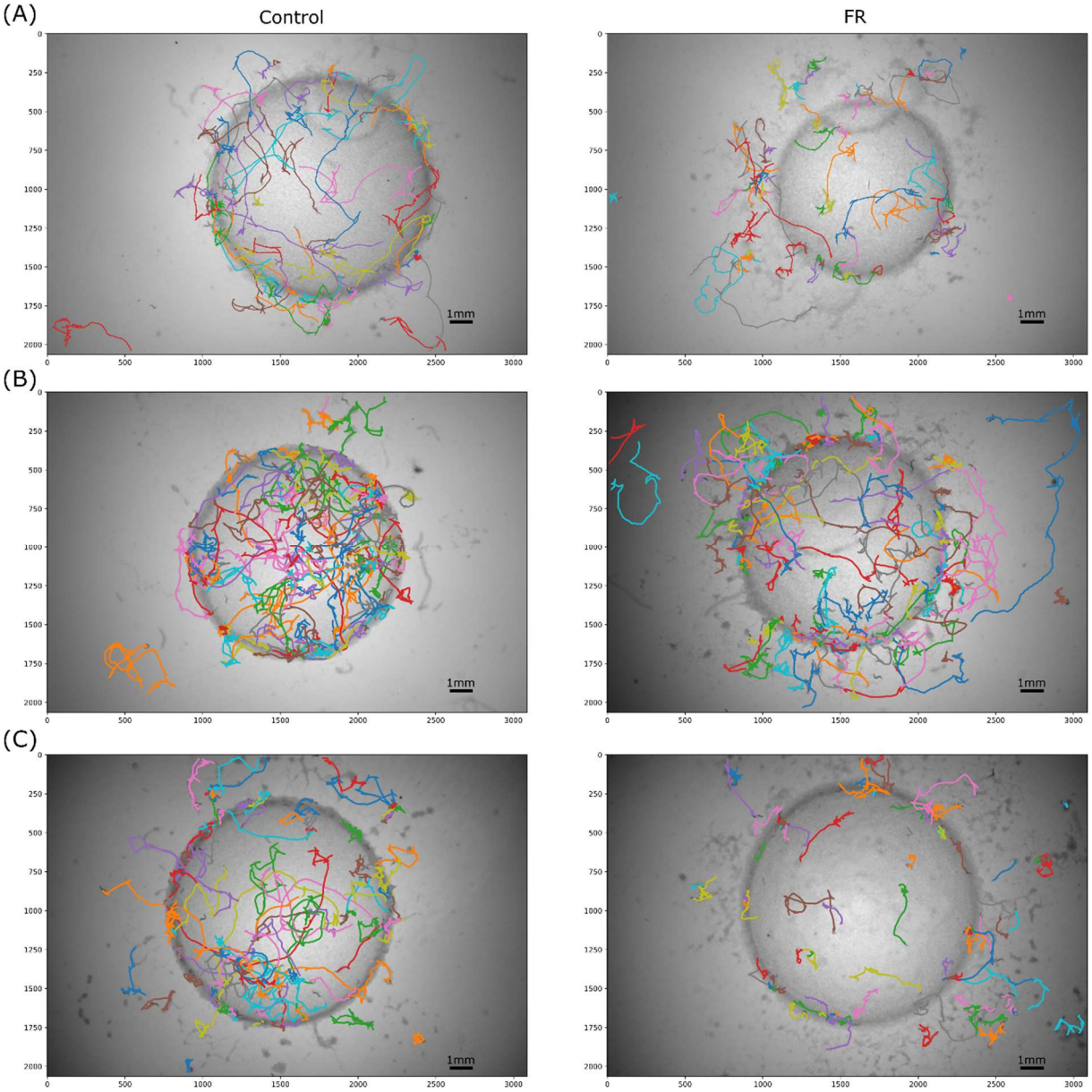

Figure 70: Tracking patterns of *Caenorhabditis elegans dgk-1*(*sy428*) with and without FR900359 (FR). Adult nematodes synchronized using bleach were recorded for five minutes on nematode growth medium with a control (1 % dimethyl sulfoxide (DMSO) mixed with *Escherichia coli* OP50) or FR (2.5 mM FR/1 % DMSO mixed with *E. coli* OP50) spot. All experiments were done in three repeats **(A)-(C)**. Figure adapted from Hanke et al, 2023[2].

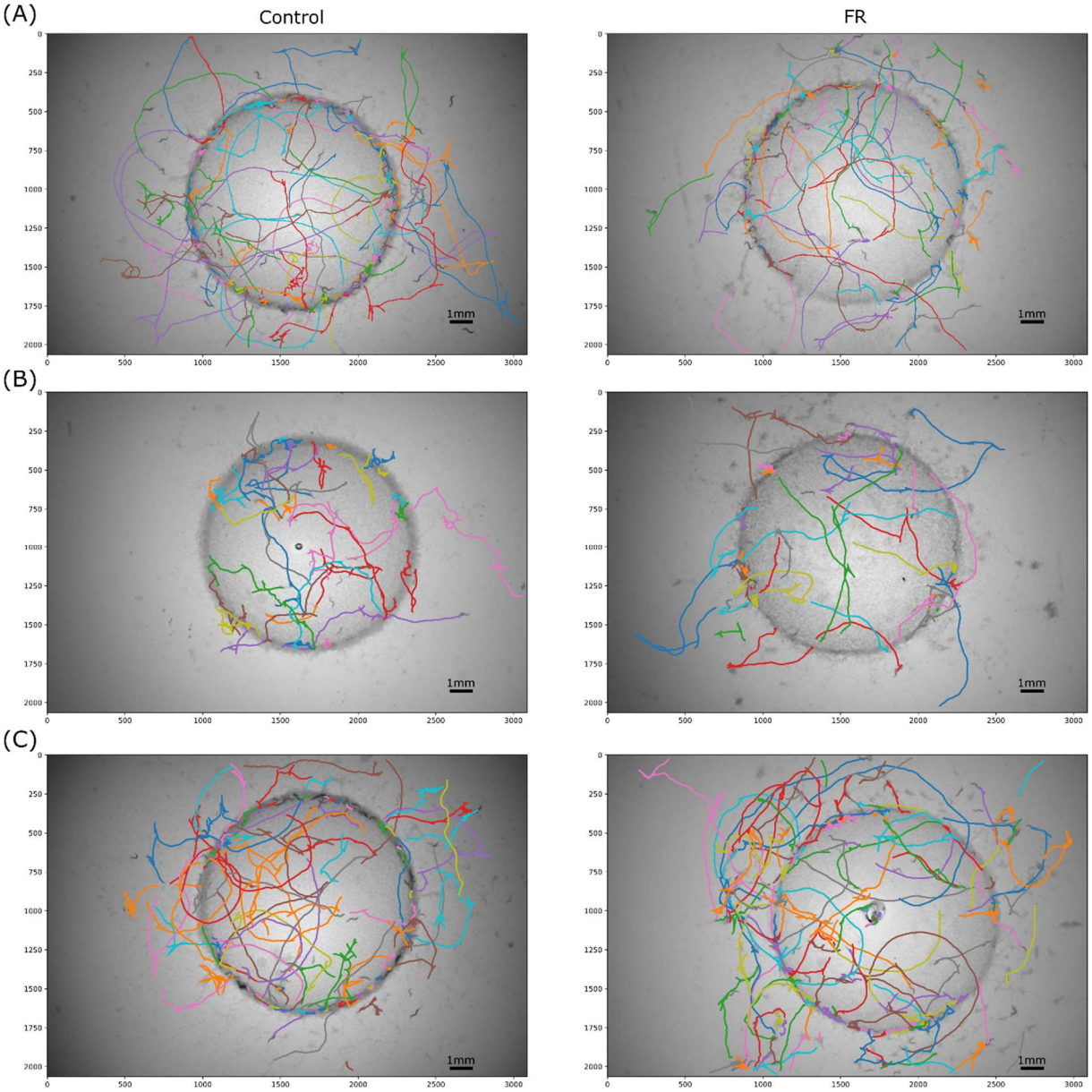

Figure 71: Tracking patterns of *Caenorhabditis elegans eat-16*(*sa609*) with and without FR900359 (FR). Adult nematodes synchronized using bleach were recorded for five minutes on nematode growth medium with a control (1 % dimethyl sulfoxide (DMSO) mixed with *Escherichia coli* OP50) or FR (2.5 mM FR/1 % DMSO mixed with *E. coli* OP50) spot. All experiments were done in three repeats **(A)**-**(C)**. Figure adapted from Hanke et al, 2023[2].

Table 26: Effect of FR-Core on the spatial distribution of *Caenorhabditis elegans* N2. Adult nematodes synchronized using bleach were recorded for five minutes on nematode growth medium with a control (1 % DMSO mixed with *Escherichia coli* OP50) or FR-Core (2.5 mM FR-Core/1 % DMSO mixed with *E. coli* OP50) spot. All experiments were done in three repeats. The spatial distribution was compared at the start and end (5 min) of the video using the modified two sample binomial test [295]. P>0.05=ns, P<0.05=*, P<0.01=**, P<0.001=**, P<0.0001=****. Adapted from Hanke et al, 2023[2].

	Nematodes in lawn (%)		
	Control	FR-Core	Modified two sample binomial test
Total	92.2 (±4.6)	94.1 (±4.1)	ns (p=0.3576)

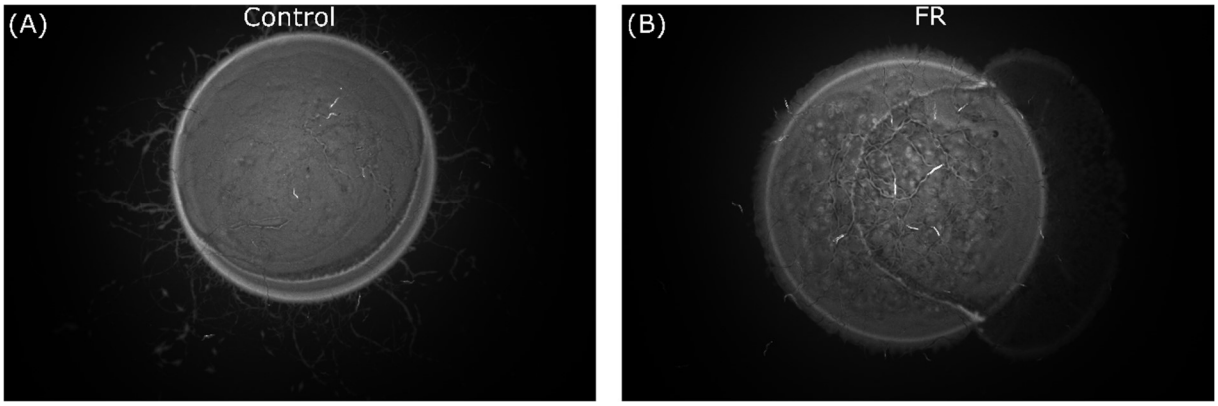

Figure 72: Egg-laying adults of *Caenorhabditis elegans egl-30*(*ad805*) after 79 hours on plate. Control **(A)** with 1 % dimethyl sulfoxide mixed with *Escherichia coli* OP50. FR **(B)** with 2.5 mM FR900359(FR)/1 % DMSO mixed with *E. coli* OP50. Images taken in dark field. Figure adapted from Hanke et al, 2023[2].

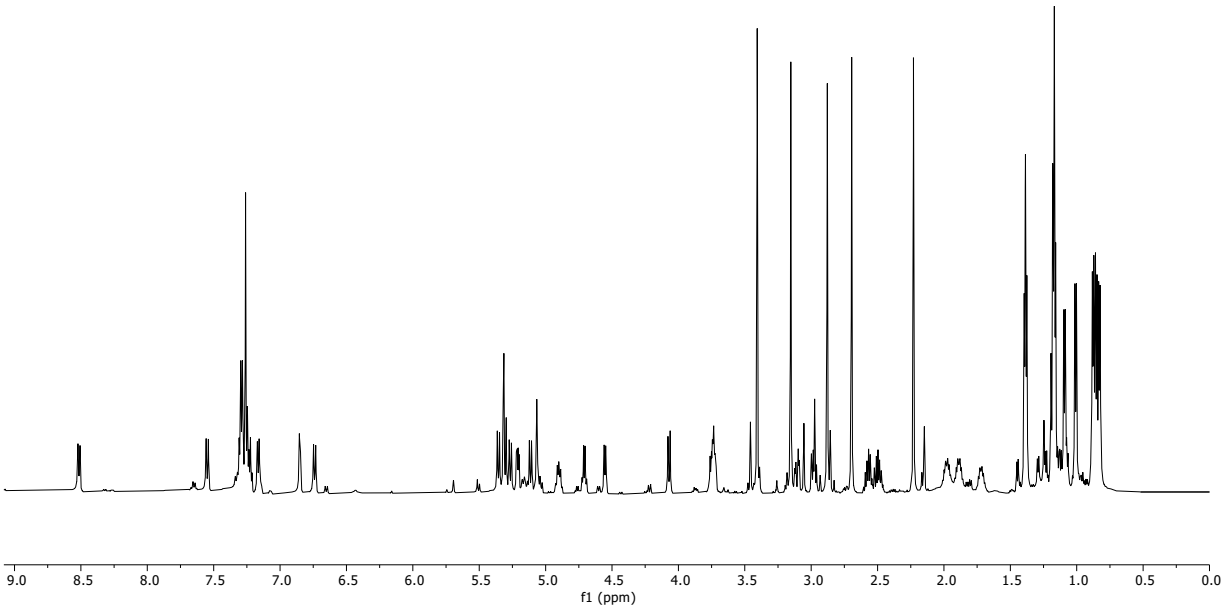

Figure 73: ^{1}H NMR spectrum of FR900359 in $CDCl_3$ (600 MHz).

Table 27: Retained eggs in the uterus of *Caenorhabditis elegans* N2 adults grown for three hours on a plate covered with *Escherichia coli* OP50 or one of the four *Chromobacterium vaccinii* MWU205 strains. Twenty worms were evaluated per bacterial strain and the worm with the highest number of retained eggs was excluded from calculations (*).

E. coli	***C. vaccinii***	***C. vaccinii ΔfrsC***	***C. vaccinii ΔvioA***	***C. vaccinii ΔfrsGvioA***
7	9	14	5	9
18	12	14	10	11

16	12	8	6	8
10	8	*20**	11	16
14	7	10	7	10
9	5	6	7	10
12	9	15	12	9
9	9	7	8	9
11	10	9	6	14
11	10	11	5	7
15	8	17	5	12
11	*27**	6	7	4
15	4	11	4	12
15	17	8	12	14
11	7	14	19	9
12	13	17	9	*24**
9	8	7	*22**	10
*21**	6	12	6	7
12	7	12	8	7
14	2	15	9	11

Publikationsliste

Henrik Harms, Anna Klöckner, Jan Schrör, Michaele Josten, Stefan Kehraus, Max Crüsemann, Wiebke Hanke, Tanja Schneider, Till F Schäberle, and Gabriele M König. Antimicrobial Dialkylresorcins from Marine-Derived Microorganisms: Insights into Their Mode of Action and Putative Ecological Relevance. Plant Medica **2018**, 84 (18), pp. 1363–1371.

DOI: https://doi.org/10.1055/a-0653-7451

Davide Malfacini, Julian Patt, Suvi Annala, Kasper Harpsøe, Funda Eryilmaz, Raphael Reher, Max Crüsemann, Wiebke Hanke, Hang Zhang, Daniel Tietze, David E Gloriam, Hans Bräuner-Osborne, Kristian Strømgaard, Gabriele M König, Asuka Inoue, Jesus Gomeza, and Evi Kostenis. Rational design of a heterotrimeric G protein α subunit with artificial inhibitor sensitivity. Journal of Biological Chemistry **2019**, 294 (15), pp. 5747–5758.

DOI: https://doi.org/10.1074/jbc.RA118.007250

Cornelia Hermes, René Richarz, Daniel A Wirtz, Julian Patt, Wiebke Hanke, Stefan Kehraus, Jan Hendrik Voß, Jim Küppers, Tsubasa Ohbayashi, Vigneshwaran Namasivayam, Judith Alenfelder, Asuka Inoue, Peter Mergaert, Michael Gütschow, Christa E Müller, Evi Kostenis, Gabriele M König, and Max Crüsemann. Thioesterase-mediated side chain transesterification generates potent Gq signaling inhibitor FR900359. Nature Communications 2021, 12 (144).

DOI: https://doi.org/10.1038/s41467-020-20418-3

Wiebke Hanke, Julian Patt, Judith Alenfelder, Jan H. Voss, Mitja M. Zdouc, Stefan Kehraus, Jung Bong Kim, Goran V. Grujičić, Vigneshwaran Namasivayam, Raphael Reher, Christa E. Müller, Evi Kostenis, Max Crüsemann and Gabriele M. König. Feature-Based Molecular Networking for the Targeted Identification of Gq Inhibiting FR900359 Derivatives. Journal of Natural Products **2021**, 84 (7), pp. 1941–1953.

DOI: https://doi.org/10.1021/acs.jnatprod.1c00194

Wiebke Hanke, Judith Alenfelder, Jun Liu, Philipp Gutbrod, Stefan Kehraus, Max Crüsemann, Peter Dörmann, Evi Kostenis, Monika Scholz, and Gabriele M. König. The Bacterial Gq Signal Transduction Inhibitor FR900359 Impairs Soil-associated Nematodes. Journal of Chemical Ecology **2023**. Open Access under a Creative Commons Attribution 4.0 International License.

DOI: https://doi.org/10.1007/s10886-023-01442-1

Danksagung

Eine Doktorarbeit ist keine One-Woman-Show, sie ist eine Teamarbeit und hat mir gezeigt, wie viele Menschen mich stärken, mir helfen und mich motivieren. All diesen Menschen möchte ich hiermit Danke sagen.

Ein großes Dankeschön geht an meine Professorin und Doktormutter Frau König. Vielen Dank, dass Sie mir mit ihrem unfassbar riesigen Wissen über die wissenschaftliche Welt der Naturstoffe zur Seite standen. Sie haben mich dazu angehalten mich zu verbessern und standen mir als Ansprechpartnerin zur Verfügung. Für mich sind Sie ein Vorbild in Sachen fachlicher Kompetenz, aber auch im Umgang mit Mitmenschen. Sie haben immer dafür gesorgt, dass ich mich wohl gefühlt habe und waren eine verlässliche Anlaufstelle für alle Sorgen. Vielen Dank, dass ich Ihre Doktorandin sein durfte.

Ein großes Dankeschön geht an dich Stefan. Pflanzenmorphologie durfte ich seit dem Master mitbetreuen und es gab für mich nichts schöneres als Teil deines Assistententeams zu sein. Auch im Labor hat mir die Zusammenarbeit immer Spaß und Freude bereitet. Deine entspannte und unkomplizierte Art hat mich immer wieder geerdet und ich werde die Zeit mit dir in guter Erinnerung behalten.

Natürlich will ich all den Mitgliedern der Arbeitsgruppe und des Instituts danken, die ich seit Beginn meines Laborpraktikums 2015/16 kennenlernen durfte: Ein Dank geht daher an alle, die sich mit mir ein Büro geteilt haben und mir viel Motivation geschenkt haben. Ein weiterer Dank geht an die, dir mit mir im Labor standen und mich fachlich unterstützt haben. Und zuletzt will ich all denen Dankeschön sagen, mit denen ich Spieleabende und anregende Gespräche erleben durfte.

Ein spezieller Dank geht an alle Masterstudenten und Praktikanten für die Zusammenarbeit und die Herausforderungen, die man gemeinsam bewältigt hat.

Cora, Cornelia, Daniel und Sophie. Bei euch möchte ich mich nicht nur als Kollegin bedanken, da mich mehr mit euch verbindet als die Laborarbeit. Sei es ein Spieleabend, eine “Dead by Daylight”- oder “Among us”-Runde, die Hochzeit von Cornelia oder der Besuch in Efringen-Kirchen. Ich freue mich darauf euch auch in Zukunft treffen zu können, sei es in Deutschland oder Neuseeland.

Judith, dein wissenschaftlicher Ehrgeiz war für mich immer Ansporn mich zu verbessern und unsere Zusammenarbeit bei meinem zweiten Paper werde ich in guter Erinnerung behalten.

Außerhalb des Instituts gab es viele Menschen, die ich durch Projekte oder die Forschergruppe treffen durfte. Danke an Christian Bonifer für die Zusammenarbeit in Bezug auf das markierte FR, an Philipp Gutbrod für die Experimente mit dem Rübenzystenwurm und an Monika Scholz und ihre Arbeitsgruppe für die tolle Erfahrung mit Fadenwürmern zu arbeiten. Dirk, der Gärtner meines Vertrauens, vielen Dank für die Zusammenarbeit an dem Projekt mit den Schildläusen und der Erdtrocknung. Lea, du hast mich am Ende meiner Dissertation als Tandem-Partnerin unterstützt, daher möchte ich einen speziellen Dank an dich richten. Gerade in den letzten Wochen, haben mich unsere Gespräche mit positiver Energie ernährt.

Danke an die DBU für die Förderung meiner Promotion und im Speziellen an Hans-Christian Schaefer, meinen Sachbearbeiter. Die DBU hat mir Einblicke in viele ökologische Projekte gewährt, die mich persönlich weiterentwickelt haben und mein Interesse für derlei Ideen entfachten. Ein spezieller Dank geht hier auch an dich Saskia, meine Tandem-Partnerin und Expertin in Sachen Umgang mit Eisbären, mit der man sich gut unterhalten und austauschen konnte.

Ein riesiges Dankeschön geht an meine Familie, meinen Freund und meine Freunde. Ich umarme euch alle und drücke euch feste. Vielen Dank an meine Eltern für die Unterstützung, das Vertrauen und all die Schubser. Danke an meine Schwester für die Ablenkung vom Alltag und all die gemeinsamen Lacher und Gespräche. Danke an den einzigartigen Biber und Freund, der mich gerade in der schwersten und letzten Phase einer Doktorarbeit immer wieder aufgebaut hat. Danke an meine Kindheitsfreundinnen, meine Schulfreundinnen, die Kommilitoninnen aus Jena und Bonn und all diejenigen, die ich abseits dieser Lebensstationen kennengelernt habe. Ich bin euch allen dankbar dafür, dass ihr meine Welt bunter, interessanter und schöner macht.

References

(1) Hanke, W.; Patt, J.; Alenfelder, J.; Voss, J. H.; Zdouc, M. M.; Kehraus, S.; Kim, J. B.; Grujičić, G. V.; Namasivayam, V.; Reher, R.; Müller, C. E.; Kostenis, E.; Crüsemann, M.; König, G. M. Feature-Based Molecular Networking for the Targeted Identification of Gq-Inhibiting FR900359 Derivatives. *Journal of natural products* **2021**, *84* (7), 1941–1953. DOI: 10.1021/acs.jnatprod.1c00194. Published Online: Jan. 7, 2021.

(2) Hanke, W.; Alenfelder, J.; Liu, J.; Gutbrod, P.; Kehraus, S.; Crüsemann, M.; Dörmann, P.; Kostenis, E.; Scholz, M.; König, G. M. The Bacterial Gq Signal Transduction Inhibitor FR900359 Impairs Soil-Associated Nematodes. *Journal of chemical ecology* **2023.** DOI: 10.1007/s10886-023-01442-1. Published Online: Jul. 15, 2023.

(3) Fierer, N. Embracing the unknown: disentangling the complexities of the soil microbiome. *Nature reviews. Microbiology* **2017**, *15* (10), 579–590. DOI: 10.1038/nrmicro.2017.87. Published Online: Aug. 21, 2017.

(4) Al-Kaisi, M. M.; Lal, R.; Olson, K. R.; Lowery, B. Fundamentals and Functions of Soil Environment. In *Soil Health and Intensification of Agroecosytems*; Elsevier, 2017; pp 1–23. DOI: 10.1016/B978-0-12-805317-1.00001-4.

(5) Pandey, V. C.; Panjak, U., Eds. *Microbial based land restoration handbook*:*Volume 2: Soil and plant health development*; CRC Press, 2022. DOI: 10.1201/9781003147077.

(6) Mishra, A.; Singh, L.; Singh, D. Unboxing the black box-one step forward to understand the soil microbiome: A systematic review. *Microbial ecology* **2022.** DOI: 10.1007/s00248-022-01962-5. Published Online: Feb. 2, 2022.

(7) Sheth, R. U.; Cabral, V.; Chen, S. P.; Wang, H. H. Manipulating Bacterial Communities by in situ Microbiome Engineering. *Trends in genetics : TIG* **2016**, *32* (4), 189–200. DOI: 10.1016/j.tig.2016.01.005. Published Online: Feb. 22, 2016.

(8) Banerjee, S.; van der Heijden, M. G. A. Soil microbiomes and one health. *Nature reviews. Microbiology* **2023**, *21* (1), 6–20. DOI: 10.1038/s41579-022-00779-w. Published Online: Aug. 23, 2022.

(9) Jansson, J. K.; Hofmockel, K. S. Soil microbiomes and climate change. *Nature reviews. Microbiology* **2020**, *18* (1), 35–46. DOI: 10.1038/s41579-019-0265-7. Published Online: Apr. 10, 2019.

(10) Afridi, M. S.; Ali, S.; Salam, A.; César Terra, W.; Hafeez, A.; Sumaira; Ali, B.; S AlTami, M.; Ameen, F.; Ercisli, S.; Marc, R. A.; Medeiros, F. H. V.; Karunakaran, R. Plant Microbiome Engineering: Hopes or Hypes. *Biology* **2022**, *11* (12). DOI: 10.3390/biology11121782. Published Online: Jul. 12, 2022.

(11) Afridi, M. S.; Javed, M. A.; Ali, S.; Medeiros, F. H. V. de; Ali, B.; Salam, A.; Sumaira; Marc, R. A.; Alkhalifah, D. H. M.; Selim, S.; Santoyo, G. New opportunities in plant microbiome engineering for increasing agricultural sustainability under stressful conditions. *Frontiers in plant science* **2022**, *13*, 899464. DOI: 10.3389/fpls.2022.899464. Published Online: Sep. 15, 2022.

(12) Wydro, U. Soil Microbiome Study Based on DNA Extraction: A Review. *Water* **2022**, *14* (24), 3999. DOI: 10.3390/w14243999.

(13) Geisen, S. The Future of (Soil) Microbiome Studies: Current Limitations, Integration, and Perspectives. *mSystems* **2021**, *6* (4), e0061321. DOI: 10.1128/mSystems.00613-21. Published Online: Aug. 24, 2021.

(14) Jansson, J. K.; Hofmockel, K. S. The soil microbiome-from metagenomics to metaphenomics. *Current opinion in microbiology* **2018**, *43*, 162–168. DOI: 10.1016/j.mib.2018.01.013. Published Online: Feb. 15, 2018.

(15) Enespa; Chandra, P. Tool and techniques study to plant microbiome current understanding and future needs: an overview. *Communicative & integrative biology*

2022, *15* (1), 209–225. DOI: 10.1080/19420889.2022.2082736. Published Online: Oct. 8, 2022.
(16) Prosser, J. I. Dispersing misconceptions and identifying opportunities for the use of 'omics' in soil microbial ecology. *Nature reviews. Microbiology* **2015**, *13* (7), 439–446. DOI: 10.1038/nrmicro3468. Published Online: Aug. 6, 2015.
(17) Dini-Andreote, F.; van Elsas, J. D. Back to the basics: The need for ecophysiological insights to enhance our understanding of microbial behaviour in the rhizosphere. *Plant Soil* **2013**, *373* (1-2), 1–15. DOI: 10.1007/s11104-013-1687-z.
(18) Poppeliers, S. W.; Sánchez-Gil, J. J.; Jonge, R. de. Microbes to support plant health: understanding bioinoculant success in complex conditions. *Current opinion in microbiology* **2023**, *73*, 102286. DOI: 10.1016/j.mib.2023.102286. Published Online: Apr. 3, 2023.
(19) GLICK, B. R.; Gamalero, E. Recent Developments in the Study of Plant Microbiomes. *Microorganisms* **2021**, *9* (7). DOI: 10.3390/microorganisms9071533. Published Online: Jul. 19, 2021.
(20) Arif, I.; Batool, M.; Schenk, P. M. Plant Microbiome Engineering: Expected Benefits for Improved Crop Growth and Resilience. *Trends in biotechnology* **2020**, *38* (12), 1385–1396. DOI: 10.1016/j.tibtech.2020.04.015. Published Online: May. 22, 2020.
(21) Topalović, O.; Hussain, M.; Heuer, H. Plants and Associated Soil Microbiota Cooperatively Suppress Plant-Parasitic Nematodes. *Frontiers in microbiology* **2020**, *11*, 313. DOI: 10.3389/fmicb.2020.00313. Published Online: Feb. 28, 2020.
(22) Maitra, S.; Brestic, M.; Bhadra, P.; Shankar, T.; Praharaj, S.; Palai, J. B.; Shah, M. M. R.; Barek, V.; Ondrisik, P.; Skalický, M.; Hossain, A. Bioinoculants-Natural Biological Resources for Sustainable Plant Production. *Microorganisms* **2021**, *10* (1). DOI: 10.3390/microorganisms10010051. Published Online: Dec. 27, 2021.
(23) GLICK, B. R. *Beneficial plant-bacterial interactions*; Life sciences; Springer, 2015. 978-3-319-13920-3.
(24) Olanrewaju, O. S.; GLICK, B. R.; Babalola, O. O. Mechanisms of action of plant growth promoting bacteria. *World journal of microbiology & biotechnology* **2017**, *33* (11), 197. DOI: 10.1007/s11274-017-2364-9. Published Online: Jun. 10, 2017.
(25) Wang, H.; Liu, R.; You, M. P.; Barbetti, M. J.; Chen, Y. Pathogen Biocontrol Using Plant Growth-Promoting Bacteria (PGPR): Role of Bacterial Diversity. *Microorganisms* **2021**, *9* (9). DOI: 10.3390/microorganisms9091988. Published Online: Sep. 18, 2021.
(26) O'Callaghan, M.; Ballard, R. A.; Wright, D. Soil microbial inoculants for sustainable agriculture: Limitations and opportunities. *Soil Use and Management* **2022**, *38* (3), 1340–1369. DOI: 10.1111/sum.12811.
(27) Kumar, J.; Ramlal, A.; Mallick, D.; Mishra, V. An Overview of Some Biopesticides and Their Importance in Plant Protection for Commercial Acceptance. *Plants (Basel, Switzerland)* **2021**, *10* (6). DOI: 10.3390/plants10061185. Published Online: Oct. 6, 2021.
(28) Khan, A. R.; Mustafa, A.; Hyder, S.; Valipour, M.; Rizvi, Z. F.; Gondal, A. S.; Yousuf, Z.; Iqbal, R.; Daraz, U. Bacillus spp. as Bioagents: Uses and Application for Sustainable Agriculture. *Biology* **2022**, *11* (12). DOI: 10.3390/biology11121763. Published Online: May. 12, 2022.
(29) Zilli, J. É.; Pacheco, R. S.; Gianluppi, V.; Smiderle, O. J.; Urquiaga, S.; Hungria, M. Biological N2 fixation and yield performance of soybean inoculated with Bradyrhizobium. *Nutr Cycl Agroecosyst* **2021**, *119* (3), 323–336. DOI: 10.1007/s10705-021-10128-7.
(30) Abdulkhair, W. M.; Alghuthaymi, M. A. Plant Pathogens. In *Plant Growth*; Rigobelo, E. C., Ed.; InTech, 2016. DOI: 10.5772/65325.

(31) Porazinska, D. L.; Giblin-Davis, R. M.; Faller, L.; Farmerie, W.; Kanzaki, N.; Morris, K.; Powers, T. O.; Tucker, A. E.; Sung, W.; Thomas, W. K. Evaluating high-throughput sequencing as a method for metagenomic analysis of nematode diversity. *Molecular ecology resources* **2009**, *9* (6), 1439–1450. DOI: 10.1111/j.1755-0998.2009.02611.x. Published Online: May. 3, 2009.
(32) Song, D.; Pan, K.; Tariq, A.; Sun, F.; Li, Z.; Sun, X.; Zhang, L.; Olusanya, O. A.; Wu, X. Large-scale patterns of distribution and diversity of terrestrial nematodes. *Applied Soil Ecology* **2017**, *114*, 161–169. DOI: 10.1016/j.apsoil.2017.02.013.
(33) Kouser, Y.; Shah, A. A.; Rasmann, S. The functional role and diversity of soil nematodes are stronger at high elevation in the lesser Himalayan Mountain ranges. *Ecology and evolution* **2021**, *11* (20), 13793–13804. DOI: 10.1002/ece3.8061. Published Online: Sep. 24, 2021.
(34) Lazarova, S.; Coyne, D.; G. Rodríguez, M. G.; Peteira, B.; Ciancio, A. Functional Diversity of Soil Nematodes in Relation to the Impact of Agriculture—A Review. *Diversity* **2021**, *13* (2), 64. DOI: 10.3390/d13020064.
(35) Bardgett, R. D.; van der Putten, W. H. Belowground biodiversity and ecosystem functioning. *Nature* **2014**, *515* (7528), 505–511. DOI: 10.1038/nature13855.
(36) van den Hoogen, J.; Geisen, S.; Routh, D.; Ferris, H.; Traunspurger, W.; Wardle, D. A.; Goede, R. G. M. de; Adams, B. J.; Ahmad, W.; Andriuzzi, W. S.; Bardgett, R. D.; Bonkowski, M.; Campos-Herrera, R.; Cares, J. E.; Caruso, T.; Brito Caixeta, L. de; Chen, X.; Costa, S. R.; Creamer, R.; Da Mauro Cunha Castro, J.; Dam, M.; Djigal, D.; Escuer, M.; Griffiths, B. S.; Gutiérrez, C.; Hohberg, K.; Kalinkina, D.; Kardol, P.; Kergunteuil, A.; Korthals, G.; Krashevska, V.; Kudrin, A. A.; Li, Q.; Liang, W.; Magilton, M.; Marais, M.; Martín, J. A. R.; Matveeva, E.; Mayad, E. H.; Mulder, C.; Mullin, P.; Neilson, R.; Nguyen, T. A. D.; Nielsen, U. N.; Okada, H.; Rius, J. E. P.; Pan, K.; Peneva, V.; Pellissier, L.; Da Carlos Pereira Silva, J.; Pitteloud, C.; Powers, T. O.; Powers, K.; Quist, C. W.; Rasmann, S.; Moreno, S. S.; Scheu, S.; Setälä, H.; Sushchuk, A.; Tiunov, A. V.; Trap, J.; van der Putten, W.; Vestergård, M.; Villenave, C.; Waeyenberge, L.; Wall, D. H.; Wilschut, R.; Wright, D. G.; Yang, J.-I.; Crowther, T. W. Soil nematode abundance and functional group composition at a global scale. *Nature* **2019**, *572* (7768), 194–198. DOI: 10.1038/s41586-019-1418-6. Published Online: Jul. 24, 2019.
(37) Ingham, R. E.; Trofymow, J. A.; Ingham, E. R.; Coleman, D. C. Interactions of Bacteria, Fungi, and their Nematode Grazers: Effects on Nutrient Cycling and Plant Growth. *Ecological Monographs* **1985**, *55* (1), 119–140. DOI: 10.2307/1942528.
(38) Procter, D. L. Global Overview of the Functional Roles of Soil-living Nematodes in Terrestrial Communities and Ecosystems. *Journal of nematology* **1990**, *22* (1), 1–7. www.ncbi.nlm.nih.gov/pmc/articles/PMC2619009/.
(39) Ferris, H. Contribution of nematodes to the structure and function of the soil food web. *Journal of nematology* **2010**, *42* (1), 63–67. www.ncbi.nlm.nih.gov/pmc/articles/PMC3380510/.
(40) Melakeberhan, H.; Bonito, G.; Kravchenko, A. N. Application of Nematode Community Analyses-Based Models towards Identifying Sustainable Soil Health Management Outcomes: A Review of the Concepts. *Soil Systems* **2021**, *5* (2), 32. DOI: 10.3390/soilsystems5020032.
(41) Yeates, G. W.; Bongers, T.; Goede, R. G. de; Freckman, D. W.; Georgieva, S. S. Feeding habits in soil nematode families and genera-an outline for soil ecologists. *Journal of nematology* **1993**, *25* (3), 315–331. www.ncbi.nlm.nih.gov/pmc/articles/PMC2619405/.
(42) Singh, S.; Singh, B.; Singh, A. P. Nematodes: A Threat to Sustainability of Agriculture. *Procedia Environmental Sciences* **2015**, *29*, 215–216. DOI: 10.1016/j.proenv.2015.07.270.

(43) Jones, J. T.; Haegeman, A.; Danchin, E. G. J.; Gaur, H. S.; Helder, J.; Jones, M. G. K.; Kikuchi, T.; Manzanilla-López, R.; Palomares-Rius, J. E.; Wesemael, W. M. L.; Perry, R. N. Top 10 plant-parasitic nematodes in molecular plant pathology. *Molecular plant pathology* **2013**, *14* (9), 946–961. DOI: 10.1111/mpp.12057. Published Online: Jan. 7, 2013.
(44) Mendoza-de Gives, P. Soil-Borne Nematodes: Impact in Agriculture and Livestock and Sustainable Strategies of Prevention and Control with Special Reference to the Use of Nematode Natural Enemies. *Pathogens (Basel, Switzerland)* **2022**, *11* (6). DOI: 10.3390/pathogens11060640. Published Online: Jan. 6, 2022.
(45) Trap, J.; Bonkowski, M.; Plassard, C.; Villenave, C.; Blanchart, E. Ecological importance of soil bacterivores for ecosystem functions. *Plant Soil* **2016**, *398* (1-2), 1–24. DOI: 10.1007/s11104-015-2671-6.
(46) Koppenhöfer, A. M.; Shapiro-Ilan, D. I.; Hiltpold, I. Entomopathogenic Nematodes in Sustainable Food Production. *Front. Sustain. Food Syst.* **2020**, *4.* DOI: 10.3389/fsufs.2020.00125.
(47) Dillman, A. R.; Sternberg, P. W. Entomopathogenic nematodes. *Current biology : CB* **2012**, *22* (11), R430-1. DOI: 10.1016/j.cub.2012.03.047.
(48) Kenney, E.; Eleftherianos, I. Entomopathogenic and plant pathogenic nematodes as opposing forces in agriculture. *International journal for parasitology* **2016**, *46* (1), 13–19. DOI: 10.1016/j.ijpara.2015.09.005. Published Online: Oct. 23, 2015.
(49) Ebone, L. A.; Kovaleski, M.; Deuner, C. C. Nematicides: history, mode, and mechanism action. *Plant Sci. Today* **2019**, *6* (2), 91–97. DOI: 10.14719/pst.2019.6.2.468.
(50) Castellano-Hinojosa, A.; Boyd, N. S.; Strauss, S. L. Impact of fumigants on non-target soil microorganisms: a review. *Journal of hazardous materials* **2022**, *427*, 128149. DOI: 10.1016/j.jhazmat.2021.128149. Published Online: Dec. 27, 2021.
(51) Sasanelli, N.; Konrat, A.; Migunova, V.; Toderas, I.; Iurcu-Straistaru, E.; Rusu, S.; Bivol, A.; Andoni, C.; Veronico, P. Review on Control Methods against Plant Parasitic Nematodes Applied in Southern Member States (C Zone) of the European Union. *Agriculture* **2021**, *11* (7), 602. DOI: 10.3390/agriculture11070602.
(52) Ayilara, M. S.; Adeleke, B. S.; Akinola, S. A.; Fayose, C. A.; Adeyemi, U. T.; Gbadegesin, L. A.; Omole, R. K.; Johnson, R. M.; Uthman, Q. O.; Babalola, O. O. Biopesticides as a promising alternative to synthetic pesticides: A case for microbial pesticides, phytopesticides, and nanobiopesticides. *Frontiers in microbiology* **2023**, *14*, 1040901. DOI: 10.3389/fmicb.2023.1040901. Published Online: Feb. 16, 2023.
(53) Gamalero, E.; GLICK, B. R. The Use of Plant Growth-Promoting Bacteria to Prevent Nematode Damage to Plants. *Biology* **2020**, *9* (11). DOI: 10.3390/biology9110381. Published Online: Jul. 11, 2020.
(54) Umetsu, N.; Shirai, Y. Development of novel pesticides in the 21st century. *Journal of pesticide science* **2020**, *45* (2), 54–74. DOI: 10.1584/jpestics.D20-201.
(55) Pires, D.; Vicente, C. S. L.; Menéndez, E.; Faria, J. M. S.; Rusinque, L.; Camacho, M. J.; Inácio, M. L. The Fight against Plant-Parasitic Nematodes: Current Status of Bacterial and Fungal Biocontrol Agents. *Pathogens (Basel, Switzerland)* **2022**, *11* (10). DOI: 10.3390/pathogens11101178. Published Online: Oct. 13, 2022.
(56) Alisjahbana, B.; Debora, J.; Susandi, E.; Darmawan, G. Chromobacterium violaceum: A Review of an Unexpected Scourge. *International journal of general medicine* **2021**, *14*, 3259–3270. DOI: 10.2147/IJGM.S272193. Published Online: Sep. 7, 2021.
(57) Martin, P. A. W.; Gundersen-Rindal, D.; Blackburn, M.; Buyer, J. Chromobacterium subtsugae sp. nov., a betaproteobacterium toxic to Colorado potato beetle and other insect pests. *International journal of systematic and evolutionary microbiology* **2007**, *57* (Pt 5), 993–999. DOI: 10.1099/ijs.0.64611-0.

(58) Young, C.-C.; Arun, A. B.; Lai, W.-A.; Chen, W.-M.; Chou, J.-H.; Shen, F.-T.; Rekha, P. D.; Kämpfer, P. Chromobacterium aquaticum sp. nov., isolated from spring water samples. *International journal of systematic and evolutionary microbiology* **2008**, *58* (Pt 4), 877–880. DOI: 10.1099/ijs.0.65573-0.
(59) Han, X. Y.; Han, F. S.; Segal, J. Chromobacterium haemolyticum sp. nov., a strongly haemolytic species. *International journal of systematic and evolutionary microbiology* **2008**, *58* (Pt 6), 1398–1403. DOI: 10.1099/ijs.0.64681-0.
(60) Kämpfer, P.; Busse, H.-J.; Scholz, H. C. Chromobacterium piscinae sp. nov. and Chromobacterium pseudoviolaceum sp. nov., from environmental samples. *International journal of systematic and evolutionary microbiology* **2009**, *59* (Pt 10), 2486–2490. DOI: 10.1099/ijs.0.008888-0. Published Online: Jul. 21, 2009.
(61) Soby, S. D.; Gadagkar, S. R.; Contreras, C.; Caruso, F. L. Chromobacterium vaccinii sp. nov., isolated from native and cultivated cranberry (Vaccinium macrocarpon Ait.) bogs and irrigation ponds. *International journal of systematic and evolutionary microbiology* **2013**, *63* (Pt 5), 1840–1846. DOI: 10.1099/ijs.0.045161-0.
(62) Menezes, C. B. A.; Tonin, M. F.; Corrêa, D. B. A.; Parma, M.; Melo, I. S. de; Zucchi, T. D.; Destéfano, S. A. L.; Fantinatti-Garboggini, F. Chromobacterium amazonense sp. nov. isolated from water samples from the Rio Negro, Amazon, Brazil. *Antonie van Leeuwenhoek* **2015**, *107* (4), 1057–1063. DOI: 10.1007/s10482-015-0397-3. Published Online: Jul. 2, 2015.
(63) Bajaj, A.; Kumar, A.; Yadav, S.; Kaur, G.; Bala, M.; Singh, N. K.; Mathan Kumar, R.; Manickam, N.; Mayilraj, S. Isolation and characterization of a novel Gram-negative bacterium Chromobacterium alkanivorans sp. nov., strain IITR-71T degrading halogenated alkanes. *International journal of systematic and evolutionary microbiology* **2016**, *66* (12), 5228–5235. DOI: 10.1099/ijsem.0.001500. Published Online: Nov. 9, 2016.
(64) Zhou, S.; Guo, X.; Wang, H.; Kong, D.; Wang, Y.; Zhu, J.; Dong, W.; He, M.; Hu, G.; Zhao, B.; Zhao, B.; Ruan, Z. Chromobacterium rhizoryzae sp. nov., isolated from rice roots. *International journal of systematic and evolutionary microbiology* **2016**, *66* (10), 3890–3896. DOI: 10.1099/ijsem.0.001284. Published Online: Aug. 7, 2016.
(65) Blackburn, M. B.; Farrar, R. R.; Sparks, M. E.; Kuhar, D.; Mitchell, A.; Gundersen-Rindal, D. E. Chromobacterium sphagni sp. nov., an insecticidal bacterium isolated from Sphagnum bogs. *International journal of systematic and evolutionary microbiology* **2017**, *67* (9), 3417–3422. DOI: 10.1099/ijsem.0.002127. Published Online: Aug. 22, 2017.
(66) Blackburn, M. B.; Farrar, R. R.; Sparks, M. E.; Kuhar, D.; Mowery, J. D.; Mitchell, A.; Gundersen-Rindal, D. E. Chromobacterium phragmitis sp. nov., isolated from estuarine marshes. *International journal of systematic and evolutionary microbiology* **2019**, *69* (9), 2681–2686. DOI: 10.1099/ijsem.0.003508.
(67) Blackburn, M. B.; Farrar, R. R.; Sparks, M. E.; Kuhar, D.; Mowery, J. D.; Mitchell, A.; Gundersen-Rindal, D. E. Chromobacterium paludis sp. nov., a novel bacterium isolated from a Chesapeake Bay marsh. *International journal of systematic and evolutionary microbiology* **2020**, *70* (12), 6142–6146. DOI: 10.1099/ijsem.0.004509.
(68) O'Hara-Hanley, K.; Harrison, A.; Soby, S. D. Chromobacterium alticapitis sp. nov. and Chromobacterium sinusclupearum sp. nov. isolated from wild cranberry bogs in the Cape Cod National Seashore, USA. *International journal of systematic and evolutionary microbiology* **2022**, *72* (6). DOI: 10.1099/ijsem.0.005410.
(69) Durán, N.; Menck, C. F. Chromobacterium violaceum: a review of pharmacological and industiral perspectives. *Critical reviews in microbiology* **2001**, *27* (3), 201–222. DOI: 10.1080/20014091096747.

(70) Kothari, V.; Sharma, S.; Padia, D. Recent research advances on Chromobacterium violaceum. *Asian Pacific journal of tropical medicine* **2017**, *10* (8), 744–752. DOI: 10.1016/j.apjtm.2017.07.022. Published Online: Aug. 19, 2017.
(71) Durán, M.; Faljoni-Alario, A.; Durán, N. Chromobacterium violaceum and its important metabolites--review. *Folia microbiologica* **2010**, *55* (6), 535–547. DOI: 10.1007/s12223-010-0088-4. Published Online: Jan. 21, 2011.
(72) Durán, N.; Justo, G. Z.; Durán, M.; Brocchi, M.; Cordi, L.; Tasic, L.; Castro, G. R.; Nakazato, G. Advances in Chromobacterium violaceum and properties of violacein-Its main secondary metabolite: A review. *Biotechnology advances* **2016**, *34* (5), 1030–1045. DOI: 10.1016/j.biotechadv.2016.06.003.
(73) Durán, N.; Justo, G. Z.; Ferreira, C. V.; Melo, P. S.; Cordi, L.; Martins, D. Violacein: properties and biological activities. *Biotechnology and applied biochemistry* **2007**, *48* (Pt 3), 127–133. DOI: 10.1042/BA20070115.
(74) Park, H.; Park, S.; Yang, Y.-H.; Choi, K.-Y. Microbial synthesis of violacein pigment and its potential applications. *Critical reviews in biotechnology* **2021**, *41* (6), 879–901. DOI: 10.1080/07388551.2021.1892579. Published Online: Mar. 17, 2021.
(75) Durán, N.; Nakazato, G.; Durán, M.; Berti, I. R.; Castro, G. R.; Stanisic, D.; Brocchi, M.; Fávaro, W. J.; Ferreira-Halder, C. V.; Justo, G. Z.; Tasic, L. Multi-target drug with potential applications: violacein in the spotlight. *World journal of microbiology & biotechnology* **2021**, *37* (9), 151. DOI: 10.1007/s11274-021-03120-4. Published Online: Aug. 16, 2021.
(76) Durán, M.; Ponezi, A. N.; Faljoni-Alario, A.; Teixeira, M. F. S.; Justo, G. Z.; Durán, N. Potential applications of violacein: a microbial pigment. *Med Chem Res* **2012**, *21* (7), 1524–1532. DOI: 10.1007/s00044-011-9654-9.
(77) Durán, N.; Castro, G. R.; Portela, R. W. D.; Fávaro, W. J.; Durán, M.; Tasic, L.; Nakazato, G. Violacein and its antifungal activity: comments and potentialities. *Letters in applied microbiology* **2022**, *75* (4), 796–803. DOI: 10.1111/lam.13760. Published Online: Jun. 22, 2022.
(78) Ballestriero, F.; Daim, M.; Penesyan, A.; Nappi, J.; Schleheck, D.; Bazzicalupo, P.; Di Schiavi, E.; Egan, S. Antinematode activity of Violacein and the role of the insulin/IGF-1 pathway in controlling violacein sensitivity in Caenorhabditis elegans. *PloS one* **2014**, *9* (10), e109201. DOI: 10.1371/journal.pone.0109201. Published Online: Aug. 10, 2014.
(79) Lyakhovchenko, N. S.; Travkin, V. M.; Senchenkov, V. Y.; Solyanikova, I. P. Bacterial Violacein: Properties, Biosynthesis and Application Prospects. *Appl Biochem Microbiol* **2022**, *58* (6), 692–700. DOI: 10.1134/S0003683822060072.
(80) Füller, J. J.; Röpke, R.; Krausze, J.; Rennhack, K. E.; Daniel, N. P.; Blankenfeldt, W.; Schulz, S.; Jahn, D.; Moser, J. Biosynthesis of Violacein, Structure and Function of l-Tryptophan Oxidase VioA from Chromobacterium violaceum. *The Journal of biological chemistry* **2016**, *291* (38), 20068–20084. DOI: 10.1074/jbc.M116.741561. Published Online: Jul. 27, 2016.
(81) McClean, K. H.; Winson, M. K.; Fish, L.; Taylor, A.; Chhabra, S. R.; Camara, M.; Daykin, M.; Lamb, J. H.; Swift, S.; Bycroft, B. W.; Stewart, G. S. A. B.; Williams, P. Quorum sensing and Chromobacterium violaceum: exploitation of violacein production and inhibition for the detection of N-acylhomoserine lactones. *Microbiology (Reading, England)* **1997**, *143 (Pt 12)*, 3703–3711. DOI: 10.1099/00221287-143-12-3703.
(82) Fuqua, W. C.; Winans, S. C.; Greenberg, E. P. Quorum sensing in bacteria: the LuxR-LuxI family of cell density-responsive transcriptional regulators. *Journal of bacteriology* **1994**, *176* (2), 269–275. DOI: 10.1128/jb.176.2.269-275.1994.
(83) Fuqua, C.; Winans, S. C.; Greenberg, E. P. Census and consensus in bacterial ecosystems: the LuxR-LuxI family of quorum-sensing transcriptional regulators. *Annual review of microbiology* **1996**, *50*, 727–751. DOI: 10.1146/annurev.micro.50.1.727.

(84) Andrighetti-Fröhner, C. R.; Antonio, R. V.; Creczynski-Pasa, T. B.; Barardi, C. R. M.; Simões, C. M. O. Cytotoxicity and potential antiviral evaluation of violacein produced by Chromobacterium violaceum. *Memorias do Instituto Oswaldo Cruz* **2003**, *98* (6), 843–848. DOI: 10.1590/S0074-02762003000600023. Published Online: Oct. 29, 2003.
(85) Alshatwi, A. A.; Subash-Babu, P.; Antonisamy, P. Violacein induces apoptosis in human breast cancer cells through up regulation of BAX, p53 and down regulation of MDM2. *Experimental and toxicologic pathology : official journal of the Gesellschaft fur Toxikologische Pathologie* **2016**, *68* (1), 89–97. DOI: 10.1016/j.etp.2015.10.002. Published Online: Oct. 28, 2015.
(86) Carvalho, D. D. de; Costa, F. T. M.; Duran, N.; Haun, M. Cytotoxic activity of violacein in human colon cancer cells. *Toxicology in vitro : an international journal published in association with BIBRA* **2006**, *20* (8), 1514–1521. DOI: 10.1016/j.tiv.2006.06.007. Published Online: Jan. 7, 2006.
(87) Ferreira, C. V.; Bos, C. L.; Versteeg, H. H.; Justo, G. Z.; Durán, N.; Peppelenbosch, M. P. Molecular mechanism of violacein-mediated human leukemia cell death. *Blood* **2004**, *104* (5), 1459–1464. DOI: 10.1182/blood-2004-02-0594. Published Online: Jun. 5, 2004.
(88) Kim, Y. J.; Yuk, N.; Shin, H. J.; Jung, H. J. The Natural Pigment Violacein Potentially Suppresses the Proliferation and Stemness of Hepatocellular Carcinoma Cells In Vitro. *International journal of molecular sciences* **2021**, *22* (19). DOI: 10.3390/ijms221910731. Published Online: Mar. 10, 2021.
(89) Souza Oliveira, P. F. de; Faria, A. V. S.; Clerici, S. P.; Akagi, E. M.; Carvalho, H. F.; Justo, G. Z.; Durán, N.; Ferreira-Halder, C. V. Violacein negatively modulates the colorectal cancer survival and epithelial-mesenchymal transition. *Journal of cellular biochemistry* **2022**, *123* (7), 1247–1258. DOI: 10.1002/jcb.30295. Published Online: Jun. 6, 2022.
(90) Neroni, B.; Zingaropoli, M. A.; Radocchia, G.; Ciardi, M. R.; Mosca, L.; Pantanella, F.; Schippa, S. Evaluation of the anti-proliferative activity of violacein, a natural pigment of bacterial origin, in urinary bladder cancer cell lines. *Oncology letters* **2022**, *23* (4), 132. DOI: 10.3892/ol.2022.13252. Published Online: Feb. 23, 2022.
(91) Lee, J.; Bae, J.; Youn, D.-Y.; Ahn, J.; Hwang, W.-T.; Bae, H.; Bae, P. K.; Kim, I.-D. Violacein-embedded nanofiber filters with antiviral and antibacterial activities. *Chemical engineering journal (Lausanne, Switzerland : 1996)* **2022**, *444*, 136460. DOI: 10.1016/j.cej.2022.136460. Published Online: Apr. 19, 2022.
(92) Dogancı, M. A.; Ay Sal, F.; Guler, H. I.; Katı, H.; Ceylan, E.; Belduz, A. O.; Bozdal, G.; Yaylı, N.; Canakcı, S. Investigation of potential inhibitor properties of violacein against HIV-1 RT and CoV-2 Spike RBD:ACE-2. *World journal of microbiology & biotechnology* **2022**, *38* (9), 161. DOI: 10.1007/s11274-022-03350-0. Published Online: Jul. 14, 2022.
(93) Aruldass, C. A.; Masalamany, S. R. L.; Venil, C. K.; Ahmad, W. A. Antibacterial mode of action of violacein from Chromobacterium violaceum UTM5 against Staphylococcus aureus and methicillin-resistant Staphylococcus aureus (MRSA). *Environmental science and pollution research international* **2018**, *25* (6), 5164–5180. DOI: 10.1007/s11356-017-8855-2. Published Online: Mar. 31, 2017.
(94) Aruldass, C. A.; Rubiyatno, R.; Venil, C. K.; Ahmad, W. A. Violet pigment production from liquid pineapple waste by Chromobacterium violaceum UTM5 and evaluation of its bioactivity. *RSC Adv.* **2015**, *5* (64), 51524–51536. DOI: 10.1039/C5RA05765E.
(95) Cauz, A. C. G.; Carretero, G. P. B.; Saraiva, G. K. V.; Park, P.; Mortara, L.; Cuccovia, I. M.; Brocchi, M.; Gueiros-Filho, F. J. Violacein Targets the Cytoplasmic Membrane of Bacteria. *ACS infectious diseases* **2019**, *5* (4), 539–549. DOI: 10.1021/acsinfecdis.8b00245. Published Online: Dec. 2, 2019.

(96) Matz, C.; Webb, J. S.; Schupp, P. J.; Phang, S. Y.; Penesyan, A.; Egan, S.; Steinberg, P.; Kjelleberg, S. Marine biofilm bacteria evade eukaryotic predation by targeted chemical defense. *PloS one* **2008**, *3* (7), e2744. DOI: 10.1371/journal.pone.0002744. Published Online: Jul. 23, 2008.
(97) Matz, C.; Deines, P.; Boenigk, J.; Arndt, H.; Eberl, L.; Kjelleberg, S.; Jürgens, K. Impact of violacein-producing bacteria on survival and feeding of bacterivorous nanoflagellates. *Applied and environmental microbiology* **2004**, *70* (3), 1593–1599. DOI: 10.1128/AEM.70.3.1593-1599.2004.
(98) Bilsland, E.; Tavella, T. A.; Krogh, R.; Stokes, J. E.; Roberts, A.; Ajioka, J.; Spring, D. R.; Andricopulo, A. D.; Costa, F. T. M.; Oliver, S. G. Antiplasmodial and trypanocidal activity of violacein and deoxyviolacein produced from synthetic operons. *BMC biotechnology* **2018**, *18* (1), 22. DOI: 10.1186/s12896-018-0428-z. Published Online: Nov. 4, 2018.
(99) Rahul, S.; Chandrashekhar, P.; Hemant, B.; Bipinchandra, S.; Mouray, E.; Grellier, P.; Satish, P. In vitro antiparasitic activity of microbial pigments and their combination with phytosynthesized metal nanoparticles. *Parasitology international* **2015**, *64* (5), 353–356. DOI: 10.1016/j.parint.2015.05.004. Published Online: May. 16, 2015.
(100) Wilkinson, M. D.; Lai, H.-E.; Freemont, P. S.; Baum, J. A Biosynthetic Platform for Antimalarial Drug Discovery. *Antimicrobial agents and chemotherapy* **2020**, *64* (5). DOI: 10.1128/AAC.02129-19. Published Online: Apr. 21, 2020.
(101) Newman, D. J.; Cragg, G. M. Natural Products as Sources of New Drugs over the Nearly Four Decades from 01/1981 to 09/2019. *Journal of natural products* **2020**, *83* (3), 770–803. DOI: 10.1021/acs.jnatprod.9b01285. Published Online: Dec. 3, 2020.
(102) Batista, B. B.; Santos, R. E. R. d. S.; Ricci-Azevedo, R.; Da Silva Neto, J. F. Production and Uptake of Distinct Endogenous Catecholate-Type Siderophores Are Required for Iron Acquisition and Virulence in Chromobacterium violaceum. *Infection and immunity* **2019**, *87* (12). DOI: 10.1128/IAI.00577-19. Published Online: Nov. 18, 2019.
(103) Ueda, H.; Nakajima, H.; Hori, Y.; Fujita, T.; Nishimura, M.; Goto, T.; Okuhara, M. FR901228, a novel antitumor bicyclic depsipeptide produced by Chromobacterium violaceum No. 968. I. Taxonomy, fermentation, isolation, physico-chemical and biological properties, and antitumor activity. *The Journal of antibiotics* **1994**, *47* (3), 301–310. DOI: 10.7164/antibiotics.47.301.
(104) Engel, J. A.; Jones, A. J.; Avery, V. M.; Sumanadasa, S. D. M.; Ng, S. S.; Fairlie, D. P.; Skinner-Adams, T.; Andrews, K. T. Profiling the anti-protozoal activity of anti-cancer HDAC inhibitors against Plasmodium and Trypanosoma parasites. *International journal for parasitology. Drugs and drug resistance* **2015**, *5* (3), 117–126. DOI: 10.1016/j.ijpddr.2015.05.004. Published Online: Jun. 20, 2015.
(105) Chua, M. J.; Arnold, M. S. J.; Xu, W.; Lancelot, J.; Lamotte, S.; Späth, G. F.; Prina, E.; Pierce, R. J.; Fairlie, D. P.; Skinner-Adams, T. S.; Andrews, K. T. Effect of clinically approved HDAC inhibitors on Plasmodium, Leishmania and Schistosoma parasite growth. *International journal for parasitology. Drugs and drug resistance* **2017**, *7* (1), 42–50. DOI: 10.1016/j.ijpddr.2016.12.005. Published Online: Dec. 23, 2016.
(106) Sun, W.; Tanaka, T. Q.; Magle, C. T.; Huang, W.; Southall, N.; Huang, R.; Dehdashti, S. J.; McKew, J. C.; Williamson, K. C.; Zheng, W. Chemical signatures and new drug targets for gametocytocidal drug development. *Scientific reports* **2014**, *4*, 3743. DOI: 10.1038/srep03743. Published Online: Jan. 17, 2014.
(107) Pojani, E.; Barlocco, D. Romidepsin (FK228), A Histone Deacetylase Inhibitor and its Analogues in Cancer Chemotherapy. *Current medicinal chemistry* **2021**, *28* (7), 1290–1303. DOI: 10.2174/0929867327666200203113926.
(108) Létévé, M.; Gonzalez, C.; Moroy, G.; Martinez, A.; Jeanblanc, J.; Legastelois, R.; Naassila, M.; Sapi, J.; Bourguet, E. Unexpected effect of cyclodepsipeptides bearing a

sulfonylhydrazide moiety towards histone deacetylase activity. *Bioorganic chemistry* **2018**, *81*, 222–233. DOI: 10.1016/j.bioorg.2018.08.016. Published Online: Oct. 8, 2018.
(109) Martin, P. A. W.; Hirose, E.; Aldrich, J. R. Toxicity of *Chromobacterium subtsugae* to Southern Green Stink Bug (Heteroptera: Pentatomidae) and Corn Rootworm (Coleoptera: Chrysomelidae). *ec* **2007**, *100* (3), 680–684. DOI: 10.1603/0022-0493(2007)100[680:tocsts]2.0.co;2.
(110) Sampson, K.; Zaitseva, J.; Stauffer, M.; Vande Berg, B.; Guo, R.; Tomso, D.; McNulty, B.; Desai, N.; Balasubramanian, D. Discovery of a novel insecticidal protein from Chromobacterium piscinae, with activity against Western Corn Rootworm, Diabrotica virgifera virgifera. *Journal of invertebrate pathology* **2017**, *142*, 34–43. DOI: 10.1016/j.jip.2016.10.004. Published Online: Oct. 28, 2016.
(111) Farrar, R. R.; Gundersen-Rindal, D.; Kuhar, D.; Blackburn, M. B. Insecticidal Activity of a Recently Described Bacterium, Chromobacterium sphagni1. *Journal of Entomological Science* **2018**, *53* (3), 333–338. DOI: 10.18474/JES17-102.1.
(112) Farrar, R. R.; Gundersen-Rindal, D. E.; Kuhar, D.; Blackburn, M. B. Insecticidal Activity of Chromobacterium phragmitis, a Recently Described Bacterium from Tidal Marshes. *Journal of Entomological Science* **2020**, *55* (1), 98. DOI: 10.18474/0749-8004-55.1.98.
(113) Farrar, R. R.; Gundersen-Rindal, D. E.; Kuhar, D.; Blackburn, M. B. Insecticidal Activity of Chromobacterium vaccinii1. *Journal of Entomological Science* **2018**, *53* (3), 339–346. DOI: 10.18474/JES17-108.1.
(114) Seur Kee Park; Hyo Yeon Lee; Ki Chung Kim. Antagonistic Effect of Chitinolytic Bacteria on Soilborne Plant Pathogens. *Korean Journal of Plant Pathology* **1995**, *11* (1), 47–52. www.ppjonline.org/journal/view.php?number=1001. Published Online: 1996.
(115) Kim, H. J.; Park, J. Y.; Han, S. H.; Lee, J. H.; Rong, X.; McSpadden Gardener, B. B.; Park, S. K.; Kim, Y. C. Draft genome sequence of the biocontrol bacterium Chromobacterium sp. strain C-61. *Journal of bacteriology* **2011**, *193* (23), 6803–6804. DOI: 10.1128/JB.06191-11.
(116) Kim, Y. C.; Jung, H.; Kim, K. Y.; Park, S. K. An effective biocontrol bioformulation against Phytophthora blight of pepper using growth mixtures of combined chitinolytic bacteria under different field conditions. *Eur J Plant Pathol* **2008**, *120* (4), 373–382. DOI: 10.1007/s10658-007-9227-4.
(117) Kim, Y. C.; Lee, J. H.; Bae, Y.-S.; Sohn, B.-K.; Park, S. K. Development of effective environmentally-friendly approaches to control Alternaria blight and anthracnose diseases of Korean ginseng. *Eur J Plant Pathol* **2010**, *127* (4), 443–450. DOI: 10.1007/s10658-010-9610-4.
(118) Park, S.-K.; Lee, M.-C.; Harman, G. E. The Biocontrol Activity of Chromobacterium sp. Strain C-61 against Rhizoctonia solani Depends on the Productive Ability of Chitinase. *The Plant Pathology Journal* **2005**, *21* (3), 275–282. DOI: 10.5423/PPJ.2005.21.3.275.
(119) Kim, H. J.; Choi, H. S.; Yang, S. Y.; Kim, I. S.; Yamaguchi, T.; Sohng, J. K.; Park, S. K.; Kim, J.-C.; Lee, C. H.; Gardener, B. M.; Kim, Y. C. Both extracellular chitinase and a new cyclic lipopeptide, chromobactomycin, contribute to the biocontrol activity of Chromobacterium sp. C61. *Molecular plant pathology* **2014**, *15* (2), 122–132. DOI: 10.1111/mpp.12070. Published Online: Nov. 9, 2013.
(120) Kim, I. S.; Yang, S. Y.; Park, S. K.; Kim, Y. C. Quorum sensing is a key regulator for the antifungal and biocontrol activity of chitinase-producing Chromobacterium sp. C61. *Molecular plant pathology* **2017**, *18* (1), 134–140. DOI: 10.1111/mpp.12379. Published Online: Dec. 4, 2016.

(121) Park, S. K.; Kim, C. W.; Kim, H.; Jung, J. S.; Harman, G. E. Cloning and high-level production of a chitinase from Chromobacterium sp. and the role of conserved or nonconserved residues on its catalytic activity. *Applied microbiology and biotechnology* **2007**, *74* (4), 791–804. DOI: 10.1007/s00253-006-0614-0. Published Online: Sep. 2, 2007.
(122) Ramirez, J. L.; Souza-Neto, J.; Torres Cosme, R.; Rovira, J.; Ortiz, A.; Pascale, J. M.; Dimopoulos, G. Reciprocal tripartite interactions between the Aedes aegypti midgut microbiota, innate immune system and dengue virus influences vector competence. *PLoS neglected tropical diseases* **2012**, *6* (3), e1561. DOI: 10.1371/journal.pntd.0001561. Published Online: Jun. 3, 2012.
(123) Caragata, E. P.; Otero, L. M.; Carlson, J. S.; Borhani Dizaji, N.; Dimopoulos, G. A Nonlive Preparation of Chromobacterium sp. Panama (Csp_P) Is a Highly Effective Larval Mosquito Biopesticide. *Applied and environmental microbiology* **2020**, *86* (11). DOI: 10.1128/AEM.00240-20. Published Online: May. 19, 2020.
(124) Ramirez, J. L.; Short, S. M.; Bahia, A. C.; Saraiva, R. G.; Dong, Y.; Kang, S.; Tripathi, A.; Mlambo, G.; Dimopoulos, G. Chromobacterium Csp_P reduces malaria and dengue infection in vector mosquitoes and has entomopathogenic and in vitro anti-pathogen activities. *PLoS pathogens* **2014**, *10* (10), e1004398. DOI: 10.1371/journal.ppat.1004398. Published Online: Oct. 23, 2014.
(125) Pereira, A. E.; Huynh, M. P.; Paddock, K. J.; Ramirez, J. L.; Caragata, E. P.; Dimopoulos, G.; Krishnan, H. B.; Schneider, S. K.; Shelby, K. S.; Hibbard, B. E. Chromobacterium Csp_P biopesticide is toxic to larvae of three Diabrotica species including strains resistant to Bacillus thuringiensis. *Scientific reports* **2022**, *12* (1), 17858. DOI: 10.1038/s41598-022-22229-6. Published Online: Oct. 25, 2022.
(126) Johnson, E. T.; Bowman, M. J.; Gomes, R. P.; Carneiro, L. C.; Dunlap, C. A. Identification of 2,4-diacetylphloroglucinol production in the genus Chromobacterium. *Scientific reports* **2023**, *13* (1), 14292. DOI: 10.1038/s41598-023-41277-0. Published Online: Aug. 31, 2023.
(127) Egorova, D. A.; Voronina, O. L.; Solovyev, A. I.; Kunda, M. S.; Aksenova, E. I.; Ryzhova, N. N.; Danilova, K. V.; Rykova, V. S.; Scherbakova, A. A.; Semenov, A. N.; Polyakov, N. B.; Grumov, D. A.; Shevlyagina, N. V.; Dolzhikova, I. V.; Romanova, Y. M.; Gintsburg, A. L. Integrated into Environmental Biofilm Chromobacterium vaccinii Survives Winter with Support of Bacterial Community. *Microorganisms* **2020**, *8* (11). DOI: 10.3390/microorganisms8111696. Published Online: Oct. 30, 2020.
(128) Pistorius, D.; Buntin, K.; Richard, E.; Rust, M.; Bouquet, C.; Wollbrett, S.; Weber, E.; Dietschin, D.; Bruccoleri, R.; Oakeley, E.; Petersen, F. Valhidepsin Lipopeptides from Chromobacterium vaccinii: Structures, Biosynthesis, and Coregulation with FR900359 Production. *Journal of natural products* **2023.** DOI: 10.1021/acs.jnatprod.2c00825. Published Online: Jun. 2, 2023.
(129) Pistorius, D.; Buntin, K.; Weber, E.; Richard, E.; Bouquet, C.; Wollbrett, S.; Regenass, H.; Peón, V.; Böhm, M.; Kessler, R.; Gempeler, T.; Haberkorn, A.; Wimmer, L.; Lanshoeft, C.; Davis, J.; Hainzl, D.; D'Alessio, J. A.; Manchado, E.; Petersen, F. Promoter-Driven Overexpression in Chromobacterium vaccinii Facilitates Access to FR900359 and Yields Novel Low Abundance Analogs. *Chemistry (Weinheim an der Bergstrasse, Germany)* **2022**, *28* (8), e202103888. DOI: 10.1002/chem.202103888. Published Online: Dec. 28, 2021.
(130) Hermes, C.; Richarz, R.; Wirtz, D. A.; Patt, J.; Hanke, W.; Kehraus, S.; Voß, J. H.; Küppers, J.; Ohbayashi, T.; Namasivayam, V.; Alenfelder, J.; Inoue, A.; Mergaert, P.; Gütschow, M.; Müller, C. E.; Kostenis, E.; König, G. M.; Crüsemann, M. Thioesterase-

mediated side chain transesterification generates potent Gq signaling inhibitor FR900359. *Nature communications* **2021**, *12* (1). DOI: 10.1038/s41467-020-20418-3.
(131) Schrage, R.; Schmitz, A.-L.; Gaffal, E.; Annala, S.; Kehraus, S.; Wenzel, D.; Büllesbach, K. M.; Bald, T.; Inoue, A.; Shinjo, Y.; Galandrin, S.; Shridhar, N.; Hesse, M.; Grundmann, M.; Merten, N.; Charpentier, T. H.; Martz, M.; Butcher, A. J.; Slodczyk, T.; Armando, S.; Effern, M.; Namkung, Y.; Jenkins, L.; Horn, V.; Stößel, A.; Dargatz, H.; Tietze, D.; Imhof, D.; Galés, C.; Drewke, C.; Müller, C. E.; Hölzel, M.; Milligan, G.; Tobin, A. B.; Gomeza, J.; Dohlman, H. G.; Sondek, J.; Harden, T. K.; Bouvier, M.; Laporte, S. A.; Aoki, J.; Fleischmann, B. K.; Mohr, K.; König, G. M.; Tüting, T.; Kostenis, E. The experimental power of FR900359 to study Gq-regulated biological processes. *Nature communications* **2015**, *6*, 10156. DOI: 10.1038/ncomms10156.
(132) Fujioka, M.; Koda, S.; Morimoto, Y.; Biemann, K. Structure of FR900359, a cyclic depsipeptide from Ardisia crenata sims. *J. Org. Chem.* **1988**, *53* (12), 2820–2825. DOI: 10.1021/jo00247a030.
(133) Dell, M.; Dunbar, K. L.; Hertweck, C. Ribosome-independent peptide biosynthesis: the challenge of a unifying nomenclature. *Natural product reports* **2022**, *39* (3), 453–459. DOI: 10.1039/D1NP00019E. Published Online: Mar. 23, 2022.
(134) Finking, R.; Marahiel, M. A. Biosynthesis of nonribosomal peptides1. *Annual review of microbiology* **2004**, *58*, 453–488. DOI: 10.1146/annurev.micro.58.030603.123615.
(135) Konz, D.; Marahiel, M. A. How do peptide synthetases generate structural diversity? *Chemistry & biology* **1999**, *6* (2), R39-48. DOI: 10.1016/S1074-5521(99)80002-7.
(136) Marahiel, M. A. A structural model for multimodular NRPS assembly lines. *Natural product reports* **2016**, *33* (2), 136–140. DOI: 10.1039/C5NP00082C.
(137) Marahiel, M. A.; Stachelhaus, T.; Mootz, H. D. Modular Peptide Synthetases Involved in Nonribosomal Peptide Synthesis. *Chemical reviews* **1997**, *97* (7), 2651–2674. DOI: 10.1021/cr960029e.
(138) McErlean, M.; Overbay, J.; van Lanen, S. Refining and expanding nonribosomal peptide synthetase function and mechanism. *Journal of industrial microbiology & biotechnology* **2019**, *46* (3-4), 493–513. DOI: 10.1007/s10295-018-02130-w. Published Online: Jan. 23, 2019.
(139) Süssmuth, R. D.; Mainz, A. Nonribosomal Peptide Synthesis-Principles and Prospects. *Angewandte Chemie (International ed. in English)* **2017**, *56* (14), 3770–3821. DOI: 10.1002/anie.201609079. Published Online: Mar. 21, 2017.
(140) Walsh, C. T. Insights into the chemical logic and enzymatic machinery of NRPS assembly lines. *Natural product reports* **2016**, *33* (2), 127–135. DOI: 10.1039/C5NP00035A.
(141) Nomenclature and symbolism for amino acids and peptides (Recommendations 1983). *Pure and Applied Chemistry* **1984**, *56* (5), 595–624. DOI: 10.1351/pac198456050595.
(142) Trauger, J. W.; Kohli, R. M.; Mootz, H. D.; Marahiel, M. A.; Walsh, C. T. Peptide cyclization catalysed by the thioesterase domain of tyrocidine synthetase. *Nature* **2000**, *407* (6801), 215–218. DOI: 10.1038/35025116.
(143) Crüsemann, M.; Reher, R.; Schamari, I.; Brachmann, A. O.; Ohbayashi, T.; Kuschak, M.; Malfacini, D.; Seidinger, A.; Pinto-Carbó, M.; Richarz, R.; Reuter, T.; Kehraus, S.; Hallab, A.; Attwood, M.; Schiöth, H. B.; Mergaert, P.; Kikuchi, Y.; Schäberle, T. F.; Kostenis, E.; Wenzel, D.; Müller, C. E.; Piel, J.; Carlier, A.; Eberl, L.; König, G. M. Heterologous Expression, Biosynthetic Studies, and Ecological Function of the Selective Gq-Signaling

Inhibitor FR900359. *Angewandte Chemie (International ed. in English)* **2018**, *57* (3), 836–840. DOI: 10.1002/anie.201707996.
(144) Baltz, R. H. Function of MbtH homologs in nonribosomal peptide biosynthesis and applications in secondary metabolite discovery. *Journal of industrial microbiology & biotechnology* **2011**, *38* (11), 1747–1760. DOI: 10.1007/s10295-011-1022-8. Published Online: Sep. 8, 2011.
(145) Bernhardt, M.; Berman, S.; Zechel, D.; Bechthold, A. Role of Two Exceptional trans Adenylation Domains and MbtH-like Proteins in the Biosynthesis of the Nonribosomal Peptide WS9324A from Streptomyces calvus ATCC 13382. *Chembiochem : a European journal of chemical biology* **2020**, *21* (18), 2659–2666. DOI: 10.1002/cbic.202000142. Published Online: Jun. 18, 2020.
(146) Herbst, D. A.; Boll, B.; Zocher, G.; Stehle, T.; Heide, L. Structural basis of the interaction of MbtH-like proteins, putative regulators of nonribosomal peptide biosynthesis, with adenylating enzymes. *The Journal of biological chemistry* **2013**, *288* (3), 1991–2003. DOI: 10.1074/jbc.M112.420182. Published Online: Nov. 28, 2012.
(147) Li, Y.; Tahlan, K.; Bignell, D. R. D. Functional Cross-Talk of MbtH-Like Proteins During Thaxtomin Biosynthesis in the Potato Common Scab Pathogen Streptomyces scabiei. *Frontiers in microbiology* **2020**, *11*, 585456. DOI: 10.3389/fmicb.2020.585456. Published Online: Oct. 15, 2020.
(148) Klöppel, S.; Richarz, R.; Wirtz, D. A.; Vasenda, N.; König, G. M.; Crüsemann, M. A Specialized Dehydrogenase Provides l-Phenyllactate for FR900359 Biosynthesis. *Chembiochem : a European journal of chemical biology* **2022**, *23* (10), e202100569. DOI: 10.1002/cbic.202100569. Published Online: Sep. 12, 2021.
(149) Li, X.; Jiang, B.; Pan, B.; Mu, W.; Zhang, T. Purification and partial characterization of Lactobacillus species SK007 lactate dehydrogenase (LDH) catalyzing phenylpyruvic acid (PPA) conversion into phenyllactic acid (PLA). *Journal of agricultural and food chemistry* **2008**, *56* (7), 2392–2399. DOI: 10.1021/jf0731503. Published Online: Dec. 3, 2008.
(150) Wirtz, D. A.; Schneberger, N.; Klöppel, S.; Richarz, R.; Geyer, M.; König, G. M.; Hagelueken, G.; Crüsemann, M. Adenylation Domain-Guided Recruitment of Trans-Acting Nonheme Monooxygenases in Nonribosomal Peptide Biosynthesis. *ACS chemical biology* **2023.** DOI: 10.1021/acschembio.3c00106. Published Online: Jun. 27, 2023.
(151) Hermes, C.; König, G. M.; Crüsemann, M. The chromodepsins - chemistry, biology and biosynthesis of a selective Gq inhibitor natural product family. *Natural product reports* **2021**, *38* (12), 2276–2292. DOI: 10.1039/D1NP00005E. Published Online: Dec. 15, 2021.
(152) Taniguchi, M.; Suzumura, K.; Nagai, K.; Kawasaki, T.; Saito, T.; Takasaki, J.; Suzuki, K.; Fujita, S.; Tsukamoto, S. Structure of YM-254890, a Novel Gq/11 Inhibitor from Chromobacterium sp. QS3666. *Tetrahedron* **2003**, *59* (25), 4533–4538. DOI: 10.1016/S0040-4020(03)00680-X.
(153) Taniguchi, M.; Nagai, K.; Arao, N.; Kawasaki, T.; Saito, T.; Moritani, Y.; Takasaki, J.; Hayashi, K.; Fujita, S.; Suzuki, K.; Tsukamoto, S. YM-254890, a novel platelet aggregation inhibitor produced by Chromobacterium sp. QS3666. *The Journal of antibiotics* **2003**, *56* (4), 358–363. DOI: 10.7164/antibiotics.56.358.
(154) Kostenis, E.; Pfeil, E. M.; Annala, S. Heterotrimeric Gq proteins as therapeutic targets? *The Journal of biological chemistry* **2020**, *295* (16), 5206–5215. DOI: 10.1074/jbc.REV119.007061. Published Online: Feb. 3, 2020.
(155) Li, J.; Ge, Y.; Huang, J.-X.; Strømgaard, K.; Zhang, X.; Xiong, X.-F. Heterotrimeric G Proteins as Therapeutic Targets in Drug Discovery. *Journal of medicinal chemistry* **2020**,

63 (10), 5013–5030. DOI: 10.1021/acs.jmedchem.9b01452. Published Online: Dec. 26, 2019.
(156) Nair, R. R.; Kiran, A.; Saini, D. K. G protein Signaling, Journeys Beyond the Plasma Membrane. *J Indian Inst Sci* **2017**, *97* (1), 95–108. DOI: 10.1007/s41745-016-0012-2.
(157) Hubbard, K. B.; Hepler, J. R. Cell signalling diversity of the Gqalpha family of heterotrimeric G proteins. *Cellular signalling* **2006**, *18* (2), 135–150. DOI: 10.1016/j.cellsig.2005.08.004. Published Online: Sep. 22, 2005.
(158) Voss, J. H.; Nagel, J.; Rafehi, M.; Guixà-González, R.; Malfacini, D.; Patt, J.; Kehraus, S.; Inoue, A.; König, G. M.; Kostenis, E.; Deupi, X.; Namasivayam, V.; Müller, C. E. Unraveling binding mechanism and kinetics of macrocyclic Gαq protein inhibitors. *Pharmacological research* **2021**, *173*, 105880. DOI: 10.1016/j.phrs.2021.105880. Published Online: Sep. 17, 2021.
(159) Kuschak, M.; Namasivayam, V.; Rafehi, M.; Voss, J. H.; Garg, J.; Schlegel, J. G.; Abdelrahman, A.; Kehraus, S.; Reher, R.; Küppers, J.; Sylvester, K.; Hinz, S.; Matthey, M.; Wenzel, D.; Fleischmann, B. K.; Pfeifer, A.; Inoue, A.; Gütschow, M.; König, G. M.; Müller, C. E. Cell-permeable high-affinity tracers for Gq proteins provide structural insights, reveal distinct binding kinetics, and identify small molecule inhibitors. *British journal of pharmacology* **2019.** DOI: 10.1111/bph.14960.
(160) Kamato, D.; Mitra, P.; Davis, F.; Osman, N.; Chaplin, R.; Cabot, P. J.; Afroz, R.; Thomas, W.; Zheng, W.; Kaur, H.; Brimble, M.; Little, P. J. Gaq proteins: molecular pharmacology and therapeutic potential. *Cellular and molecular life sciences : CMLS* **2017**, *74* (8), 1379–1390. DOI: 10.1007/s00018-016-2405-9. Published Online: Apr. 11, 2016.
(161) Rosenbaum, D. M.; Rasmussen, S. G. F.; Kobilka, B. K. The structure and function of G-protein-coupled receptors. *Nature* **2009**, *459* (7245), 356–363. DOI: 10.1038/nature08144.
(162) Insel, P. A.; Sriram, K.; Gorr, M. W.; Wiley, S. Z.; Michkov, A.; Salmerón, C.; Chinn, A. M. GPCRomics: An Approach to Discover GPCR Drug Targets. *Trends in pharmacological sciences* **2019**, *40* (6), 378–387. DOI: 10.1016/j.tips.2019.04.001. Published Online: Aug. 5, 2019.
(163) Fredriksson, R.; Lagerström, M. C.; Lundin, L.-G.; Schiöth, H. B. The G-protein-coupled receptors in the human genome form five main families. Phylogenetic analysis, paralogon groups, and fingerprints. *Molecular pharmacology* **2003**, *63* (6), 1256–1272. DOI: 10.1124/mol.63.6.1256.
(164) Matthey, M.; Roberts, R.; Seidinger, A.; Simon, A.; Schröder, R.; Kuschak, M.; Annala, S.; König, G. M.; Müller, C. E.; Hall, I. P.; Kostenis, E.; Fleischmann, B. K.; Wenzel, D. Targeted inhibition of Gq signaling induces airway relaxation in mouse models of asthma. *Science translational medicine* **2017**, *9* (407). DOI: 10.1126/scitranslmed.aag2288.
(165) Carr, R.; Koziol-White, C.; Zhang, J.; Lam, H.; An, S. S.; Tall, G. G.; Panettieri, R. A.; Benovic, J. L. Interdicting Gq Activation in Airway Disease by Receptor-Dependent and Receptor-Independent Mechanisms. *Molecular pharmacology* **2016**, *89* (1), 94–104. DOI: 10.1124/mol.115.100339. Published Online: Oct. 13, 2015.
(166) Klepac, K.; Kilić, A.; Gnad, T.; Brown, L. M.; Herrmann, B.; Wilderman, A.; Balkow, A.; Glöde, A.; Simon, K.; Lidell, M. E.; Betz, M. J.; Enerbäck, S.; Wess, J.; Freichel, M.; Blüher, M.; König, G.; Kostenis, E.; Insel, P. A.; Pfeifer, A. The Gq signalling pathway inhibits brown and beige adipose tissue. *Nature communications* **2016**, *7*, 10895. DOI: 10.1038/ncomms10895. Published Online: Sep. 3, 2016.
(167) Machida, K.; Arai, D.; Katsumata, R.; Otsuka, S.; Yamashita, J. K.; Ye, T.; Tang, S.; Fusetani, N.; Nakao, Y. Sameuramide A, a new cyclic depsipeptide isolated from an

ascidian of the family Didemnidae. *Bioorganic & medicinal chemistry* **2018**, *26* (13), 3852–3857. DOI: 10.1016/j.bmc.2018.06.042. Published Online: Jun. 30, 2018.
(168) Annala, S.; Feng, X.; Shridhar, N.; Eryilmaz, F.; Patt, J.; Yang, J.; Pfeil, E. M.; Cervantes-Villagrana, R. D.; Inoue, A.; Häberlein, F.; Slodczyk, T.; Reher, R.; Kehraus, S.; Monteleone, S.; Schrage, R.; Heycke, N.; Rick, U.; Engel, S.; Pfeifer, A.; Kolb, P.; König, G.; Bünemann, M.; Tüting, T.; Vázquez-Prado, J.; Gutkind, J. S.; Gaffal, E.; Kostenis, E. Direct targeting of Gαq and Gα11 oncoproteins in cancer cells. *Science signaling* **2019**, *12* (573). DOI: 10.1126/scisignal.aau5948.
(169) Lapadula, D.; Farias, E.; Randolph, C. E.; Purwin, T. J.; McGrath, D.; Charpentier, T. H.; Zhang, L.; Wu, S.; Terai, M.; Sato, T.; Tall, G. G.; Zhou, N.; Wedegaertner, P. B.; Aplin, A. E.; Aguirre-Ghiso, J.; Benovic, J. L. Effects of Oncogenic Gαq and Gα11 Inhibition by FR900359 in Uveal Melanoma. *Molecular cancer research : MCR* **2019**, *17* (4), 963–973. DOI: 10.1158/1541-7786.MCR-18-0574. Published Online: Dec. 19, 2018.
(170) Onken, M. D.; Noda, S. E.; Kaltenbronn, K. M.; Frankfater, C.; Makepeace, C. M.; Fettig, N.; Piggott, K. D.; Custer, P. L.; Ippolito, J. E.; Blumer, K. J. Oncogenic Gq/11 signaling acutely drives and chronically sustains metabolic reprogramming in uveal melanoma. *The Journal of biological chemistry* **2022**, *298* (1), 101495. DOI: 10.1016/j.jbc.2021.101495. Published Online: Dec. 14, 2021.
(171) Miyamae, A.; Fujioka, M.; Koda, S.; Morimoto, Y. Structural studies of FR900359, a novel cyclic depsipeptide from Ardisia crenata sims(Myrsinaceae). *J. Chem. Soc., Perkin Trans. 1* **1989** (5), 873. DOI: 10.1039/P19890000873.
(172) Meleka, M. M.; Edwards, A. J.; Xia, J.; Dahlen, S. A.; Mohanty, I.; Medcalf, M.; Aggarwal, S.; Moeller, K. D.; Mortensen, O. V.; Osei-Owusu, P. Anti-hypertensive mechanisms of cyclic depsipeptide inhibitor ligands for Gq/11 class G proteins. *Pharmacological research* **2019**, *141*, 264–275. DOI: 10.1016/j.phrs.2019.01.012. Published Online: Oct. 1, 2019.
(173) Reher, R.; Kuschak, M.; Heycke, N.; Annala, S.; Kehraus, S.; Dai, H.-F.; Müller, C. E.; Kostenis, E.; König, G. M.; Crüsemann, M. Applying Molecular Networking for the Detection of Natural Sources and Analogues of the Selective Gq Protein Inhibitor FR900359. *Journal of natural products* **2018**, *81* (7), 1628–1635. DOI: 10.1021/acs.jnatprod.8b00222.
(174) Taniguchi, M.; Suzumura, K.; Nagai, K.; Kawasaki, T.; Takasaki, J.; Sekiguchi, M.; Moritani, Y.; Saito, T.; Hayashi, K.; Fujita, S.; Tsukamoto, S.; Suzuki, K. YM-254890 analogues, novel cyclic depsipeptides with Galpha(q/11) inhibitory activity from Chromobacterium sp. QS3666. *Bioorganic & medicinal chemistry* **2004**, *12* (12), 3125–3133. DOI: 10.1016/j.bmc.2004.04.006.
(175) Blin, K.; Shaw, S.; Augustijn, H. E.; Reitz, Z. L.; Biermann, F.; Alanjary, M.; Fetter, A.; Terlouw, B. R.; Metcalf, W. W.; Helfrich, E. J. N.; van Wezel, G. P.; Medema, M. H.; Weber, T. antiSMASH 7.0: new and improved predictions for detection, regulation, chemical structures and visualisation. *Nucleic acids research* **2023.** DOI: 10.1093/nar/gkad344. Published Online: Apr. 5, 2023.
(176) Medema, M. H.; Blin, K.; Cimermancic, P.; Jager, V. de; Zakrzewski, P.; Fischbach, M. A.; Weber, T.; Takano, E.; Breitling, R. antiSMASH: rapid identification, annotation and analysis of secondary metabolite biosynthesis gene clusters in bacterial and fungal genome sequences. *Nucleic acids research* **2011**, *39* (Web Server issue), W339-46. DOI: 10.1093/nar/gkr466.
(177) Katajamaa, M.; Miettinen, J.; Oresic, M. MZmine: toolbox for processing and visualization of mass spectrometry based molecular profile data. *Bioinformatics (Oxford, England)* **2006**, *22* (5), 634–636. DOI: 10.1093/bioinformatics/btk039. Published Online: Oct. 1, 2006.

(178) Pluskal, T.; Castillo, S.; Villar-Briones, A.; Oresic, M. MZmine 2: modular framework for processing, visualizing, and analyzing mass spectrometry-based molecular profile data. *BMC bioinformatics* **2010**, *11*, 395. DOI: 10.1186/1471-2105-11-395.
(179) Olivon, F.; Grelier, G.; Roussi, F.; Litaudon, M.; Touboul, D. MZmine 2 Data-Preprocessing To Enhance Molecular Networking Reliability. *Analytical chemistry* **2017**, *89* (15), 7836–7840. DOI: 10.1021/acs.analchem.7b01563.
(180) Nothias, L.-F.; Petras, D.; Schmid, R.; Dührkop, K.; Rainer, J.; Sarvepalli, A.; Protsyuk, I.; Ernst, M.; Tsugawa, H.; Fleischauer, M.; Aicheler, F.; Aksenov, A. A.; Alka, O.; Allard, P.-M.; Barsch, A.; Cachet, X.; Caraballo-Rodriguez, A. M.; Da Silva, R. R.; Dang, T.; Garg, N.; Gauglitz, J. M.; Gurevich, A.; Isaac, G.; Jarmusch, A. K.; Kameník, Z.; Kang, K. B.; Kessler, N.; Koester, I.; Korf, A.; Le Gouellec, A.; Ludwig, M.; Martin H, C.; McCall, L.-I.; McSayles, J.; Meyer, S. W.; Mohimani, H.; Morsy, M.; Moyne, O.; Neumann, S.; Neuweger, H.; Nguyen, N. H.; Nothias-Esposito, M.; Paolini, J.; Phelan, V. V.; Pluskal, T.; Quinn, R. A.; Rogers, S.; Shrestha, B.; Tripathi, A.; van der Hooft, J. J. J.; Vargas, F.; Weldon, K. C.; Witting, M.; Yang, H.; Zhang, Z.; Zubeil, F.; Kohlbacher, O.; Böcker, S.; Alexandrov, T.; Bandeira, N.; Wang, M.; Dorrestein, P. C. Feature-based molecular networking in the GNPS analysis environment. *Nature methods* **2020**, *17* (9), 905–908. DOI: 10.1038/s41592-020-0933-6.
(181) Wang, M.; Carver, J. J.; Phelan, V. V.; Sanchez, L. M.; Garg, N.; Peng, Y.; Nguyen, D. D.; Watrous, J.; Kapono, C. A.; Luzzatto-Knaan, T.; Porto, C.; Bouslimani, A.; Melnik, A. V.; Meehan, M. J.; Liu, W.-T.; Crüsemann, M.; Boudreau, P. D.; Esquenazi, E.; Sandoval-Calderón, M.; Kersten, R. D.; Pace, L. A.; Quinn, R. A.; Duncan, K. R.; Hsu, C.-C.; Floros, D. J.; Gavilan, R. G.; Kleigrewe, K.; Northen, T.; Dutton, R. J.; Parrot, D.; Carlson, E. E.; Aigle, B.; Michelsen, C. F.; Jelsbak, L.; Sohlenkamp, C.; Pevzner, P.; Edlund, A.; McLean, J.; Piel, J.; Murphy, B. T.; Gerwick, L.; Liaw, C.-C.; Yang, Y.-L.; Humpf, H.-U.; Maansson, M.; Keyzers, R. A.; Sims, A. C.; Johnson, A. R.; Sidebottom, A. M.; Sedio, B. E.; Klitgaard, A.; Larson, C. B.; P, C. A. B.; Torres-Mendoza, D.; Gonzalez, D. J.; Silva, D. B.; Marques, L. M.; Demarque, D. P.; Pociute, E.; O'Neill, E. C.; Briand, E.; Helfrich, E. J. N.; Granatosky, E. A.; Glukhov, E.; Ryffel, F.; Houson, H.; Mohimani, H.; Kharbush, J. J.; Zeng, Y.; Vorholt, J. A.; Kurita, K. L.; Charusanti, P.; McPhail, K. L.; Nielsen, K. F.; Vuong, L.; Elfeki, M.; Traxler, M. F.; Engene, N.; Koyama, N.; Vining, O. B.; Baric, R.; Silva, R. R.; Mascuch, S. J.; Tomasi, S.; Jenkins, S.; Macherla, V.; Hoffman, T.; Agarwal, V.; Williams, P. G.; Dai, J.; Neupane, R.; Gurr, J.; Rodríguez, A. M. C.; Lamsa, A.; Zhang, C.; Dorrestein, K.; Duggan, B. M.; Almaliti, J.; Allard, P.-M.; Phapale, P.; Nothias, L.-F.; Alexandrov, T.; Litaudon, M.; Wolfender, J.-L.; Kyle, J. E.; Metz, T. O.; Peryea, T.; Nguyen, D.-T.; VanLeer, D.; Shinn, P.; Jadhav, A.; Müller, R.; Waters, K. M.; Shi, W.; Liu, X.; Zhang, L.; Knight, R.; Jensen, P. R.; Palsson, B. O.; Pogliano, K.; Linington, R. G.; Gutiérrez, M.; Lopes, N. P.; Gerwick, W. H.; Moore, B. S.; Dorrestein, P. C.; Bandeira, N. Sharing and community curation of mass spectrometry data with Global Natural Products Social Molecular Networking. *Nature biotechnology* **2016**, *34* (8), 828–837. DOI: 10.1038/nbt.3597.
(182) Yang, J. Y.; Sanchez, L. M.; Rath, C. M.; Liu, X.; Boudreau, P. D.; Bruns, N.; Glukhov, E.; Wodtke, A.; Felicio, R. de; Fenner, A.; Wong, W. R.; Linington, R. G.; Zhang, L.; Debonsi, H. M.; Gerwick, W. H.; Dorrestein, P. C. Molecular networking as a dereplication strategy. *Journal of natural products* **2013**, *76* (9), 1686–1699. DOI: 10.1021/np400413s.
(183) Yu, J. S.; Seo, H.; Kim, G. B.; Hong, J.; Yoo, H. H. MS-Based Molecular Networking of Designer Drugs as an Approach for the Detection of Unknown Derivatives for Forensic and Doping Applications: A Case of NBOMe Derivatives. *Analytical chemistry* **2019**, *91* (9), 5483–5488. DOI: 10.1021/acs.analchem.9b00294. Published Online: Apr. 18, 2019.

(184) Mohimani, H.; Gurevich, A.; Mikheenko, A.; Garg, N.; Nothias, L.-F.; Ninomiya, A.; Takada, K.; Dorrestein, P. C.; Pevzner, P. A. Dereplication of peptidic natural products through database search of mass spectra. *Nature chemical biology* **2017**, *13* (1), 30–37. DOI: 10.1038/nchembio.2219. Published Online: Oct. 31, 2016.
(185) Wandy, J.; Zhu, Y.; van der Hooft, J. J. J.; Daly, R.; Barrett, M. P.; Rogers, S. Ms2lda.org: web-based topic modelling for substructure discovery in mass spectrometry. *Bioinformatics (Oxford, England)* **2018**, *34* (2), 317–318. DOI: 10.1093/bioinformatics/btx582.
(186) van der Hooft, J. J. J.; Wandy, J.; Barrett, M. P.; Burgess, K. E. V.; Rogers, S. Topic modeling for untargeted substructure exploration in metabolomics. *Proceedings of the National Academy of Sciences of the United States of America* **2016**, *113* (48), 13738–13743. DOI: 10.1073/pnas.1608041113. Published Online: Nov. 16, 2016.
(187) Gurevich, A.; Mikheenko, A.; Shlemov, A.; Korobeynikov, A.; Mohimani, H.; Pevzner, P. A. Increased diversity of peptidic natural products revealed by modification-tolerant database search of mass spectra. *Nature microbiology* **2018**, *3* (3), 319–327. DOI: 10.1038/s41564-017-0094-2. Published Online: Jan. 22, 2018.
(188) Dührkop, K.; Nothias, L.-F.; Fleischauer, M.; Reher, R.; Ludwig, M.; Hoffmann, M. A.; Petras, D.; Gerwick, W. H.; Rousu, J.; Dorrestein, P. C.; Böcker, S. Systematic classification of unknown metabolites using high-resolution fragmentation mass spectra. *Nature biotechnology* **2021**, *39* (4), 462–471. DOI: 10.1038/s41587-020-0740-8. Published Online: Nov. 23, 2020.
(189) Dührkop, K.; Fleischauer, M.; Ludwig, M.; Aksenov, A. A.; Melnik, A. V.; Meusel, M.; Dorrestein, P. C.; Rousu, J.; Böcker, S. SIRIUS 4: a rapid tool for turning tandem mass spectra into metabolite structure information. *Nature methods* **2019**, *16* (4), 299–302. DOI: 10.1038/s41592-019-0344-8. Published Online: Mar. 18, 2019.
(190) Morohoshi, T.; Kato, M.; Fukamachi, K.; Kato, N.; Ikeda, T. N-acylhomoserine lactone regulates violacein production in Chromobacterium violaceum type strain ATCC 12472. *FEMS microbiology letters* **2008**, *279* (1), 124–130. DOI: 10.1111/j.1574-6968.2007.01016.x.
(191) Bangera, M. G.; Thomashow, L. S. Identification and characterization of a gene cluster for synthesis of the polyketide antibiotic 2,4-diacetylphloroglucinol from Pseudomonas fluorescens Q2-87. *Journal of bacteriology* **1999**, *181* (10), 3155–3163. DOI: 10.1128/JB.181.10.3155-3163.1999.
(192) Ngoka, L. C. M.; Gross, M. L. A nomenclature system for labeling cyclic peptide fragments. *J Am Soc Mass Spectrom* **1999**, *10* (4), 360–363. DOI: 10.1016/S1044-0305(99)00006-9.
(193) Biemann, K. Mass spectrometry of peptides and proteins. *Annual review of biochemistry* **1992**, *61*, 977–1010. DOI: 10.1146/annurev.bi.61.070192.004553.
(194) Roepstorff, P.; Fohlman, J. Proposal for a common nomenclature for sequence ions in mass spectra of peptides. *Biomedical mass spectrometry* **1984**, *11* (11), 601. DOI: 10.1002/bms.1200111109.
(195) Reher, R. Ecological and Chemical Studies on the Gq-protein Inhibitor FR900359, Rheinische Friedrich-Wilhelms-Universität Bonn, 2018. hdl.handle.net/20.500.11811/7644.
(196) Schröder, R.; Janssen, N.; Schmidt, J.; Kebig, A.; Merten, N.; Hennen, S.; Müller, A.; Blättermann, S.; Mohr-Andrä, M.; Zahn, S.; Wenzel, J.; Smith, N. J.; Gomeza, J.; Drewke, C.; Milligan, G.; Mohr, K.; Kostenis, E. Deconvolution of complex G protein-coupled receptor signaling in live cells using dynamic mass redistribution measurements. *Nature biotechnology* **2010**, *28* (9), 943–949. DOI: 10.1038/nbt.1671. Published Online: Aug. 15, 2010.

(197) Schröder, R.; Schmidt, J.; Blättermann, S.; Peters, L.; Janssen, N.; Grundmann, M.; Seemann, W.; Kaufel, D.; Merten, N.; Drewke, C.; Gomeza, J.; Milligan, G.; Mohr, K.; Kostenis, E. Applying label-free dynamic mass redistribution technology to frame signaling of G protein-coupled receptors noninvasively in living cells. *Nature protocols* **2011**, *6* (11), 1748–1760. DOI: 10.1038/nprot.2011.386. Published Online: Oct. 20, 2011.

(198) Nishimura, A.; Kitano, K.; Takasaki, J.; Taniguchi, M.; Mizuno, N.; Tago, K.; Hakoshima, T.; Itoh, H. Structural basis for the specific inhibition of heterotrimeric Gq protein by a small molecule. *Proceedings of the National Academy of Sciences of the United States of America* **2010**, *107* (31), 13666–13671. DOI: 10.1073/pnas.1003553107.

(199) Carlier, A.; Fehr, L.; Pinto-Carbó, M.; Schäberle, T.; Reher, R.; Dessein, S.; König, G.; Eberl, L. The genome analysis of Candidatus Burkholderia crenata reveals that secondary metabolism may be a key function of the Ardisia crenata leaf nodule symbiosis. *Environmental microbiology* **2016**, *18* (8), 2507–2522. DOI: 10.1111/1462-2920.13184.

(200) Reher, R.; Kühl, T.; Annala, S.; Benkel, T.; Kaufmann, D.; Nubbemeyer, B.; Odhiambo, J. P.; Heimer, P.; Bäuml, C. A.; Kehraus, S.; Crüsemann, M.; Kostenis, E.; Tietze, D.; König, G. M.; Imhof, D. Deciphering Specificity Determinants for FR900359-Derived Gq α Inhibitors Based on Computational and Structure-Activity Studies. *ChemMedChem* **2018**, *13* (16), 1634–1643. DOI: 10.1002/cmdc.201800304.

(201) Frediansyah, A.; Manuhara, Y. S. W.; Kristanti, A. N.; Luqman, A.; Wibowo, A. T. Fermentation in Minimal Media and Fungal Elicitation Enhance Violacein and Deoxyviolacein Production in Two Janthinobacterium Strains. *Fermentation* **2022**, *8* (12), 714. DOI: 10.3390/fermentation8120714.

(202) Alem, D.; Marizcurrena, J. J.; Saravia, V.; Davyt, D.; Martinez-Lopez, W.; Castro-Sowinski, S. Production and antiproliferative effect of violacein, a purple pigment produced by an Antarctic bacterial isolate. *World journal of microbiology & biotechnology* **2020**, *36* (8), 120. DOI: 10.1007/s11274-020-02893-4. Published Online: Jul. 18, 2020.

(203) Priya, K.; Sulaiman, J.; How, K. Y.; Yin, W.-F.; Chan, K.-G. Production of N-acyl homoserine lactones by Chromobacterium haemolyticum KM2 isolated from the river water in Malaysia. *Archives of microbiology* **2018**, *200* (7), 1135–1142. DOI: 10.1007/s00203-018-1526-y. Published Online: May. 23, 2018.

(204) Rekha, P. D.; Young, C.-C.; Arun, A. B. Identification of N-acyl-l-homoserine lactones produced by non-pigmented Chromobacterium aquaticum CC-SEYA-1(T) and pigmented Chromobacterium subtsugae PRAA4-1(T). *3 Biotech* **2011**, *1* (4), 239–245. DOI: 10.1007/s13205-011-0029-1. Published Online: Oct. 14, 2011.

(205) Rodrigues, A. M. S.; Lami, R.; Escoubeyrou, K.; Intertaglia, L.; Mazurek, C.; Doberva, M.; Pérez-Ferrer, P.; Stien, D. Straightforward N-Acyl Homoserine Lactone Discovery and Annotation by LC-MS/MS-based Molecular Networking. *Journal of proteome research* **2022**, *21* (3), 635–642. DOI: 10.1021/acs.jproteome.1c00849. Published Online: Jan. 2, 2022.

(206) Wang, J.; Quan, C.; Wang, X.; Zhao, P.; Fan, S. Extraction, purification and identification of bacterial signal molecules based on N-acyl homoserine lactones. *Microbial biotechnology* **2011**, *4* (4), 479–490. DOI: 10.1111/j.1751-7915.2010.00197.x. Published Online: Aug. 16, 2010.

(207) Min, L.-J.; Wu, X.-Q.; Li, D.-W.; Chen, K.; Guo, L.; Ye, J.-R. Burkholderia pyrrocinia JK-SH007 Enhanced Seed Germination, Cucumber Seedling Growth and Tomato Fruit via Catecholate-Siderophore-Mediation. *International Journal of Agriculture and Biology* **2019** (22), 779–786. DOI: 10.17957/IJAB/15.1130.

(208) Timofeeva, A. M.; Galyamova, M. R.; Sedykh, S. E. Bacterial Siderophores: Classification, Biosynthesis, Perspectives of Use in Agriculture. *Plants (Basel, Switzerland)* **2022**, *11* (22). DOI: 10.3390/plants11223065. Published Online: Dec. 11, 2022.
(209) Yu, X.; Ai, C.; Xin, L.; Zhou, G. The siderophore-producing bacterium, Bacillus subtilis CAS15, has a biocontrol effect on Fusarium wilt and promotes the growth of pepper. *European Journal of Soil Biology* **2011**, *47* (2), 138–145. DOI: 10.1016/j.ejsobi.2010.11.001.
(210) Zhang, S.; Deng, Z.; Borham, A.; Ma, Y.; Wang, Y.; Hu, J.; Wang, J.; Bohu, T. Significance of Soil Siderophore-Producing Bacteria in Evaluation and Elevation of Crop Yield. *Horticulturae* **2023**, *9* (3), 370. DOI: 10.3390/horticulturae9030370.
(211) Abdul-Tehrani, H.; Hudson, A. J.; Chang, Y. S.; Timms, A. R.; Hawkins, C.; Williams, J. M.; Harrison, P. M.; Guest, J. R.; Andrews, S. C. Ferritin mutants of Escherichia coli are iron deficient and growth impaired, and fur mutants are iron deficient. *Journal of bacteriology* **1999**, *181* (5), 1415–1428. DOI: 10.1128/jb.181.5.1415-1428.1999.
(212) Payne, S. M. Detection, isolation, and characterization of siderophores. *Methods in enzymology* **1994**, *235*, 329–344. DOI: 10.1016/0076-6879(94)35151-1.
(213) Miethke, M.; Marahiel, M. A. Siderophore-based iron acquisition and pathogen control. *Microbiology and molecular biology reviews : MMBR* **2007**, *71* (3), 413–451. DOI: 10.1128/MMBR.00012-07.
(214) Biessy, A.; Filion, M. Phloroglucinol Derivatives in Plant-Beneficial Pseudomonas spp.: Biosynthesis, Regulation, and Functions. *Metabolites* **2021**, *11* (3). DOI: 10.3390/metabo11030182. Published Online: Mar. 20, 2021.
(215) Julian, W. T.; Vasilchenko, A. V.; Shpindyuk, D. D.; Poshvina, D. V.; Vasilchenko, A. S. Bacterial-Derived Plant Protection Metabolite 2,4-Diacetylphloroglucinol: Effects on Bacterial Cells at Inhibitory and Subinhibitory Concentrations. *Biomolecules* **2020**, *11* (1). DOI: 10.3390/biom11010013. Published Online: Dec. 25, 2020.
(216) Khan, F.; Tabassum, N.; Bamunuarachchi, N. I.; Kim, Y.-M. Phloroglucinol and Its Derivatives: Antimicrobial Properties toward Microbial Pathogens. *Journal of agricultural and food chemistry* **2022**, *70* (16), 4817–4838. DOI: 10.1021/acs.jafc.2c00532. Published Online: Apr. 13, 2022.
(217) Shanahan, P.; O'sullivan, D. J.; Simpson, P.; Glennon, J. D.; O'gara, F. Isolation of 2,4-diacetylphloroglucinol from a fluorescent pseudomonad and investigation of physiological parameters influencing its production. *Applied and environmental microbiology* **1992**, *58* (1), 353–358. DOI: 10.1128/aem.58.1.353-358.1992.
(218) Sidana, J.; Foley, W. J.; Singh, I. P. Isolation and quantitation of ecologically important phloroglucinols and other compounds from Eucalyptus jensenii. *Phytochemical analysis : PCA* **2012**, *23* (5), 483–491. DOI: 10.1002/pca.2345. Published Online: Sep. 1, 2012.
(219) Vöing, K.; Harrison, A.; Soby, S. D. Draft Genome Sequence of Chromobacterium vaccinii, a Potential Biocontrol Agent against Mosquito (Aedes aegypti) Larvae. *Genome announcements* **2015**, *3* (3). DOI: 10.1128/genomeA.00477-15. Published Online: May. 21, 2015.
(220) Schmidt, Y.; van der Voort, M.; Crüsemann, M.; Piel, J.; Josten, M.; Sahl, H.-G.; Miess, H.; Raaijmakers, J. M.; Gross, H. Biosynthetic origin of the antibiotic cyclocarbamate brabantamide A (SB-253514) in plant-associated Pseudomonas. *Chembiochem : a European journal of chemical biology* **2014**, *15* (2), 259–266. DOI: 10.1002/cbic.201300527.
(221) El Maddah, F.; Kehraus, S.; Nazir, M.; Almeida, C.; König, G. M. Insights into the Biosynthetic Origin of 3-(3-Furyl)alanine in Stachylidium sp. 293 K04 Tetrapeptides.

Journal of natural products **2016**, *79* (11), 2838–2845. DOI: 10.1021/acs.jnatprod.6b00601. Published Online: Oct. 27, 2016.
(222) Arroo, R. R. J.; Bhambra, A. S.; Hano, C.; Renda, G.; Ruparelia, K. C.; Wang, M. F. Analysis of plant secondary metabolism using stable isotope-labelled precursors. *Phytochemical analysis : PCA* **2021**, *32* (1), 62–68. DOI: 10.1002/pca.2955. Published Online: Jul. 24, 2020.
(223) Hautbergue, T.; Jamin, E. L.; Costantino, R.; Tadrist, S.; Meneghetti, L.; Tabet, J.-C.; Debrauwer, L.; Oswald, I. P.; Puel, O. Combination of Isotope Labeling and Molecular Networking of Tandem Mass Spectrometry Data To Reveal 69 Unknown Metabolites Produced by Penicillium nordicum. *Analytical chemistry* **2019**, *91* (19), 12191–12202. DOI: 10.1021/acs.analchem.9b01634. Published Online: Nov. 9, 2019.
(224) Stokvis, E.; Rosing, H.; Beijnen, J. H. Stable isotopically labeled internal standards in quantitative bioanalysis using liquid chromatography/mass spectrometry: necessity or not? *Rapid communications in mass spectrometry : RCM* **2005**, *19* (3), 401–407. DOI: 10.1002/rcm.1790.
(225) Hanke, W. *Investigation of a microbial producer of FR900359*, 2018.
(226) Hermes, C. Investigations into side chain assembly and attachment during biosynthesis of the G protein inhibitor FR900359, Rheinische Friedrich-Wilhelms-Universität Bonn, 2021. hdl.handle.net/20.500.11811/9126.
(227) ATKINSON, D. E.; MELVIN, S.; FOX, S. W. Effects of rho-fluorophenylalanine on the growth of Lactobacillus arabinosus. *Archives of biochemistry and biophysics* **1951**, *31* (2), 205–211. DOI: 10.1016/0003-9861(51)90207-X.
(228) Dunn, N. W.; Holloway, B. W. Pleiotrophy of p-fluorophenylalanine-resistant and antibiotic hypersensitive mutants of Pseudomonas aeruginosa. *Genetical research* **1971**, *18* (2), 185–197. DOI: 10.1017/S0016672300012593.
(229) MITCHELL, H. K.; NIEMANN, C. The competitive inhibition of the metabolism of alpha-amino acids by their halogenated analogs. *Journal of the American Chemical Society* **1947**, *69* (5), 1232. DOI: 10.1021/ja01197a525.
(230) Pratt, E. A.; Ho, C. Incorporation of fluorotryptophans into proteins of escherichia coli. *Biochemistry* **1975**, *14* (13), 3035–3040. DOI: 10.1021/bi00684a037.
(231) Hai, Y.; Huang, A.; Tang, Y. Biosynthesis of Amino Acid Derived α-Pyrones by an NRPS-NRPKS Hybrid Megasynthetase in Fungi. *Journal of natural products* **2020**, *83* (3), 593–600. DOI: 10.1021/acs.jnatprod.9b00989. Published Online: Nov. 3, 2020.
(232) Rivera-Chávez, J.; Raja, H. A.; Graf, T. N.; Burdette, J. E.; Pearce, C. J.; Oberlies, N. H. Biosynthesis of Fluorinated Peptaibols Using a Site-Directed Building Block Incorporation Approach. *Journal of natural products* **2017**, *80* (6), 1883–1892. DOI: 10.1021/acs.jnatprod.7b00189. Published Online: Aug. 6, 2017.
(233) Inoue, M.; Sumii, Y.; Shibata, N. Contribution of Organofluorine Compounds to Pharmaceuticals. *ACS omega* **2020**, *5* (19), 10633–10640. DOI: 10.1021/acsomega.0c00830. Published Online: Apr. 22, 2020.
(234) van Pham, H. T.; Kim, J. Cultivation of unculturable soil bacteria. *Trends in biotechnology* **2012**, *30* (9), 475–484. DOI: 10.1016/j.tibtech.2012.05.007. Published Online: Jul. 7, 2012.
(235) Berendsen, B.; Pikkemaat, M.; Römkens, P.; Wegh, R.; van Sisseren, M.; Stolker, L.; Nielen, M. Occurrence of chloramphenicol in crops through natural production by bacteria in soil. *Journal of agricultural and food chemistry* **2013**, *61* (17), 4004–4010. DOI: 10.1021/jf400570c. Published Online: Apr. 19, 2013.
(236) Kennedy, C. D.; Wilderotter, S.; Payne, M.; Buda, A. R.; Kleinman, P. J.; Bryant, R. B. A geospatial model to quantify mean thickness of peat in cranberry bogs. *Geoderma* **2018**, *319*, 122–131. DOI: 10.1016/j.geoderma.2017.12.032.

(237) Putnam, R. A.; Nelson, J. O.; Clark, J. M. The persistence and degradation of chlorothalonil and chlorpyrifos in a cranberry bog. *Journal of agricultural and food chemistry* **2003**, *51* (1), 170–176. DOI: 10.1021/jf020744r.
(238) Nguyen, T. M.; Seo, C.; Ji, M.; Paik, M.-J.; Myung, S.-W.; Kim, J. Effective Soil Extraction Method for Cultivating Previously Uncultured Soil Bacteria. *Applied and environmental microbiology* **2018**, *84* (24). DOI: 10.1128/AEM.01145-18.
(239) Deutschen Sammlung von Mikroorganismen und Zellkulturen. *Medium 12*:*Soil Extract Medium*. www.dsmz.de/microorganisms/medium/pdf/DSMZ_Medium12.pdf.
(240) Hamaki, T.; Suzuki, M.; Fudou, R.; Jojima, Y.; Kajiura, T.; Tabuchi, A.; Sen, K.; Shibai, H. Isolation of novel bacteria and actinomycetes using soil-extract agar medium. *Journal of bioscience and bioengineering* **2005**, *99* (5), 485–492. DOI: 10.1263/jbb.99.485.
(241) Vilain, S.; Luo, Y.; Hildreth, M. B.; Brözel, V. S. Analysis of the life cycle of the soil saprophyte Bacillus cereus in liquid soil extract and in soil. *Applied and environmental microbiology* **2006**, *72* (7), 4970–4977. DOI: 10.1128/AEM.03076-05.
(242) Vaz Jauri, P.; Bakker, M. G.; Salomon, C. E.; Kinkel, L. L. Subinhibitory antibiotic concentrations mediate nutrient use and competition among soil streptomyces. *PloS one* **2013**, *8* (12), e81064. DOI: 10.1371/journal.pone.0081064. Published Online: May. 12, 2013.
(243) Arseneault, T.; Filion, M. Biocontrol through antibiosis: exploring the role played by subinhibitory concentrations of antibiotics in soil and their impact on plant pathogens. *Canadian Journal of Plant Pathology* **2017**, *39* (3), 267–274. DOI: 10.1080/07060661.2017.1354335.
(244) Beier, S.; Bertilsson, S. Bacterial chitin degradation-mechanisms and ecophysiological strategies. *Frontiers in microbiology* **2013**, *4*, 149. DOI: 10.3389/fmicb.2013.00149. Published Online: Jun. 14, 2013.
(245) Kudela, R. M. Characterization and deployment of Solid Phase Adsorption Toxin Tracking (SPATT) resin for monitoring of microcystins in fresh and saltwater. *Harmful Algae* **2011**, *11*, 117–125. DOI: 10.1016/j.hal.2011.08.006.
(246) Kudela, R. M. Passive Sampling for Freshwater and Marine Algal Toxins. In *Recent Advances in the Analysis of Marine Toxins*; Comprehensive Analytical Chemistry; Elsevier, 2017; pp 379–409. DOI: 10.1016/bs.coac.2017.08.006.
(247) Tuttle, R. N.; Demko, A. M.; Patin, N. V.; Kapono, C. A.; Donia, M. S.; Dorrestein, P.; Jensen, P. R. Detection of Natural Products and Their Producers in Ocean Sediments. *Applied and environmental microbiology* **2019**, *85* (8). DOI: 10.1128/AEM.02830-18. Published Online: Apr. 4, 2019.
(248) Cao, J.; Pliquett, U.; Yang, L.; Wiedemeier, S.; Cahill, B.; Michael Köhler, J. Contactless optical and impedimetric sensing for droplet-based dose-response investigations of microorganisms. *Sensors and Actuators B: Chemical* **2022**, *372*, 132688. DOI: 10.1016/j.snb.2022.132688.
(249) Hu, B.; Xu, P.; Ma, L.; Chen, D.; Wang, J.; Dai, X.; Huang, L.; Du, W. One cell at a time: droplet-based microbial cultivation, screening and sequencing. *Marine life science & technology* **2021**, *3* (2), 169–188. DOI: 10.1007/s42995-020-00082-8. Published Online: Jan. 19, 2021.
(250) Santana-Pereira, A. L. R.; Sandoval-Powers, M.; Monsma, S.; Zhou, J.; Santos, S. R.; Mead, D. A.; Liles, M. R. Discovery of Novel Biosynthetic Gene Cluster Diversity From a Soil Metagenomic Library. *Frontiers in microbiology* **2020**, *11*, 585398. DOI: 10.3389/fmicb.2020.585398. Published Online: Jul. 12, 2020.
(251) Lokits, A. D.; Indrischek, H.; Meiler, J.; Hamm, H. E.; Stadler, P. F. Tracing the evolution of the heterotrimeric G protein α subunit in Metazoa. *BMC evolutionary biology* **2018**, *18* (1), 51. DOI: 10.1186/s12862-018-1147-8. Published Online: Nov. 4, 2018.

(252) Mendoza, A. de; Sebé-Pedrós, A.; Ruiz-Trillo, I. The evolution of the GPCR signaling system in eukaryotes: modularity, conservation, and the transition to metazoan multicellularity. *Genome biology and evolution* **2014**, *6* (3), 606–619. DOI: 10.1093/gbe/evu038.
(253) Altschul, S. F.; Madden, T. L.; Schäffer, A. A.; Zhang, J.; Zhang, Z.; Miller, W.; Lipman, D. J. Gapped BLAST and PSI-BLAST: a new generation of protein database search programs. *Nucleic acids research* **1997**, *25* (17), 3389–3402. DOI: 10.1093/nar/25.17.3389.
(254) Altschul, S. F.; Wootton, J. C.; Gertz, E. M.; Agarwala, R.; Morgulis, A.; Schäffer, A. A.; Yu, Y.-K. Protein database searches using compositionally adjusted substitution matrices. *The FEBS journal* **2005**, *272* (20), 5101–5109. DOI: 10.1111/j.1742-4658.2005.04945.x.
(255) Malfacini, D.; Patt, J.; Annala, S.; Harpsøe, K.; Eryilmaz, F.; Reher, R.; Crüsemann, M.; Hanke, W.; Zhang, H.; Tietze, D.; Gloriam, D. E.; Bräuner-Osborne, H.; Strømgaard, K.; König, G. M.; Inoue, A.; Gomeza, J.; Kostenis, E. Rational design of a heterotrimeric G protein α subunit with artificial inhibitor sensitivity. *The Journal of biological chemistry* **2019**, *294* (15), 5747–5758. DOI: 10.1074/jbc.RA118.007250. Published Online: Nov. 2, 2019.
(256) Brenner, S. The genetics of Caenorhabditis elegans. *Genetics* **1974**, *77* (1), 71–94. DOI: 10.1093/genetics/77.1.71.
(257) Harris, T. W.; Arnaboldi, V.; Cain, S.; Chan, J.; Chen, W. J.; Cho, J.; Davis, P.; Gao, S.; Grove, C. A.; Kishore, R.; Lee, R. Y. N.; Muller, H.-M.; Nakamura, C.; Nuin, P.; Paulini, M.; Raciti, D.; Rodgers, F. H.; Russell, M.; Schindelman, G.; Auken, K. V.; Wang, Q.; Williams, G.; Wright, A. J.; Yook, K.; Howe, K. L.; Schedl, T.; Stein, L.; Sternberg, P. W. WormBase: a modern Model Organism Information Resource. *Nucleic acids research* **2020**, *48* (D1), D762-D767. DOI: 10.1093/nar/gkz920.
(258) Davis, P.; Zarowiecki, M.; Arnaboldi, V.; Becerra, A.; Cain, S.; Chan, J.; Chen, W. J.; Cho, J.; Da Veiga Beltrame, E.; Diamantakis, S.; Gao, S.; Grigoriadis, D.; Grove, C. A.; Harris, T. W.; Kishore, R.; Le, T.; Lee, R. Y. N.; Luypaert, M.; Müller, H.-M.; Nakamura, C.; Nuin, P.; Paulini, M.; Quinton-Tulloch, M.; Raciti, D.; Rodgers, F. H.; Russell, M.; Schindelman, G.; Singh, A.; Stickland, T.; van Auken, K.; Wang, Q.; Williams, G.; Wright, A. J.; Yook, K.; Berriman, M.; Howe, K. L.; Schedl, T.; Stein, L.; Sternberg, P. W. WormBase in 2022-data, processes, and tools for analyzing Caenorhabditis elegans. *Genetics* **2022**, *220* (4). DOI: 10.1093/genetics/iyac003.
(259) Brundage, L.; Avery, L.; Katz, A.; Kim, U. J.; Mendel, J. E.; Sternberg, P. W.; Simon, M. I. Mutations in a C. elegans Gqalpha gene disrupt movement, egg laying, and viability. *Neuron* **1996**, *16* (5), 999–1009. DOI: 10.1016/s0896-6273(00)80123-3.
(260) Dayi, M.; Kanzaki, N.; Sun, S.; Ide, T.; Tanaka, R.; Masuya, H.; Okabe, K.; Kajimura, H.; Kikuchi, T. Additional description and genome analyses of Caenorhabditis auriculariae representing the basal lineage of genus Caenorhabditis. *Scientific reports* **2021**, *11* (1), 6720. DOI: 10.1038/s41598-021-85967-z. Published Online: Mar. 24, 2021.
(261) Sudhaus, W.; Giblin-Davis, R.; Kiontke, K. Description of Caenorhabditis angaria n. sp. (Nematoda: Rhabditidae), an associate of sugarcane and palm weevils (Coleoptera: Curculionidae). *Nematol* **2011**, *13* (1), 61–78. DOI: 10.1163/138855410X500334.
(262) Dey, A.; Jeon, Y.; Wang, G.-X.; Cutter, A. D. Global population genetic structure of Caenorhabditis remanei reveals incipient speciation. *Genetics* **2012**, *191* (4), 1257–1269. DOI: 10.1534/genetics.112.140418. Published Online: May. 29, 2012.
(263) Félix, M.-A.; Braendle, C.; Cutter, A. D. A streamlined system for species diagnosis in Caenorhabditis (Nematoda: Rhabditidae) with name designations for 15 distinct

biological species. *PloS one* **2014**, *9* (4), e94723. DOI: 10.1371/journal.pone.0094723. Published Online: Nov. 4, 2014.
(264) Baird, S. E. Natural and experimental associations of Caenorhabditis remanei with Trachelipus rathkii and other terrestrial isopods. *Nematol* **1999**, *1* (5), 471–475. DOI: 10.1163/156854199508478.
(265) Hironaka, M.; Kiontke, K.; Sudhaus, W. Description of Caenorhabditis japonica n. sp. (Nematoda: Rhabditida) associated with the burrower bug Parastrachia japonensis (Heteroptera: Cydnidae) in Japan. *Nematol* **2002**, *4* (8), 933–941. DOI: 10.1163/156854102321122557.
(266) Yoshiga, T.; Ishikawa, Y.; Tanaka, R.; Hironaka, M.; Okumura, E. Species-specific and female host-biased ectophoresy in the roundworm Caenorhabditis japonica. *Die Naturwissenschaften* **2013**, *100* (2), 205–208. DOI: 10.1007/s00114-013-1011-z. Published Online: Jan. 17, 2013.
(267) Schulenburg, H.; Félix, M.-A. The Natural Biotic Environment of Caenorhabditis elegans. *Genetics* **2017**, *206* (1), 55–86. DOI: 10.1534/genetics.116.195511.
(268) Cutter, A. D. Caenorhabditis evolution in the wild. *BioEssays : news and reviews in molecular, cellular and developmental biology* **2015**, *37* (9), 983–995. DOI: 10.1002/bies.201500053. Published Online: Jun. 30, 2015.
(269) Abebe, E.; Jumba, M.; Bonner, K.; Gray, V.; Morris, K.; Thomas, W. K. An entomopathogenic Caenorhabditis briggsae. *The Journal of experimental biology* **2010**, *213* (Pt 18), 3223–3229. DOI: 10.1242/jeb.043109.
(270) Pires-daSilva, A.; Sommer, R. J. Conservation of the global sex determination gene tra-1 in distantly related nematodes. *Genes & development* **2004**, *18* (10), 1198–1208. DOI: 10.1101/gad.293504.
(271) Herrmann, M.; Mayer, W. E.; Sommer, R. J. Nematodes of the genus Pristionchus are closely associated with scarab beetles and the Colorado potato beetle in Western Europe. *Zoology (Jena, Germany)* **2006**, *109* (2), 96–108. DOI: 10.1016/j.zool.2006.03.001. Published Online: Apr. 17, 2006.
(272) Kumari, S. Aphelenchus avenae (Nematoda: Aphelenchidae) under the rhizosphere of Brassica napus. *Helminthologia* **2012**, *49* (1), 57–59. DOI: 10.2478/s11687-012-0009-y.
(273) Kanzaki, N.; Maehara, N.; Aikawa, T.; Togashi, K. First report of parthenogenesis in the genus Bursaphelenchus Fuchs, 1937: a description of Bursaphelenchus okinawaensis sp. nov. isolated from Monochamus maruokai (Coleoptera: Cerambycidae). *Zoological science* **2008**, *25* (8), 861–873. DOI: 10.2108/zsj.25.861.
(274) Zheng, J.; Peng, D.; Chen, L.; Liu, H.; Chen, F.; Xu, M.; Ju, S.; Ruan, L.; Sun, M. The Ditylenchus destructor genome provides new insights into the evolution of plant parasitic nematodes. *Proceedings. Biological sciences* **2016**, *283* (1835). DOI: 10.1098/rspb.2016.0942.
(275) Htay, C.; Peng, H.; Huang, W.; Kong, L.; He, W.; Holgado, R.; Peng, D. The development and molecular characterization of a rapid detection method for Rice root-knot nematode (Meloidogyne graminicola). *Eur J Plant Pathol* **2016**, *146* (2), 281–291. DOI: 10.1007/s10658-016-0913-y.
(276) Elling, A. A. Major emerging problems with minor meloidogyne species. *Phytopathology* **2013**, *103* (11), 1092–1102. DOI: 10.1094/ PHYTO-01-13-0019-RVW.
(277) Sijmons, P. C. Plant-nematode interactions. *Plant molecular biology* **1993**, *23* (5), 917–931. DOI: 10.1007/BF00021809.
(278) Siddique, S.; Radakovic, Z. S.; Hiltl, C.; Pellegrin, C.; Baum, T. J.; Beasley, H.; Bent, A. F.; Chitambo, O.; Chopra, D.; Danchin, E. G. J.; Grenier, E.; Habash, S. S.; Hasan, M. S.; Helder, J.; Hewezi, T.; Holbein, J.; Holterman, M.; Janakowski, S.; Koutsovoulos, G. D.;

Kranse, O. P.; Lozano-Torres, J. L.; Maier, T. R.; Masonbrink, R. E.; Mendy, B.; Riemer, E.; Sobczak, M.; Sonawala, U.; Sterken, M. G.; Thorpe, P.; van Steenbrugge, J. J. M.; Zahid, N.; Grundler, F.; Eves-van den Akker, S. The genome and lifestage-specific transcriptomes of a plant-parasitic nematode and its host reveal susceptibility genes involved in trans-kingdom synthesis of vitamin B5. *Nature communications* **2022**, *13* (1), 6190. DOI: 10.1038/s41467-022-33769-w. Published Online: Oct. 19, 2022.

(279) Flock, T.; Ravarani, C. N. J.; Sun, D.; Venkatakrishnan, A. J.; Kayikci, M.; Tate, C. G.; Veprintsev, D. B.; Babu, M. M. Universal allosteric mechanism for Gα activation by GPCRs. *Nature* **2015**, *524* (7564), 173–179. DOI: 10.1038/nature14663. Published Online: Jun. 7, 2015.

(280) Trinquet, E.; Bouhelal, R.; Dietz, M. Monitoring Gq-coupled receptor response through inositol phosphate quantification with the IP-One assay. *Expert opinion on drug discovery* **2011**, *6* (10), 981–994. DOI: 10.1517/17460441.2011.608658. Published Online: Aug. 9, 2011.

(281) Trinquet, E.; Fink, M.; Bazin, H.; Grillet, F.; Maurin, F.; Bourrier, E.; Ansanay, H.; Leroy, C.; Michaud, A.; Durroux, T.; Maurel, D.; Malhaire, F.; Goudet, C.; Pin, J.-P.; Naval, M.; Hernout, O.; Chrétien, F.; Chapleur, Y.; Mathis, G. D-myo-inositol 1-phosphate as a surrogate of D-myo-inositol 1,4,5-tris phosphate to monitor G protein-coupled receptor activation. *Analytical biochemistry* **2006**, *358* (1), 126–135. DOI: 10.1016/j.ab.2006.08.002. Published Online: Aug. 30, 2006.

(282) Unal, H. Calcium Mobilization Assay to Measure the Activity of Gq-coupled Receptors. *BIO-PROTOCOL* **2013**, *3* (12). DOI: 10.21769/bioProtoc.790.

(283) Patt, J.; Alenfelder, J.; Pfeil, E. M.; Voss, J. H.; Merten, N.; Eryilmaz, F.; Heycke, N.; Rick, U.; Inoue, A.; Kehraus, S.; Deupi, X.; Müller, C. E.; König, G. M.; Crüsemann, M.; Kostenis, E. An experimental strategy to probe Gq contribution to signal transduction in living cells. *The Journal of biological chemistry* **2021**, *296*, 100472. DOI: 10.1016/j.jbc.2021.100472. www.ncbi.nlm.nih.gov/pmc/articles/PMC8024710/. Published Online: Feb. 25, 2021.

(284) Zhang, Y.; Kowal, D.; Kramer, A.; Dunlop, J. Evaluation of FLIPR Calcium 3 Assay Kit--a new no-wash fluorescence calcium indicator reagent. *Journal of biomolecular screening* **2003**, *8* (5), 571–577. DOI: 10.1177/1087057103257240.

(285) Liu, K.; Titus, S.; Southall, N.; Zhu, P.; Inglese, J.; Austin, C. P.; Zheng, W. Comparison on functional assays for Gq-coupled GPCRs by measuring inositol monophospate-1 and intracellular calcium in 1536-well plate format. *Current chemical genomics* **2008**, *1*, 70–78. DOI: 10.2174/1875397300801010070. Published Online: Nov. 7, 2008.

(286) Miller, K. G.; Emerson, M. D.; McManus, J. R.; Rand, J. B. RIC-8 (Synembryn): a novel conserved protein that is required for G(q)alpha signaling in the C. elegans nervous system. *Neuron* **2000**, *27* (2), 289–299. DOI: 10.1016/s0896-6273(00)00037-4.

(287) Chan, P.; Thomas, C. J.; Sprang, S. R.; Tall, G. G. Molecular chaperoning function of Ric-8 is to fold nascent heterotrimeric G protein α subunits. *Proceedings of the National Academy of Sciences of the United States of America* **2013**, *110* (10), 3794–3799. DOI: 10.1073/pnas.1220943110. Published Online: Feb. 19, 2013.

(288) Tall, G. G.; Krumins, A. M.; Gilman, A. G. Mammalian Ric-8A (synembryn) is a heterotrimeric Galpha protein guanine nucleotide exchange factor. *The Journal of biological chemistry* **2003**, *278* (10), 8356–8362. DOI: 10.1074/jbc.M211862200. Published Online: Dec. 30, 2002.

(289) Himmelreich, S.; Masuho, I.; Berry, J. A.; MacMullen, C.; Skamangas, N. K.; Martemyanov, K. A.; Davis, R. L. Dopamine Receptor DAMB Signals via Gq to Mediate

Forgetting in Drosophila. *Cell reports* **2017**, *21* (8), 2074–2081. DOI: 10.1016/j.celrep.2017.10.108.
(290) Jose, A. M.; Koelle, M. R. Domains, amino acid residues, and new isoforms of Caenorhabditis elegans diacylglycerol kinase 1 (DGK-1) important for terminating diacylglycerol signaling in vivo. *The Journal of biological chemistry* **2005**, *280* (4), 2730–2736. DOI: 10.1074/jbc.M409460200. Published Online: Nov. 24, 2004.
(291) Miller, K. G.; Emerson, M. D.; Rand, J. B. Goα and Diacylglycerol Kinase Negatively Regulate the Gqα Pathway in C. elegans. *Neuron* **1999**, *24* (2), 323–333. DOI: 10.1016/s0896-6273(00)80847-8.
(292) Hajdu-Cronin, Y. M.; Chen, W. J.; Patikoglou, G.; Koelle, M. R.; Sternberg, P. W. Antagonism between G(o)alpha and G(q)alpha in Caenorhabditis elegans: the RGS protein EAT-16 is necessary for G(o)alpha signaling and regulates G(q)alpha activity. *Genes & development* **1999**, *13* (14), 1780–1793. DOI: 10.1101/gad.13.14.1780.
(293) Pradel, E.; Zhang, Y.; Pujol, N.; Matsuyama, T.; Bargmann, C. I.; Ewbank, J. J. Detection and avoidance of a natural product from the pathogenic bacterium Serratia marcescens by Caenorhabditis elegans. *Proceedings of the National Academy of Sciences of the United States of America* **2007**, *104* (7), 2295–2300. DOI: 10.1073/pnas.0610281104. Published Online: Jan. 31, 2007.
(294) Matsuki, M.; Kunitomo, H.; Iino, Y. Goalpha regulates olfactory adaptation by antagonizing Gqalpha-DAG signaling in Caenorhabditis elegans. *Proceedings of the National Academy of Sciences of the United States of America* **2006**, *103* (4), 1112–1117. DOI: 10.1073/pnas.0506954103. Published Online: Jan. 17, 2006.
(295) Wong, K.-F.; Wong, W.-K.; Lin, M.-S. Forward selection two sample binomial test. *Journal of data science* **2014**, *12* (4), 279–294. www.ncbi.nlm.nih.gov/pmc/articles/PMC4914133/#:~:text=TFisher%27s%20exact%20test%20(FET)%20is,it%20is%20a%20conditional%20test.
(296) Lints, R.; Hall, D. H. WormAtlas Hermaphrodite Handbook - Reproductive System - Egg-laying Apparatus. *WormAtlas* **2004.** DOI: 10.3908/wormatlas.1.24.
(297) Collins, K. M.; Bode, A.; Fernandez, R. W.; Tanis, J. E.; Brewer, J. C.; Creamer, M. S.; Koelle, M. R. Activity of the C. elegans egg-laying behavior circuit is controlled by competing activation and feedback inhibition. *eLife* **2016**, *5.* DOI: 10.7554/eLife.21126. Published Online: Nov. 16, 2016.
(298) Bohlmann, H.; Sobczak, M. The plant cell wall in the feeding sites of cyst nematodes. *Frontiers in plant science* **2014**, *5*, 89. DOI: 10.3389/fpls.2014.00089. Published Online: Mar. 19, 2014.
(299) Lilley, C. J.; Atkinson, H. J.; Urwin, P. E. Molecular aspects of cyst nematodes. *Molecular plant pathology* **2005**, *6* (6), 577–588. DOI: 10.1111/J.1364-3703.2005.00306.X.
(300) Ngala, B.; Mariette, N.; Ianszen, M.; Dewaegeneire, P.; Denis, M.-C.; Porte, C.; Piriou, C.; Robilliard, E.; Couetil, A.; Nguema-Ona, E.; Yvin, J.-C.; Gobert, V.; Beury, A.; Le Roux, A.-C.; Montarry, J.; Fournet, S. Hatching Induction of Cyst Nematodes in Bare Soils Drenched With Root Exudates Under Controlled Conditions. *Frontiers in plant science* **2020**, *11*, 602825. DOI: 10.3389/fpls.2020.602825. Published Online: Aug. 1, 2021.
(301) Urwin, P. E.; Lilley, C. J.; Atkinson, H. J. Ingestion of double-stranded RNA by preparasitic juvenile cyst nematodes leads to RNA interference. *Molecular plant-microbe interactions : MPMI* **2002**, *15* (8), 747–752. DOI: 10.1094/MPMI.2002.15.8.747.
(302) Masler, E. P. Responses of Heterodera glycines and Meloidogyne incognita to exogenously applied neuromodulators. *Journal of helminthology* **2007**, *81* (4), 421–427. DOI: 10.1017/S0022149X07850243. Published Online: Nov. 16, 2007.

(303) Griffin, C.; Fitters, P. Spontaneous and induced activity of Heterorhabditis megidis infective juveniles during storage. *Nematol* **2004**, *6* (6), 911–917. DOI: 10.1163/1568541044038597.
(304) Schroeder, N. E.; MacGuidwin, A. E. Behavioural quiescence reduces the penetration and toxicity of exogenous compounds in second-stage juveniles of Heterodera glycines. *Nematol* **2010**, *12* (2), 277–287. DOI: 10.1163/138855409X12506855979712.
(305) Wallace, H. R. Undulatory locomotion of the plant parasitic nematode Meloidogyne javanica. *Parasitology* **1968**, *58* (2), 377–391. DOI: 10.1017/S0031182000069419.
(306) Daub, M. The beet cyst nematode (Heterodera schachtii): an ancient threat to sugar beet crops in Central Europe has become an invisible actor. In *Integrated nematode management: state-of-the-art and visions for the future*; Sikora, R. A., Desaeger, J., Molendijk, L., Eds.; CABI, 2021; pp 394–399. DOI: 10.1079/9781789247541.0055.
(307) Almasri, H.; Liberti, J.; Brunet, J.-L.; Engel, P.; Belzunces, L. P. Mild chronic exposure to pesticides alters physiological markers of honey bee health without perturbing the core gut microbiota. *Scientific reports* **2022**, *12* (1), 4281. DOI: 10.1038/s41598-022-08009-2. Published Online: Nov. 3, 2022.
(308) Chianese, R.; Viggiano, A.; Urbanek, K.; Cappetta, D.; Troisi, J.; Scafuro, M.; Guida, M.; Esposito, G.; Ciuffreda, L. P.; Rossi, F.; Berrino, L.; Fasano, S.; Pierantoni, R.; Angelis, A. de; Meccariello, R. Chronic exposure to low dose of bisphenol A impacts on the first round of spermatogenesis via SIRT1 modulation. *Scientific reports* **2018**, *8* (1), 2961. DOI: 10.1038/s41598-018-21076-8. Published Online: Feb. 13, 2018.
(309) Berg, G.; Rybakova, D.; Fischer, D.; Cernava, T.; Vergès, M.-C. C.; Charles, T.; Chen, X.; Cocolin, L.; Eversole, K.; Corral, G. H.; Kazou, M.; Kinkel, L.; Lange, L.; Lima, N.; Loy, A.; Macklin, J. A.; Maguin, E.; Mauchline, T.; McClure, R.; Mitter, B.; Ryan, M.; Sarand, I.; Smidt, H.; Schelkle, B.; Roume, H.; Kiran, G. S.; Selvin, J.; Souza, R. S. C. de; van Overbeek, L.; Singh, B. K.; Wagner, M.; Walsh, A.; Sessitsch, A.; Schloter, M. Microbiome definition re-visited: old concepts and new challenges. *Microbiome* **2020**, *8* (1), 103. DOI: 10.1186/s40168-020-00875-0. Published Online: Jun. 30, 2020.
(310) LACKEY, J. B. Stream enrichment and microbiota. *Public health reports (Washington, D.C. : 1896)* **1956**, *71* (7), 708–718. www.ncbi.nlm.nih.gov/pmc/articles/PMC2031044/.
(311) Ağagündüz, D.; Cocozza, E.; Cemali, Ö.; Bayazıt, A. D.; Nanì, M. F.; Cerqua, I.; Morgillo, F.; Saygılı, S. K.; Berni Canani, R.; Amero, P.; Capasso, R. Understanding the role of the gut microbiome in gastrointestinal cancer: A review. *Frontiers in pharmacology* **2023**, *14*, 1130562. DOI: 10.3389/fphar.2023.1130562. Published Online: Jan. 24, 2023.
(312) Li, X.; Liu, Y.; Yang, X.; Li, C.; Song, Z. The Oral Microbiota: Community Composition, Influencing Factors, Pathogenesis, and Interventions. *Frontiers in microbiology* **2022**, *13*, 895537. DOI: 10.3389/fmicb.2022.895537. Published Online: Apr. 29, 2022.
(313) Nagata, N.; Takeuchi, T.; Masuoka, H.; Aoki, R.; Ishikane, M.; Iwamoto, N.; Sugiyama, M.; Suda, W.; Nakanishi, Y.; Terada-Hirashima, J.; Kimura, M.; Nishijima, T.; Inooka, H.; Miyoshi-Akiyama, T.; Kojima, Y.; Shimokawa, C.; Hisaeda, H.; Zhang, F.; Yeoh, Y. K.; Ng, S. C.; Uemura, N.; Itoi, T.; Mizokami, M.; Kawai, T.; Sugiyama, H.; Ohmagari, N.; Ohno, H. Human Gut Microbiota and Its Metabolites Impact Immune Responses in COVID-19 and Its Complications. *Gastroenterology* **2023**, *164* (2), 272–288. DOI: 10.1053/j.gastro.2022.09.024. Published Online: Sep. 23, 2022.
(314) Perler, B. K.; Friedman, E. S.; Wu, G. D. The Role of the Gut Microbiota in the Relationship Between Diet and Human Health. *Annual review of physiology* **2023**, *85*,

449–468. DOI: 10.1146/annurev-physiol-031522-092054. Published Online: Nov. 14, 2022.
(315) Peixoto, R. S.; Harkins, D. M.; Nelson, K. E. Advances in Microbiome Research for Animal Health. *Annual review of animal biosciences* **2021**, *9*, 289–311. DOI: 10.1146/annurev-animal-091020-075907. Published Online: Dec. 14, 2020.
(316) Jin, Y.; Li, W.; Ba, X.; Li, Y.; Wang, Y.; Zhang, H.; Li, Z.; Zhou, J. Gut microbiota changes in horses with Chlamydia. *BMC microbiology* **2023**, *23* (1), 246. DOI: 10.1186/s12866-023-02986-8. Published Online: Sep. 2, 2023.
(317) Tabbabi, A.; Mizushima, D.; Yamamoto, D. S.; Kato, H. Effects of host species on microbiota composition in Phlebotomus and Lutzomyia sand flies. *Parasites & vectors* **2023**, *16* (1), 310. DOI: 10.1186/s13071-023-05939-2. Published Online: Aug. 31, 2023.
(318) Bettenfeld, P.; Cadena I Canals, J.; Jacquens, L.; Fernandez, O.; Fontaine, F.; van Schaik, E.; Courty, P.-E.; Trouvelot, S. The microbiota of the grapevine holobiont: A key component of plant health. *Journal of advanced research* **2022**, *40*, 1–15. DOI: 10.1016/j.jare.2021.12.008. Published Online: Dec. 22, 2021.
(319) Tiziani, R.; Miras-Moreno, B.; Malacrinò, A.; Vescio, R.; Lucini, L.; Mimmo, T.; Cesco, S.; Sorgonà, A. Drought, heat, and their combination impact the root exudation patterns and rhizosphere microbiome in maize roots. *Environmental and Experimental Botany* **2022**, *203*, 105071. DOI: 10.1016/j.envexpbot.2022.105071.
(320) Wichard, T. From model organism to application: Bacteria-induced growth and development of the green seaweed Ulva and the potential of microbe leveraging in algal aquaculture. *Seminars in cell & developmental biology* **2023**, *134*, 69–78. DOI: 10.1016/j.semcdb.2022.04.007. Published Online: Apr. 19, 2022.
(321) Mueller, U. G.; Linksvayer, T. A. Microbiome breeding: conceptual and practical issues. *Trends in microbiology* **2022**, *30* (10), 997–1011. DOI: 10.1016/j.tim.2022.04.003. Published Online: May. 18, 2022.
(322) Yadav, M.; Chauhan, N. S. Microbiome therapeutics: exploring the present scenario and challenges. *Gastroenterology report* **2022**, *10*, goab046. DOI: 10.1093/gastro/goab046. Published Online: Nov. 15, 2021.
(323) Mimee, M.; Citorik, R. J.; Lu, T. K. Microbiome therapeutics - Advances and challenges. *Advanced drug delivery reviews* **2016**, *105* (Pt A), 44–54. DOI: 10.1016/j.addr.2016.04.032. Published Online: May. 5, 2016.
(324) Celine Bichay. Erstes fäkales Mikro-biota-Präparat aus menschlichen Stuhlproben zugelassen. *Deutsche Apothekerzeitung,* Jan 11, 2023. www.deutsche-apotheker-zeitung.de/news/artikel/2023/01/11/mit-faekaler-mikrobiota-gegen-clostridioides-difficile (accessed 2023-09-13).
(325) Guo, M. Soil Health Assessment and Management: Recent Development in Science and Practices. *Soil Systems* **2021**, *5* (4), 61. DOI: 10.3390/soilsystems5040061.
(326) Shah, A. M.; Khan, I. M.; Shah, T. I.; Bangroo, S. A.; Kirmani, N. A.; Nazir, S.; Malik, A. R.; Aezum, A. M.; Mir, Y. H.; Hilal, A.; Biswas, A. Soil Microbiome: A Treasure Trove for Soil Health Sustainability under Changing Climate. *Land* **2022**, *11* (11), 1887. DOI: 10.3390/land11111887.
(327) Saleem, M.; Hu, J.; Jousset, A. More Than the Sum of Its Parts: Microbiome Biodiversity as a Driver of Plant Growth and Soil Health. *Annu. Rev. Ecol. Evol. Syst.* **2019**, *50* (1), 145–168. DOI: 10.1146/annurev-ecolsys-110617-062605.
(328) Suman, J.; Rakshit, A.; Ogireddy, S. D.; Singh, S.; Gupta, C.; Chandrakala, J. Microbiome as a Key Player in Sustainable Agriculture and Human Health. *Front. Soil Sci.* **2022**, *2.* DOI: 10.3389/fsoil.2022.821589.
(329) Khatri, S.; Dubey, S.; Sharma, S. Microbiome-based approaches to enhance soil health in arable land. In *New and Future Developments in Microbial Biotechnology and*

Bioengineering; Elsevier, 2022; pp 333–344. DOI: 10.1016/B978-0-323-85163-3.00017-X.
(330) Martin, P. A.; Soby, S. Insecticidal strains of Chromobacterium vaccinii sp. nov. for control of insects. US201414338549 20140723.
(331) Ebadzadsahrai, G.; Higgins Keppler, E. A.; Soby, S. D.; Bean, H. D. Inhibition of Fungal Growth and Induction of a Novel Volatilome in Response to Chromobacterium vaccinii Volatile Organic Compounds. *Frontiers in microbiology* **2020**, *11*, 1035. DOI: 10.3389/fmicb.2020.01035. Published Online: May. 20, 2020.
(332) Kawaletz, H.; Mölder, I.; Annighöfer, P.; Terwei, A.; Zerbe, S.; Ammer, C. Pot experiments with woody species – a review. *Forestry: An International Journal of Forest Research* **2014**, *87* (4), 482–491. DOI: 10.1093/forestry/cpu017.
(333) Passioura, J. B. Viewpoint: The perils of pot experiments. *Functional plant biology : FPB* **2006**, *33* (12), 1075–1079. DOI: 10.1071/FP06223.
(334) Yadav, P.; Kumari, A.; Sundari, S. K. "ASURE": A multi-potential plant bioassay as a pre-determinative microbial efficiency testing tool for bioinoculant studies. *MethodsX* **2020**, *7*, 100685. DOI: 10.1016/j.mex.2019.09.037. Published Online: Oct. 4, 2019.
(335) Myers, O. D.; Sumner, S. J.; Li, S.; Barnes, S.; Du, X. One Step Forward for Reducing False Positive and False Negative Compound Identifications from Mass Spectrometry Metabolomics Data: New Algorithms for Constructing Extracted Ion Chromatograms and Detecting Chromatographic Peaks. *Analytical chemistry* **2017**, *89* (17), 8696–8703. DOI: 10.1021/acs.analchem.7b00947.
(336) Djoumbou Feunang, Y.; Eisner, R.; Knox, C.; Chepelev, L.; Hastings, J.; Owen, G.; Fahy, E.; Steinbeck, C.; Subramanian, S.; Bolton, E.; Greiner, R.; Wishart, D. S. ClassyFire: automated chemical classification with a comprehensive, computable taxonomy. *Journal of cheminformatics* **2016**, *8*, 61. DOI: 10.1186/s13321-016-0174-y. Published Online: Apr. 11, 2016.
(337) Kim, H. W.; Wang, M.; Leber, C. A.; Nothias, L.-F.; Reher, R.; Kang, K. B.; van der Hooft, J. J. J.; Dorrestein, P. C.; Gerwick, W. H.; Cottrell, G. W. NPClassifier: A Deep Neural Network-Based Structural Classification Tool for Natural Products. *Journal of natural products* **2021**, *84* (11), 2795–2807. DOI: 10.1021/acs.jnatprod.1c00399. Published Online: Oct. 18, 2021.
(338) Kiontke, K. C.; Félix, M.-A.; Ailion, M.; Rockman, M. V.; Braendle, C.; Pénigault, J.-B.; Fitch, D. H. A. A phylogeny and molecular barcodes for Caenorhabditis, with numerous new species from rotting fruits. *BMC evolutionary biology* **2011**, *11*, 339. DOI: 10.1186/1471-2148-11-339. Published Online: Nov. 21, 2011.
(339) Tsuda, K.; Futai, K. Description of Caenorhabditis auriculariae n. sp.(Nematoda: Rhabditida) from Fruiting Bodies of Auricularia polytricha. *Jpn. J. Nematol.* **1999**, *29* (1), 18–23. DOI: 10.3725/jjn1993.29.1_18.
(340) Stevens, L.; Rooke, S.; Falzon, L. C.; Machuka, E. M.; Momanyi, K.; Murungi, M. K.; Njoroge, S. M.; Odinga, C. O.; Ogendo, A.; Ogola, J.; Fèvre, E. M.; Blaxter, M. The Genome of Caenorhabditis bovis. *Current biology : CB* **2020**, *30* (6), 1023-1031.e4. DOI: 10.1016/j.cub.2020.01.074. Published Online: Feb. 27, 2020.
(341) Morris, G. M.; Huey, R.; Lindstrom, W.; Sanner, M. F.; Belew, R. K.; Goodsell, D. S.; Olson, A. J. AutoDock4 and AutoDockTools4:Automated docking with selective receptor flexibility. *Journal of computational chemistry* **2009**, *30* (16), 2785–2791. DOI: 10.1002/jcc.21256.
(342) Sanner, M. F. Python: a programming language for software integration and development. *Journal of molecular graphics & modelling* **1999**, *17* (1), 57–61.

(343) Namasivayam, V.; Günther, R. pso@autodock:A fast flexible molecular docking program based on Swarm intelligence. *Chemical biology & drug design* **2007**, *70* (6), 475–484. DOI: 10.1111/j.1747-0285.2007.00588.x.
(344) Allan, D. B.; Caswell, T.; Keim, N. C.; van der Wel, C. M. *soft-matter/trackpy: Trackpy v0.4.2*; Zenodo, 2019. DOI: 10.5281/zenodo.3492186.
(345) Bonnard, E.; Liu, J.; Zjacic, N.; Alvarez, L.; Scholz, M. *Automatically tracking feeding behavior in populations of foraging C. elegans*, 2022. DOI: 10.1101/2022.01.20.477072.
(346) Sijmons, P. C.; Grundler, F. M.; Mende, N.; Burrows, P. R.; Wyss, U. Arabidopsis thaliana as a new model host for plant-parasitic nematodes. *The Plant Journal* **1991**, *1* (2), 245–254. DOI: 10.1111/j.1365-313X.1991.00245.x.
(347) Gutbrod, P.; Gutbrod, K.; Nauen, R.; Elashry, A.; Siddique, S.; Benting, J.; Dörmann, P.; Grundler, F. M. W. Inhibition of acetyl-CoA carboxylase by spirotetramat causes growth arrest and lipid depletion in nematodes. *Scientific reports* **2020**, *10* (1), 12710. DOI: 10.1038/s41598-020-69624-5. Published Online: Jul. 29, 2020.